

## CONTENTS

There are no problems and therefore, no problem solutions for the "read-only" Chapters 4, 9, and 13.

### **PART I Semiconductor Fundamentals**

<b>CHAPTER 1</b> Semiconductors: A General Introduction	1-1
<b>CHAPTER 2</b> Carrier Modeling	2-1
<b>CHAPTER 3</b> Carrier Action	3-1

### **PART IIA *pn* Junction Diodes**

<b>CHAPTER 5</b> <i>pn</i> Junction Electrostatics	5-1
<b>CHAPTER 6</b> <i>pn</i> Junction Diode: I-V Characteristics	6-1
<b>CHAPTER 7</b> <i>pn</i> Junction Diode: Small-Signal Admittance	7-1
<b>CHAPTER 8</b> <i>pn</i> Junction Diode: Transient Response	8-1

### **PART IIB BJTs and Other Junction Devices**

<b>CHAPTER 10</b> BJT Fundamentals	10-1
<b>CHAPTER 11</b> BJT Static Characteristics	11-1
<b>CHAPTER 12</b> BJT Dynamic Response Modeling	12-1
<b>CHAPTER 14</b> MS Contacts and Schottky Diodes	14-1
<b>R2 Part II</b> Supplement and Review	R2-1

### **PART III Field Effect Devices**

<b>CHAPTER 15</b> Field Effect Introduction--The J-FET and MESFET	15-1
<b>CHAPTER 16</b> MOS Fundamentals	16-1
<b>CHAPTER 17</b> MOSFETs-- <i>The Essentials</i>	17-1
<b>CHAPTER 18</b> Nonideal MOS	18-1
<b>CHAPTER 19</b> Modern FET Structures	19-1



## CHAPTER 1

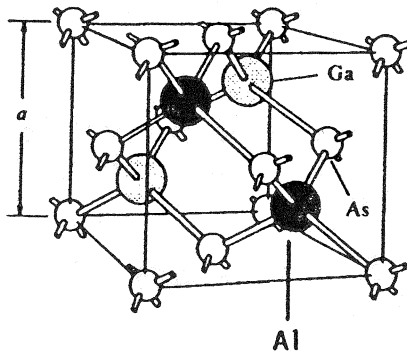
### 1.1

- (a) From Table 1.1...
- (i) Si or Ge
  - (ii) AlP, AlAs, AlSb, GaN, GaP, GaAs, GaSb, InP, InAs, or InSb
- (b) Crystalline material has the same atomic pattern or order throughout the material, while polycrystalline material has crystalline subsections that are misaligned with respect to each other.
- (c) A *unit cell* is a small portion of a crystal that could be used to reproduce the crystal.  
(The preceding is from the first sentence of Subsection 1.2.1.)
- (d) 

<u>Unit cell</u>	<u>Atoms/unit cell</u>
simple cubic.....	1
bcc.....	2
fcc.....	4
diamond.....	8
- (e)  $1\text{\AA} = 10^{-8} \text{ cm}$
- (f)  $a$  (one lattice constant)
- (g) 4
- (h) As summarized in Table 1.3: ( )--crystal plane, { }--equivalent planes, [ ]--crystal direction, and < >--equivalent directions.
- (i) See Subsection 1.3.2.

### 1.2

In the  $\text{Al}_{0.5}\text{Ga}_{0.5}\text{As}$  unit cell, pictured below, fcc sublattice sites containing the Column III elements are equally occupied by Al and Ga atoms.



### 1.3

(a) Ge crystallizes in the diamond lattice where there are 8 atoms per unit cell (see Subsection 1.2.3). Thus

$$\text{DENSITY} = \frac{8}{a^3} = \frac{8}{(5.65 \times 10^{-8})^3} = 4.44 \times 10^{22} \text{ atoms/cm}^3$$

### 1.4

(a) From Fig. 1.3(c), we conclude nearest-neighbors in the bcc lattice lie along the unit cell body diagonal. Since the body diagonal of a cube is equal to  $\sqrt{3}$  times a cube side length (the lattice constant  $a$ ),

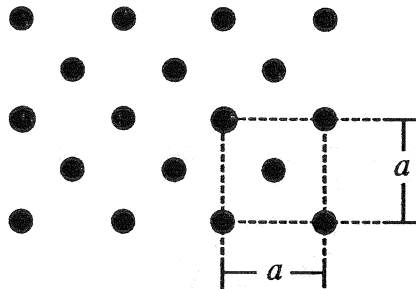
$$\left( \frac{\text{Nearest-Neighbor}}{\text{Distance}} \right) = \frac{\sqrt{3}}{2} a$$

(b) From Fig. 1.3(d), nearest-neighbors in the fcc lattice are concluded to lie along a *cube-face* diagonal. The diagonal of a cube face is equal to  $\sqrt{2}$  times a cube side length. Thus

$$\left( \frac{\text{Nearest-Neighbor}}{\text{Distance}} \right) = \frac{\sqrt{2}}{2} a$$

### 1.5

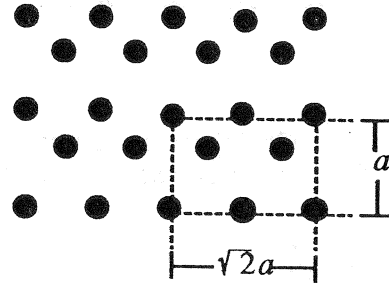
(a) Looking at Fig. 1.4(a) one concludes



(b) For Si at room temperature  $a = 5.43 \times 10^{-8} \text{ cm}$ . From the above figure one concludes that there are  $(1/4 \times 4 \text{ corner atoms}) + 1 \text{ body atom} = 2 \text{ atoms}$  per an area of  $a^2$  on the (100) surface. Thus one has

$$\frac{2}{a^2} = \frac{2}{(5.43 \times 10^{-8})^2} = 6.78 \times 10^{14} \text{ Si atoms/cm}^2$$

(c) For a (110) plane one has the atom placement pictured below



(d) On the (110) plane in the area  $a \times \sqrt{2}a$  one has  $(1/4 \times 4 \text{ corner atoms}) + (1/2 \times 2 \text{ edge atoms}) + 2 \text{ body atoms} = 4 \text{ atoms}$ . Thus one has

$$\frac{4}{\sqrt{2}a^2} = \frac{2\sqrt{2}}{(5.43 \times 10^{-8})^2} = 9.59 \times 10^{14} \text{ Si atoms/cm}^2$$

(e) MATLAB program script (paralleling Exercise 1.3)...

```
%Solution to Problem 1.5(e)
N=input('input number of atoms on (100) face of unit cell, N = ');
a=input('lattice constant in angstrom, a = ');
surfaceden=N*(1.0e16)/(a^2)      %number of atoms/cm^2
```

(Note: This and all other problem solutions are available on disk.)

## 1.6

(a) (i) Following the procedure outlined in the text

1, 3, 1	...intercepts (normalized)
1, 1/3, 1	...[1/intercept]s
3, 1, 3	...reduction to lowest whole-number set
<b>(313)</b>	...Miller index notation for plane

(ii) As noted in the text near the end of Subsection 1.2.4, the normal to a plane in the cubic crystal system has the same Miller indices as the plane.

**[313]** ...Miller index notation for normal to plane

(b) (i) Again following the Miller indexing procedure,

1, 1, 1/2	...normalized intercepts
1, 1, 2	...[1/intercept]s
1, 1, 2	...lowest whole-number set
<b>(112)</b>	...Miller indices of plane

(ii) Assume the vector has a length  $d$ . Its projections along the  $x$ ,  $y$ , and  $z$  axes are then 0, 0, and  $d$ , respectively. Reducing to the lowest possible whole-number set and enclosing in square brackets, then yields

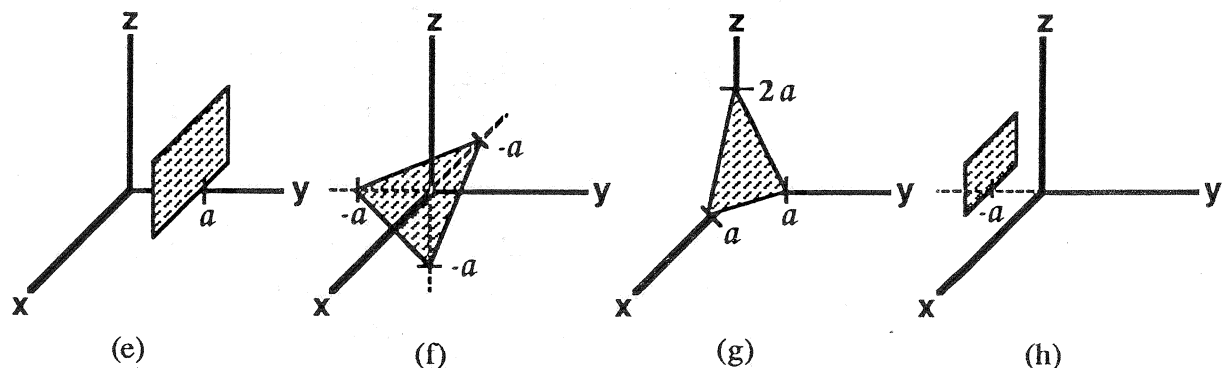
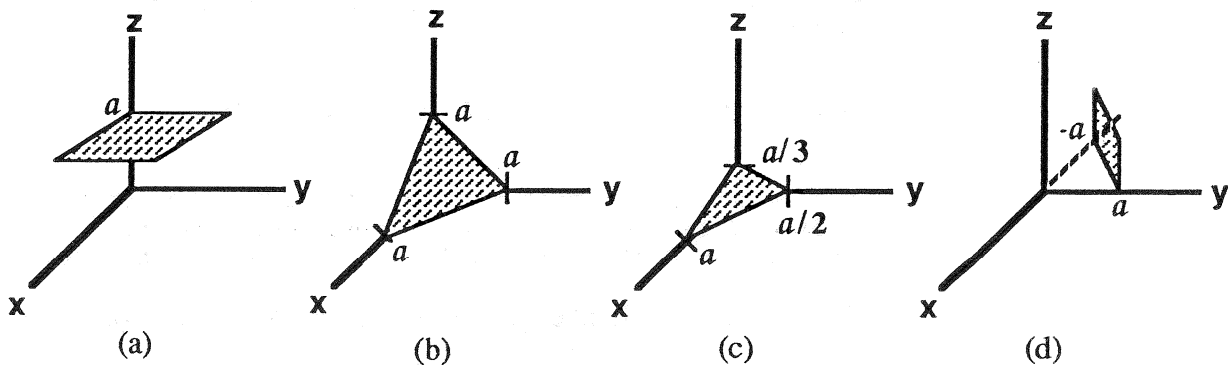
**[001]** ...Miller indices of direction vector

### 1.7

For each of the given planes, the Miller indexing procedure must be reversed to determine the intercepts of the given plane on the coordinate axes. Using part (c) as an example, one proceeds as follows:

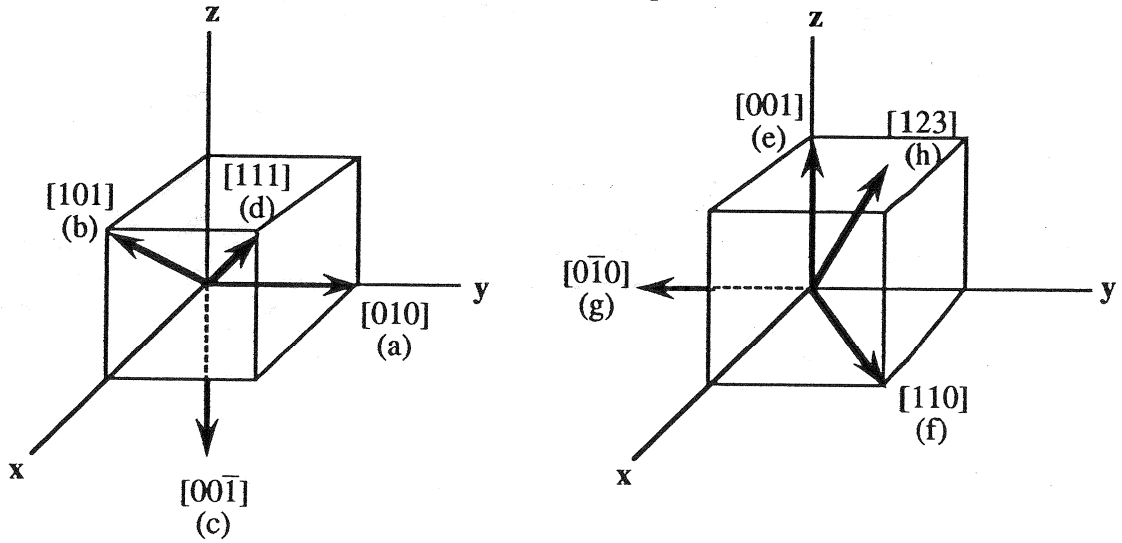
(123)	...Miller indices
1, 2, 3	...[1/intercept]s
1, 1/2, 1/3	...intercepts

The plane in question intercepts the  $x$ ,  $y$ ,  $z$  coordinate axes at  $a$ ,  $a/2$ , and  $a/3$ , respectively. Note that any multiple of the cited intercept set – such as  $3a$ ,  $2a$ ,  $a$  – would also be correct. All such planes are parallel equivalent planes.



### 1.8

Miller indices may be viewed as specifying the projection (in arbitrary units) of the to-be-pictured vectors along the coordinate axes. For example, [010] corresponds to a vector with a unit projection along the y-axis and no projection along the x- or z-axes. In other words, [010] is coincident with the +y coordinate axis. The other required direction vectors are deduced in a similar manner and are as pictured below.



### 1.9

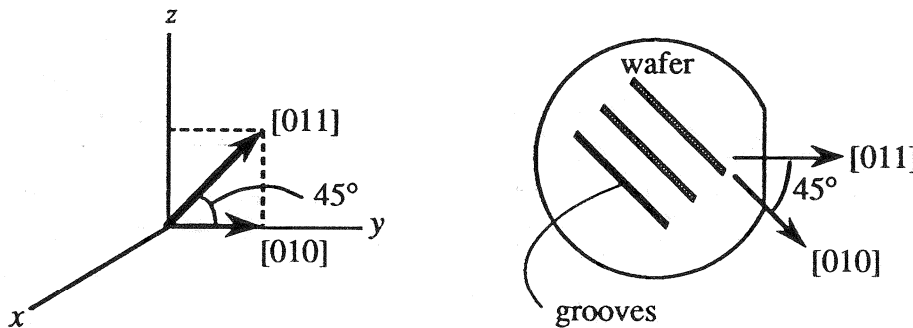
As noted in the problem statement, two directions  $[h_1k_1l_1]$  and  $[h_2k_2l_2]$  will be mutually perpendicular if

$$h_1h_2 + k_1k_2 + l_1l_2 = 0$$

- (a) Here  $[h_1k_1l_1] = [100]$ , requiring  $h_2 = 0$ . All directions  $[0k_2l_2]$  are perpendicular to  $[100]$ . Two specific simple examples are  $[001]$  and  $[011]$ .
- (b) Given  $[h_1k_1l_1] = [111]$ , one requires the Miller indices of the perpendicular direction to be such that  $h_2 + k_2 + l_2 = 0$ . Two specific examples are  $[01\bar{1}]$  and  $[11\bar{2}]$ .

### 1.10

As shown in the following left-hand figure, when the [011] and [010] directions are pictured simultaneously, it becomes obvious that the angle between the two directions is  $45^\circ$ . Alternatively, the angle between the two directions can be computed using the  $\cos(\theta)$  relationship in Problem 1.9. Specifically, given  $[h_1k_1l_1] = [011]$  and  $[h_2k_2l_2] = [010]$ ,  $\cos(\theta) = 1/\sqrt{2}$  and  $\theta = 45^\circ$ . The required positioning of the "grooves" on the wafer's surface is pictured in the following right-hand figure.

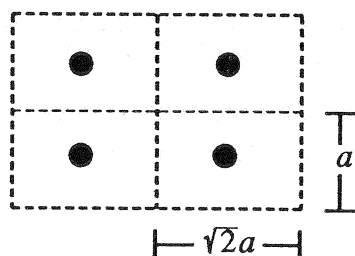


### 1.11

(a) If the Fig. P1.11 unit cell is conceptually copied and the cells stacked like blocks in a nursery, one concludes the resulting lattice is a simple cubic lattice.

(b) There is one atom inside the unit cell and the unit cell volume is  $a^3$ . Thus atoms/unit volume =  $1/a^3$ .

(c) For a (110) surface plane the atom positioning would be as pictured below.



$$\frac{\text{atoms}}{\text{unit area}} = \frac{1 \text{ atom}}{(a)(\sqrt{2}a)} = \frac{1}{\sqrt{2}a^2}$$

(d) [111] ... The specified vector has equal projections on the three coordinate axes.

### 1.12

Equivalent planes: (a) 6, (b) 12, (c) 8.

Equivalent directions: (d) 6, (e) 12, (f) 8.

NOTE: The answers may be deduced from geometrical considerations – or – by noting the total number of possible combinations of the given, and negatives of the given, Miller indices.

### 1.13

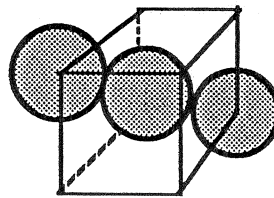
(a) In the simple cubic lattice the nearest-neighbor distance is  $a$ , where  $a$  is the side length of the cube, and the atomic radius  $r$  is therefore  $a/2$ . Moreover, there is one atom per unit cell. Thus

$$\text{Occupied volume} = \frac{4}{3}\pi r^3 = \frac{4}{3}\pi (a/2)^3 = \pi a^3/6$$

$$\text{Total cell volume} = a^3$$

$$\text{Ratio} = \frac{\text{Occupied volume}}{\text{Total volume}} = \frac{\pi}{6}$$

(b) In the body centered cubic lattice the atom in the center and any one of the cube corner atoms are nearest neighbors. Thus 1/2 the nearest neighbor distance is  $r = \sqrt{3} a/4$ . Also, there are two atoms per unit cell.



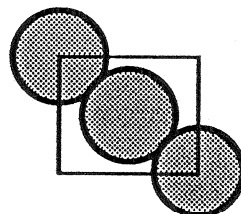
$$\text{diagonal} = 4r = \sqrt{3} a$$

$$\text{Occupied volume} = 2(\frac{4}{3}\pi r^3) = \frac{8}{3}\pi (\sqrt{3} a/4)^3 = \frac{\sqrt{3}}{8}\pi a^3$$

$$\text{Total cell volume} = a^3$$

$$\text{Ratio} = \frac{\text{Occupied volume}}{\text{Total volume}} = \frac{\sqrt{3}\pi}{8}$$

(c) For a face centered cubic lattice, the closest atoms lie in a cube face. Also, there are four atoms per unit cell in the fcc lattice.



$$\text{face diagonal} = 4r = \sqrt{2} a; r = \sqrt{2} a/4$$

$$\text{Occupied volume} = 4\left(\frac{4}{3}\pi r^3\right) = \frac{16}{3}\pi (\sqrt{2} a/4)^3 = \frac{\sqrt{2}}{6}\pi a^3$$

$$\text{Total volume} = a^3$$

$$\text{Ratio} = \frac{\sqrt{2}\pi}{6}$$

(d) As emphasized in Fig. 1.4(c), the atom in the upper front corner of the unit cell and the atom along the cube diagonal 1/4 of the way down the diagonal are nearest neighbors. Since the diagonal of the cube is equal to  $\sqrt{3}$  times a cube side length, the center-to-center distance between nearest-neighbor atoms in the diamond lattice is  $\sqrt{3} a/4$ , and the atomic radius  $r = \sqrt{3} a/8$ . Moreover, there are eight atoms per unit cell in the diamond lattice. Thus

$$\text{Occupied volume} = 8\left(\frac{4}{3}\pi r^3\right) = \frac{32}{3}\pi (\sqrt{3} a/8)^3 = \frac{\sqrt{3}}{16}\pi a^3$$

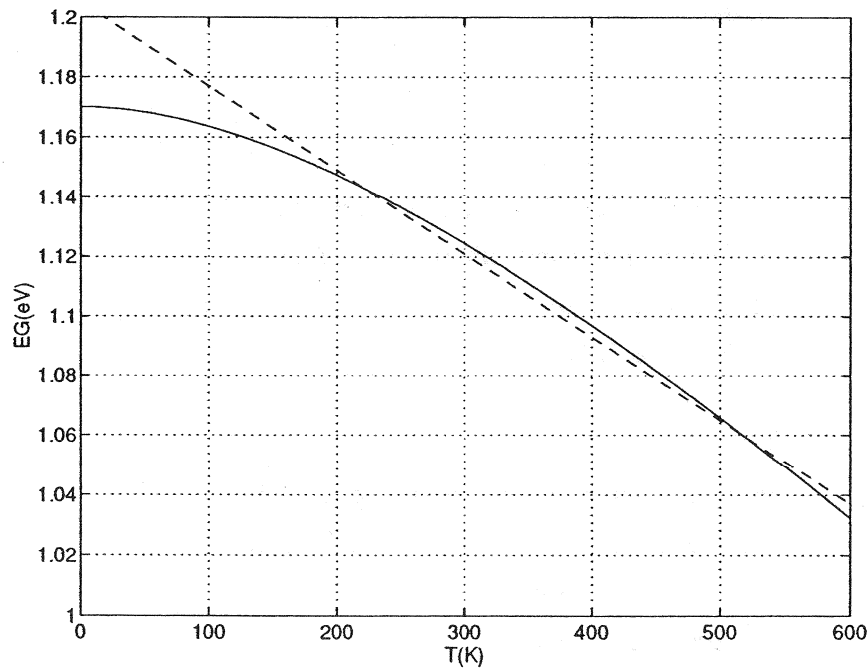
$$\text{Total volume} = a^3$$

$$\text{Ratio} = \frac{\sqrt{3}\pi}{16}$$

## CHAPTER 2

### 2.1

(a)/(b) The MATLAB program script yielding both the part (a) and part (b) results is listed below. A combined plot comparing the part (a) result (solid-line) and part (b) result (dashed-line) is included before the program script. At  $T = 300$  K the part (a) relationship yields  $E_G(300K) = 1.1245$  eV.



MATLAB program script...

```
%EG Computation (EG versus T)
close
clear
%Parabolic Fit Parameters
EG0=1.170;
a=4.730e-4;
b=636;
%Parabolic computation and plot
T=[0:5:600];
```

```

EG=EG0-a.* (T.^2)./(T+b);
EG300=EG0-a.* (300.^2)./(300+b);
plot(T,EG); axis([0 600 1.0 1.2]); grid;
xlabel('T(K)'); ylabel('EG(eV)');
hold on
%Linear computation and plot
EG0=1.205;
a=2.8e-4;
EG=EG0-a.*T;
plot(T,EG, 'b--');
hold off
%T=300K result
EG300

```

## 2.2

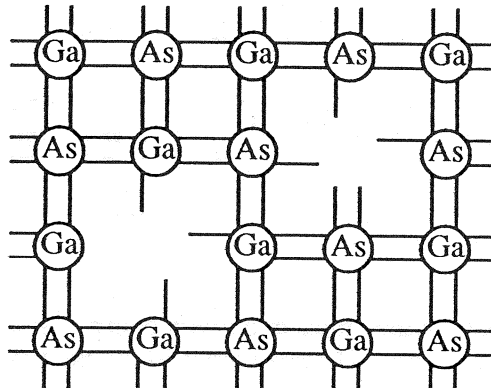
- (a) See Fig. 2.4(a).
- (b) See Fig. 2.4(b) or the left-hand side of Fig. 2.7(b).
- (c) See the left-hand side of Fig. 2.7(c).
- (d) See Fig. 2.10(a).
- (e) See Fig. 2.10(b).

## 2.3

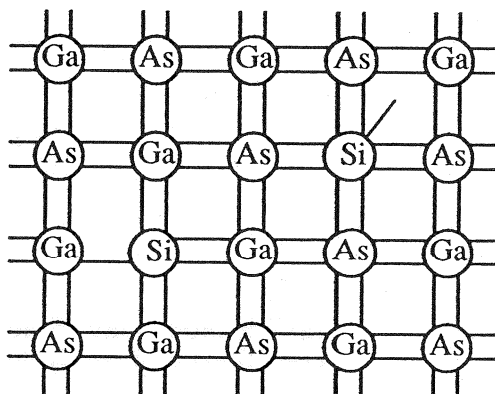
- (a) See the right-hand side of Fig. 2.7(b).
- (b) See the right-hand side of Fig. 2.7(c).
- (c) See Fig. 2.13(a).
- (d) See Fig. 2.13(b).
- (e) See the extreme left-hand side of either Fig. 2.13(a) or Fig. 2.22(b).
- (f) See the extreme left-hand side of Fig. 2.13(b).
- (g) See the extreme right-hand side of Fig. 2.16.
- (h) See the extreme left-hand side of Fig. 2.18.
- (i) See the middle of Fig. 2.18.
- (j) See the extreme right-hand side of Fig. 2.18.
- (k) See Fig. 2.19.
- (l) See Fig. 2.19.

2.4

- (a) The removal of the column III Ga atom with three valence electrons leaves five dangling bonds in the vicinity of the vacancy. The removal of the column V As atom with five valence electrons leaves three dangling bonds in the vicinity of the vacancy.
- (b) When a Si atom with four valence electrons is inserted into the missing Ga site, there is one extra electron that does not fit snugly into the bonding pattern. Conversely, when a Si atom is inserted into the missing As site, there are one too few bonds to complete the bonding scheme.--There is a hole in the bonding scheme.



Answer-(a)

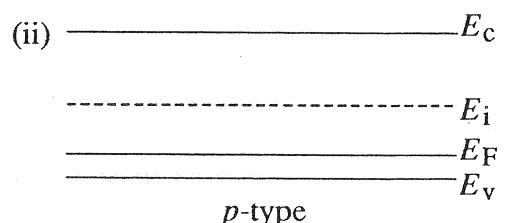
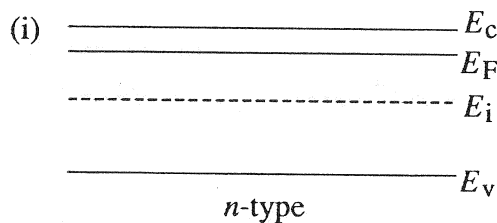


Answer-(b)

(c) **n-type** ... The extra electron noted in part (b) is readily released yielding an increase in the electron concentration.

(d) **p-type** ... The missing bond noted in part (b) is readily filled at room temperature yielding an increase in the hole concentration.

(e)



## 2.5

As noted in Subsection 2.4.1,  $g_c(E)dE$  represents the number of conduction band states/cm<sup>3</sup> lying in the energy range between  $E$  and  $E + dE$ . It follows that the number of states/cm<sup>3</sup> in the conduction band lying between energies  $E_c$  and  $E_c + \gamma kT$  is simply obtained by integrating  $g_c(E)dE$  over the noted range of energies.

$$\begin{aligned} \text{states/cm}^3 &= \int_{E_c}^{E_c+\gamma kT} g_c(E)dE = \frac{m_n^* \sqrt{2m_n^*}}{\pi^2 \hbar^3} \int_{E_c}^{E_c+\gamma kT} \sqrt{E - E_c} dE \\ &= \frac{2}{3} \frac{m_n^* \sqrt{2m_n^*}}{\pi^2 \hbar^3} (E - E_c)^{3/2} \Big|_{E_c}^{E_c+\gamma kT} = \boxed{\frac{2}{3} \left( \frac{m_n^* \sqrt{2m_n^*}}{\pi^2 \hbar^3} \right) (\gamma kT)^{3/2}} \end{aligned}$$

## 2.6

(a) The probability of electrons occupying states at a given energy under equilibrium conditions is given by the Fermi function. Here we are told the energy of interest is  $E = E_F$ . Thus

$$f(E_F) = \frac{1}{1 + e^{(E_F - E_F)/kT}} = \frac{1}{2}$$

(b) The desired probability is again given by the Fermi function. Here we are told  $E_F = E_c$  and the energy of interest is  $E = E_c + kT$ . Consequently,

$$f(E_c + kT) = \frac{1}{1 + e^{[(E_c+kT) - E_c]/kT}} = \frac{1}{1 + e^1} = 0.269$$

(c) The problem statement indicates  $f(E_c+kT) = 1 - f(E_c+kT)$ , or

$$\frac{1}{1 + e^{(E_c+kT-E_F)/kT}} = 1 - \frac{1}{1 + e^{(E_c+kT-E_F)/kT}} = \frac{e^{(E_c+kT-E_F)/kT}}{1 + e^{(E_c+kT-E_F)/kT}} = \frac{1}{1 + e^{(E_F-E_c-kT)/kT}}$$

Thus we must have

$$E_c + kT - E_F = E_F - (E_c + kT)$$

or

$$\boxed{E_F = E_c + kT}$$

## 2.7

The distribution of electrons in the conduction band is given by  $g_c(E)f(E)$ ; the distribution of holes in the valence band is given by  $g_v(E)[1 - f(E)]$ . Working with the electron distribution we note,

$$f(E) = \frac{1}{1 + e^{(E - E_F)/kT}} \equiv e^{-(E - E_F)/kT}$$

...for all  $E \geq E_c$  if the semiconductor is nondegenerate

Thus

$$\begin{aligned} g_c(E)f(E) &= \frac{m_n^* \sqrt{2m_n^*(E-E_c)}}{\pi^2 \hbar^3} e^{-(E-E_F)/kT} \\ &= \kappa (E-E_c)^{1/2} e^{-(E-E_F)/kT} \quad \dots \kappa \equiv \frac{m_n^* \sqrt{2m_n^*}}{\pi^2 \hbar^3} \end{aligned}$$

The extrema points of any function are obtained by taking the derivative of the function and setting the derivative equal to zero.

$$\begin{aligned} \frac{d}{dE}[g_c(E)f(E)] &= \frac{\kappa}{2(E-E_c)^{1/2}} e^{-(E-E_F)/kT} - \frac{\kappa(E-E_c)^{1/2}}{kT} e^{-(E-E_F)/kT} \\ &\text{set} \\ &= 0 \end{aligned}$$

Clearly

$$\frac{1}{2\sqrt{E_{\text{peak}}-E_c}} = \frac{\sqrt{E_{\text{peak}}-E_c}}{kT}$$

or

$$E_{\text{peak}} - E_c = kT/2$$

and

$$E_{\text{peak}} = E_c + kT/2 \quad \dots \text{for electrons in the conduction band}$$

The development leading to the peak energy of  $E_{\text{peak}} = E_v - kT/2$  for holes in the valence band is completely analogous.

## 2.8

The electron population at any energy is given by  $g_c(E)f(E)$ . Also, since the semiconductor is nondegenerate

$$f(E) = \frac{1}{1 + e^{(E - E_F)/kT}} \approx e^{-(E - E_F)/kT} \quad \text{...for all } E > E_c$$

The electron population at  $E = E_c + 5kT$  normalized to the peak electron population at  $E = E_c + kT/2$  is therefore

$$\begin{aligned} \text{ratio} &= \frac{g_c(E_c+5kT)f(E_c+5kT)}{g_c(E_c+kT/2)f(E_c+kT/2)} \\ &\approx \frac{\sqrt{5kT}}{\sqrt{kT/2}} \frac{e^{-(E_c+5kT-E_F)/kT}}{e^{-(E_c+kT/2-E_F)/kT}} = \sqrt{10} e^{-4.5} = 3.51 \times 10^{-2} \end{aligned}$$

## 2.9

The hole and electron distributions are given respectively by

$$\begin{aligned} (\text{electron dist.}) &= g_c(E)f(E) \approx \frac{m_n^* \sqrt{2m_n^*}}{\pi^2 \hbar^3} \sqrt{E - E_c} e^{-(E - E_F)/kT} \\ &= \left( \frac{m_n^* \sqrt{2m_n^*}}{\pi^2 \hbar^3} e^{-E_G/4kT} \right) \sqrt{E - E_c} e^{-(E - E_c)/kT} \end{aligned}$$

and

$$\begin{aligned} (\text{hole dist.}) &= g_v(E)[1 - f(E)] \approx \frac{m_p^* \sqrt{2m_p^*}}{\pi^2 \hbar^3} \sqrt{E_v - E} e^{(E - E_F)/kT} \\ &= \left( \frac{m_p^* \sqrt{2m_p^*}}{\pi^2 \hbar^3} e^{-3E_G/4kT} \right) \sqrt{E_v - E} e^{-(E_v - E)/kT} \end{aligned}$$

Note that the approximate (non-degenerate) expressions for the Fermi function established in Subsection 2.4.2 were employed in writing down the carrier distributions.

The required MATLAB program script and resultant plots are presented below. Computations were performed employing  $E_G = 1.12 \text{ eV}$ ,  $kT = 0.0259 \text{ eV}$ ,  $m_n^*/m_0 = 1.18$  and  $m_p^*/m_0 = 0.81$  from Table 2.1, and  $\hbar = 6.63 \times 10^{-34} \text{ joule-sec}$  and  $m_0 = 9.11 \times 10^{-31} \text{ kg}$  from the table of physical constants (inside back cover).

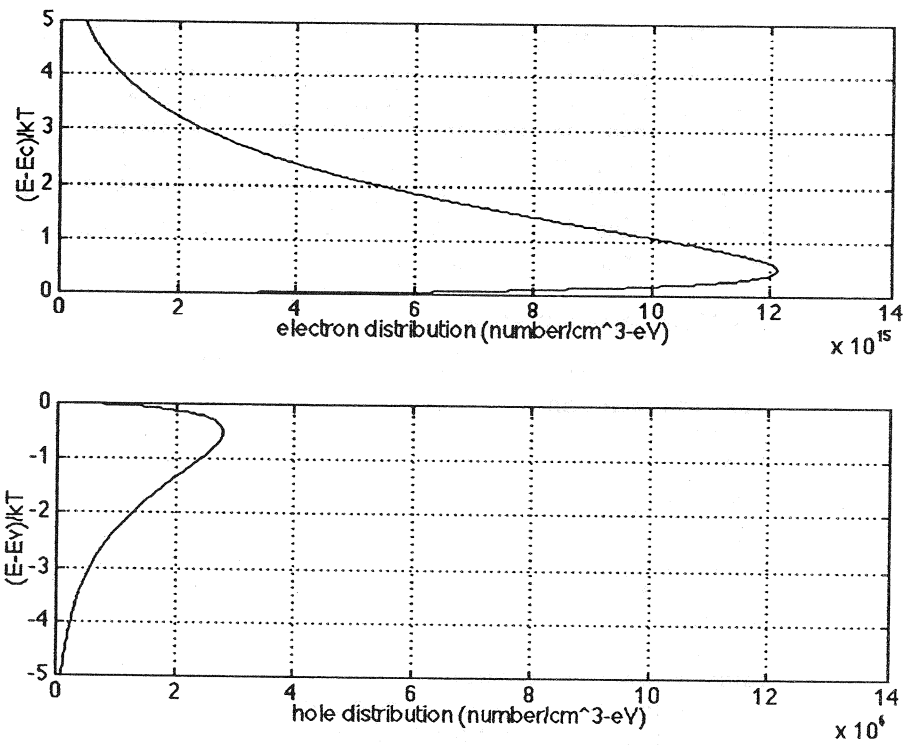
The plots are clearly consistent with Fig. 2.16 in the text. (Note that the electron distribution scale is multiplied by  $10^{15}$  while the hole distribution scale is multiplied by  $10^6$ .) The distributions peak at  $kT/2$  from the band edges graphically reconfirming the peak positions noted in Problem 2.7.

#### MATLAB program script...

```
%Problem 2.9...Carrier Distributions
%Initialization
close
clear
%Constants
EG=1.12;
kT=0.0259;
m0=9.11e-31;
mnr=1.18;
mpr=0.81;
hbar=6.63e-34/(2*pi);
c1=1.6e-19;      %joules = c1*eV
c2=1.0e-6        %m^3=c2*cm^3

%Computation
deltaE=linspace(0,5*kT);           %deltaE = E-Ec or Ev-E in eV
A=m0*sqrt(2*m0)/(pi^2*hbar^3);
An=mnr^(3/2)*A; Ap=mpr^(3/2)*A;
e_dist=c1*c2*An*exp(-EG/(4*kT)).*sqrt(c1*deltaE).*exp(-deltaE/kT);
h_dist=c1*c2*Ap*exp(-3*EG/(4*kT)).*sqrt(c1*deltaE).*exp(-deltaE/kT);
%Note use of c1 and c2 to make distribution units number/cm^3-eV

%Plots
subplot(2,1,1), plot(e_dist,deltaE/kT); grid
xlabel('electron distribution (number/cm^3-eV)');
ylabel('(E-Ec)/kT')
subplot(2,1,2), plot(h_dist,-deltaE/kT); grid
axis([0,1.4e7,-5,0])
xlabel('hole distribution (number/cm^3-eV)');
ylabel('(E-Ev)/kT')
```



## 2.10

(a) Utilizing Eq. (2.6a), the approximate (nondegenerate) expression for the Fermi function established in Subsection 2.4.2, Eq. (2.13a), and Eq. (2.16a), one obtains

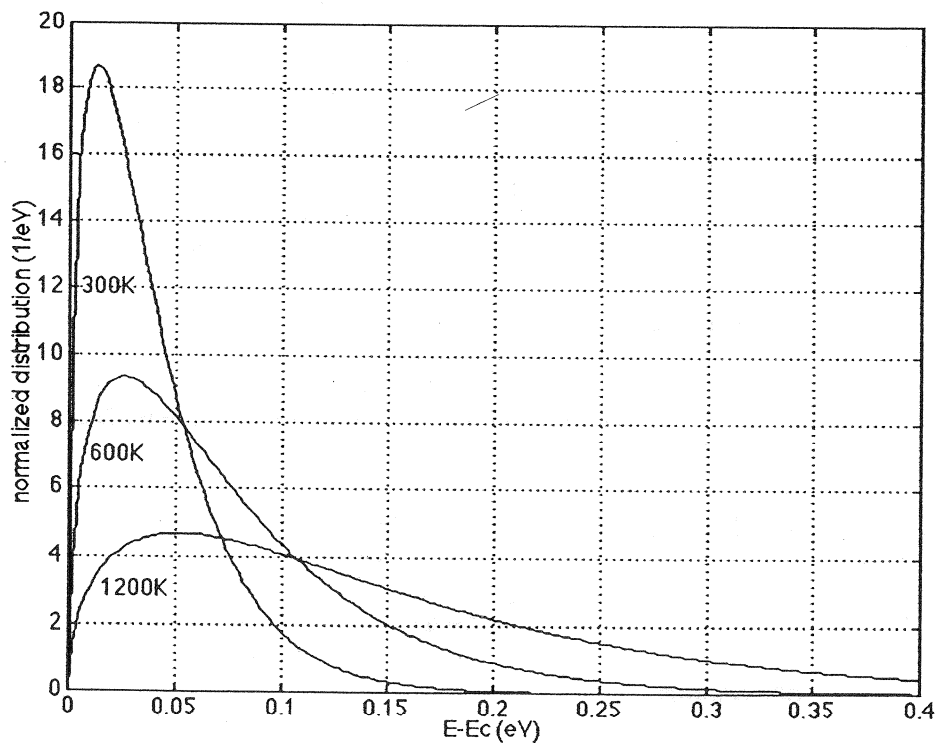
$$\begin{aligned}
 \text{(normalized dist.)} &= \frac{g_c(E)f(E)}{n} \approx \frac{\left(m_n^* \sqrt{2m_n^*} / \pi^2 \hbar^3\right) \sqrt{E - E_c} e^{-(E-E_F)/kT}}{2 \left(m_n^* kT / 2\pi\hbar^2\right)^{3/2} e^{(E_F-E_c)/kT}} \\
 &= \frac{2\sqrt{E - E_c}}{\sqrt{\pi}(kT)^{3/2}} e^{-(E-E_c)/kT}
 \end{aligned}$$

(b) A plot of the normalized electron distribution versus energy for three different temperatures and the MATLAB program script yielding the plot are given below. From the plot one observes that the peak energy, which occurs at  $kT/2$ , moves to progressively higher energies with increasing  $T$ . More significantly, the distribution becomes less peaked in nature and the height of the peak decreases with increasing temperature.

MATLAB program script...

```
%Problem 2.10...Normalized Electron Distribution as a function of T
%Initialization
close
clear

%Computation and plot
k=8.617e-5;
T=[300 600 1200];
kT=k.*T;
E_Ec=linspace(0,0.4);
for i=1:3,
    dist=2*sqrt(E_Ec)/(sqrt(pi)*kT(i)^(3/2)).*exp(-E_Ec/kT(i));
    y(i,:)=dist;
end
plot(E_Ec,y); grid
axis([0,0.4,0,20])
xlabel('E-Ec (eV)'); ylabel('normalized distribution (1/eV)');
text(.005,12,'300K','Color','yellow');
text(.01,7,'600K','Color','magenta');
text(.015,3,'1200K','Color','cyan')
```



## 2.11

Substituting the Eq.(2.6b) expression for  $g_v(E)$  and the Eq.(2.7) expression for  $f(E)$  into Eq.(2.8b), one obtains

$$1 - \frac{1}{1 + e^{(E - E_F)/kT}} = \frac{1}{1 + e^{(E_F - E)/kT}}$$

and

$$p = \frac{m_p^* \sqrt{2m_p^*}}{\pi^2 \hbar^3} \int_{E_{\text{bottom}}}^{E_v} \frac{\sqrt{E_v - E} dE}{1 + e^{(E_F - E)/kT}} \quad (2.9)'$$

Now letting

$$\eta = \frac{E_v - E}{kT} \quad (2.10a)'$$

$$\eta_v = \frac{E_v - E_F}{kT} \quad (2.10b)'$$

$$E_{\text{bottom}} \rightarrow -\infty \quad (2.10c)'$$

yields

$$p = \frac{m_p^* \sqrt{2m_p^*} (kT)^{3/2}}{\pi^2 \hbar^3} \int_0^\infty \frac{\eta^{1/2} d\eta}{1 + e^{\eta - \eta_v}} \quad (2.11)'$$

Recognizing

$$F_{1/2}(\eta_v) \equiv \int_0^\infty \frac{\eta^{1/2} d\eta}{1 + e^{\eta - \eta_v}} \quad \dots \text{Fermi-Dirac integral of order } 1/2 \quad (2.12)'$$

and defining

$$N_v = 2 \left[ \frac{m_p^* kT}{2\pi \hbar^2} \right]^{3/2} \quad (2.13b)$$

one obtains

$$p = N_V \frac{2}{\sqrt{\pi}} F_{1/2}(\eta_v) \quad (2.14b)$$

If the semiconductor is nondegenerate, such that  $E_F \geq E_v + 3kT$ , then  $\eta_v \leq -3$ . Since  $\eta \geq 0$  in the Fermi-Dirac integral,  $\exp(\eta - \eta_v) \geq \exp(3)$  for all  $\eta$ . Thus one obtains

$$F_{1/2}(\eta_v) \approx \int_0^\infty \eta^{1/2} e^{-(\eta - \eta_v)} d\eta = \frac{\sqrt{\pi}}{2} e^{(E_v - E_F)/kT}$$

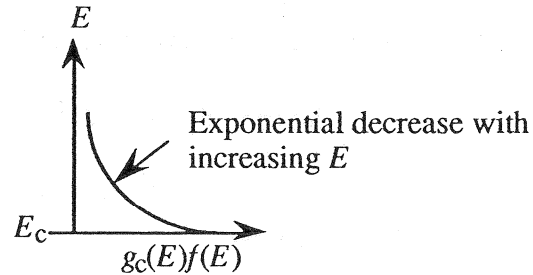
Substituting this approximate relationship into Eq.(2.14b) finally yields

$$p = N_V e^{(E_v - E_F)/kT} \quad (2.16b)$$

## 2.12

(a) electron distribution  $= g_c(E)f(E) \approx (N_C/kT) e^{-(E-E_F)/kT}$

where use has been made of the fact that the semiconductor is nondegenerate ( $E_F < E_c - 3kT$ ). Thus



(b) Following the procedure outlined in Subsection 2.5.1 of the text, if

$$g_c(E) = N_C/kT \quad \dots E \geq E_c$$

then

$$n = \int_{E_c}^{E_{top}} g_c(E)f(E)dE = \frac{N_C}{kT} \int_{E_c}^{E_{top}} \frac{dE}{1 + e^{(E-E_F)/kT}}$$

Let

$$\eta = \frac{E - E_c}{kT}; \quad \eta_c = \frac{E_F - E_c}{kT}; \quad E_{top} \rightarrow \infty$$

This yields

$$n = N_C \int_0^{\infty} \frac{d\eta}{1 + e^{\eta - \eta_c}}$$

The integral here can be performed in closed-form.

$$n = N_C [\eta - \ln(1+e^{\eta - \eta_c})]_0^{\infty} = N_C [\eta_c + \ln(1+e^{-\eta_c})]$$

The relationship analogous to Eqs.(2.14a) is therefore

$$n = N_C [\eta_c + \ln(1+e^{-\eta_c})]$$

If the semiconductor is nondegenerate,  $\eta_c \leq -3$ . Thus

$$\ln(1+e^{-\eta_c}) = \ln[e^{-\eta_c}(1+e^{\eta_c})] = -\eta_c + \ln(1+e^{\eta_c})$$

$$\equiv -\eta_c + e^{\eta_c} \quad \text{...since } \exp(\eta_c) \ll 1 \text{ and } \ln(1+x) \approx x \text{ if } x \ll 1.$$

We therefore conclude

$$n = N_C e^{\eta_c} = N_C e^{(E_F - E_c)/kT}$$

The above holds for a nondegenerate semiconductor and is the desired relationship analogous to Eq.(2.16a). Actually, the relationship has turned out to be identical to Eq.(2.16a).

### 2.13

(a) Rewriting Eqs.(2.13), one obtains

$$N_C = N_0 \left( \frac{m_n^*}{m_0} \right)^{3/2}$$

$$N_V = N_0 \left( \frac{m_p^*}{m_0} \right)^{3/2}$$

where

$$N_0 \equiv 2 \left[ \frac{m_0 kT}{2\pi\hbar^2} \right]^{3/2}$$

Using the numbers cited in the problem statement, the  $k$ -value given on the inside back cover, and remembering to convert from eV to joules, one calculates

$$\begin{aligned} N_0 &= 2 \left[ \frac{2\pi (9.109 \times 10^{-31})(8.617 \times 10^{-5})(300)(1.602 \times 10^{-19})}{(6.625 \times 10^{-34})^2} \right]^{3/2} \\ &= 2.510 \times 10^{25}/\text{m}^3 = 2.510 \times 10^{19}/\text{cm}^3 \end{aligned}$$

and therefore

$$N_{C,V} = (2.510 \times 10^{19}/\text{cm}^3) (m^*/m_0)^{3/2}$$

(b)	Semiconductor	<u><math>N_C (\text{cm}^{-3})</math></u>	<u><math>N_V (\text{cm}^{-3})</math></u>
	Si	$3.22 \times 10^{19}$	$1.83 \times 10^{19}$
	Ge	$1.02 \times 10^{19}$	$5.42 \times 10^{18}$
	GaAs	$4.26 \times 10^{17}$	$9.41 \times 10^{18}$

## 2.14

(a) Referring to Fig. 2.20, one concludes:

- (i)  $n_i(\text{Si}) = n_i(\text{Ge}, 300\text{K})$  at  $T \cong 430\text{K}$ .
- (ii)  $n_i(\text{GaAs}) = n_i(\text{Ge}, 300\text{K})$  at  $T \cong 600\text{K}$ .

(b) With the differences in the effective masses neglected,

$$\frac{n_{iA}}{n_{iB}} = \frac{e^{-E_{GA}/2kT}}{e^{-E_{GB}/2kT}} = e^{(E_{GB}-E_{GA})/2kT} = e^{1/0.0518} = 2.42 \times 10^8$$

## 2.15

The MATLAB program script implementing the requested  $n_i(\text{Ge})$  vs.  $T$  computation is reproduced below along with sample numerical results. As must be the case since the same computational equation was used in both cases, the numerical results are found to be consistent with the values displayed in Fig. 2.20.

MATLAB program script...

```
%Problem 2.15...ni versus T for Ge
%Initialization
close; clear
%Computation
k=8.617e-5;
T=[225:25:475];
ni=(1.76e16).*(T.^1.5).*exp(-0.392./ (k.*T));
%Display result on screen
j=length(T);
fprintf('\n\nT(K)          ni(Ge)\n');
for ii=1:j,
fprintf('%-10.f%-10.3e\n',T(ii),ni(ii));
end
```

<u>T(K)</u>	<u>ni(Ge)</u>
225	9.841e+10
250	8.705e+11
275	5.251e+12
300	2.375e+13
325	8.597e+13
350	2.611e+14
375	6.888e+14
400	1.620e+15
425	3.463e+15
450	6.838e+15
475	1.263e+16

## 2.16

(a) As  $T \rightarrow 0$ ,  $n \rightarrow 0$  and  $p \rightarrow 0$ . (See the discussion in Subsection 2.5.7.)

(b) Since  $N \gg n_i$ , one would have

$$n = N_D \text{ and } p = n_i^2/N_D \quad \dots \text{if a donor}$$

$$p = N_A \text{ and } n = n_i^2/N_A \quad \dots \text{if an acceptor}$$

We are told  $n = N$  and  $p = n_i^2/N$ . Clearly the impurity is a **donor**.

(c) Here we are given the minority carrier concentration,  $n = 10^5/\text{cm}^3$ . As long as the Si is nondegenerate, one can always write

$$np = n_i^2$$

Thus

$$p = n_i^2/n = \frac{(10^{10})^2}{10^5} = 10^{15}/\text{cm}^3$$

Note: From previous problems we recognize that the above carrier concentrations do indeed correspond to a nondegenerate semiconductor.

(d) Given  $E_F - E_i = 0.259\text{eV}$  and  $T = 300\text{K}$ ,

$$n = n_i e^{(E_F - E_i)/kT} = (10^{10}) e^{0.259/0.0259} = 2.20 \times 10^{14}/\text{cm}^3$$

$$p = n_i e^{(E_i - E_F)/kT} = (10^{10}) e^{-0.259/0.0259} = 4.54 \times 10^5/\text{cm}^3$$

(e) Employing the  $np$  product relationship,

$$np = n^2/2 = n_i^2$$

$$n = \sqrt{2}n_i = 1.414 \times 10^{13}/\text{cm}^3$$

Next employing the charge neutrality relationship,

$$p - n + N_D - N_A = n/2 - n + N_D = 0$$

$$N_D = n/2 = n_i/\sqrt{2} = 0.707 \times 10^{13}/\text{cm}^3$$

### 2.17

(a) At room temperature in Si,  $n_i = 10^{10}/\text{cm}^3$ . Thus here  $N_D \gg N_A$ ,  $N_D \gg n_i$  and

$$n = N_D = 10^{15}/\text{cm}^3$$

$$p = n_i^2/N_D = 10^5/\text{cm}^3$$

(b) Since  $N_A \gg N_D$  and  $N_A \gg n_i$ ,

$$p = N_A = 10^{16}/\text{cm}^3$$

$$n = n_i^2/N_A = 10^4/\text{cm}^3$$

(c) Here we must retain both  $N_A$  and  $N_D$ , but  $N_D - N_A \gg n_i$ .

$$n = N_D - N_A = 10^{15}/\text{cm}^3$$

$$p = n_i^2/(N_D - N_A) = 10^5/\text{cm}^3$$

(d) We deduce from Fig. 2.20 that, at 450K,  $n_i(\text{Si}) \approx 5 \times 10^{13}/\text{cm}^3$ . Clearly,  $n_i$  is comparable to  $N_D$  and we must use Eq.(2.29a).

$$n = \frac{N_D}{2} + \left[ \left( \frac{N_D}{2} \right)^2 + n_i^2 \right]^{1/2} = 1.21 \times 10^{14}/\text{cm}^3$$

$$p = \frac{n_i^2}{n} = \frac{(5 \times 10^{13})^2}{1.21 \times 10^{14}} = 2.07 \times 10^{13}/\text{cm}^3$$

(e) We conclude from Fig. 2.20 that, at 650K,  $n_i \approx 10^{16}/\text{cm}^3$ . Here  $n_i \gg N_D$ . Thus

$$n = n_i \approx 10^{16}/\text{cm}^3$$

$$p = n_i \approx 10^{16}/\text{cm}^3$$

## 2.18

(i) As established in the text [Eq.(2.36)],

$$E_i = \frac{E_c + E_v}{2} + \frac{3}{4} kT \ln(m_p^*/m_n^*)$$

Taking  $m_p^*/m_n^*$  to be temperature independent and employing the values listed in Table 2.1, one concludes

<u>part</u>	<u>T(K)</u>	<u>kT (eV)</u>	<u><math>E_i</math> displacement from midgap (eV)</u>
(a-c)	300	0.0259	-0.0073
(d)	450	0.0388	-0.0109
(e)	650	0.0560	-0.0158

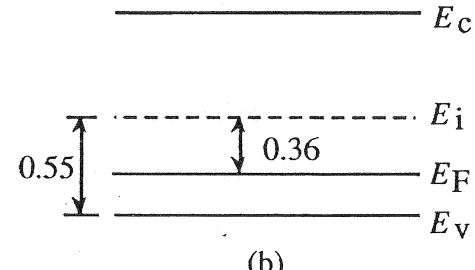
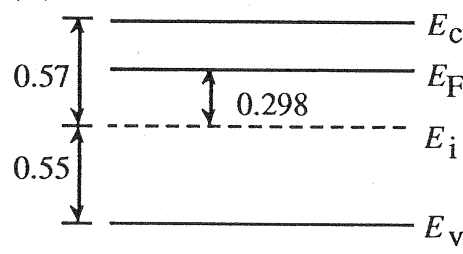
Alternatively, the  $m_p^*/m_0$  and  $m_n^*/m_0$  versus  $T$  fit-relationships cited in Exercise 2.4 may be used to compute the  $m_p^*/m_n^*$  ratio. One finds

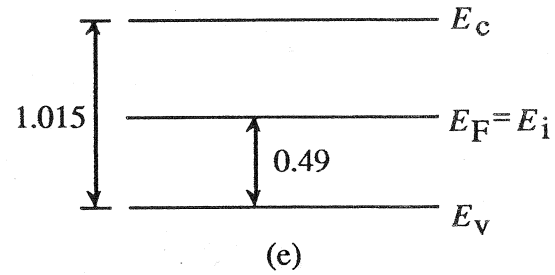
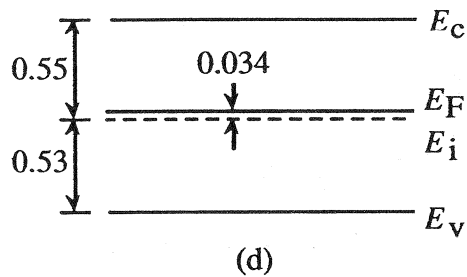
<u>part</u>	<u>T(K)</u>	<u><math>m_p^*/m_n^*</math></u>	<u>kT (eV)</u>	<u><math>E_i</math> displacement from midgap (eV)</u>
(a-c)	300	0.680	0.0259	-0.0075
(d)	450	0.703	0.0388	-0.0103
(e)	650	0.719	0.0560	-0.0139

(ii)  $E_F - E_i$  is computed using the appropriate version of Eq.(2.37) or (2.38).

- (a)  $E_F - E_i = kT \ln(N_D/n_i) = 0.0259 \ln(10^{15}/10^{10}) = 0.298 \text{ eV}$
- (b)  $E_i - E_F = kT \ln(N_A/n_i) = 0.0259 \ln(10^{16}/10^{10}) = 0.358 \text{ eV}$
- (c)  $E_F - E_i = kT \ln[(N_D-N_A)/n_i] = 0.0259 \ln(10^{15}/10^{10}) = 0.298 \text{ eV}$
- (d)  $E_F - E_i = kT \ln(n/n_i) = 0.0388 \ln(1.21 \times 10^{14}/5 \times 10^{13}) = 0.034 \text{ eV}$
- (e)  $E_F - E_i = kT \ln(n/n_i) \approx 0 \quad \dots (n \approx n_i)$

(iii)





### 2.19

(a) A sample MATLAB program that computes  $n$ ,  $p$ , and  $E_F-E_i$  given  $T$ ,  $N_D$ , and  $N_A$  is listed below. The program incorporates the  $n_i(T)$  computation given in the solution to Exercise 2.4a.

MATLAB program script...

```
%Calculation of n,p and EF-Ei (nondegenerate, fully ionized)
%Initialization
clear; close
%Specification of basic parameters
T=input('Please input the temperature, T, in Kelvin...T=');
NA=input('Please input NA(cm-3)...NA=');
ND=input('Please input ND(cm-3)...ND=');
k=8.617e-5;
Nnet=ND-NA;
%ni computation (from Exercise 2.4a solution)
%Constants and T-range
A=2.510e19;
Eex=0.0074; %Value was adjust to match S&G ni(300K) value
%
%Band Gap vs. T
EG0=1.17;
a=4.730e-4;
b=636;
EG=EG0-a.* (T.^2)./(T+b);
%
%Effective mass ratio (mnr=mn*/m0, mpr=mp*/m0)
mnr=1.028 + (6.11e-4).*T - (3.09e-7).*T.^2;
mpr=0.610 + (7.83e-4).*T - (4.46e-7).*T.^2;
%
%Actual ni calculation
ni=A.*((T./300).^1.5).*((mnr.*mpr).^(0.75)).*exp(-(EG-Eex)./(2.*k.*T));
```

```

%Computation of n, p, and EF-Ei
if Nnet==0,
    n=ni;
    p=ni;
    EFi=0;
elseif Nnet>0,
    n=Nnet/2+sqrt((Nnet/2)^2+ni^2);
    p=ni^2/n;
    EFi=k*T*log(n/ni);
else
    p=-Nnet/2+sqrt((Nnet/2)^2+ni^2);
    n=ni^2/p;
    EFi=-k*T*log(p/ni);
end
%Printout of results
format compact;
n
p
EFi

```

(b) Results obtained employing the part (a) program are tabulated below. The Problem 2.17/2.18 part (d) and (e) results are slightly different because of inaccuracies in reading the elevated temperature values of  $n_i$  from Fig. 2.20.

Part	$T$ (K)	$N_A$ (cm $^{-3}$ )	$N_D$ (cm $^{-3}$ )	$n_i$ (cm $^{-3}$ )	$n$ (cm $^{-3}$ )	$p$ (cm $^{-3}$ )	$E_F-E_i$ (eV)
(a)	300	0	$10^{15}$	$1.00 \times 10^{10}$	$1.00 \times 10^{15}$	$1.00 \times 10^5$	0.298
(b)	300	$10^{16}$	0	$1.00 \times 10^{10}$	$1.00 \times 10^4$	$1.00 \times 10^{16}$	-0.357
(c)	300	$9 \times 10^{15}$	$10^{16}$	$1.00 \times 10^{10}$	$1.00 \times 10^{15}$	$1.00 \times 10^5$	0.298
(d)	450	0	$10^{14}$	$4.71 \times 10^{13}$	$1.19 \times 10^{14}$	$1.87 \times 10^{13}$	0.0359
(e)	650	0	$10^{14}$	$1.146 \times 10^{16}$	$1.151 \times 10^{16}$	$1.141 \times 10^{16}$	$2.44 \times 10^{-4}$

## 2.20

There is more than one way to work this problem, with alternative approaches likely to yield slightly different answers. The most straightforward approach is recorded here.

At the onset of degeneracy

$$E_F = E_C - 3kT \quad \dots n\text{-type semiconductor}$$

$$E_F = E_V + 3kT \quad \dots p\text{-type semiconductor}$$

and the maximum nondegenerate carrier concentrations are therefore

$$n = N_C e^{(E_F - E_c)/kT} = N_C e^{-3}$$

$$p = N_V e^{(E_v - E_F)/kT} = N_V e^{-3}$$

However

$$n \equiv N_D \quad \dots n\text{-type Si at room T}$$

$$p \equiv N_A \quad \dots p\text{-type Si at room T}$$

Thus

$$N_{D\max} = N_C e^{-3} = (3.22 \times 10^{19}) e^{-3} = 1.60 \times 10^{18}/\text{cm}^3$$

$$N_{A\max} = N_V e^{-3} = (1.83 \times 10^{19}) e^{-3} = 9.11 \times 10^{17}/\text{cm}^3$$

$N_C$  and  $N_V$  were computed using the expression  $N_{C,V} = (2.51 \times 10^{19}/\text{cm}^3)(m_{n,p}^*/m_0)^{3/2}$  and the effective mass values in Table 2.1. The cited computational relationship is given in the text below Eq.(2.14b). Also see Problem 2.13.

## 2.21

The MATLAB program listed below computes  $E_F - E_i$  vs.  $N_A$  or  $N_D$  up to the nondegenerate limit ( $N_A$  or  $N_D \leq 10^{18}/\text{cm}^3$ ) and yields results very similar to Fig. 2.21.

MATLAB program script...

```
%EF-Ei versus NA or ND (nondegenerate, fully ionized, 300K)
clear; close
%Specification of basic parameters
kT=0.0259;
ni=1.0e10;
NB=logspace(13,18); %NB=ND or NA
%Computation of EF-Ei versus doping
EFiD=kT.*log(NB./ni);
EFiA=-EFiD;

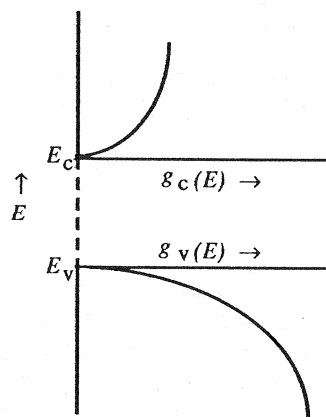
%Plot out Fermi level positioning
semilogx(NB, EFiD, NB, EFiA);
axis([1.0e13,1.0e18,-0.56 0.56]);
grid; xlabel('ND or NA'); ylabel('EF-Ei');
text(1.0e14,0.30,'Donor'); text(1.0e14,-0.30,'Acceptor');
```

## 2.22

(a) Because  $m_n^* \ll m_p^*$  in GaAs, the density of states in the conduction band is considerably smaller than the density of states in the valence band at a given energy displacement from the respective band edges. To be precise, using the effective mass values from Table 2.1,

$$\frac{g_c(E_c + \Delta E)}{g_v(E_v - \Delta E)} = \left( \frac{m_n^*}{m_p^*} \right)^{3/2} = \left( \frac{0.066}{0.52} \right)^{3/2} = 0.045$$

The required sketch is shown below.



(b)  $E_i$  will lie **ABOVE** midgap. Because the density of states is smaller in the conduction band, the Fermi level must be displaced from the middle of the band gap toward the conduction band edge to achieve an equal number of filled states in the two bands.

(c) Employing  $kT = 0.0259$  eV and the effective mass values from Table 2.1, we find

$$E_i = \frac{E_c + E_v}{2} + \frac{3}{4} kT \ln(m_p^*/m_n^*) \quad \dots \text{Eq.(2.36)}$$

$$= \frac{E_c + E_v}{2} + \frac{3}{4} (0.0259) \ln(0.52/0.066)$$

or

$$E_i = \frac{E_c + E_v}{2} + 0.040 \text{ eV}$$

$E_i$  lies **approximately 0.04 eV above midgap** in GaAs at room temperature. (Note that the displacement from midgap is considerably larger for GaAs compared to Si. However, the room temperature displacement of 0.04 eV is still only  $0.04/1.42 = 2.8\%$  of the total band gap.)

(d) Using the results of Problems 2.13 and 2.20, we know

$$N_C = 4.26 \times 10^{17}/\text{cm}^3$$

...GaAs

$$N_V = 9.41 \times 10^{18}/\text{cm}^3$$

at 300K

and

$$N_{Dlmax} = N_C e^{-3} = (4.26 \times 10^{17}) e^{-3} = 2.12 \times 10^{16}/\text{cm}^3$$

$$N_{Almax} = N_V e^{-3} = (9.41 \times 10^{18}) e^{-3} = 4.68 \times 10^{17}/\text{cm}^3$$

Please note that *n-type GaAs becomes degenerate at relatively low donor dopings*. This fact is very important in the modeling of certain GaAs devices; constructive use is made of this fact in other GaAs devices.

### 2.23

(a) At temperatures  $T \rightarrow 0$  K there are essentially no filled levels above  $E_F$  and all levels below  $E_F$  are filled. (The foregoing was pointed out in the Fermi function discussion.) Moreover, as  $T \rightarrow 0$  K, freeze-out occurs and  $p \rightarrow 0$ ; all the acceptors are emptied of electrons. Now,  $E_F$  can't be below  $E_V$  because that would mean  $p \neq 0$ . Likewise,  $E_F$  can't be above  $E_A$  because that would mean all of the acceptor are filled with electrons. We therefore conclude  $E_V < E_F < E_A$ ; the Fermi level as  $T \rightarrow 0$  K lies somewhere between  $E_V$  and  $E_A$ .

(b) The  $E_F - E_i$  vs.  $T$  program and plot result are displayed below. Please note:

(i)  $n_i$  was computed using the simple experimental-fit relationship quoted in part (b) of Exercise 2.4. (The  $T$ -range of the computation here is beyond the quoted  $T$ -range of the relationship but the error introduced is small.)

(ii) Eq. (2.29b) was used to compute  $p$  because  $n_i$  is comparable to  $N_A$  at the upper end of the temperature range.

(iii) The approximate positioning of  $E_C$  and  $E_V$  vs.  $T$  were added to the plot assuming  $E_C - E_i = E_G/2$  and  $E_i - E_V = E_G/2$ .  $E_G$  vs.  $T$  was computed employing the relationship from Problem 2.1.

MATLAB program script...

```
%EF-Ei versus T (nondegenerate, fully ionized)
clear; close

%Specification of basic parameters
NA=1.0e14;
T=[200:5:500];
k=8.617e-5;
```

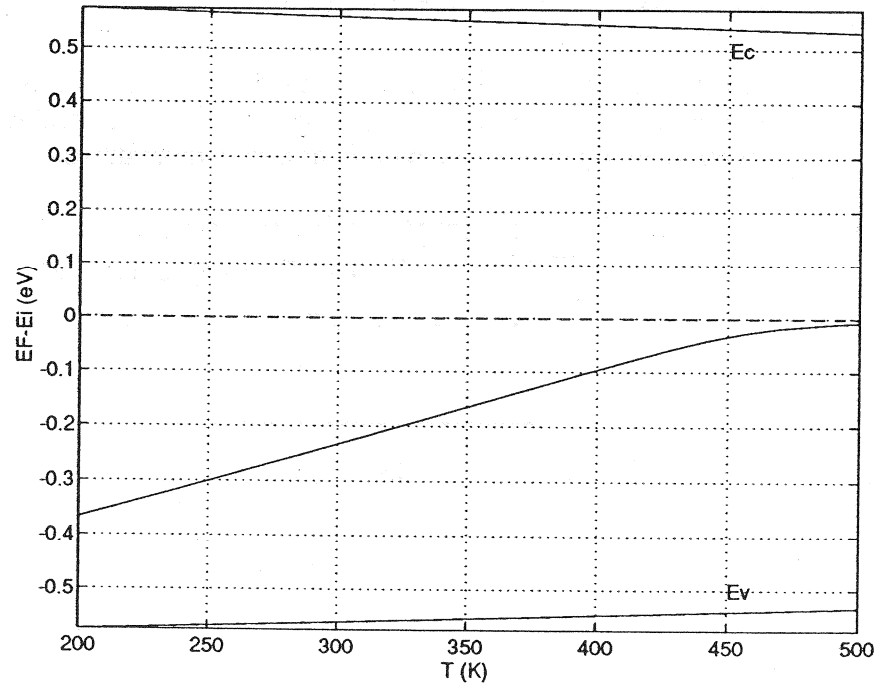
```

ni=(3.10e16).* (T.^1.5).*exp(-0.603./(k.*T));
EG=1.205-(2.8e-4).*T;
Ei=0.0.*T;
plot(T,EG,'b--');

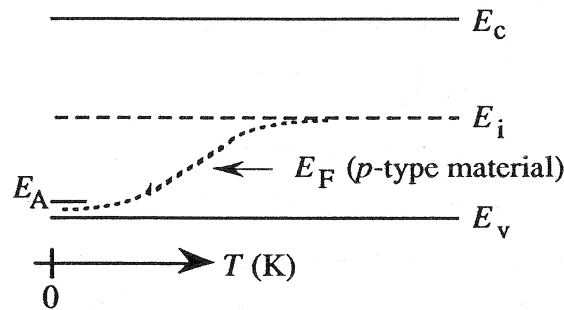
%Computation of EF-Ei versus T
p=NA./2+sqrt((NA./2).^2+ni.^2);
EFI=-k*T.*log(p./ni);

%Plot out Fermi level positioning
plot(T,EFI)
axis([200,500,-EG(1)/2,EG(1)/2])
hold on
plot(T,EG/2,'w-',T,-EG/2,'w-',T,Ei,'w--')
grid; xlabel('T (K)'); ylabel('EF-Ei (eV)')
text(450,0.5,'Ec'); text(450,-0.5,'Ev')
hold off

```

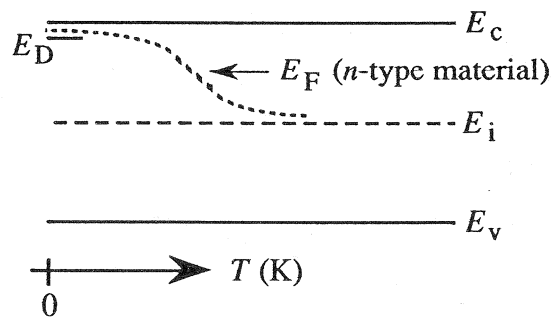


(c) Combining the results of parts (a) and (b), we see that for a p-type material,  $E_F$  starts out near  $E_V$  at  $T \approx 0$  K. For increasing  $T$ ,  $E_F$  moves closer and closer to  $E_i$ , eventually merging with  $E_i$  at high temperatures.



(d) As  $N_A$  is increased the Fermi level moves closer to  $E_V$  at all temperatures.

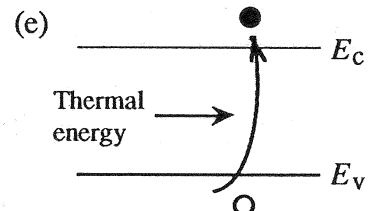
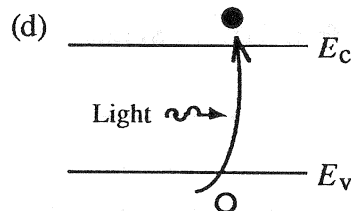
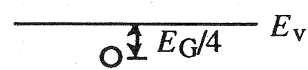
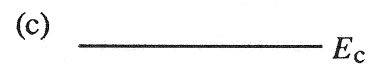
(e) By analogy, in a donor doped material,  $E_F$  will lie between  $E_D$  and  $E_c$  as  $T \rightarrow 0$  K. For increasing  $T$ ,  $E_F$  will move down from near the conduction band toward  $E_i$ . Eventually,  $E_F$  will merge with  $E_i$  at high temperatures.



## CHAPTER 3

### 3.1

(a) See Fig. 3.10(a).



(f) See Fig. 3.15(a).

(g) See Fig. 3.15(b).

(h) See Fig. 3.15(e)

### 3.2

(a) Given:  $v_d = 10^3 \text{ cm/sec}$

$$\mathcal{E} = \Delta V/L = 2 \text{ V/cm}$$

$$\mu_p = v_d/\mathcal{E} = 500 \text{ cm}^2/\text{V}\cdot\text{sec}$$

(b) (i) Lattice scattering

(ii) Ionized impurity scattering

(See the *Relationship to Scattering* discussion in Subsection 3.1.3.)

(c)  $\mu_{\text{intrinsic}}$  is higher than  $\mu_{\text{heavily doped}}$

Reason: In intrinsic material the scattering is due exclusively to lattice scattering. In heavily doped materials, ionized impurity scattering is also important. The more scattering there is, the lower the mobility.

(d) Given  $N_{D1}$  and  $N_{A2} \gg n_i$ , we know from Eqs. (3.8) that

$$\rho = \frac{1}{q\mu_n N_{D1}} \quad \dots \text{n-type wafer 1}; \quad \rho = \frac{1}{q\mu_p N_{A2}} \quad \dots \text{p-type wafer 2}$$

In most semiconductors including GaAs,  $\mu_n$  is greater than  $\mu_p$  for a given doping and system temperature. Since we are given  $N_{D1} = N_{A2}$ , taking the wafer temperatures to be the same, and with  $\mu_n > \mu_p$ , we conclude from the above equations that  $\rho(\text{wafer 2}) > \rho(\text{wafer 1})$ . Note that the conclusion here is consistent with Fig. 3.8(b).

(e)  $D_N = (kT/q)\mu_n = (0.0259)(1300) = 33.7 \text{ cm}^2/\text{sec}$

(f)  $\Delta p \ll n_0, \quad n \approx n_0 \quad \dots \text{if n-type}$

$$\Delta n \ll p_0, \quad p \approx p_0 \quad \dots \text{if p-type}$$

(g) R-G center

(h) Increase. Per Eq. (3.33a),  $\tau_p = 1/c_p N_T$ . Since  $N_T$  decreased after processing,  $\tau_p$  increased.

### 3.3

The MATLAB program script required to complete part (b) of Exercise 3.1 is listed below. Except for labeling and elimination of the  $10^{15}/\text{cm}^3$  curves which lie almost on top of the  $10^{14}/\text{cm}^3$  curves, the output is identical to the solid line portions of Fig. 3.7. (A slightly modified version of the program was in fact used to produce Fig. 3.7.)

MATLAB program script ...

```
%Mobility versus Temperature (Si)
%Initialization
clear; close
T=logspace(log10(200),log10(500));
s=menu('Choose the carrier type','Electrons','Holes');
%Fit Parameters
NDref=1.3e17; NAref=2.35e17;
μnmin=92; μpmin=54.3;
μn0=1268; μp0=406.9;
an=0.91; ap=0.88;
TNref=2.4; Tμmin=-0.57;
Tμn0=-2.33; Tμp0=-2.23;
Ta=-0.146;
%Mobility Calculation
for i=14:18,
    N=10.^i;
    if s==1,
        %Electrons
        NDrefT=NDref*(T./300).^TNref;
        μnminT=μnmin.* (T./300).^Tμmin;
        μn0T=μn0.* (T./300).^Tμn0;
        anT=an.* (T./300).^Ta;
        μn=μnminT+μn0T./(1+(N./NDrefT).^anT);
        y=μn;
    else
        %Holes
        NArefT=NAref*(T./300).^TNref;
        μpminT=μpmin.* (T./300).^Tμmin;
        μp0T=μp0.* (T./300).^Tμp0;
        apT=ap.* (T./300).^Ta;
        μp=μpminT+μp0T./(1+(N./NArefT).^apT);
        y=μp;
    end
    %Plotting results
    if i==14,
```

```

if s==1,
    %Electrons
    loglog(T,y); grid;
    axis([1e2,1e3,1e2,1e4]);
    xlabel('T (K)');
    ylabel('Electron mobility (cm2/V-sec)');
    text(220,3300,'ND=1.0e14');
    text(220,230,'ND=1.0e18');
    text(600,6500,'SILICON');
else
    %Holes
    loglog(T,y); grid;
    axis([1e2,1e3,1e2,1e4]);
    xlabel('T (K)');
    ylabel('Hole mobility (cm2/V-sec)');
    text(205,1150,'NA=1.0e14');
    text(205,125,'NA=1.0e18');
    text(600,6500,'SILICON');
end
elseif i>=15,
    hold on
    loglog(T,y);
else
end
end

```

### 3.4

(a) (Optional reading assignment.)

(b) MATLAB program script ...

```

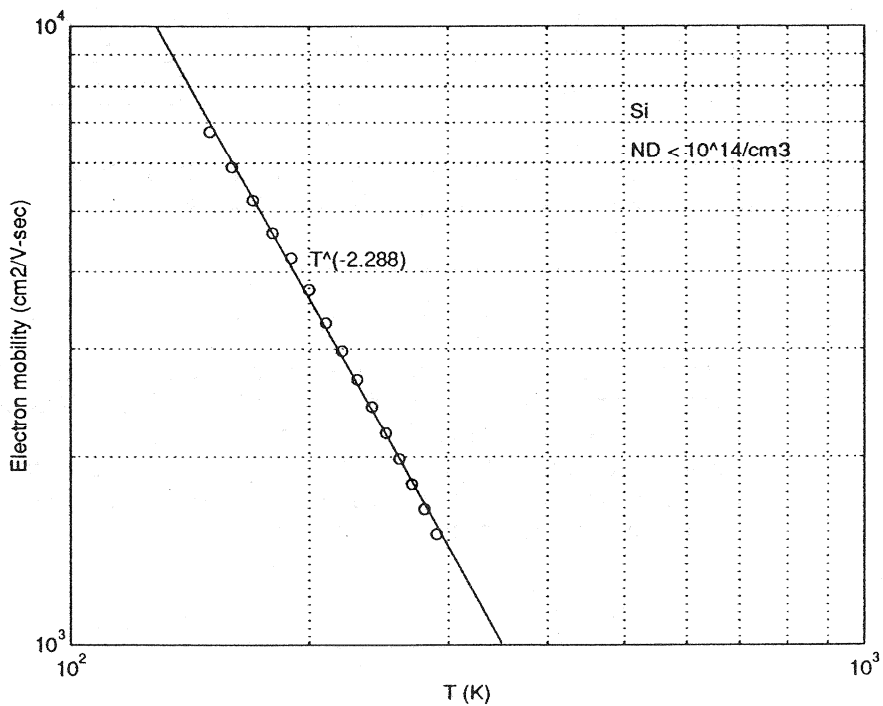
%Mobility vs. T(K) Data
%Determining the power-dependence exponent
clear; close
%Input data and take log of data
T=150:10:290;
μn=[6757 5910 5216 4619 4209 3743 3306 2978 2675 2415 2185 ...
    1985 1805 1646 1501];
x=log(T);
y=log(μn);
%Perform least-squares fit to data
c=polyfit(x,y,1);
a=c(2);
b=-c(1);

```

```

Tfit=120:10:350;
yfit=exp(a).*Tfit.^(-b);
%Plot data, draw fit line, note fit value
loglog(T,μn,'o',Tfit,yfit); grid
axis([1e2,1e3,1e3,1e4]);
xlabel('T (K)'); ylabel('Electron mobility (cm2/V-sec)');
text(200,4200,['T(-1,num2str(b),')']);
text(510,6300,'ND < 1014/cm3');
text(510,7300,'Si');

```



- (c) The agreement between experiment and the text plot is impressive. The experimentally determined  $b$  fit value is almost identical to the  $b$ -value noted on the text plot, 2.29 versus 2.3. The magnitude of the measured mobility is also in close agreement with the Fig. 3.7(a) plot. A lowly-doped sample was employed, of course, so that lattice scattering would dominate and a power-law dependence would be observed.

### 3.5

(a) In an intrinsic semiconductor  $n = p = n_i$  and

$$\rho = \frac{1}{q(\mu_n + \mu_p)n_i}$$

The  $\rho_{\text{intrinsic}}$  values recorded in the following table were computed using the maximum mobility values deduced from Fig. 3.5 and the  $n_i$  values read from Fig. 2.20 or the tables adjacent to Fig. 2.20.

Semi	$\mu_n$ (cm <sup>2</sup> /V-sec)	$\mu_p$ (cm <sup>2</sup> /V-sec)	$n_i$ (cm <sup>-3</sup> )	$\rho_{\text{intrinsic}}$ ( $\Omega\cdot\text{cm}$ )	$\rho_{\text{max}}$ ( $\Omega\cdot\text{cm}$ )
Ge	~4000	~1900	$2.5 \times 10^{13}$	42.4	45.3
Si	1358	461	$10^{10}$	$3.44 \times 10^5$	$3.95 \times 10^5$
GaAs	~8000	~400	$2.25 \times 10^6$	$3.31 \times 10^8$	$7.76 \times 10^8$

(b) If the  $np$  product relationship is used to eliminate  $p$  in terms of  $n$  in the general resistivity relationship (Eq. 3.7), one obtains

$$\rho = \frac{1}{q(\mu_n n + \mu_p n_i^2/n)}$$

Following the standard procedure for determining the maximum of a function, we can find the maximum resistivity by differentiating  $\rho$  with respect to  $n$  and setting the result equal to zero. In performing the differentiation, we assume  $d\mu_n/dn = 0$  and  $d\mu_p/dn = 0$ . This is reasonable since the maximum resistivity is expected to occur at very low carrier concentrations (low dopings) where the mobilities are essentially doping (and therefore  $n$ ) independent. Proceeding as described,

$$\frac{d\rho}{dn} = -\frac{1}{q(\mu_n n + \mu_p n_i^2/n)^2} (\mu_n - \mu_p n_i^2/n^2) = 0$$

and at the resistivity maximum  $\mu_n = \mu_p n_i^2/n^2$ , or

$$n = \sqrt{\mu_p/\mu_n} n_i$$

Substituting the  $n$  value at the maximum back into the general resistivity expression then yields,

$$\rho_{\text{max}} = \frac{1}{q(\sqrt{\mu_n \mu_p} n_i + \sqrt{\mu_n \mu_p} n_i)} = \frac{1}{2q\sqrt{\mu_n \mu_p} n_i}$$

The  $\rho_{\text{max}}$  values computed from the foregoing expression are recorded in the part (a) table.

3.6

$$(a) \quad \rho = \frac{1}{q\mu_n N_D} \quad \dots \text{Eq.(3.8a)}$$

$$= \frac{1}{(1.6 \times 10^{-19})(1248)(10^{16})} = 0.501 \text{ ohm-cm} \quad \dots \mu_n \text{ from Fig. 3.5(a)}$$

$$\rho \approx 0.5 \text{ ohm-cm} \quad \dots \text{by inspection from Fig. 3.8(a)}$$

(b) Since  $N_A = N_D$ ,  $n = p = n_i = 10^{10}/\text{cm}^3$ . Moreover, the total number of scattering centers is  $N_D + N_A = 2 \times 10^{16}/\text{cm}^3$ . Thus, from Fig. 3.5(a),  $\mu_n = 1165 \text{ cm}^2/\text{V-sec}$ ,  $\mu_p = 419 \text{ cm}^2/\text{V-sec}$ , and

$$\rho = \frac{1}{q(\mu_n + \mu_p)n_i} = \frac{1}{(1.6 \times 10^{-19})(1584)(10^{10})} = 3.95 \times 10^5 \text{ ohm-cm}$$

(c) Here  $n = p = n_i = 10^{10}/\text{cm}^3$ . With  $N_A = 0$  and  $N_D = 0$ , one has the maximum possible carrier mobilities. From Fig. 3.5(a),  $\mu_{n\max} = 1358 \text{ cm}^2/\text{V-sec}$  and  $\mu_{p\max} = 461 \text{ cm}^2/\text{V-sec}$ .

$$\rho = \frac{1}{q(\mu_n + \mu_p)n_i} = \frac{1}{(1.6 \times 10^{-19})(1819)(10^{10})} = 3.44 \times 10^5 \text{ ohm-cm}$$

Because of the lower mobilities in compensated material,  $\rho(\text{part b}) > \rho(\text{part c})$ .

$$(d) \quad R = \rho l/A$$

$$\rho = RA/l = (500)(10^{-2})/(1) = 5 \text{ ohm-cm}$$

Since the bar is *n*-type, we conclude from Fig. 3.8(a) that  $N_D \cong 9 \times 10^{14}/\text{cm}^3$ .

(e) For a sample where  $N_D \gg n_i$ ,  $\rho = 1/q\mu_n N_D$ . Furthermore, since the sample is lightly doped, lattice scattering will dominate and  $\mu_n$  will decrease with increasing  $T$ . Fig. 3.7a confirms the preceding observation. Thus, with  $\rho \propto 1/\mu_n$ , heating up the sample causes the resistivity to increase.

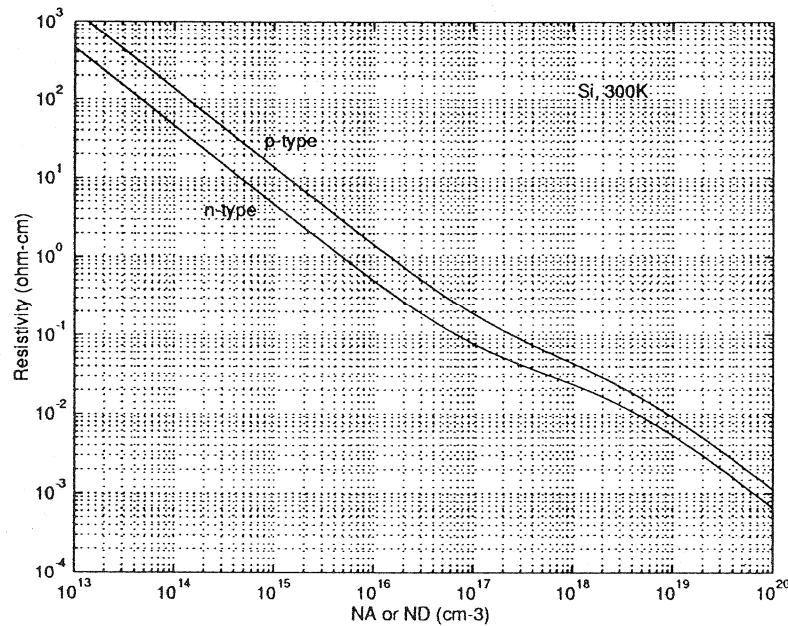
### 3.7

The problem is to produce a plot of the Si 300K resistivity versus doping. The required MATLAB program script and output plot are reproduced below. Formed employing the same computation relationships and parametric values, the MATLAB produced plot should be identical to Fig. 3.8 in the text.

MATLAB program script ...

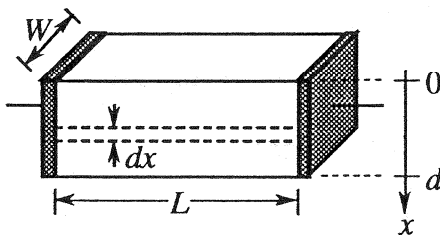
```
%Resistivity versus Dopant Concentration (Si, 300K)
%Initialization
clear; close
q=1.6e-19;
%Fit Parameters
NDref=1.3e17; NAref=2.35e17;
μnmin=92; μpmin=54.3;
μn0=1268; μp0=406.9;
an=0.91; ap=0.88;
%Resistivity Calculation
N=logspace(13,20);
μn=μnmin+μn0./(1+(N/NDref).^an);
μp=μpmin+μp0./(1+(N/NAref).^ap);
rhon=(1)./(q.*μn.*N);
rhop=(1)./(q.*μp.*N);
(continued at right)
```

```
%Plotting results
loglog(N,rhon,N,rhop); grid;
axis([1e13,1e20,1e-4,1e3]);
xlabel('NA or ND (cm-3)');
ylabel('Resistivity (ohm-cm)');
text(8.0e14,30,'p-type');
text(2.0e14,4,'n-type');
text(1.1e18,130,'Si, 300K');
```



### 3.8

(a) Consider the bar-shaped resistor pictured below. Note that the  $x$ -coordinate is oriented vertically, with  $x = 0$  positioned at the top of the bar. For a uniformly doped semiconductor bar,  $R = 1/G = \rho L/A$ , where  $R$  is the resistance,  $G$  the conductance,  $L$  the bar length, and  $A$  the bar cross-sectional area. In the given problem, however,  $N_D$  and therefore  $\rho = 1/q\mu_n N_D$  are a function of  $x$ .



Let us conceptually break the bar up into small  $dx$  sections. Within a  $dx$  section, the doping is approximately constant and the conductance of a small section ( $dG$ ) is given by

$$dG = d(1/R) = \frac{Wdx}{\rho L} = \frac{W}{L} q\mu_n N_D dx$$

The  $dx$  sections are in parallel and therefore the conductance of the sections simply add to yield the total conductance.

$$G = \sum dG = \int_0^d \frac{W}{L} q\mu_n N_D dx \quad \text{or} \quad R = 1/G = \frac{L/W}{q \int_0^d \mu_n N_D dx}$$

(b) The required  $R$  versus  $N_{D0}$  plot and MATLAB program script are reproduced below. Note that, consistent with the presented plot and given  $L = W$ ,  $R \rightarrow 1/qd\mu_n N_{DB} = 9.21 \times 10^4$  ohms if  $N_{D0} \rightarrow 0$ .

MATLAB program script ...

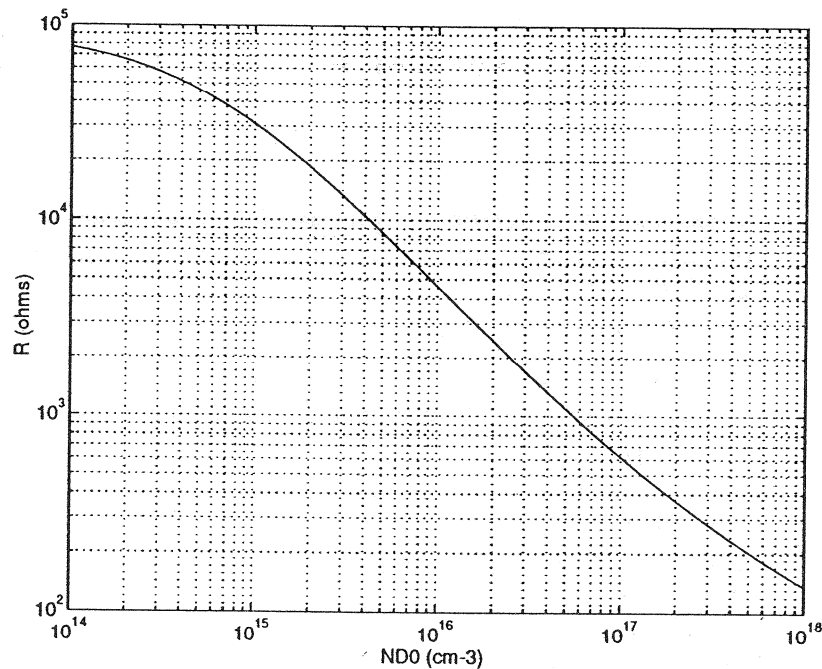
```
%IC Resistor, resistance calculation
%Rintg, a function subprogram, is a run-time requirement
%Initialization
clear; close
global ND0 i

%Constants and Resistor Parameters
q=1.6e-19;
ND0=logspace(14,18);
d=5.0e-4; %d in cm
```

```

%Resistance Calculation
% A change of variable to x'=x/d was made in
% evaluating the R integral
j=length(ND0);
for i=1:j
R(i)=(1)./(q*d.*quad8('Rintg',0,1));
end
%Plotting result
loglog(ND0,R); grid
xlabel('ND0 (cm-3)'); ylabel('R (ohms)')
-----
function [y] = Rintg(x)
global ND0 i
%ND Calculation
NDB=1.0e14;
ND=NDB+ND0(i).*exp((-5).*x); %Note that a*d=5
%Mobility Calculation
μnmin=92; μn0=1268;
NDref=1.3e17; an=0.91;
μn=μnmin+μn0./(1+(ND./NDref).^an);
%Integrand
y=μn.*ND;

```

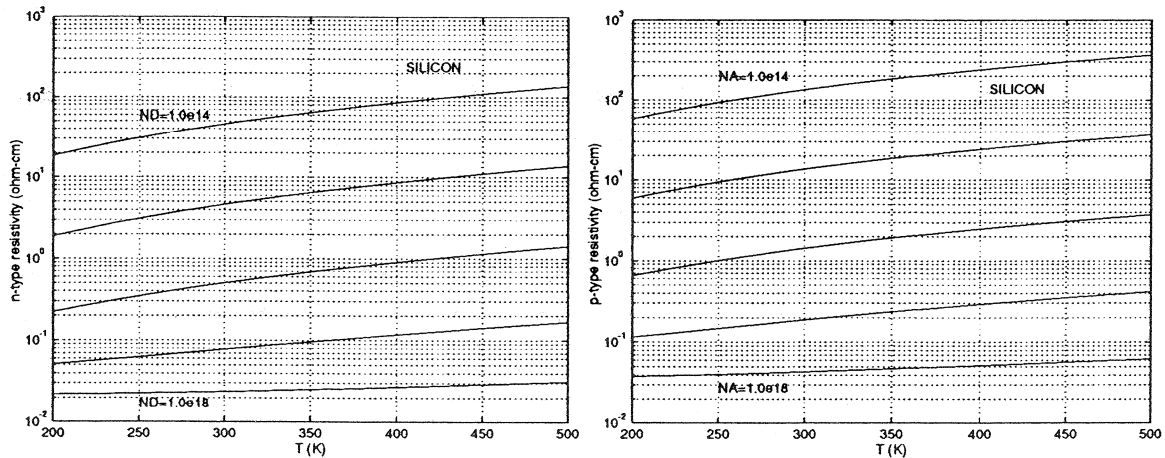


### 3.9

(a) It is a relatively simple matter to modify the Problem 3.3 program to obtain  $\rho$  versus  $T$  plots. The only required computational changes involve the  $\rho$  computation itself. This is accomplished by replacing the y-lines in the program with  $y = 1/q\mu_n N$  or  $y = 1/q\mu_p N$  as appropriate. Cosmetic changes to the comments, labels, and label positions are obviously necessary. The  $T=\logspace$  assignment is best replaced with a  $T=linspace$  assignment, the  $\loglog$  calls must be replaced by  $\text{semilogy}$  calls, and the old  $\text{axis}$  command must also be deleted or revised. The modified program yielding the  $\rho$  versus  $T$  plots reproduced below is included on the instructor's disk as program P\_03\_09.m.

At the higher temperatures  $n_i$  becomes comparable to the smaller  $N_D$  and  $N_A$  values. Specifically,  $n_i = 2.72 \times 10^{14}/\text{cm}^3$  at  $T = 500$  K. To be correct,  $\rho$  must be computed using Eq. (3.7), with the carrier concentrations calculated using Eqs. (2.29). The use of Eqs. (2.29) in turn requires that  $n_i$  be supplementally calculated as a function of  $T$ . The corrections noted here, corrections which primarily affect only the  $N_D$  and  $N_A = 10^{14}/\text{cm}^3$  curves, would require a significant modification of the original program.

(b) The agreement with the plots cited in the semiconductor literature is excellent over the entire range of mutually plotted temperatures and dopings!



### 3.10

(This is clearly an open-ended problem with several alternative solution approaches and many possible solutions. What follows is only one possible approach and solution.)

(a) The choice of sensor dimensions is totally arbitrary. A relatively small cross section would be advisable to permit a more rapid response to temperature changes. (One might consider sawing up a wafer to fabricate the sensor.) To be specific, let us assume the sensor is **bar-like**, with length  $l = 1 \text{ cm}$  and cross-sectional area  $A = 1\text{mm}\times1\text{mm} = 10^{-2}\text{cm}^2$ . Considering the resistance of the sensor, we know

$$R = \rho l/A \quad \text{or} \quad \rho = (A/l)R$$

where the resistance is restricted to

$$1 \Omega \leq R \leq 1000 \Omega$$

But we have chosen

$$A/l = 10^{-2} \text{ cm}$$

We therefore require

$$10^{-2} \Omega\text{-cm} \leq \rho \leq 10 \Omega\text{-cm}$$

at all measurement temperatures.

The doping must be chosen such the  $\rho$  falls within the cited range over the operating temperature range ( $-30^\circ\text{C} \leq T \leq 40^\circ\text{C}$ ). At room temperature and taking the Si to be *n*-type, reference to Fig. 3.8(a) indicates that we must have

$$4.5 \times 10^{14}/\text{cm}^3 \leq N_D \leq 4.5 \times 10^{18}/\text{cm}^3$$

Anticipating changes in the allowed  $N_D$  range at higher and lower temperatures, let us choose  $N_D$  in the middle of the above noted range, say  $N_D = 10^{16}/\text{cm}^3$ , and check to see if the  $\rho$  requirement is met at the temperature extremes. Referring to Fig. 3.7(a), we conclude

$$\text{at } T = -30^\circ\text{C} = 243 \text{ K}, \mu_n \sim 1800 \text{ cm}^2/\text{V}\text{-sec} \text{ and } \rho = 0.347 \Omega\text{-cm}$$

$$\text{at } T = 40^\circ\text{C} = 313 \text{ K}, \mu_n \sim 1100 \text{ cm}^2/\text{V}\text{-sec} \text{ and } \rho = 0.568 \Omega\text{-cm}$$

The computed extrema temperature values fall comfortably within the allowable  $\rho$ -range. Previously boldfaced items are then the acceptable design solution.

$$(b) \quad R = \frac{\rho l}{A} = \frac{1}{q\mu_n N_D} \frac{l}{A}$$

$$\frac{dR}{dT} = \frac{1}{qN_D} \frac{l}{A} \frac{d}{dT} \left( \frac{1}{\mu_n} \right) = - \frac{l}{A} \frac{1}{q\mu_n^2 N_D} \frac{d\mu_n}{dT}$$

For maximum sensitivity it is preferable to use the lowest possible doping. As can be deduced from Fig. 3.7(a), both  $|d\mu_n/dT|$  and  $1/q\mu_n^2 N_D$  decrease with increasing doping concentrations.

(c) Technically, the temperature sensor can be used at any temperature where

$$10^{-2} \Omega\text{-cm} \leq \rho = 1/q\mu_n N_D \leq 10 \Omega\text{-cm}$$

or

$$62.5 \text{ cm}^2/\text{V}\cdot\text{sec} \leq \mu_n \leq 6.25 \times 10^4 \text{ cm}^2/\text{V}\cdot\text{sec} \quad (N_D = 10^{16}/\text{cm}^3)$$

Inspecting Fig. 3.7(a), the temperature range of operation is at least  $200\text{K} \leq T \leq 500\text{K}$ . At temperatures approaching  $100\text{K}$  and lower, the mobility is expected to decrease with decreasing  $T$ . The sensor would still work but  $R$  would begin to increase with decreasing  $T$ . More than likely the contacts to the device would fail before the lower mobility limit is reached at very high  $T$ .

(d) Computation of the sensor  $R$  versus  $T$  were made using the  $\mu_n$  versus  $T$  fit relationship given in Exercise 3.1.

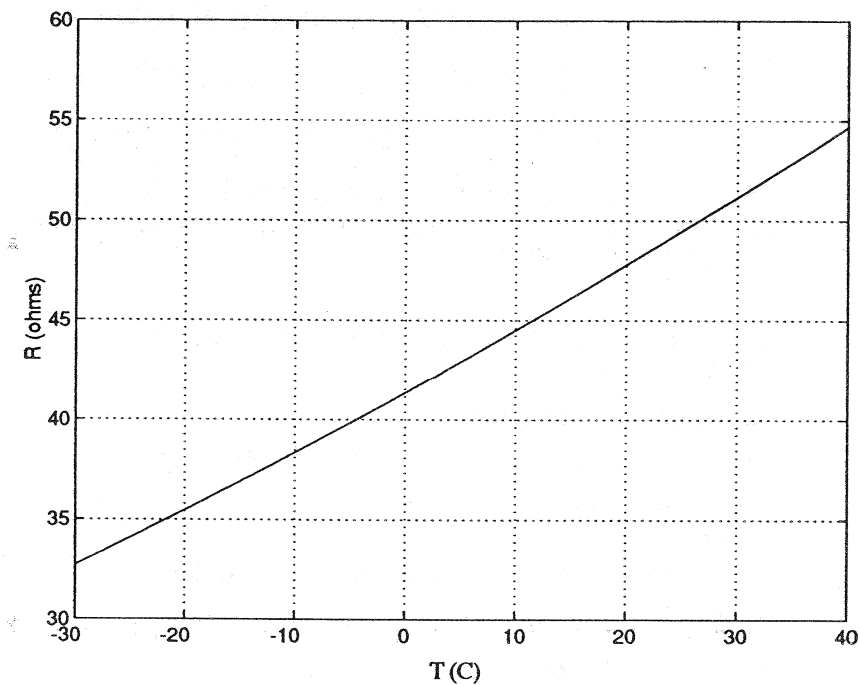
MATLAB program script ...

```
%R vs. T of Temperature Sensor (Problem 3.10d)
%Initialization
clear; close
%Constants, parameters, and independent variable
q=1.6e-19;
ND=1.0e16;
l=1; %l=length of bar-like sensor
A=0.01; %A=cross-sectional area
TC=linspace(-30,40);
T=273.18+TC;

%Electron mobility computation
%Fit Parameters
NDref=1.3e17; an=0.91;
μnmin=92; μn0=1268;
TNref=2.4; Ta=-0.146;
Tμn0=-2.33; Tμmin=-0.57;
%Computation
NDrefT=NDref*(T./300).^TNref;
μnminT=μnmin.* (T./300).^Tμmin;
μn0T=μn0.* (T./300).^Tμn0;
anT=an.* (T./300).^Ta;
μn=μnminT+μn0T./(1+(ND./NDrefT).^anT);

%R Computation
R=(l/A)./(q.*μn.*ND);
```

```
%Plot  
plot(TC,R); grid  
axis([-30,40,30,60])  
xlabel('T (C)'); ylabel('R (ohms)')
```



### 3.11

In Problems 2.7 and 2.8 it is noted that the peak in the electron distribution versus energy inside the conduction band occurs at  $E_c + kT/2$ . Moreover, as explained in Subsection 3.1.5,  $E - E_c$  is interpreted to be the kinetic energy (KE) of electrons in the conduction band. Thus

$$KE_{\text{peak}} = \frac{1}{2} m^* v_{\text{peak}}^2 = E_{\text{peak}} - E_c = kT/2$$

Setting  $m^* = m_0$ , we obtain

$$v_{\text{peak}} = \sqrt{\frac{kT}{m_0}} = \left[ \frac{(0.0259)(1.6 \times 10^{-19})}{9.11 \times 10^{-31}} \right]^{1/2} = 6.75 \times 10^4 \text{ m/sec} = 6.75 \times 10^6 \text{ cm/sec}$$

### 3.12

The brief explanation how one arrives at a given answer, an explanation applicable to all the energy band diagrams, is given immediately below. Sketches indicating the *general form* of the expected answers follow the explanations.

- (a) Yes for all cases. The semiconductor is concluded to be in equilibrium because the Fermi level has the same energy value (it is constant) as a function of position.
- (b)  $V$  vs.  $x$  has the same functional form as the "upside down" of  $E_c$  (or  $E_i$  or  $E_v$ ). The sketches that follow were constructed taking the arbitrary reference voltage to be  $V = 0$  at  $x = 0$ .
- (c)  $\mathcal{E}$  vs.  $x$  is determined by simply noting the slope of the energy bands as a function of position.
- (d) For electrons,  $PE = E_c - E_F$  and  $KE = E - E_c$ ; for holes  $PE = E_F - E_v$  and  $KE = E_v - E$ .
- (e) The general carrier concentration variation with position can be deduced by noting  $E_F - E_i$  vs.  $x$ . Under equilibrium conditions,  $n = n_i \exp[(E_F - E_i)/kT]$  and  $p = n_i \exp[(E_i - E_F)/kT]$  if the semiconductor is nondegenerate.
- (f) Since  $J_{N\text{drift}} = q\mu_n n \mathcal{E}$ , the general variation of  $J_{N\text{drift}}$  with position can be deduced by conceptually forming the product of the  $\mathcal{E}$  vs.  $x$  dependence sketched in part (c) and the  $n$  vs.  $x$  dependence sketched in part (e). Under equilibrium conditions,  $J_N = J_{N\text{drift}} + J_{N\text{diff}} = 0$ . Thus  $J_{N\text{diff}} = -J_{N\text{drift}}$ .

Diagram (a)

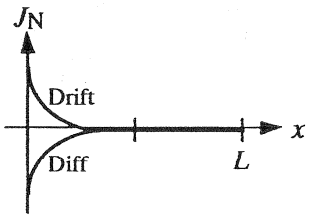
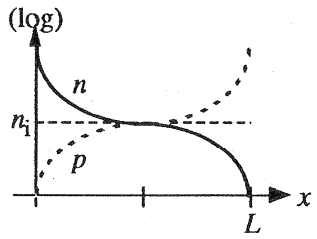
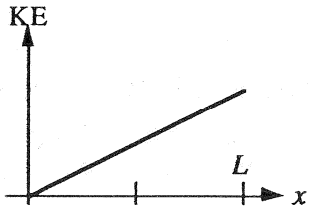
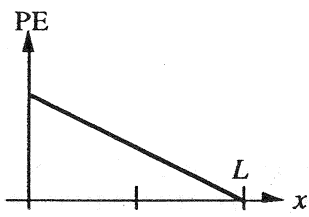
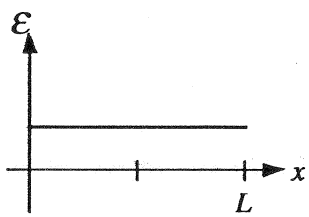
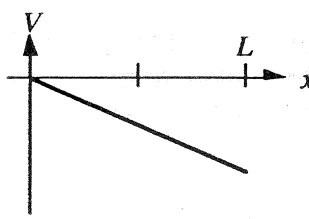


Diagram (b)

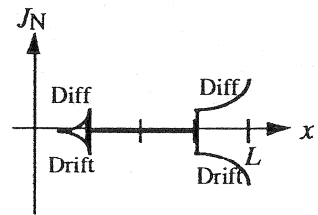
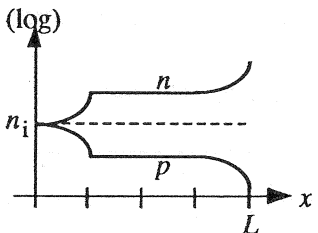
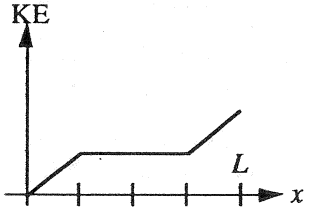
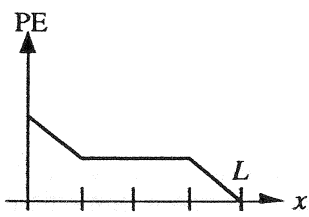
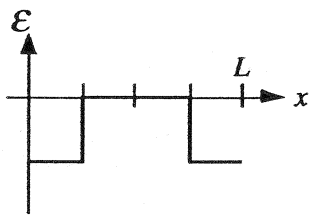
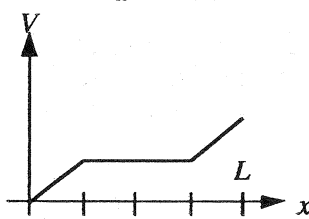
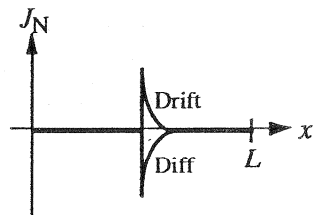
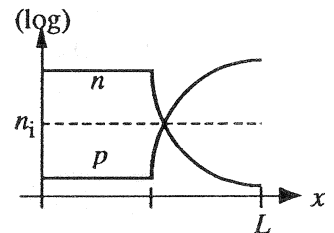
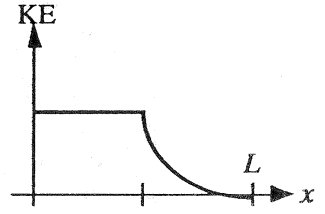
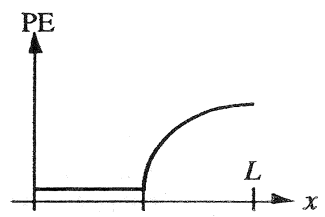
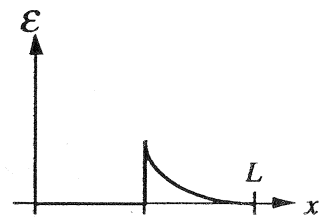
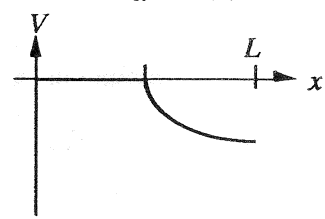


Diagram (c)



### Diagram (d)

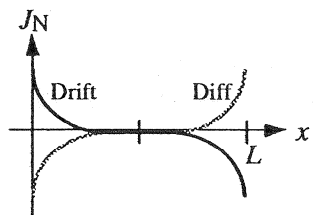
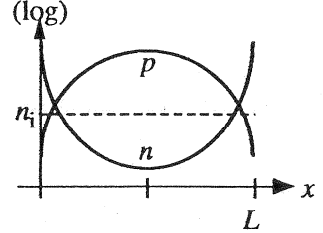
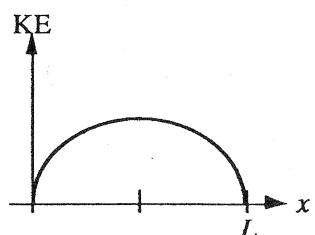
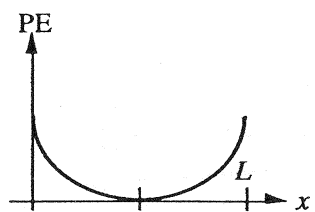
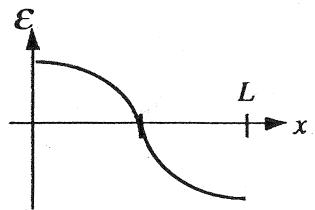
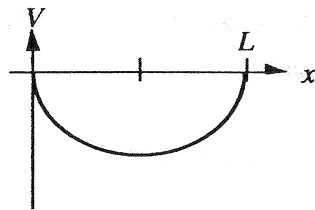
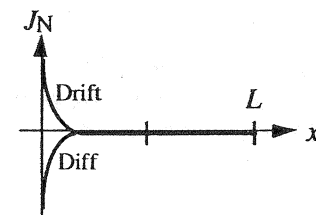
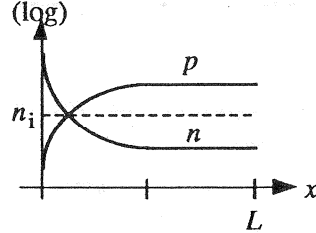
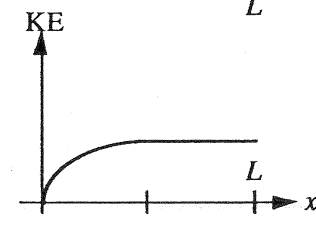
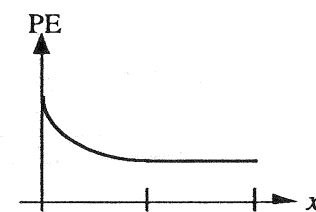
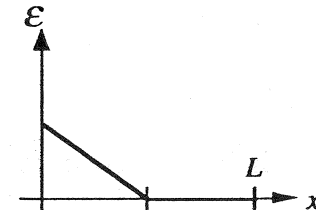
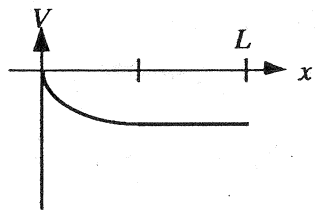
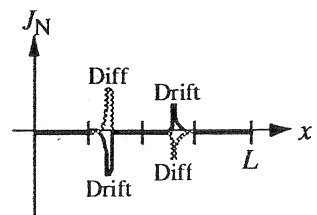
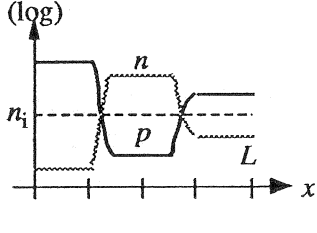
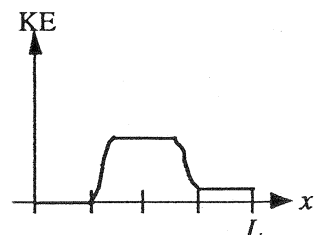
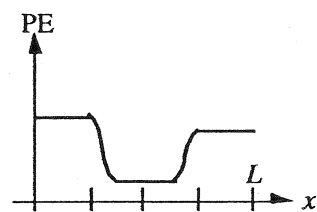
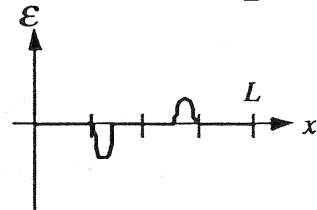
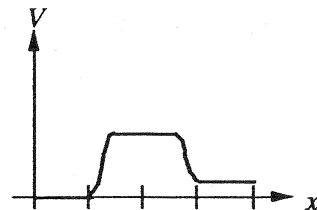


Diagram (e)



### Diagram (f)



### 3.13

(a) (i) We know  $E_F = \text{constant}$  on the diagram since equilibrium conditions prevail.

$$(ii) \dots p(x) = n_i e^{(a-x)/b} = n_i e^{(E_i - E_F)/kT}$$

Therefore

$$E_i - E_F = kT(a-x)/b \quad \dots \text{a linear function of } x$$

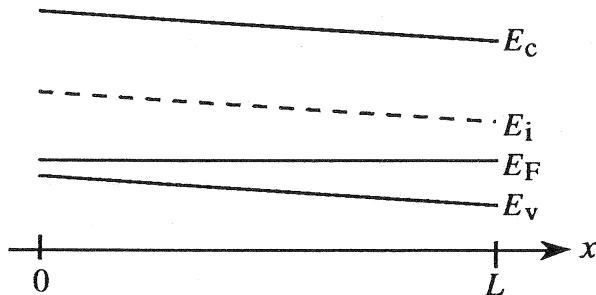
Moreover

$$\text{at } x = 0, E_i - E_F = kTa/b = 18kT = 0.466 \text{ eV}$$

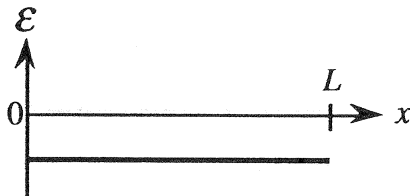
$$\text{at } x = L, E_i - E_F = kT(a-L)/b = 10kT = 0.259 \text{ eV}$$

$$(iii) E_G(\text{Si}) = 1.12 \text{ eV at room temperature and } E_i \equiv (E_c + E_v)/2.$$

Using the above information one concludes...



(b)



The above  $\mathcal{E}$  versus  $x$  plot can be deduced by inspection from the slope of the energy band diagram. Quantitatively,

$$\mathcal{E} = \frac{1}{q} \frac{dE_i}{dx} = -\frac{kT/q}{b} = -\frac{0.0259}{10^{-5}} = -2.59 \times 10^3 \text{ V/cm}$$

(c) The direction of the electric field is such as to accelerate minority carrier electrons in the  $+x$  direction. The built-in electric field should indeed assist in the transport of minority carrier electrons from  $x = 0$  to  $x = L$ .

### 3.14

(a) Since  $D = (kT/q)\mu$  and  $kT/q$  is not a function of the doping, a sketch of the  $D_N$  and  $D_P$  variation with  $N_A$  or  $N_D$  must have the same identical shape as the  $\mu_n$  and  $\mu_p$  plots in Fig. 3.5(a).

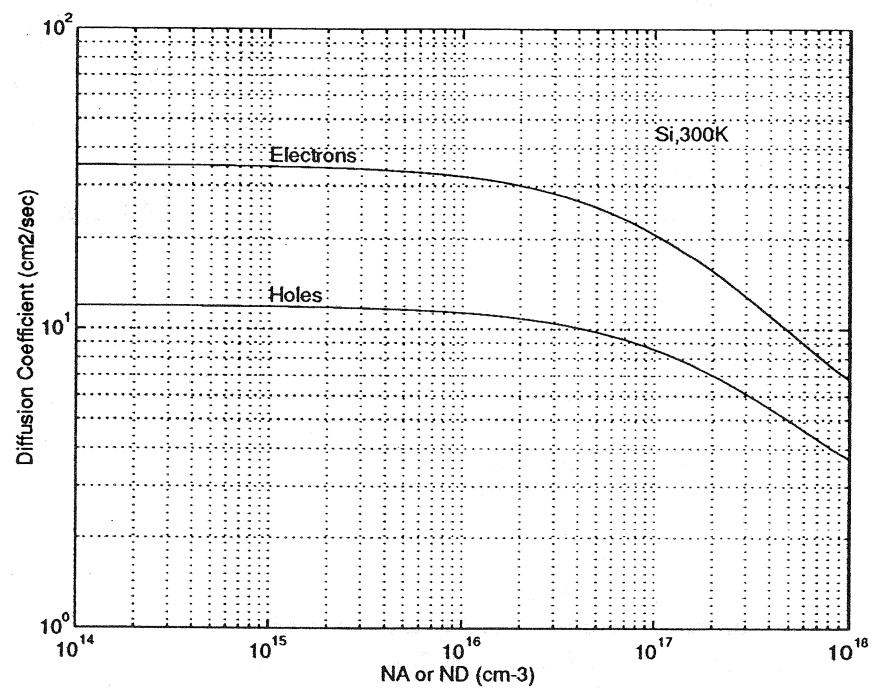
(b) MATLAB program script ...

```
%Diffusion Coefficient versus Dopant Concentration (Si, 300K)
%Initialization
clear; close
k=8.617e-5;
T=300;

%Fit Parameters
NDref=1.3e17; NAref=2.35e17;
μnmin=92; μpmin=54.3;
μn0=1268; μp0=406.9;
an=0.91; ap=0.88;

%Diffusion Coefficient Calculation
N=logspace(14,18);
μn=μnmin+μn0./(1+(N/NDref).^an);
μp=μpmin+μp0./(1+(N/NAref).^ap);
DN=k.*T.*μn;
DP=k.*T.*μp;

%Plotting results
loglog(N, DN, N, DP); grid;
axis([1e14, 1e18, 1, 1e2]);
xlabel('NA or ND (cm-3)');
ylabel('Diffusion Coefficient (cm2/sec)');
text(1.0e15, 38, 'Electrons');
text(1.0e15, 13, 'Holes');
text(1.0e17, 45, 'Si, 300K');
```



- (c) The Einstein relationship used to convert mobility data to diffusion coefficient data assumes a modified form if the semiconductor is degenerate. At room temperature, Si becomes degenerate for doping concentrations in excess of roughly  $10^{18}/\text{cm}^3$ .

### 3.15

By definition

$$\begin{aligned} n &= n_0 + \Delta n \\ p &= p_0 + \Delta p \end{aligned}$$

which when substituted into Eq. (3.35) gives

$$\begin{aligned} \left. \frac{\partial p}{\partial t} \right|_{\substack{i-\text{thermal} \\ R-G}} &= \left. \frac{\partial n}{\partial t} \right|_{\substack{i-\text{thermal} \\ R-G}} = \frac{n_i^2 - (n_0 + \Delta n)(p_0 + \Delta p)}{\tau_p(n_0 + \Delta n + n_i) + \tau_n(p_0 + \Delta p + p_i)} \\ &= \frac{n_i^2 - n_0 p_0 - n_0 \Delta p - p_0 \Delta p - \Delta p^2}{\tau_p(n_0 + \Delta p + n_i) + \tau_n(p_0 + \Delta p + n_i)} \end{aligned}$$

In the latter form of the preceding equation we have set  $n_1 = p_1 = n_i$  and  $\Delta n = \Delta p$  in accordance with the assumptions in the problem statement. The above equation is valid for both  $n$ - and  $p$ -type materials. To be specific, let us assume the semiconductor is  $n$ -type.

Examining the numerator of the simplified expression we note

$$n_0 p_0 = n_i^2; \text{ the } n_i^2 \text{ and } -n_0 p_0 \text{ terms cancel}$$

$$n_0 \Delta p \gg p_0 \Delta p \dots \text{since } n_0 \gg p_0 \text{ in an } n\text{-type material}$$

$$n_0 \Delta p \gg \Delta p^2 \dots \text{since } \Delta p \ll n_0 \text{ under low-level injection}$$

All but the  $n_0 \Delta p$  term may be neglected.

Examining the denominator of the simplified expression we note

$$\tau_p(n_0 + \Delta p + n_i) \approx \tau_p n_0 \dots n_0 \gg \Delta p \text{ and } n_0 \gg n_i$$

$$\tau_p n_0 \gg \tau_n(p_0 + \Delta p + n_i) \dots \text{since } \tau_p \sim \tau_n, \text{ and } n_0 \gg p_0 + \Delta p + n_i$$

All but the  $\tau_p n_0$  term may be neglected.

We therefore conclude

$$\left. \frac{\partial p}{\partial t} \right|_{\substack{i-\text{thermal} \\ R-G}} = -\frac{n_0 \Delta p}{\tau_p n_0} = -\frac{\Delta p}{\tau_p} \dots n\text{-type material}$$

The reduced relationship is indeed just the special-case Eq. (3.34a).

### 3.16

- (a) One assumes the minority carrier drift current is negligible compared to the diffusion current in deriving the equation; i.e., diffusion is taken to be the dominant mode of minority carrier transport — hence the name DIFFUSION equation.
- (b) The equation is only valid for minority carriers.
- (c) The recombination-generation term appearing in the equation, namely  $-\Delta n_p/\tau_n$ , is valid only under low-level injection conditions.

### 3.17

$$\frac{\partial \Delta p_n}{\partial t} = D_p \frac{\partial^2 \Delta p_n}{\partial x^2} - \frac{\Delta p_n}{\tau_p} + G_L \quad \dots \text{Hole minority carrier diff. eq.}$$

$$\frac{\partial \Delta p_n}{\partial t} = 0 \quad \dots \text{steady state}$$

$$\frac{\Delta p_n}{\tau_p} \Rightarrow 0 \quad \dots \text{R-G neglected}$$

$$G_L = 0 \quad \dots \text{no light}$$

Thus

$$\frac{d^2 \Delta p_n}{dx^2} = 0$$

$$\Delta p_n(x) = A + Bx \quad \dots \text{general solution}$$

$$\Delta p_n(0) = \Delta p_{n0} = A \quad \dots \text{boundary condition no. 1}$$

$$\Delta p_n(L) = 0 = A + BL \quad \dots \text{boundary condition no. 2}$$

$$\text{or } B = -A/L = -\Delta p_{n0}/L$$

So finally

$\Delta p_n(x) = \Delta p_{n0} (1 - x/L) \quad \dots 0 \leq x \leq L$

3.18

(a)  $\Delta n = n - n_0 = -n_0 \quad (n_0 = n_i^2/N_A = 10^{20}/10^{16} = 10^4/\text{cm}^3)$

(b) **Generation**. There is a deficit of carriers at  $t = 0^+$  and therefore the R-G process operates to eliminate the deficit by adding (generating) carriers.

(c) **Yes**.  $|\Delta n| = n_0 = 10^4/\text{cm}^3 \ll p_0 = N_A = 10^{16}/\text{cm}^3$

(d).....  $\frac{\partial \Delta n_p}{\partial t} = D_N \frac{\partial^2 \Delta n_p}{\partial x^2} - \frac{\Delta n_p}{\tau_n} + G_L \quad \dots \text{minority carrier diff. eq.}$

$G_L = 0$  since light is not affecting the wafer and the  $D_N(\partial^2 \Delta n_p / \partial x^2)$  term is zero because there is no concentration gradient. Thus

$$\frac{d\Delta n_p}{dt} = -\frac{\Delta n_p}{\tau_n} \quad \dots \text{simplified equation}$$

$$\Delta n_p(0) = -n_0 \quad \dots \text{boundary condition}$$

$$\Delta n_p(t) = A e^{-t/\tau_n} \quad \dots \text{general solution}$$

$$-n_0 = A \quad \dots \text{applying b.c.}$$

$$\boxed{\Delta n_p(t) = -n_0 e^{-t/\tau_n}}$$

### 3.19

Since  $G_{L0}$  is applied for a time  $t \gg \tau_n$ , steady state conditions will prevail prior to  $t = 0$ . Analogous to Sample Problem No. 1 discussed in the text, we can therefore state that

$$\Delta n_p(0) = G_{L0}\tau_n$$

Note that since the light intensity is reduced at  $t = 0$ ,  $\Delta n_p(0) = \Delta n_{p\max}$ , and

$\Delta n_{p\max} = G_{L0}\tau_n = 10^{16} \times 10^{-6} = 10^{10}/\text{cm}^3 \ll p_0 \approx N_A = 10^{14}/\text{cm}^3$ . Low level injection conditions clearly prevail at all times. Also, all other conditions needed for use of the minority carrier diffusion equation have been met. Thus, we need to solve

$$\frac{\partial \Delta n_p}{\partial t} = D_N \frac{\partial^2 \Delta n_p}{\partial x^2} - \frac{\Delta n_p}{\tau_n} + G_L$$

which, for the problem at hand, simplifies to

$$\frac{d\Delta n_p}{dt} = -\frac{\Delta n_p}{\tau_n} + \frac{G_{L0}}{2} \quad \dots t > 0$$

This equation is subject to the boundary condition,

$$\Delta n_p(0) = G_{L0}\tau_n$$

One obtains

$$\Delta n_p(t) = \frac{G_{L0}\tau_n}{2} + A e^{-t/\tau_n} \quad \dots \text{general solution}$$

and applying the boundary condition,

$$G_{L0}\tau_n = \frac{G_{L0}\tau_n}{2} + A \Rightarrow A = \frac{G_{L0}\tau_n}{2}$$

$$\Delta n_p(t) = \frac{G_{L0}\tau_n}{2} (1 + e^{-t/\tau_n})$$

### 3.20

Since  $\Delta n_p(x) \ll p_0$ , we have low level injection. All conditions for use of the minority carrier diffusion equation are satisfied except possibly  $\mathcal{E} = 0$ . However, we do not expect a small non-uniform distribution of minority carriers to give rise to a significant  $\mathcal{E}$ -field. Thus, assuming  $\mathcal{E} \equiv 0$ , we can write in general

$$\frac{\partial \Delta n_p}{\partial t} = D_N \frac{\partial^2 \Delta n_p}{\partial x^2} - \frac{\Delta n_p}{\tau_n} + G_L$$

Simplifying...

$$\frac{\partial \Delta n_p}{\partial t} = 0 \quad \dots \text{steady state}$$

$$0 = D_N \frac{d^2 \Delta n_p}{dx^2} - \frac{\Delta n_p}{\tau_n} + G_L \quad \dots \text{equation to be solved}$$

Solving...

$$\Delta n_p(x) = G_L \tau_n + A e^{-x/L_N} + B e^{x/L_N} \quad (L_N = \sqrt{D_N \tau_n})$$

Boundary conditions...

$$(1) \Delta n_p(0) = 0 \quad \dots \text{given}$$

$$(2) \Delta n_p(\infty) = G_L \tau_n$$

The second boundary condition follows from the fact that far from  $x = 0$  the concentration gradient caused by the extraction of carriers at  $x = 0$  must vanish. If  $D_N(d^2 \Delta n_p / dx^2) \rightarrow 0$ ,  $\Delta n_p = G_L \tau_n$  as deduced from the simplified minority carrier diffusion equation. Thus

$$B = 0 \quad \dots \text{applying boundary condition (2)}$$

$$0 = G_L \tau_n + A \quad \dots \text{applying boundary condition (1)}$$

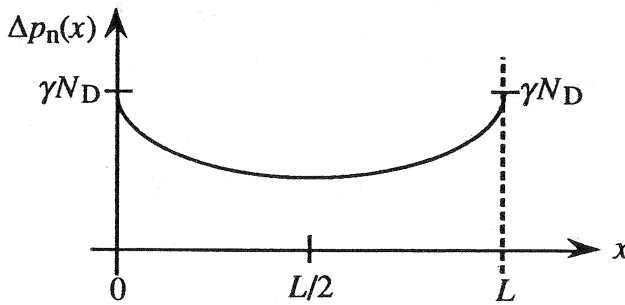
$$\text{or } A = -G_L \tau_n$$

and

$$\boxed{\Delta n_p(x) = G_L \tau_n (1 - e^{-x/L_N})}$$

### 3.21

(a) With a  $\gamma N_D$  excess of holes being created at the bar ends, some of the excess will move into the bar interior via diffusion. Recombination will systematically reduce the excess as it moves into the bar. A distribution of excess minority carriers symmetrical about the center of the bar is expected because both ends of the bar are being perturbed in an identical manner. The expected general form of the  $\Delta p_n(x)$  solution is therefore as sketched below.



(b) [Yes]. As is obvious from the qualitative sketch,

$$\Delta p_{nlmax} = \gamma N_D = 10^{-3} N_D$$

but  $n_0 \approx N_D$  ( $N_D \gg n_i$ )

therefore  $\Delta p_{nlmax} \ll n_0$  as required for low-level injection

(c) Inside the bar  $G_L = 0$  and steady state conditions prevail making  $\partial \Delta p_n / \partial t = 0$ . Thus the minority carrier diffusion equation simplifies to

$$0 = D_P \frac{d^2 \Delta p_n}{dx^2} - \frac{\Delta p_n}{\tau_p}$$

(d) Referring to solution no. 1 in Table 3.2, the general solution to the part (c) differential equation is

$$\Delta p_n(x) = A e^{-x/L_P} + B e^{x/L_P} \quad \dots L_P = \sqrt{D_P \tau_p}$$

The boundary conditions are

$$\Delta p_n(0) = \gamma N_D \quad \text{and} \quad \Delta p_n(L) = \gamma N_D$$

$$(e) \dots \quad J_P = q \mu_{pp} \mathcal{E} - q D_P \frac{dp}{dx} = -q D_P \frac{dp}{dx} = -q D_P \frac{d \Delta p_n}{dx}$$

The first simplification above follows from the fact that  $\mathcal{E} \approx 0$  and the drift current is assumed to be negligible compared with the diffusion current. This is consistent with the

prior use of the minority carrier diffusion equation. Secondly,  $dp/dx = d\Delta p_n/dx$  because  $p = p_0 + \Delta p$  and  $dp_0/dx = 0$ . Now,

$$\left. \frac{d\Delta p_n}{dx} \right|_{x=0} = \left[ -\frac{A}{L_P} e^{-x/L_P} + \frac{B}{L_P} e^{x/L_P} \right] \Big|_{x=0} = \frac{B - A}{L_P}$$

Thus

$$J_P \Big|_{x=0} = -qD_P \left. \frac{d\Delta p_n}{dx} \right|_{x=0} = -q \frac{D_P}{L_P} (B - A)$$

### 3.22

(a) Far to the negative side of  $x = 0$  there will be no perturbation and

$$p(-\infty) = p_0 = n_i^2/N_D = 10^{20}/10^{18} = 10^2/\text{cm}^3$$

(b) We expect a concentration gradient near  $x = 0$  due to diffusion, but as  $x \rightarrow \infty$  the gradient should vanish. Thus, far from  $x = 0$  the carriers generated by the light must just balance the carriers being annihilated by thermal R-G under steady state conditions; i.e.,

$$G_L = \Delta p_n(\infty)/\tau_p$$

or  $\Delta p_n(\infty) = G_L \tau_p = (10^{15})(10^{-6}) = 10^9/\text{cm}^3$

and  $p(\infty) = p_0 + \Delta p_n(\infty) \equiv \Delta p_n(\infty) = 10^9/\text{cm}^3$

(c) **Yes**. The largest  $\Delta p_n$  will occur at  $x = \infty$  and

$$\Delta p_n(\infty) = 10^9/\text{cm}^3 \ll n_0 = N_D = 10^{18}/\text{cm}^3$$

(d) For  $x < 0$  ...

$$0 = D_P \frac{d^2 \Delta p_n}{dx^2} - \frac{\Delta p_n}{\tau_p}$$

$$\Delta p_n(x) = Ae^{-x/L_P} + Be^{x/L_P}$$

$$\Delta p_n(-\infty) = 0 \Rightarrow A = 0$$

$$\Delta p_n(x) = Be^{x/L_P} \quad \text{and} \quad \frac{d\Delta p_n(x)}{dx} = \frac{B}{L_P} e^{x/L_P}$$

For  $x > 0$  ...

$$0 = D_P \frac{d^2 \Delta p_n}{dx^2} - \frac{\Delta p_n}{\tau_p} + G_L$$

$$\Delta p_n(x) = G_L \tau_p + A' e^{-x/L_P} + B' e^{x/L_P}$$

$$\Delta p_n(\infty) = G_L \tau_p \quad \Rightarrow \quad B' = 0$$

$$\Delta p_n(x) = G_L \tau_p + A' e^{-x/L_P} \quad \text{and} \quad \frac{d\Delta p_n(x)}{dx} = -\frac{A'}{L_P} e^{-x/L_P}$$

At  $x = 0$  ...

$$B = G_L \tau_p + A' \quad \dots \text{continuity of } \Delta p_n(x)$$

$$B/L_P = -A'/L_P \quad \dots \text{continuity of } d\Delta p_n(x)/dx$$

$$\text{or} \quad B = -A' = G_L \tau_p / 2$$

and

$$\Delta p_n(x) = \begin{cases} \frac{1}{2} G_L \tau_p e^{x/L_P} & \dots x \leq 0 \\ G_L \tau_p \left(1 - \frac{1}{2} e^{-x/L_P}\right) & \dots x \geq 0 \end{cases}$$

### 3.23

(a) The snake-like pattern provides a relatively large area for light absorption while making the film length/width ratio, and hence the dark resistance, as large as possible.

$$(b) \quad R = \rho l/A$$

$$\text{with } \rho \equiv 1/q\mu_n N_D \quad \text{and} \quad A = (\text{width})(\text{thickness}) = wt$$

$$\text{or} \quad R = \frac{l}{q\mu_n N_D wt} = \frac{3}{(1.6 \times 10^{-19})(100)(10^{13})(3 \times 10^{-2})(5 \times 10^{-4})}$$

$$= 1.25 \times 10^9 \text{ ohms}$$

(c) Under low-level injection conditions, one could assert  $G_L = \Delta p/\tau_p$ . However, with the light-on resistance much less than the dark resistance, it is clear that one actually has high level ( $n \gg n_0$ ) injection. The usual relationships cannot be used.

3.24

(a)  $n_0 = n_i e^{(E_F - E_i)/kT} = (10^{10})e^{0.3/0.0259} = 1.07 \times 10^{15}/\text{cm}^3$

$p_0 = n_i e^{(E_i - E_F)/kT} = (10^{10})e^{-0.3/0.0259} = 9.32 \times 10^4/\text{cm}^3$

(b)  $n = n_i e^{(F_N - E_i)/kT} = (10^{10})e^{0.318/0.0259} = 2.15 \times 10^{15}/\text{cm}^3$

$p = n_i e^{(E_i - F_P)/kT} = (10^{10})e^{0.3/0.0259} = 1.07 \times 10^{15}/\text{cm}^3$

(c)  $N_D \equiv n_0 = 1.07 \times 10^{15}/\text{cm}^3$

(d) [No] Due to illumination,  $\Delta p \approx n_0$  and  $n$  differs significantly from  $n_0$ . For low level injection one must have  $\Delta p \ll n_0$  and  $n \approx n_0$ .

(e)  $\rho_{\text{before}} \equiv \frac{1}{q\mu_n N_D} = \frac{1}{(1.6 \times 10^{-19})(1345)(1.07 \times 10^{15})} = 4.34 \text{ ohm-cm}$

$$\begin{aligned}\rho_{\text{after}} &= \frac{1}{q(\mu_n n + \mu_p p)} = \frac{1}{(1.6 \times 10^{-19})[(1345)(2.15 \times 10^{15}) + (458)(1.07 \times 10^{15})]} \\ &= 1.85 \text{ ohm-cm}\end{aligned}$$

### 3.25

(1) Since  $\mathcal{E} \equiv 0$ ,  $E_c$ ,  $E_i$ , and  $E_v$  will be position independent.

(2) Given  $n \equiv N_D$ , it follows that  $F_N \equiv E_F$  and

$$E_F - E_i \equiv kT \ln(N_D/n_i) = (0.0259)\ln(10^{15}/10^{10}) = 0.298 \text{ eV}$$

$$(3) \quad p = p_0 + \Delta p_n = n_i^2/N_D + n_i(1-x/L) = n_i e^{(E_i - F_P)/kT}$$

$$p_0 = n_i^2/N_D = 10^5/\text{cm}^3$$

and

$$\Delta p_n = n_i(1-x/L) = (10^{10})(1-x/L)$$

Clearly

$$\text{at } x=0, p \equiv n_i \text{ and } F_P = E_i$$

$$\text{at } x=L, p = p_0 \text{ and } F_P = E_F$$

For most  $x$  (except values near  $x=L$ ),  $\Delta p_n \gg p_0$   
and

$$e^{(E_i - F_P)/kT} \equiv 1 - x/L$$

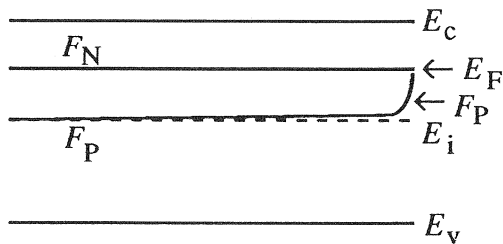
$$E_i - F_P = kT \ln(1 - x/L) \Rightarrow F_P - E_i = 0.0027 \text{ eV if } x/L = 0.1$$

$$F_P - E_i = 0.018 \text{ eV if } x/L = 0.5$$

$$F_P - E_i = 0.060 \text{ eV if } x/L = 0.9$$

From the calculations note that  $F_P$  stays fairly close to  $E_i$  until  $x \approx L$ .

Putting all the above information together, one concludes,



### 3.26

(a) In constructing the plot, all energies are referenced to  $E_V$  and normalized by  $kT$ . Specifically,

$$(F_N - E_V)/kT = E_G/2kT + \ln(N_D/n_i)$$

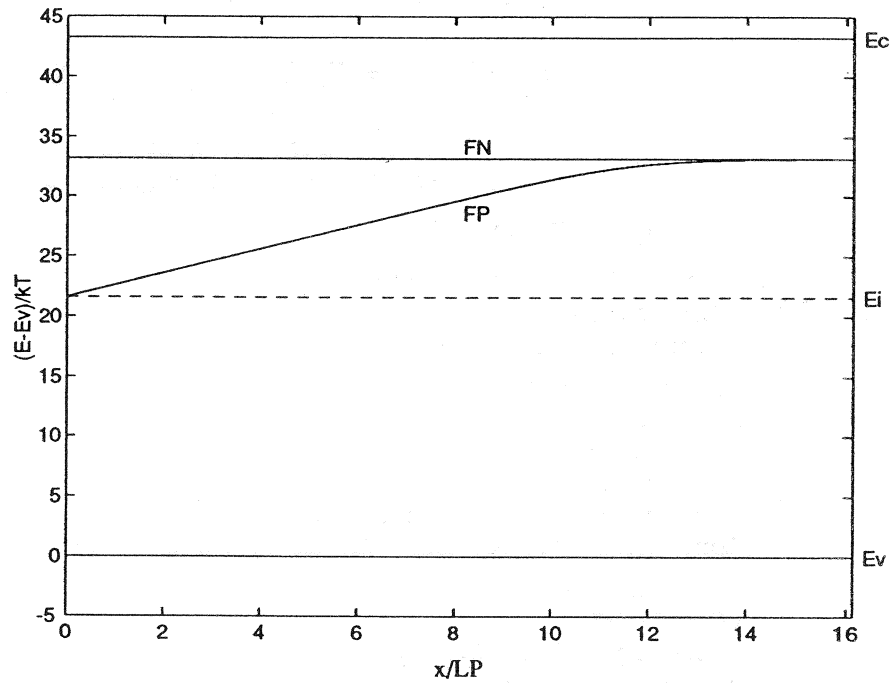
$$(F_P - E_V)/kT = E_G/2kT - \ln[p_0/n_i + (\Delta p_{n0}/n_i)e^{-x/L_P}]$$

Because the independent variable is taken to be  $x/L_P$ , it is not necessary to compute  $L_P$ . The  $\tau_p$  given in the problem statement is not required in performing the computations.

MATLAB program script ...

```
%Quasi-Fermi level plot
%Initialization
clear; close
%Input parameters
EG=1.12;
kT=0.0259;
ni=1.0e10;
ND=input('Input ND in cm-3, ND = ');
Δpn0=input('Input Δpn0 in cm-3, Δpn0 = ');
%Calculations
p0=ni^2/ND;
zmax=log(100*Δpn0/p0);
z=linspace(0, zmax); %z=x/LP
%All energies referenced to Ev and normalized by kT
Ec=EG/kT;
FN=EG/(2*kT)+log(ND/ni);
FP=EG/(2*kT)-log(p0/ni+Δpn0/ni).*exp(-z));
%Plotting results
plot(z,FP,'r');
axis([0, zmax, -5, 45])
xlabel('x/LP'); ylabel('(E-Ev)/kT')
hold on
x=[0, zmax];
y1=[Ec, Ec]; y2=[FN, FN]; plot(x,y1,x,y2,'b')
y3=[Ec/2, Ec/2]; y4=[0, 0]; plot(x,y3,'--',x,y4,'y')
zput=zmax+0.2;
text(zput, 43.2, 'Ec'); text(zput, 21.6, 'Ei'); text(zput, 0, 'Ev')
text(zput/2, FN+1, 'FN'); text(zput/2, FP(50)-1, 'FP')
```

(b) The program output with  $N_D = 10^{15}/\text{cm}^3$  and  $\Delta p_{n0} = 10^{10}/\text{cm}^3$  that is displayed below compares favorably with the sketch in Exercise 3.5. The sketch shows a greater  $x$ -length of the band diagram. Also, in producing the text sketch, the graphic artist incorrectly added some curvature to the near  $x = 0$  part of the  $F_P$  line.



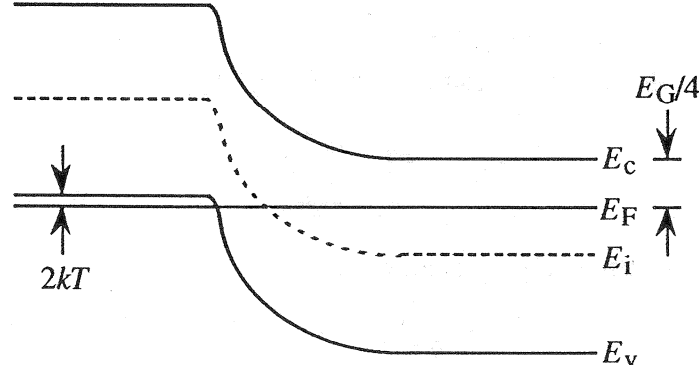
## CHAPTER 5

### 5.1

- (a) False
- (b) True
- (c) False
- (d) True
- (e) True
- (f) False
- (g) True
- (h) True
- (i) False
- (j) True

### 5.2

(a)

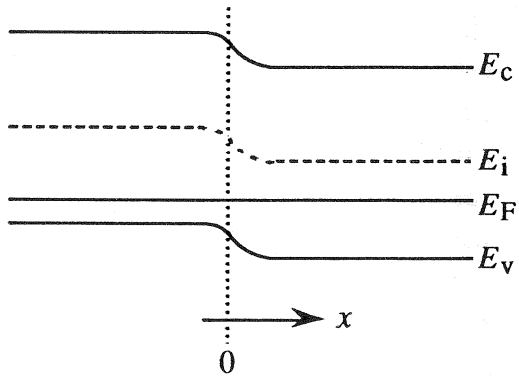


(b) Employing Eq. (5.12),

$$\begin{aligned}V_{bi} &= \frac{1}{q} [(E_i - E_F)_p\text{-side} + (E_F - E_i)_n\text{-side}] \\&\approx \frac{1}{q} (E_G/2 + 2kT + E_G/4) = \frac{1}{q} (3E_G/4 + 2kT) = \frac{3}{4} (1.12) + 2(0.0259) \\&= 0.89 \text{ V}\end{aligned}$$

### 5.3

(a) Because  $N_{A1} > N_{A2}$  and  $p = n_i \exp[(E_i - E_F)/kT] \approx N_A$  far from the junction, it follows that  $(E_i - E_F)_{x<0} > (E_i - E_F)_{x>0}$ . The energy band diagram must therefore be of the form



(b) Given that the dopings are nondegenerate, the same development leading to Eq. (5.10) can be employed, except

$$n(x_n) \equiv n_i^2/N_{A2}$$

$$n(-x_p) \equiv n_i^2/N_{A1}$$

which when substituted into Eq. (5.8) yields

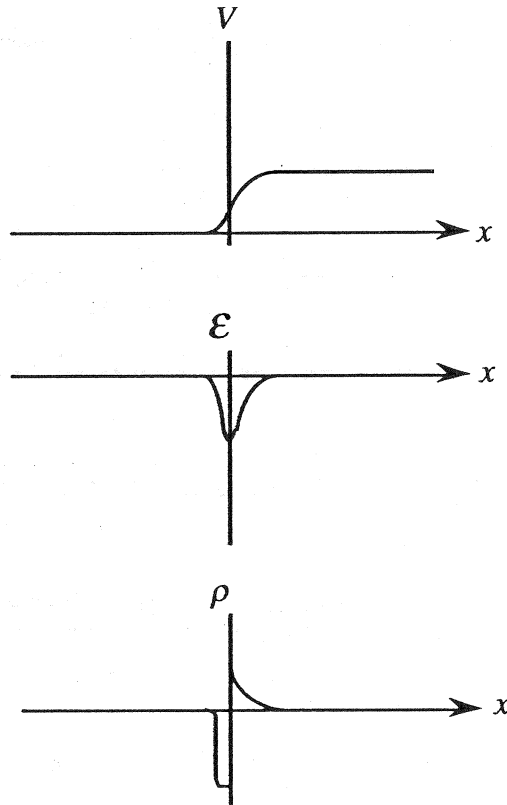
$$V_{bi} = \frac{kT}{q} \ln\left(\frac{N_{A1}}{N_{A2}}\right)$$

Alternatively, one can write

$$\begin{aligned} V_{bi} &= \frac{1}{q} [E_i(-\infty) - E_i(+\infty)] = \frac{1}{q} [(E_i - E_F)_{p1\text{-side}} - (E_i - E_F)_{p2\text{-side}}] \\ &= \frac{1}{q} [kT \ln(N_{A1}/n_i) - kT \ln(N_{A2}/n_i)] = \frac{kT}{q} \ln(N_{A1}/N_{A2}) \end{aligned}$$

Note that, as must be the case,  $V_{bi} \rightarrow 0$  if  $N_{A1} = N_{A2}$ .

(c)



(It should be emphasized that the above are rough sketches. The exact functional dependencies cannot be deduced employing a graphical approach.)

(d) **No**. It is true that the minus charge shown on the  $x < 0$  portion of the part (c)  $\rho$ -plot is caused by a depletion of holes on the higher-doped  $N_{A1}$ -side of the junction, leading to a net charge associated with the ionized acceptors. The plus charge on the  $N_{A2}$ -side of the junction, however, cannot be attributed to ionized donors. There is no donor doping! The only other source of a positive charge is holes.—There is a hole concentration on the  $n$ -side of the junction in *excess* of  $N_{A2}$ . [The hole excess on the  $N_{A2}$ -side of the junction can actually be inferred from the energy band diagram in part (a).] Since  $p > N_{A2}$  near the junction, we cannot invoke the depletion approximation.

5.4

(a)  $V_{bi} = \frac{kT}{q} \ln\left(\frac{N_A N_D}{n_i^2}\right) = (0.0259) \ln\left[\frac{(2 \times 10^{15})(10^{15})}{(10^{20})}\right] = 0.614 \text{ V}$

(b)  $x_p = \left[ \frac{2K_S \epsilon_0}{q} \frac{N_D}{N_A(N_A+N_D)} V_{bi} \right]^{1/2} = 3.655 \times 10^{-5} \text{ cm}$

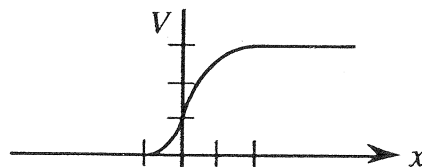
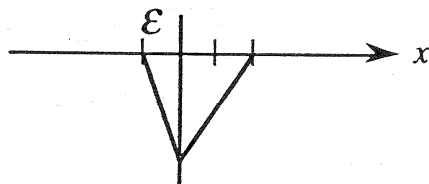
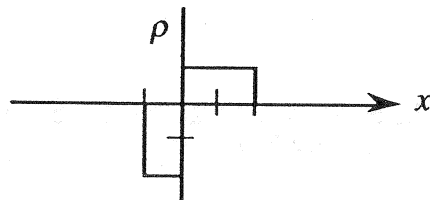
$$x_n = \left[ \frac{2K_S \epsilon_0}{q} \frac{N_A}{N_D(N_A+N_D)} V_{bi} \right]^{1/2} = 7.31 \times 10^{-5} \text{ cm}$$

$$W = x_n + x_p = 1.10 \times 10^{-4} \text{ cm}$$

(c)  $\mathcal{E}(0) = -\frac{qN_D}{K_S \epsilon_0} x_n = -\frac{(1.6 \times 10^{-19})(10^{15})(7.31 \times 10^{-5})}{(11.8)(8.85 \times 10^{-14})} = -1.12 \times 10^4 \text{ V/cm}$

(d)  $V(0) = \frac{qN_A}{2K_S \epsilon_0} x_p^2 = \frac{(1.6 \times 10^{-19})(2 \times 10^{15})(3.655 \times 10^{-5})^2}{(2)(11.8)(8.85 \times 10^{-14})} = 0.205 \text{ V}$

(e)



5.5

$$(a) V_{bi} = \frac{kT}{q} \ln \left( \frac{N_A N_D}{n_i^2} \right) = (0.0259) \ln \left[ \frac{(10^{17})(10^{15})}{(10^{20})} \right] = 0.716 \text{ V}$$

$$(b) x_p = \left[ \frac{2K_S \epsilon_0}{q} \frac{N_D}{N_A(N_A+N_D)} V_{bi} \right]^{1/2} = 9.62 \times 10^{-7} \text{ cm}$$

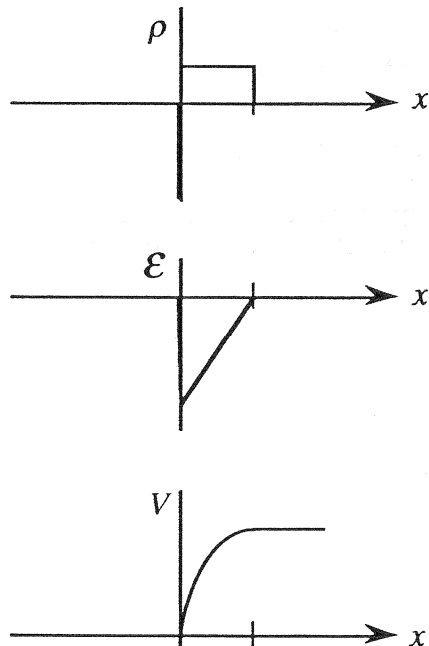
$$x_n = \left[ \frac{2K_S \epsilon_0}{q} \frac{N_A}{N_D(N_A+N_D)} V_{bi} \right]^{1/2} = 9.62 \times 10^{-5} \text{ cm}$$

$$W = x_n + x_p = 9.72 \times 10^{-5} \text{ cm}$$

$$(c) E(0) = -\frac{qN_D}{K_S \epsilon_0} x_n = -\frac{(1.6 \times 10^{-19})(10^{15})(9.62 \times 10^{-5})}{(11.8)(8.85 \times 10^{-14})} = -1.47 \times 10^4 \text{ V/cm}$$

$$(d) V(0) = \frac{qN_A}{2K_S \epsilon_0} x_p^2 = \frac{(1.6 \times 10^{-19})(10^{17})(9.62 \times 10^{-7})^2}{(2)(11.8)(8.85 \times 10^{-14})} = 7.09 \times 10^{-3} \text{ V}$$

(e)



In Problem 5.4 the widths of the  $n$ - and  $p$ -sides of the depletion region and the corresponding variation of the electrostatic variables are comparable reflecting the fact that  $N_A \sim N_D$ . Here with  $N_A \gg N_D$ , we find the depletion width and potential drop lie almost exclusively on the lowly doped  $n$ -side of the junction.

## 5.6

The MATLAB program listed below (and included on the Instructor's disk as m-file P\_05\_06.m) can be used to establish the expected answers for a given set of instructor specified parameters.

### MATLAB program script...

```
%Problem 5.6
%Initialization
clear; format compact

%Constants and Parameters
q=1.6e-19; e0=8.85e-14;
ni=1.0e10; kT=0.0259;
KS=11.8;

NA=input('Input NA in cm-3, NA=');
ND=input('Input ND in cm-3, ND=');
VA=input('Input VA in volts, VA=');

%(a) Vbi...the built-in-voltage
format compact
Vbi=kT*log(NA*ND/ni^2)

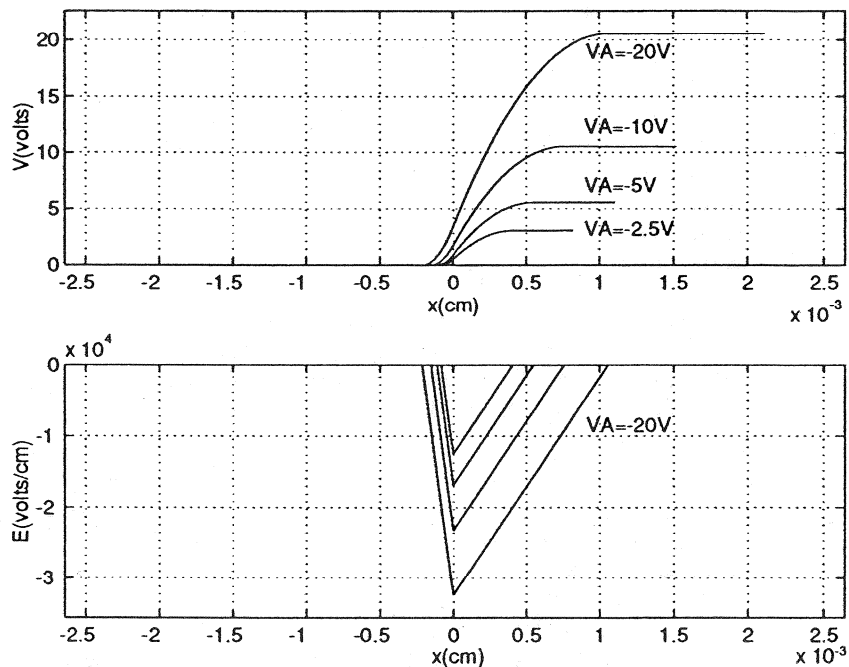
%(b) xp, xn, and W
xp=sqrt(2*KS*e0/q*(Vbi-VA)*ND/(NA*(NA+ND)));
xn=sqrt(2*KS*e0/q*(Vbi-VA)*NA/(ND*(NA+ND)));
W=xn+xp

%(c) Electric field at x = 0
E0=-q*ND/(KS*e0)*xn

%(d) Electrostatic potential at x = 0
V0=q*NA/(2*KS*e0)*xp^2
fprintf('UNITS...\npxp(cm), xn(cm), W(cm)')
fprintf('\nVbi(volts), E0(V/cm), V0(volts)\n')
```

### 5.7

(a)/(b)/(c) Constructed in accordance with suggestions provided in the problem statement, the P\_05\_07.m program yielding the desired results, along with sample output, are displayed below. The program produces a plot of 1 to 4 simultaneous  $E$  and  $V$  versus  $x$  curves corresponding to different applied voltages. In addition, a listing of relevant parameters and computational constants is sent to the Command window.



#### COMPUTATIONAL RESULTS

NA =  $1.0000e+15$   
ND =  $2.0000e+14$   
VA = -20  
Vbi = 0.5547  
xn = 0.0011  
xp =  $2.1147e-04$   
W = 0.0013  
E0 =  $-3.2400e+04$   
V0 = 3.4258

### MATLAB program script...

```

%This program computes and plots the ELECTROSTATIC VARIABLES (V, E).
%It also provides an output of key computational parameters.
%A Si step junction maintained at 300K is assumed.
%The solution is based on the depletion approximation.
fprintf('\n\nELECTROSTATIC VARIABLES COMPUTATION (step,Si,300K)');

%Initialization
clear; close
format compact

%Constants
q=1.6e-19;
k=8.617e-5;
e0=8.85e-14;

%Parameters
ni=1.0e10;
kT=0.0259;
KS=11.8;

%Variables
NA=input('Input the p-side doping, NA = ');
ND=input('Input the n-side doping, ND = ');
s=input('Specify the number of curves to compute (1-4), ');
VA=input('Specify the minimum applied bias, VA = ');

%Computation Proper
for ii=1:s
    %Built-in Voltage
    Vbi=kT*log(NA*ND/ni^2);
    %xn, xp, and W
    X=(2*KS*e0)*(Vbi-VA)/q;
    xn=sqrt(X*NA/(ND*(NA+ND)));
    xp=sqrt(X*ND/(NA*(NA+ND)));
    W=xn+xp;
    %p-side electrostatic variables
    x=linspace(-xp,0);
    Vp=(q*NA/(2*KS*e0))*(xp+x).^2;
    Ep=-(q*NA/(KS*e0))*(xp+x);
    %n-side electrostatic variables
    xx=linspace(0,xn);
    Vn=Vbi-VA-(q*ND/(2*KS*e0))*(xn-xx).^2;
    En=-(q*ND/(KS*e0))*(xn-xx);
    xxx=[xx,2*xn];
    Vn=[Vn,Vn(100)];

```

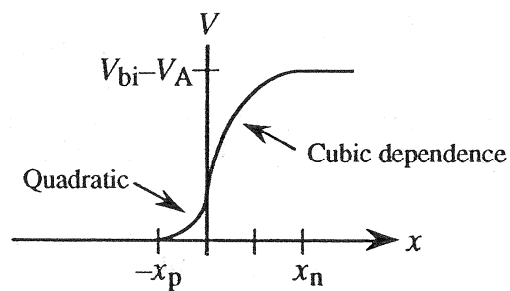
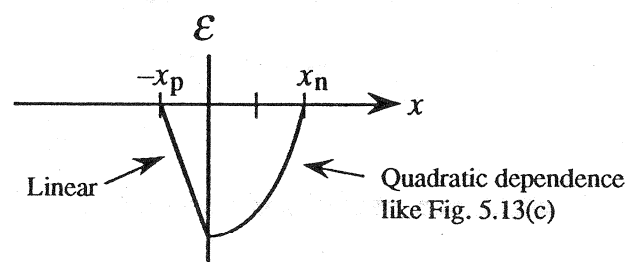
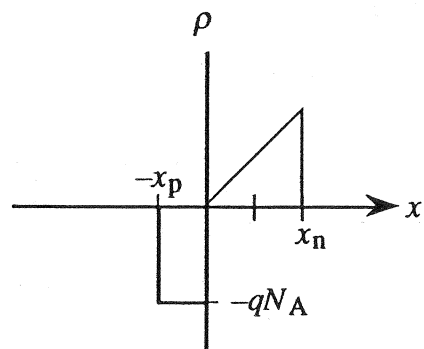
```

%Plotting results
if ii==1,
    Emax=1.1*En(1);
    Vmax=1.1*Vn(100);
    xmax=2.5*max(xn,xp);
else
end
subplot(2,1,1), plot(x,Vp,xxx,Vn);
axis([-xmax,xmax,0,Vmax]); grid on
xlabel('x(cm)'); ylabel('V(volts)');
hold on
subplot(2,1,2), plot(x,Ep,xx,En);
axis([-xmax,xmax,Emax,0]); grid on
xlabel('x(cm)'); ylabel('E(volts/cm)');
hold on
%Print out numerical results
fprintf('\n\nCOMPUTATIONAL RESULTS\n')
NA, ND, VA, Vbi, xn, xp, W, E0=En(1),
V0=Vn(1)
%Recycle
VA=VA/2;
end
hold off

```

### 5.8

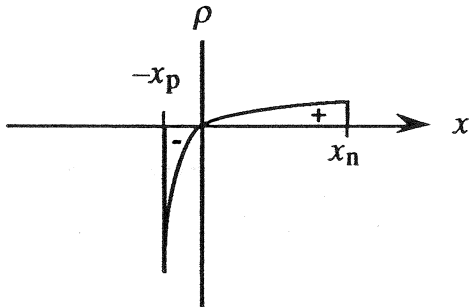
Essentially, the solution is just a superposition of the step junction solution for  $x < 0$  and the linearly graded solution for  $x > 0$ .



5.9

(a) The carrier concentrations are assumed to be negligible compared to the net doping concentration in a region  $-x_p \leq x \leq x_n$  straddling the metallurgical junction. The charge density outside the depletion region is taken to be identically zero.

(b) We must have  $\rho = q(N_D - N_A)$  for  $-x_p \leq x \leq x_n$  and the total (+) charge must equal the total (-) charge.



(c) Since based on the depletion approximation

$$\rho = \begin{cases} qN_0(1 - e^{-\alpha x}) & \dots -x_p \leq x \leq x_n \\ 0 & \dots x \leq -x_p \text{ and } x \geq x_n \end{cases}$$

substitution into Poisson's equation gives

$$\frac{dE}{dx} = \begin{cases} \frac{qN_0}{K_S \epsilon_0} (1 - e^{-\alpha x}) & \dots -x_p \leq x \leq x_n \\ 0 & \dots x \leq -x_p \text{ and } x \geq x_n \end{cases}$$

Separating variables and integrating from the  $-x_p$  depletion region edge where  $E = 0$  to an arbitrary point  $x$  in the depletion region, one obtains

$$E(x) = \frac{qN_0}{K_S \epsilon_0} \int_{-x_p}^x (1 - e^{-\alpha x'}) dx' = \frac{qN_0}{K_S \epsilon_0} \left( x' + \frac{e^{-\alpha x'}}{\alpha} \right) \Big|_{-x_p}^x = \frac{qN_0}{K_S \epsilon_0} \left( x + \frac{e^{-\alpha x}}{\alpha} + x_p - \frac{e^{\alpha x_p}}{\alpha} \right)$$

or

$$E(x) = \frac{qN_0}{K_S \epsilon_0} \left[ (x + x_p) + \frac{1}{\alpha} (e^{-\alpha x} - e^{\alpha x_p}) \right] \quad \dots -x_p \leq x \leq x_n$$

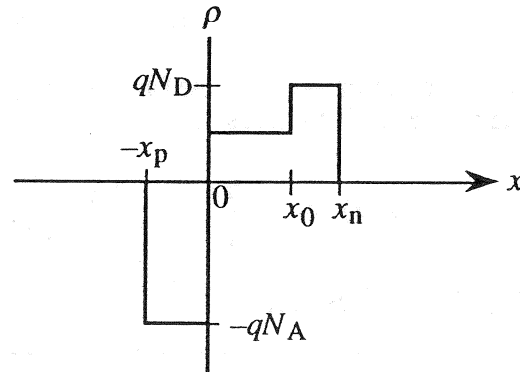
### 5.10

(a) Given that  $x_n > x_0$  for all applied biases of interest, then surely  $x_n > x_0$  under equilibrium ( $V_A = 0$ ) conditions. Now, the derivation of the Eq. (5.8)  $V_{bi}$  relationship is valid for an arbitrary nondegenerate doping profile. Moreover,  $n(-x_p) = n_i^2/N_A$ , and with  $x_n > x_0$ ,  $n(x_n) = N_D$  for the given junction profile, just like in a standard step junction. Assuming the  $p$ - and  $x_n > x_0$   $n$ -region dopings to be nondegenerate, the standard Eq. (5.10) result therefore applies,

$$V_{bi} = \frac{kT}{q} \ln \left( \frac{N_A N_D}{n_i^2} \right)$$

(This problem points out that only the dopings at the depletion region edges are relevant in determining  $V_{bi}$ .)

(b) Since  $\rho = q(N_D - N_A)$  for  $-x_p \leq x \leq x_n$  and zero elsewhere under the depletion approximation, we conclude



(c) Invoking the depletion approximation gives

$$\rho = \begin{cases} 0 & \dots x < -x_p \\ -qN_A & \dots -x_p \leq x \leq 0 \\ qN_D/2 & \dots 0 \leq x \leq x_0 \\ qN_D & \dots x_0 \leq x \leq x_n \\ 0 & \dots x > x_n \end{cases}$$

Substituting into Poisson's equation then yields

$$\frac{dE}{dx} = \begin{cases} -qN_A/K_S \epsilon_0 & \dots -x_p \leq x \leq 0 \\ qN_D/2K_S \epsilon_0 & \dots 0 \leq x \leq x_0 \\ qN_D/K_S \epsilon_0 & \dots x_0 \leq x \leq x_n \end{cases}$$

Separating variables and integrating from the depletion region edges where  $\mathcal{E} = 0$  to arbitrary points in the  $p$ -region and  $x_n > x_0$   $n$ -region yield the same relationships and results as in the standard step-junction analysis. To obtain the  $0 \leq x \leq x_0$  solution, we can either integrate from  $x = 0$  where  $\mathcal{E}$  is known from the  $p$ -region solution to an arbitrary point in the  $0 \leq x \leq x_0$  region, or we can start the integration at  $x = x_n$  where  $\mathcal{E}$  is known from the  $x_n > x_0$   $n$ -region solution and integrate backward into the lighter-doped  $n$ -region. Taking the former approach we can write

$$\int_{\mathcal{E}(0)}^{\mathcal{E}(x)} d\mathcal{E} = \frac{qN_D}{2K_S\epsilon_0} \int_0^x dx'$$

or

$$\mathcal{E}(x) = \mathcal{E}(0) + \frac{qN_D}{2K_S\epsilon_0} x = \frac{-qN_A}{K_S\epsilon_0} x_p + \frac{qN_D}{2K_S\epsilon_0} x \quad \dots 0 \leq x \leq x_0$$

If the integration is performed from  $x = x_n$  backward into the lighter doped  $n$ -region, one obtains the equivalent result

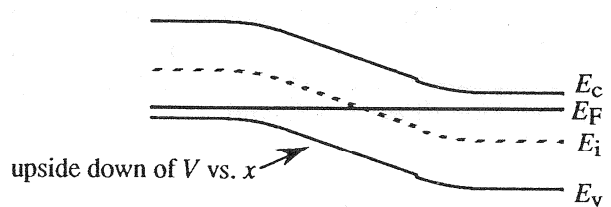
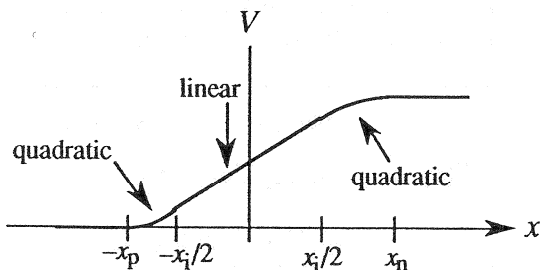
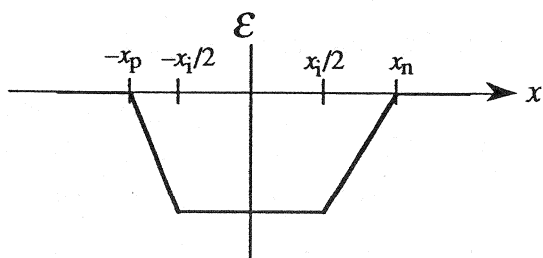
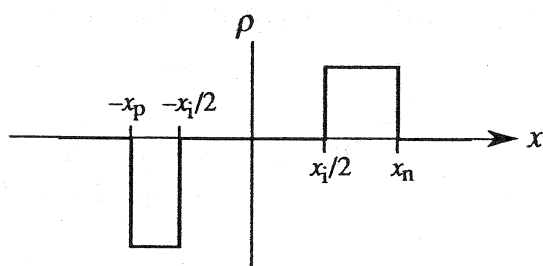
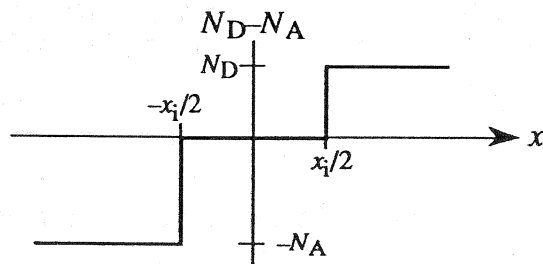
$$\mathcal{E}(x) = -\frac{qN_D}{K_S\epsilon_0} \left( x_n - \frac{x_0}{2} - \frac{x}{2} \right) \quad \dots 0 \leq x \leq x_0$$

Thus the final result is

$$\mathcal{E}(x) = \begin{cases} -(qN_A/K_S\epsilon_0)(x_p+x) & \dots -x_p \leq x \leq 0 \\ -(q/K_S\epsilon_0)(N_Ax_p - N_Dx/2) & \dots 0 \leq x \leq x_0 \\ \text{or} \\ -(qN_D/K_S\epsilon_0)(x_n - x_0/2 - x/2) & \dots 0 \leq x \leq x_0 \\ -(qN_D/K_S\epsilon_0)(x_n - x) & \dots x_0 \leq x \leq x_n \end{cases}$$

5.11

(a)



(b) The derivation of the Eq. (5.8)  $V_{bi}$  relationship is valid for an arbitrary doping profile. Moreover,  $n(x_n) = N_D$  and  $n(-x_p) = n_i^2/N_A$  for the  $p$ - $i$ - $n$  diode just like a step-junction  $pn$  diode. Assuming the  $p$ - and  $n$ -region dopings to be nondegenerate, the standard Eq.(5.10) result therefore applies and

$$V_{bi} = \frac{kT}{q} \ln\left(\frac{N_A N_D}{n_i^2}\right)$$

(This problem points out that only the dopings at the depletion region edges are relevant in determining  $V_{bi}$ .)

(c) Invoking the depletion approximation, we can write

$$\rho = \begin{cases} 0 & \dots x < -x_p \\ -qN_A & \dots -x_p \leq x \leq -x_i/2 \\ 0 & \dots -x_i/2 \leq x \leq x_i/2 \\ qN_D & \dots x_i/2 \leq x \leq x_n \\ 0 & \dots x > x_n \end{cases}$$

Substitution into Poisson's equation yields

$$\frac{dE}{dx} = \begin{cases} -qN_A/K_S \epsilon_0 & \dots -x_p \leq x \leq -x_i/2 \\ 0 & \dots -x_i/2 \leq x \leq x_i/2 \\ qN_D/K_S \epsilon_0 & \dots x_i/2 \leq x \leq x_n \end{cases}$$

Separating variables and integrating from the depletion region edges where  $E = 0$  to arbitrary points in the  $n$ - and  $p$ -regions yield the same relationships and results as in the step junction analysis. In the  $i$ -region,  $E = \text{constant} = E(-x_i/2)$ . Thus we conclude

$$E(x) = \begin{cases} -(qN_A/K_S \epsilon_0)(x_p + x) & \dots -x_p \leq x \leq -x_i/2 \\ -(qN_A/K_S \epsilon_0)(x_p - x_i/2) & \dots -x_i/2 \leq x \leq x_i/2 \\ -(qN_D/K_S \epsilon_0)(x_n - x) & \dots x_i/2 \leq x \leq x_n \end{cases}$$

Setting  $E(x) = -dV/dx$ , separating variables, and integrating from the depletion region edges to arbitrary points in the  $n$ - and  $p$ -regions again yields the same relationships and results as in the step junction analysis. Introducing  $E(-x_i/2) \equiv E_i$  and  $V(-x_i/2) \equiv V_i$ , we note that in the  $i$ -region  $dV/dx = -E_i$  and

$$\int_{V_i}^{V(x)} dV = -\mathcal{E}_i \int_{-x_i/2}^x dx'$$

or

$$V(x) = V_i - \mathcal{E}_i(x + x_i/2)$$

Thus

$V(x) = \begin{cases} (qN_A/2K_S\varepsilon_0)(x_p+x)^2 & \dots -x_p \leq x \leq -x_i/2 \\ (qN_A/2K_S\varepsilon_0)[(x_p-x_i/2)(x_p+x_i/2+2x)] & \dots -x_i/2 \leq x \leq x_i/2 \\ V_{bi}-V_A - (qN_D/2K_S\varepsilon_0)(x_n-x)^2 & \dots x_i/2 \leq x \leq x_n \end{cases}$
--

To determine  $x_n$  and  $x_p$  we require  $\mathcal{E}(x)$  and  $V(x)$  to be continuous at  $x = x_i/2$ , or

$$N_A(x_p - x_i/2) = N_D(x_n - x_i/2)$$

and

$$(qN_A/2K_S\varepsilon_0)[(x_p - x_i/2)(x_p + 3x_i/2)] = V_{bi} - V_A - (qN_D/2K_S\varepsilon_0)(x_n - x_i/2)^2$$

Solving for  $x_n - x_i/2$  from the first equation directly above, substituting into the second equation, and rearranging, gives

$$(x_p - x_i/2)^2 + \frac{2N_D x_i}{N_A + N_D} (x_p - x_i/2) - \frac{2K_S\varepsilon_0}{q} \frac{N_D}{N_A(N_A + N_D)} (V_{bi} - V_A) = 0$$

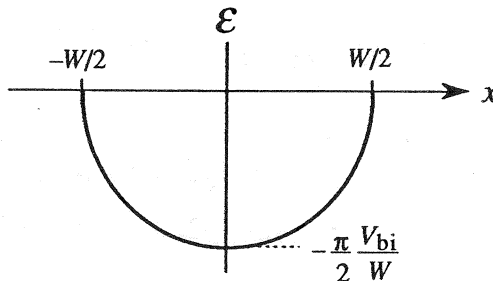
Finally, solving the quadratic equation yields

$x_p - \frac{x_i}{2} = \frac{N_D}{N_A} \left( x_n - \frac{x_i}{2} \right) = \frac{N_D x_i}{N_A + N_D} + \left[ \left( \frac{N_D x_i}{N_A + N_D} \right)^2 + \frac{2K_S\varepsilon_0}{q} \frac{N_D}{N_A(N_A + N_D)} (V_{bi} - V_A) \right]^{1/2}$
--

where the (+) root has been chosen because  $x_p - x_i/2$  must be greater than zero. Note that the result here reduces to Eq. (5.34) if  $x_i \rightarrow 0$ .

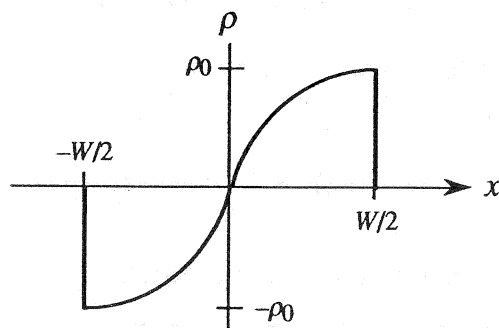
5.12

(a)  $\mathcal{E}(x) = -\frac{dV}{dx} = -\frac{\pi}{2} \frac{V_{bi}}{W} \cos\left(\frac{\pi x}{W}\right) \quad \dots -\frac{W}{2} \leq x \leq \frac{W}{2}$



(b) Poisson's equation states  $d\mathcal{E}/dx = \rho/K_S \epsilon_0$ . Thus

$$\rho(x) = K_S \epsilon_0 \frac{d\mathcal{E}}{dx} = \left(\frac{\pi^2}{2} \frac{K_S \epsilon_0 V_{bi}}{W^2}\right) \sin\left(\frac{\pi x}{W}\right) \equiv \rho_0 \sin\left(\frac{\pi x}{W}\right) \quad \dots -\frac{W}{2} \leq x \leq \frac{W}{2}$$



(c) Under the depletion approximation

$$\rho = q(N_D - N_A) \quad \dots -W/2 \leq x \leq W/2$$

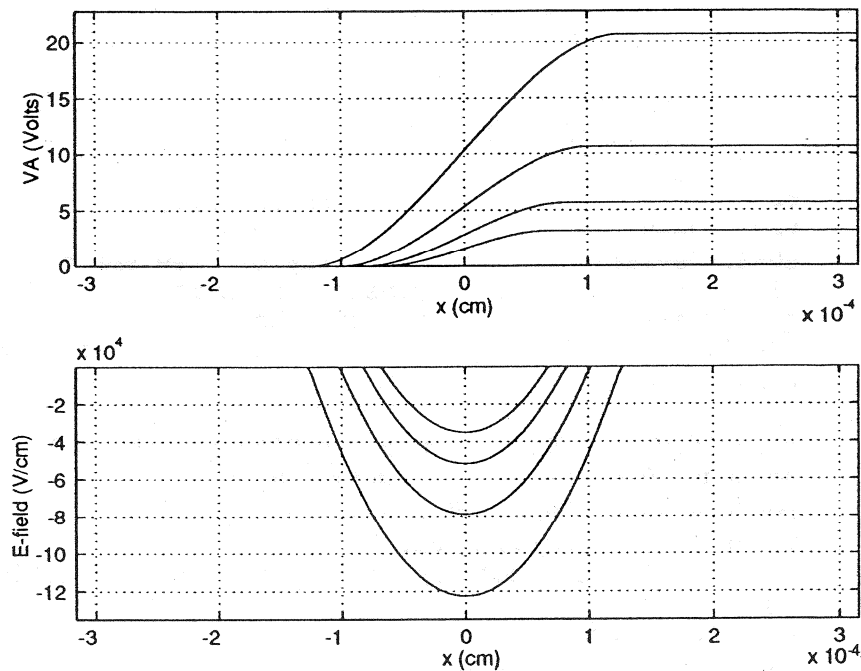
Thus

$$N_D - N_A = \rho/q \quad \dots -W/2 \leq x \leq W/2$$

The  $N_D - N_A$  plot is identical in shape to the  $\rho$ -plot, with the limiting y-axis values modified to  $-\rho_0/q$  and  $\rho_0/q$ .

### 5.13

(a)/(b)/(c) Sample linearly graded junction results,  $E$  versus  $x$  and  $V$  versus  $x$  plots plus an output list of relevant parameters and computational constants, are displayed below. These results were generated by the MATLAB program P\_05\_13.m listed on the following pages. Note that Vbi.m, a subprogram used in the iteration procedure to determine the built-in voltage, must be present at runtime. We might mention that, having been developed later, the program presented here is somewhat more sophisticated and efficient than the step-junction computational program constructed as a solution to Problem 5.7.



### COMPUTATIONAL RESULTS

$$a = 1.0000e+20$$

$$Vbi = 6.6725e-01$$

$$VA = -2.0000e+01 \quad -1.0000e+01 \quad -5.0000e+00 \quad -2.5000e+00$$

$$W = 2.5286e-04 \quad 2.0283e-04 \quad 1.6428e-04 \quad 1.3531e-04$$

$$E0 = -1.2260e+05 \quad -7.8888e+04 \quad -5.1748e+04 \quad -3.5110e+04$$

$$V0 = 2.0667e+01 \quad 1.0667e+01 \quad 5.6672e+00 \quad 3.1672e+00$$

## MATLAB program script...

```
%A Si LINEARLY-GRADED junction maintained at 300K is assumed.  
%The ELECTROSTATIC VARIABLES (V,E) are computed and plotted as  
%a function of position; the program also provides an output  
%of key computational parameters.  
%The solution is based on the depletion approximation.  
%The function file Vbi.m is required for the program to run.  
  
%User Input  
% a is the dopant gradient constant in cm(-4)  
% VA is the applied voltage in volts  
  
% Initialization  
clear; close  
format short e  
format compact  
global aa e0 ni qq KS k T  
  
% Constants  
T=300; % Temperature in Kelvin  
k=8.617e-5; % Boltzmann constant  
e0=8.85e-14; % permittivity of free space  
ni=1e10; % intrinsic concentration in Si at 300K  
q=1.602e-19; % electronic charge  
KS=11.8; % Dielectric constant of Si at 300K  
  
%User input  
disp('');  
disp('Linearly Graded Junction Electrostatics');  
a=input('Please enter a (cm-4), a=');  
VA0=input('Please enter VA (volts), VA=');  
  
%Iterate to determine Vbi  
aa=a; %This is necessary because the fzero function uses a and q  
qq=q;  
Vbi=fzero('Vbi',1);  
  
%Computational constants  
for n = 1:4,  
    VA(n)=VA0/2^(n-1);  
    W(n)=(12*KS*e0*(Vbi-VA(n)) / (q*a))^(1/3);  
    xn(n)=W(n)/2;  
    xp(n)=W(n)/2;  
end  
  
%Computation proper  
xMAX=2.5*max(xn);  
x=[linspace(-xMAX,0) linspace(0,xMAX)];  
for n=1:4,  
    Ex(n,:)=(x>=-xn(n) & x<=xn(n)).*q*a.* (x.^2-xn(n)^2)/(2*KS*e0);  
    Vmax(n)=Vbi-VA(n);
```

```

Vx(n,:)=(x>=-xn(n) & x<=xn(n)).*q*a/(6*KS*e0).* (2*(xn(n))^3 ...
+3*(xn(n))^2.*x-x.^3)+(x>xn(n))*Vmax(n);
end
% plot V vs x
subplot(2,1,1), plot(x,Vx); grid on
axis([-xMAX,xMAX,0,1.1*max(Vmax)])
xlabel('x (cm)'); ylabel('VA (Volts)')
% plot E-field vs x
Exx=[Ex(1,:) Ex(2,:) Ex(3,:) Ex(4,:)];
Emin=1.1*min(Exx);
subplot(2,1,2), plot(x,Ex); grid on
axis([-xMAX xMAX Emin 0])
xlabel('x (cm)'); ylabel('E-field (V/cm)')
pause
%Print out numerical results to Command window
fprintf('\n\nCOMPUTATIONAL RESULTS\n')
a, Vbi, VA, W, E0=Ex(:,100)', V0=Vx(:,200)'

```

*Subprogram Vbi.m*

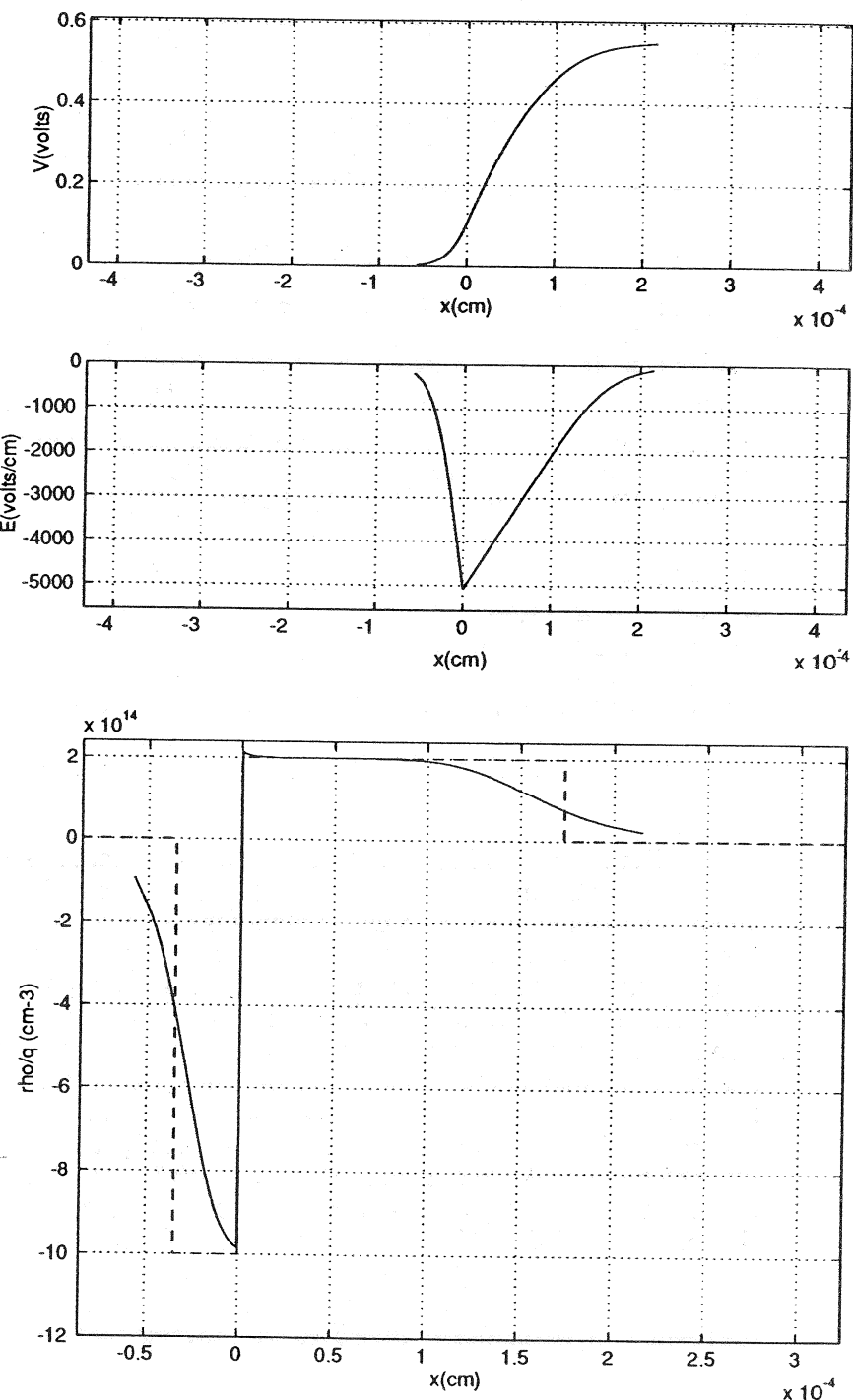
```

function y = f(Vbi);
global aa e0 ni qq KS k T
q=qq; a=aa;
y = Vbi-2*k*T*log(a*(12*KS*e0*Vbi/(q*a))^(1/3)/(2*ni));

```

### 5.14

(a)/(b) The exact solution  $\mathcal{E}$ ,  $V$ , and  $\rho$  versus  $x$  computations for both parts (a) and (b) are performed by the m-file P\_05\_14.m on the Instructor's disk. The program may take several minutes to execute. Sample output is displayed on the next page. When the exact  $\mathcal{E}$  and  $V$  vs.  $x$  solutions for a step junction are compared with the approximate solutions based on the depletion approximation, one finds the two sets of solutions are very similar in the vicinity of the metallurgical junction but deviate significantly as one approaches the semiconductor bulk. Whereas the  $\mathcal{E}$  and  $V$  results are pretty much as expected, the exact  $\rho/q$  vs.  $x$  plot may come as somewhat of a surprise. Under equilibrium conditions, the true charge density profile is very crudely modeled by the depletion approximation, especially on the heavily doped side of the junction. Also, if examined carefully, the charge density plot exhibits a slight peak near  $x = 0$  on the lightly doped side of the junction. The cited feature reflects an *excess of minority carriers* or "inversion layer" on the lightly doped side of the junction. This spill-over of carriers from the other side of the junction becomes more pronounced for highly asymmetrical junctions and leads to the computed difference in the  $x = 0$   $\mathcal{E}$ -field. We should note that the "inversion layer" disappears and the depletion approximation dramatically improves with reverse biasing.



## CHAPTER 6

### 6.1

- (a) Majority carrier injection (diffusion) to the opposite side of the junction.
- (b) Minority carriers wandering into the depletion region and being accelerated (drifting) to the opposite side of the junction.
- (c) The reverse bias current is expected to be *small* because it arises from *minority carriers* which are few in number. The reverse bias current *saturates* because a small voltage all but eliminates majority carrier injection across the junction, and the remaining current due to minority carriers is independent of the applied voltage.
- (d) generation and diffusion
- (e) The primary reason is that  $\mathcal{E} \neq 0$ . Also, low level injection conditions seldom apply;  $\partial n / \partial t$  thermal R-G  $\neq -\Delta n_p / \tau_n$  and  $\partial p / \partial t$  thermal R-G  $\neq -\Delta p_n / \tau_p$ .
- (f) There is NO a priori justification.
- (g) A diode where the contacts are far removed (several minority carrier diffusion lengths) from the edges of the depletion region.
- (h)  $np = n_i^2 e^{qV_A/kT} \quad \dots -x_p \leq x \leq x_n$
- (i)  $I_0$  is the extrapolated intercept of the straight-line region on the  $I$  (log scale) axis.
- (j) True

### 6.2

The graphical ideal-device/Si-300K device comparison of  $I$ - $V$  characteristics is presented on the next page. (Also see Fig. 6.6, Fig. 6.17, and Exercise 6.9.) The causes of the deviations noted in the sketches are:

#### *Causes*

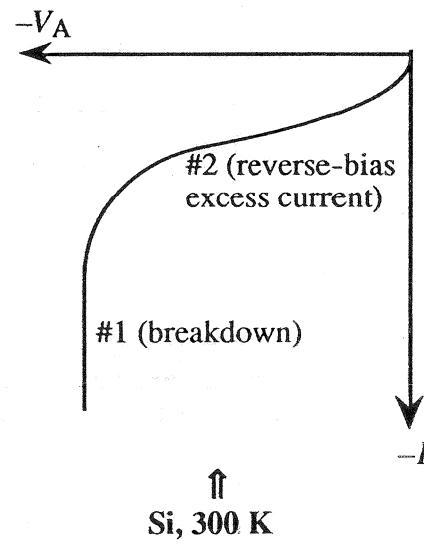
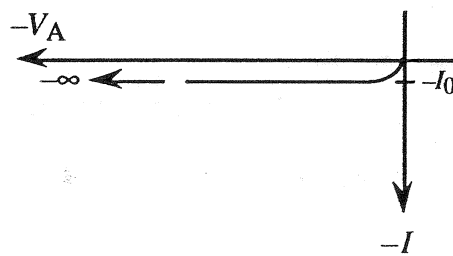
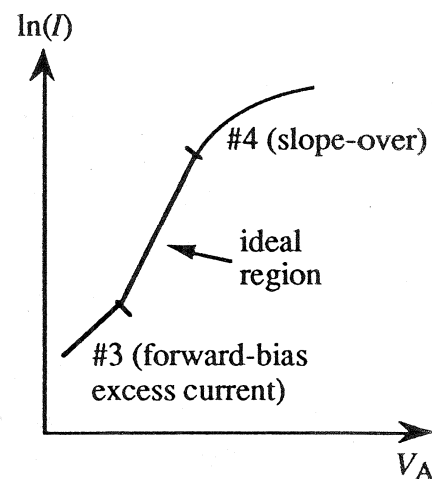
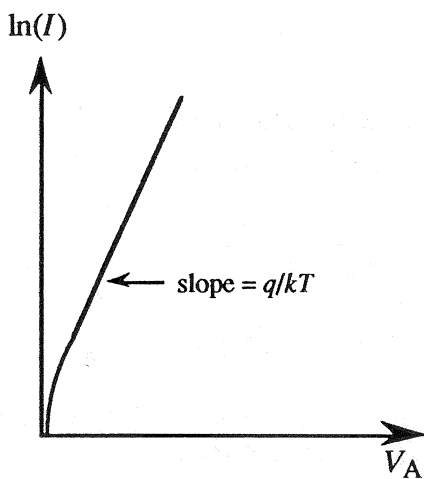
Deviation #1...Breakdown is caused by *avalanching* in the depletion region or tunneling through the depletion region (the *Zener process*). The latter is important if  $V_{BR} \lesssim 4V$ .

Deviation #2...Results from generation of carriers in the depletion region. (This was ignored in the ideal diode derivation.)

Deviation #3...Results from recombination of carriers in the depletion region.

Deviation #4...The slope-over on a log scale results from series resistance (bulk and/or contact resistance). An  $\exp(qV_A/2kT)$  region at large forward biases, if observed, is due to high-level injection.

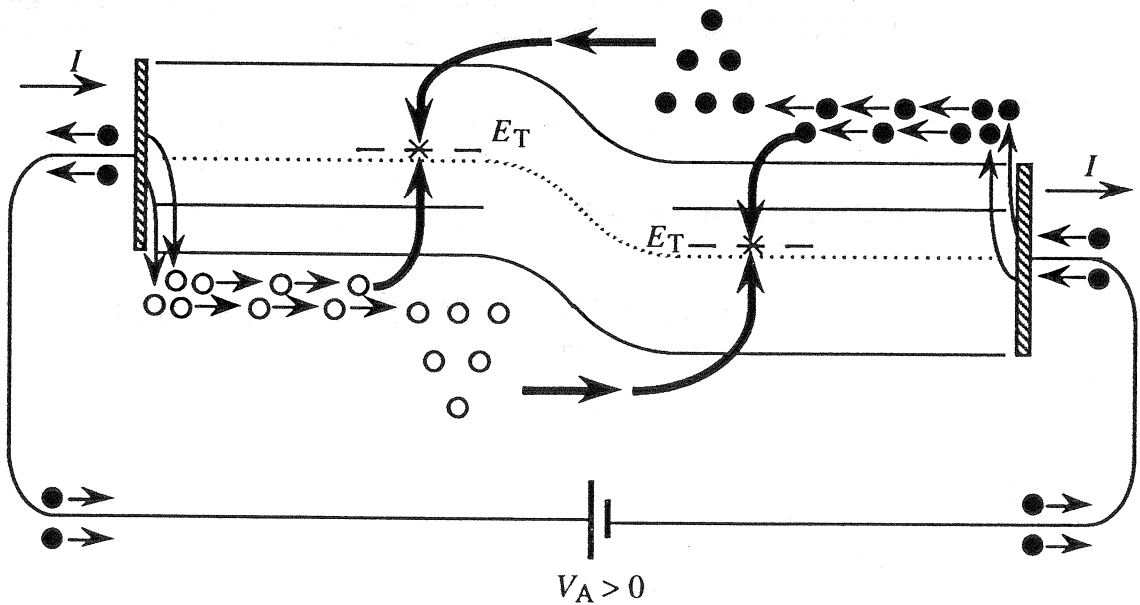
### Graphical Comparison



### 6.3

(a)/(b)/(c) To first order, the sketches here should be essentially identical to Fig. 6.1(a)–(c), except the Fermi level on the *p*-side is close to or actually in the valence band. Although it is perhaps unreasonable to expect from someone who has read only through Subsection 6.1.1 in the text, the majority carrier hole concentration on the *p*-side of the junction should also be visualized as much larger than the majority carrier electron concentration on the *n*-side of the junction. Likewise, the hole minority carrier concentration on the *n*-side is much greater than the electron minority carrier concentration on the *p*-side in a *p*<sup>+</sup>-*n* diode. Consequently, one would expect the hole component of the current to dominate over the electron component of the current under both forward and reverse biases.—The hole current arrows in the part (b) and (c) diagrams should be significantly larger than the electron current arrows. Note that the qualitative conclusion here is consistent with the formula-based observations made in Subsection 6.1.4.

### 6.4



## 6.5

If  $V_A \neq 0$ ,  $V(x_n) = V_{bi} - V_A$  and Eq. (5.5) in the Subsection 5.1.4 derivation assumes the modified form

$$-\int_{-x_p}^{x_n} \mathcal{E} dx = V_{bi} - V_A$$

Continuing to assume  $J_N = 0$  when  $V_A \neq 0$  then leads to the modified Eq. (5.8) relationship

$$V_{bi} - V_A = \frac{kT}{q} \ln \left[ \frac{n(x_n)}{n(-x_p)} \right]$$

or

$$\frac{n(x_n)}{n(-x_p)} = e^{q(V_{bi}-V_A)/kT} = \frac{N_A N_D}{n_i^2} e^{-qV_A/kT}$$

where the second form of the preceding equation is obtained by eliminating  $V_{bi}$  using Eq. (5.10). Finally, noting  $n(x_n) = N_D$ , simplifying, and solving for  $n(-x_p)$  yields

$$n(-x_p) = \frac{n_i^2}{N_A} e^{qV_A/kT}$$

and since  $n_0(-x_p) = n_i^2/N_A$ ,

$$\Delta n(-x_p) = \frac{n_i^2}{N_A} (e^{qV_A/kT} - 1) \quad \dots \text{Eq. (6.15)}$$

## 6.6

The MATLAB Diary session leading to the desired result was copied to a wordprocessor, irrelevant entries eliminated, and the results condensed into boxed regions. The modified version is reproduced below. Please note that  $I$  at  $V_A = -0.1V$  and  $V_A = -50V$  are nearly identical, indicating the saturation current has all but reached the saturation value at only  $V_A = -0.1V$ . Also note the small size of the room temperature saturation current,  $\sim 10^{-13} A$ , and the hugh increase in current at the elevated temperature.

### MATLAB Diary session...

```
%Given: n+ -p step junction with  
NA=1.0e15;  
taun=1.0e-6;  
A=1.0e-3;  
  
%Universal constants  
q=1.6e-19;  
k=8.617e-5;  
  
%(a) Currents at T=300K  
T=300;  
μn=1345; %Value from Fig. 3.5(a)  
DN=k*T*μn;  
LN=sqrt(DN*taun);  
ni=1.0e10;  
I0=q*A*DN/LN*ni^2/NA;  
VA=[-50 -0.1 0.1 0.5];  
I=I0*(exp(VA./(k*T))-1)
```

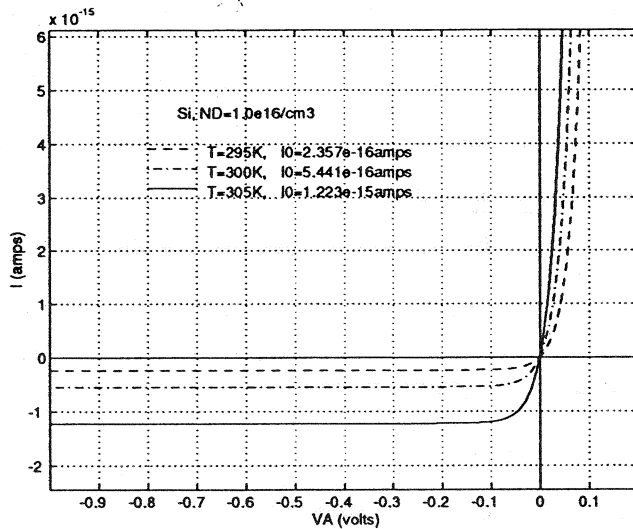
I = -9.4345e-14 A	...for $V_A = -50V$
-9.2374e-14 A	...for $V_A = -0.1V$
4.4212e-12 A	...for $V_A = 0.1V$
2.3696e-05 A	...for $V_A = 0.5V$

```
%(b) Currents at T=500K  
ni=2.716e14; %Value from table in Exercise 2.4  
T=500;  
μn=(1345)*(T/300)^(-2.3); %See Fig. 3.7a (approx. value)  
DN=k*T*μn;  
LN=sqrt(DN*taun);  
I0=q*A*DN/LN*ni^2/NA;  
I=I0*(exp(VA./(k*T))-1)
```

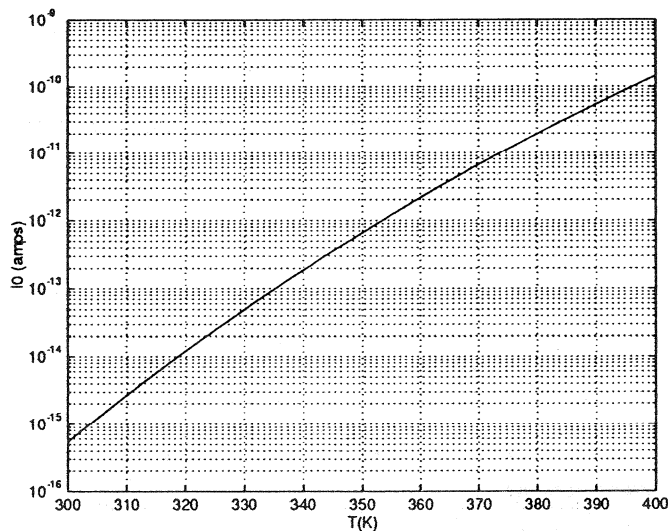
I = -4.9932e-05 A	...for $V_A = -50V$
-4.5030e-05 A	...for $V_A = -0.1V$
4.5866e-04 A	...for $V_A = 0.1V$
5.4745e+00 A	...for $V_A = 0.5V$

## 6.7

(a) Sample ideal-diode  $I-V T$ -dependence plot



(b)  $I_0$  versus  $T$  plot



(c) MATLAB m-files P\_06\_07a.m and P\_06\_07b.m, available on the Instructor's disk, were used to generate the part (a) and part (b) plots, respectively. Both plots verify the very strong temperature dependence of the ideal-diode  $I-V$  characteristics. Only a 5 K rise in temperature leads to a very significant increase in the part (a) current; the part (b) plot exhibits over a  $10^5$  increase in  $I_0$  associated with a 100 K increase in temperature!

## 6.8

(a) Let us examine the minority carrier diffusion equation for hole. In general

$$\frac{\partial \Delta p_n}{\partial t} = D_p \frac{\partial^2 \Delta p_n}{\partial x^2} - \frac{\Delta p_n}{\tau_p} + G_L$$

For the steady state problem at hand  $\partial \Delta p_n / \partial t = 0$ . Also,  $\partial^2 \Delta p_n / \partial x^2 = 0$  if one goes far from the junction on the *n*-side where the carrier perturbation introduced by the junction has decayed to zero. Thus

$$0 = - \frac{\Delta p_n(x \rightarrow \infty)}{\tau_p} + G_L$$

or

$$\Delta p_n(x \rightarrow \infty) = G_L \tau_p \quad \Leftarrow \text{boundary condition}$$

(b) One simply parallels the ideal diode derivation to obtain the desired  $I-V_A$  relationship. Given a  $p^+ - n$  junction, however, we need consider only the lightly doped *n*-side of the junction. Specifically, under steady state conditions and with  $x'$  as defined in Fig. 6.5(a), we must solve

$$0 = D_p \frac{d^2 \Delta p_n}{dx'^2} - \frac{\Delta p_n}{\tau_p} + G_L$$

subject to the boundary conditions

$$\Delta p_n(x' = 0) = (n_i^2/N_D)(e^{qV_A/kT} - 1)$$

$$\Delta p_n(x' \rightarrow \infty) = G_L \tau_p$$

The general solution is

$$\Delta p_n(x') = G_L \tau_p + A_1 e^{-x'/L_p} + A_2 e^{x'/L_p}$$

Because  $\exp(x'/L_p) \rightarrow \infty$  as  $x' \rightarrow \infty$ , the only way the second boundary condition can be satisfied is for  $A_2$  to be identically zero. With  $A_2 = 0$ , the application of the first boundary condition yields

$$\Delta p_n(x' = 0) = G_L \tau_p + A_1 = (n_i^2/N_D)(e^{qV_A/kT} - 1)$$

or

$$A_1 = (n_i^2/N_D)(e^{qV_A/kT} - 1) - G_L \tau_p$$

and

$$\Delta p_n(x') = G_L \tau_p + [(n_i^2/N_D)(e^{qV_A/kT} - 1) - G_L \tau_p] e^{-x'/L_p}$$

The associated hole current density is then

$$J_P(x') = -qD_P \frac{d\Delta p_n}{dx'} = q \frac{D_P}{L_P} \left[ (n_i^2/N_D) (e^{qV_A/kT} - 1) - G_L \tau_p \right] e^{-x'/L_P}$$

and for a  $p^+-n$  diode

$$I = AJ = A[J_N(x=-x_p) + J_P(x=x_n)] \equiv AJ_P(x'=0)$$

or

$$I = qA \frac{D_P}{L_P} \frac{n_i^2}{N_D} (e^{qV_A/kT} - 1) - qA \frac{D_P \tau_p}{L_P} G_L$$

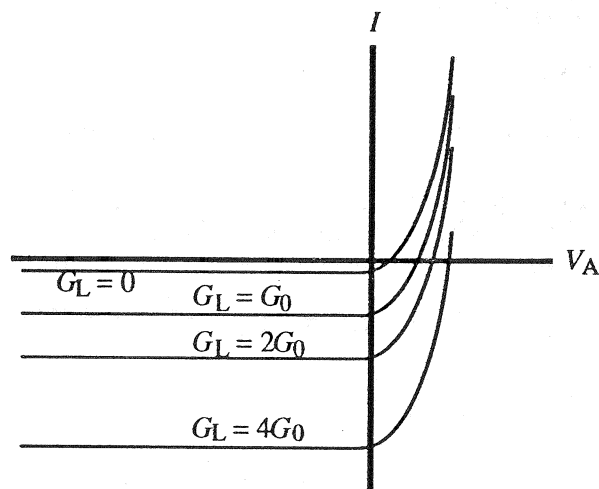
Finally noting  $D_P \tau_p = L_P^2$ , we conclude

$$I = I_0 (e^{qV_A/kT} - 1) + I_L$$

$$\text{where } I_0 = qA \frac{D_P}{L_P} \frac{n_i^2}{N_D}$$

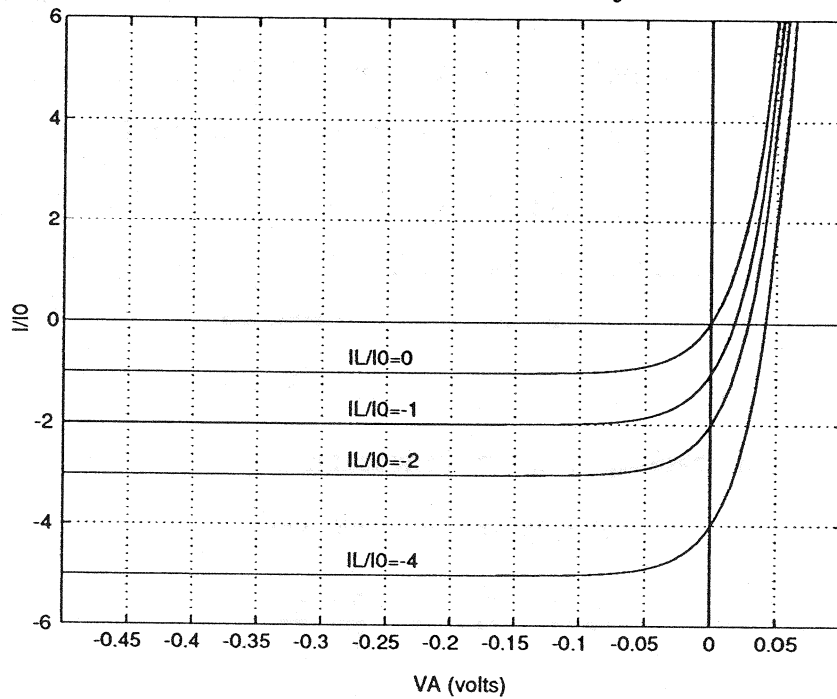
$$I_L = -qAL_P G_L$$

(c) In constructing the characteristics we note that the usual ideal-diode characteristic results if  $G_L = 0$ . A  $G_L \neq 0$  characteristic is obtained by subtracting the same constant value from all  $I$ -values on the dark ( $G_L = 0$ ) curve. Effectively, the entire dark  $I-V$  curve is simply translated downward by an amount equal to  $I_L$ . Since  $I_L \propto G_L$ , the downward translation increases in proportion to  $G_L$ . The characteristics are concluded to be of the form sketched below.



## 6.9

General nature of the  $I-V$  characteristics of a solar cell subject to illumination...



MATLAB program script used to generate the characteristics...

```
%Solar Cell Characteristics
%Initialization
clear; close
%Constants
k=8.617e-5; T=300;
%Computation Proper
VA=linspace(-0.5,0.1);
I1=exp(VA./(k*T))-1; %I/I0 with IL/I0=0
I2=I1-1; I3=I1-2; I4=I1-4;
I=[I1; I2; I3; I4];
%Plotting Result
plot(VA,I)
axis([-0.5 0.1 -6 6]); grid
xlabel('VA (volts)'); ylabel('I/I0');
text(-0.28,-0.7,'IL/I0=0'); text(-0.28,-1.7,'IL/I0=-1');
text(-0.28,-2.7,'IL/I0=-2'); text(-0.28,-4.7,'IL/I0=-4');
xx=[-0.5 0.1]; xy=[0 0]; yx=[0 0]; yy=[-6 6];
hold on
plot(xx,xy,'-w',yx,yy,'-w')
```

### 6.10

(a) [Reverse biased] — there is a deficit of minority carrier in the quasineutral region immediately adjacent to the depletion region.

(b) Low-level injection DOES prevail. As required for low-level injection

$$|\Delta n_p|_{\max} \approx n_{p0} \ll p_p \quad \dots \text{for } x \leq -x_p$$

$$|\Delta p_n|_{\max} \approx p_{n0} \ll n_n \quad \dots \text{for } x \geq x_n$$

(c) Since we have low level injection,

$$N_A \approx p_{p0} \approx p_p = 10^{14}/\text{cm}^3$$

$$N_D \approx n_{n0} \approx n_n = 10^{15}/\text{cm}^3$$

(d) Invoking the law of the junction,

$$n(-x_p)p(-x_p) = n_i^2 e^{qV_A/kT}$$

or

$$V_A = \frac{kT}{q} \ln \left[ \frac{n(-x_p)p(-x_p)}{n_i^2} \right]$$

As deduced from Fig. P6.10,

$$n(-x_p) = 10^3/\text{cm}^3$$

$$p(-x_p) = 10^{14}/\text{cm}^3$$

and

$$n_i = \sqrt{n(\infty)p(\infty)} = \sqrt{n(-\infty)p(-\infty)} = \sqrt{10^{20}} = 10^{10}/\text{cm}^3$$

The foregoing manipulation to obtain  $n_i$  was necessary because the semiconductor used in fabricating the diode was not specified in the problem statement. Lastly, substituting into the  $V_A$  expression gives

$$V_A = (0.0259) \ln \left[ \frac{(10^3)(10^{14})}{10^{20}} \right] = -0.18\text{V}$$

### 6.11

Under equilibrium conditions

$$\begin{aligned} p_{p0} &= N_A = 10^{17}/\text{cm}^3 & n_{n0} &= N_D = 10^{16}/\text{cm}^3 \\ n_{p0} &= n_i^2/N_A = 10^3/\text{cm}^3 & p_{n0} &= n_i^2/N_D = 10^4/\text{cm}^3 \end{aligned}$$

Invoking the depletion edge boundary conditions (Eqs. 6.15 and 6.18) gives

$$\Delta n_p(-x_p) = (n_i^2/N_A)(e^{qV_A/kT} - 1) = (10^3)e^{23.03} = 10^{13}/\text{cm}^3$$

$$\Delta p_n(x_n) = (n_i^2/N_D)(e^{qV_A/kT} - 1) = (10^4)e^{23.03} = 10^{14}/\text{cm}^3$$

Since the perturbed carrier concentrations in the quasineutral regions are greatest at the depletion region edges, and since  $\Delta n_p(-x_p) \ll p_{p0}$  and  $\Delta p_n(x_n) \ll n_{n0}$ , we have low-level injection. This makes  $p_p \approx p_{p0}$  everywhere on the  $p$ -side of the junction and  $n_n \approx n_{n0}$  everywhere on the  $n$ -side of the junction.

Next invoking the ideal diode solution, we can write

$$n_p = n_{p0} + \Delta n_p(-x_p)e^{-x''/L_N}$$

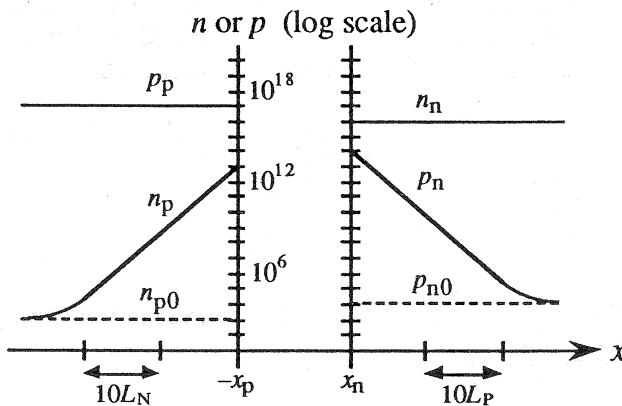
and

$$p_n = p_{n0} + \Delta p_n(x_n)e^{-x'/L_P}$$

Thus at points 0, 10, and 20 diffusion lengths from the depletion region edges we compute

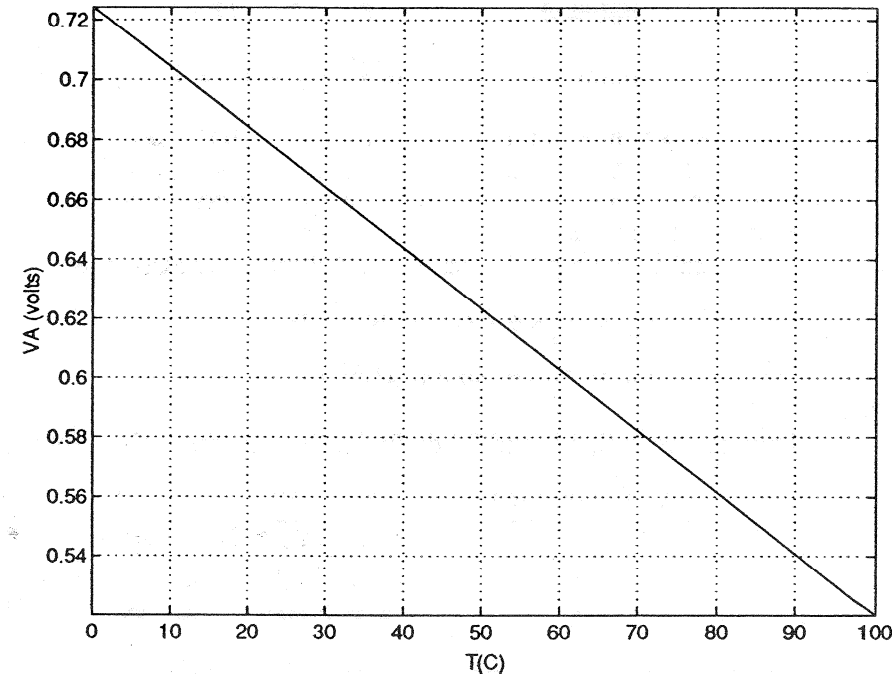
$x''/L_N$ or $x'/L_P$	$n_p(\text{cm}^{-3})$	$p_n(\text{cm}^{-3})$
0	$10^{13}$	$10^{14}$
10	$4.54 \times 10^8$	$4.54 \times 10^9$
20	$2.16 \times 10^4$	$2.16 \times 10^5$ (~5% $n_{p0}$ or $p_{n0}$ contribution)

The sketch constructed using the foregoing data is shown below.



### 6.12

(a) Reproduced below is the requested sample plot of the  $V_A$  versus  $T$  expected from the specified  $pn$  diode temperature sensor when the forward bias current through the diode is held constant at  $I = 10^{-4}$  A. The plot was produced using MATLAB file P\_06\_12.m supplied on the Instructor's disk. Note the nearly linear dependence of  $V_A$  on the ambient temperature. A linear temperature dependence of the monitored parameter is of course highly desirable in producing a temperature sensor.



(b) After running the program with a given  $I$  setting, the Command window in MATLAB can be used to access the  $V_A$  values corresponding to  $T = 0^\circ\text{C}$  and  $T = 100^\circ\text{C}$ . For the two currents cited in the problem one finds:

$I$	$V_A$ (volts) at $T = 0^\circ\text{C}$	$V_A$ (volts) at $T = 100^\circ\text{C}$	$\Delta V_A / \Delta T$ (V/ $^\circ\text{C}$ )
$10^{-4}$	0.724	0.520	$2.04 \times 10^{-3}$
$10^{-3}$	0.779	0.594	$1.85 \times 10^{-3}$

The computation results clearly indicate the sensitivity of the sensor is greater when  $I = 10^{-4}$  A.

### 6.13

(a) As read from Fig. 6.11,  $V_{BR} \equiv 320$  V.

$$(b) W = \left[ \frac{2K_S \epsilon_0}{qN_D} (V_{bi} - V_A) \right]^{1/2} = \left[ \frac{2K_S \epsilon_0}{qN_D} V_{BR} \right]^{1/2} = \left[ \frac{(2)(11.8)(8.85 \times 10^{-14})(320)}{(1.6 \times 10^{-19})(10^{15})} \right]^{1/2}$$

$$= 2.04 \times 10^{-3} \text{ cm} = 20.4 \mu\text{m}$$

$$(c) |E|_{max} = |\mathcal{E}(0)| = \frac{qN_D}{K_S \epsilon_0} x_n = \frac{qN_D}{K_S \epsilon_0} W = \frac{(1.6 \times 10^{-19})(10^{15})(2.04 \times 10^{-3})}{(11.8)(8.85 \times 10^{-14})}$$

$$= 3.13 \times 10^5 \text{ V/cm}$$

### 6.14

(a) As the student hopefully discovers, the problem statement is very misleading. Although a possible solution approach, the modification of Exercise 6.2 to obtain the desired reverse-bias  $I/I_0$  versus  $V_A$  plot is extremely inefficient. With the current normalized by  $I_0$ , one can write

$$I/I_0 = M(e^{qV_A/kT} - 1) \quad \dots V_A \leq 0$$

The only parameters required for the computation are  $m$  and  $N_D$ . Moreover, except for the normally inconsequential portion of the plot near  $V_A = 0$ , and the fact that the  $x$ -axis is not normalized to  $V_{BR}$ , the plot produced is *identical* to the  $m = 6$  plot in Exercise 6.5.

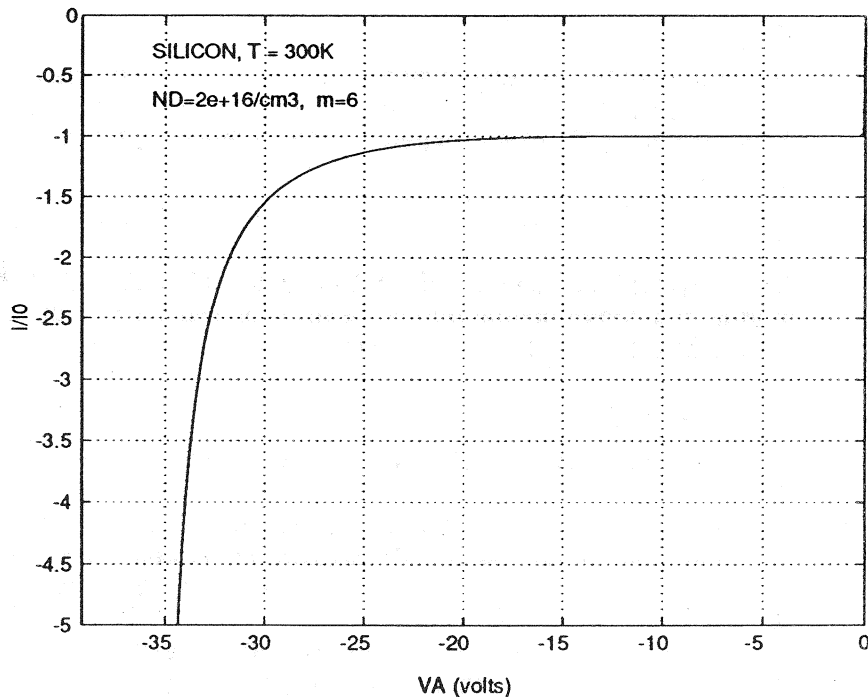
MATLAB program script...

```
% Breakdown-included Reverse Bias I-VA Characteristics
%
% This program assumes an ideal diode with the one modification
% that avalanche multiplication is taken into account using:
% M=1/(1-(abs(VA)/VBR)^m).
%
% Appropriate for Si diodes at 300K, VBR is calculated from
% VBR = 60*(ND/1e16)^(-3/4)
%
% Initialization
clear; close
%
% Computational Constants
kT=0.0259;
ND=input('Input the n-side doping, ND = ');
m=input('Input the value of m (3≤m≤6), m = ');
```

```

% VBR, M calculation
VBR=60*(ND/1e16)^(-3/4);
VA1=linspace(-VBR+.1,-0.1,200);
VA2=linspace(-0.1,0,25);
VA=[VA1,VA2];
M=(1-abs(VA./VBR).^m).^(-1);
% I/I0 Calculation
Iratio=M.* (exp(VA./(kT))-1);
% Plot
plot(VA',Iratio')
axis([-1.1*VBR(1),0,-5,0]); grid
xlabel('VA (volts)'); ylabel('I/I0')
text(-VBR,-0.3,'SILICON, T = 300K')
text(-VBR,-0.7,['ND=',num2str(ND(1)), '/cm3, m=',num2str(m)])

```



- (b) Like in Exercise 6.5, the approach to breakdown becomes more gradual with decreasing values of  $m$ . Varying  $N_D$  has no effect on the general shape of the curve, although the breakdown voltage does of course increase with  $N_D$ .

### 6.15

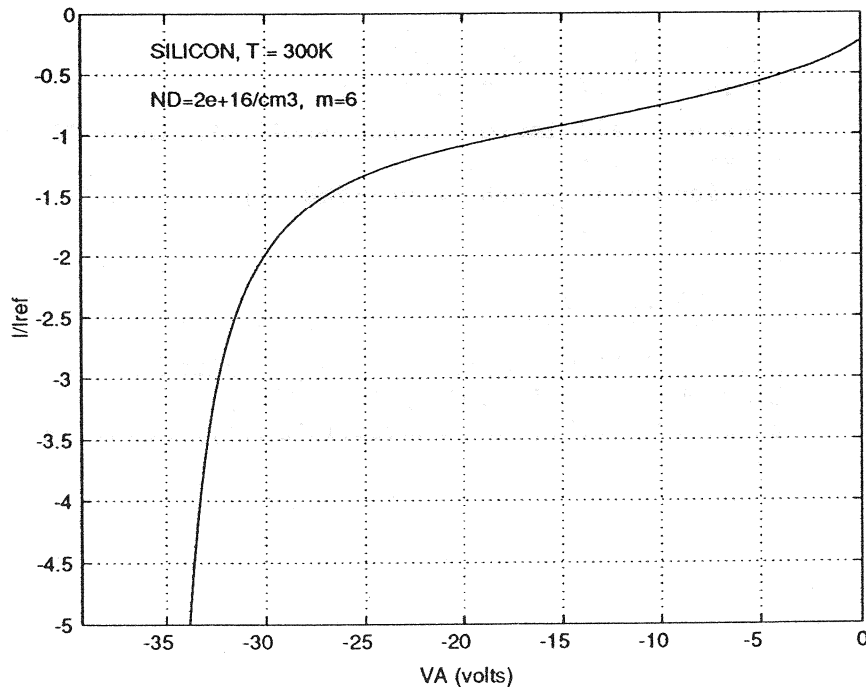
If normalized properly, the  $\tau_0$  supplied in the statement of the problem is not required. Specifically,

$$\frac{I_{R-G}(V_A)}{|I_{R-G}(-V_{BR}/2)|} = -M \frac{W(V_A)}{W(-V_{BR}/2)} = -M \sqrt{\frac{V_{bi}-V_A}{V_{bi}+V_{BR}/2}} \quad \dots \text{reverse biases} > \text{few } kT/q$$

where, assuming a  $p^+-n$  junction,

$$V_{bi} \equiv E_G/2q + (kT/q) \ln(N_D/n_i)$$

As might be suspected from the fact that the  $I_{R-G}$  current typically dominates in reverse-biased Si diodes at room temperature, the sample computational plot reproduced below has a general shape very close to the experimental data presented in Fig. 6.10(b). The  $N_D$  employed in the sample computation was even chosen to yield a close approximation to the observed  $V_{BR}$ . Note, however, that the final approach to  $V_{BR}$  in the theoretical plot is more gradual than that observed experimentally.



MATLAB program script (Problem 6.15)...

```
% Breakdown-included Reverse Bias I-VA Characteristics
% Si, p+n, 300K
% This program assumes Ireverse=IR-G
% Avalanche multiplication is taken into account using:
% M=1/(1-(abs(VA)/VBR)^m).
%
% VBR is calculated from
% VBR = 60*(ND/1e16)^(-3/4)
% Initialization
clear; close
% Universal and System Constants
kT=0.0259;
EG=1.12;
ni=1.0e10;
ND=input('Input the n-side doping, ND = ');
m=input('Input the m value (3≤m≤6), m = ');
%
% VBR, M calculation
VBR=60*(ND/1e16)^(-3/4);
VA=linspace(-VBR+0.1,-0.1,200);
M=(1-abs(VA./VBR).^m).^(1-m);
%
% Current Calculation [Iratio=IRG(VA)/|IRG(-VBR/2)|]
Vbi=EG/2+kT.*log(ND./ni);
Wratio=sqrt((Vbi-VA)./(Vbi+VBR/2));
Iratio=-M.*Wratio;
%
% Plot
plot(VA,Iratio)
axis([-1.1*VBR(1),0,-5,0]); grid
xlabel ('VA (volts)'); ylabel ('I/Iref');
text(-VBR,-0.3,'SILICON, T = 300K')
text(-VBR,-0.7,['ND=',num2str(ND(1)), '/cm3, m=',num2str(m)])
```

### 6.16

We know

$$I_{\text{DIFF}} = -I_0 = -qA \frac{n_i^2}{N_D} \frac{D_P}{L_P}$$

and

$$I_{\text{R-G}} = -qA \frac{n_i}{2\tau_0} W$$

Equating  $I_{\text{DIFF}}$  and  $I_{\text{R-G}}$  yields the requirement

$$\frac{n_i}{N_D} \frac{D_P}{L_P} = \frac{W}{2\tau_0}$$

Assuming  $\tau_0 = \tau_p$ , as suggested in the problem statement, and solving for  $n_i$ , gives

$$n_i(T_D) = N_D \frac{L_P}{2D_P \tau_p} W = N_D \frac{W}{2L_P}$$

where  $T_D$  is the transition temperature above which the diffusion component of the current is expected to dominate. With  $V_{bi} - V_A = V_{BR}/2$  and  $V_{BR}$  read from Fig. 6.11, we compute

$$W = \left[ \frac{2K_S \epsilon_0}{qN_D} (V_{bi} - V_A) \right]^{1/2} = \left[ \frac{K_S \epsilon_0}{qN_D} V_{BR} \right]^{1/2} = \left[ \frac{(11.8)(8.85 \times 10^{-14})(55)}{(1.6 \times 10^{-19})(10^{16})} \right]^{1/2} \\ = 1.89 \times 10^{-4} \text{ cm}$$

and

$$n_i(T_D) = N_D \frac{W}{2L_P} = \frac{(10^{16})(1.89 \times 10^{-4})}{(2)(10^{-2})} \cong 10^{14}/\text{cm}^3$$

From the Fig. 2.20 plot of  $n_i$  versus  $T$  we conclude  $T_D \cong 470 \text{ K}$ .

### 6.17

Let  $x_1$  and  $x_2$  be the ends of the  $d$ -region, with  $d = x_2 - x_1$ . Also let  $\tau_{01}$  and  $\tau_{02}$  be the generation lifetime outside and inside the  $d$ -region, respectively. Clearly, based on Eq. (6.42),

$$\begin{aligned} I_{R-G} &= -qA \int_{-x_p}^{x_n} \frac{n_i}{\tau_p(n_1/n_i) + \tau_n(p_1/n_i)} dx \\ &= -qA \left[ \int_{-x_p}^{x_1} \frac{n_i}{2\tau_{01}} dx + \int_{x_1}^{x_2} \frac{n_i}{2\tau_{02}} dx + \int_{x_2}^{x_n} \frac{n_i}{2\tau_{01}} dx \right] \\ &= -qA \left[ \frac{n_i}{2\tau_{01}} (W-d) + \frac{n_i}{2\tau_{02}} d \right] \end{aligned}$$

Since  $\tau_n$  and  $\tau_p$  are both proportional to  $1/N_T$ , it follows that  $\tau_{02} = \tau_{01}/3$  and

$$I_{R-G} = -\frac{qAn_i}{2\tau_{01}} (W + 2d)$$

### 6.18

At the desired  $I$ -value, we infer from the statement of the problem that

$$V_A = V_J + IR_S = 1.1V_J$$

or

$$V_J = 10IR_S$$

Thus at the specified operational point (invoking Eq. 6.49),

$$I = I_0 e^{qV_J/kT} = I_0 e^{(10IR_S)/(kT/q)} = (10^{-14}) e^{(10IR_S)/(0.0259)}$$

An iterative technique, employing the fzero function in MATLAB for example, must be used to numerically solve the transcendental equation for  $I$ . We find...

- (a) If  $R_S = 2 \Omega$ ,  $I = 37.5 \text{ mA}$ .
- (b) If  $R_S = 20 \Omega$ ,  $I = 3.44 \text{ mA}$ .

### 6.19

The lines drawn manually by the author through the straight-line regions (roughly  $0.12V \leq V_A \leq 0.5V$  and  $0.64V \leq V_A \leq 0.76V$ ) on the Fig. P6.19 plot were found to pass through the  $(V_A, I)$  points

$$\begin{array}{ll} (0.20V, 10^{-10}A), (0.92V, 1A) & \dots 0.64V \leq V_A \leq 0.76V \text{ region} \\ (0V, 10^{-9}A), (1V, 2 \times 10^{-2}A) & \dots 0.12V \leq V_A \leq 0.5V \text{ region} \end{array}$$

Employing the relationships presented in Exercise 6.7, we conclude

$$n_1 = \frac{0.92 - 0.20}{(0.0259) \ln(1/10^{-10})} = 1.21$$

$$n_2 = \frac{1}{(0.0259) \ln(2 \times 10^{-2}/10^{-9})} = 2.30$$

$$I_{01} = I/e^{qV_A/n_1 kT} \Big|_{V_A=0.2V} = (10^{-10})/e^{0.2/[(1.21)(0.0259)]} \cong 1.7 \times 10^{-13} A$$

$$I_{02} = (\text{extrapolated } V_A=0 \text{ intercept}) \cong 10^{-9} A$$

A MATLAB program, listed after the discussion of results and incorporating the polyfit function, was used to effect a least squares fit to the data in the straight-line regions. The fit yields

$$\ln(I) = -29.68 + 32.45V_A \quad \dots 0.64V \leq V_A \leq 0.76V$$

$$n_1 = 1.19$$

$$I_{01} = 1.29 \times 10^{-13} A$$

$$\ln(I) = -20.57 + 16.67V_A \quad \dots 0.12V \leq V_A \leq 0.5V$$

$$n_2 = 2.32$$

$$I_{02} = 1.16 \times 10^{-9} A$$

The agreement between the manual and least-square approaches is amazingly good. As a general rule, data which has minimal noise can be accurately analyzed using the manual approach. In either case, the  $n_1$  and  $n_2$  values came out a bit larger than expected. (The author believes the high value for  $n_2$  was caused by a non-negligible shunt conductance.—See Prob. 6.21.) Note, however, that  $I_{02} \gg I_{01}$  as expected.

### MATLAB fit program script...

```
%Least squares fit for Problem 6.19.  
%Initialization  
clear; format short e  
format compact  
%Data  
s=menu('CHOOSE VOLTAGE REGION', '0.64V≤VA≤0.76V', '0.12V≤VA≤0.5V');  
if s==1,  
    VA=0.64:0.02:0.76;  
    I=[1.359e-4, 2.531e-4, 4.852e-4, 9.444e-4, 1.841e-3, 3.518e-3, 6.433e-3];  
else  
    VA=0.12:0.02:0.5;  
    I=[8.210e-9, 1.183e-8, 1.73e-8, 2.449e-8, 3.416e-8, 4.764e-8, 6.501e-8, ...  
        8.866e-8, 1.209e-7, 1.666e-7, 2.305e-7, 3.201e-7, 4.462e-7, 6.285e-7, ...  
        8.845e-7, 1.249e-6, 1.776e-6, 2.527e-6, 3.615e-6, 5.2e-6];  
end  
%Computation  
y=log(I);  
p=polyfit(VA,y,1);  
y0=p(2)  
slope=p(1)  
nj=1/(0.0259*slope)  
I0=exp(y0)
```

### 6.20

We take the slope-over in the  $I$ - $V$  characteristics for  $V_A \geq 0.8V$  to be caused by the series resistance,  $R_S$ . In what follows, we determine the extrapolated "ideal" ( $R_S=0$ ) voltage required to achieve a given current level by employing the least squares fit to the near-ideal data region established in Prob. 6.19. Specifically,

$$I = I_{01} e^{qV_A/n_1 kT} = (1.29 \times 10^{-13}) e^{V_A / [(1.19)(0.0259)]}$$

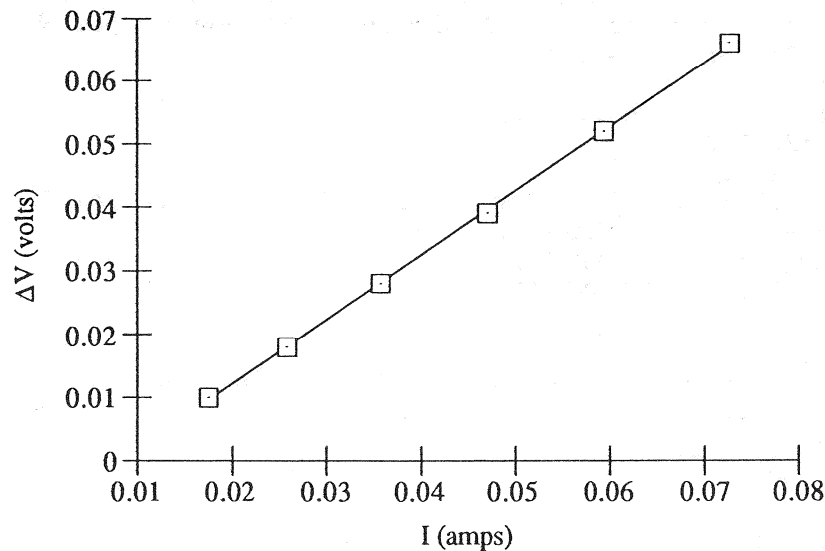
or

$$V_A(\text{ideal}) = (1.19)(0.0259) \ln(I / 1.29 \times 10^{-13})$$

One computes...

$I$ (amps)	$V_A$ (observed)	$V_A$ (ideal)	$\Delta V$
0.01752	0.800	0.790	0.010
0.02585	0.820	0.802	0.018
0.03579	0.840	0.812	0.028
0.04706	0.860	0.821	0.039
0.05941	0.880	0.828	0.052
0.07264	0.900	0.834	0.066

Plotting the data...



A least squares fit to the data yields  $\Delta V = -0.0082 + 1.02I$ , and  $R_S = \text{slope} = 1.02 \text{ ohm}$ .

### 6.21

(a) This part of the problem was included to make sure that the student had the correct computational relationships. Obviously, the total current flowing through the device is equal to the current through the ideal representation plus the current through  $R_{SH}$ . Since  $V_J$  is the voltage drop across  $R_{SH}$ , we conclude

$$I = I_J + I_{SH} = I_J + V_J/R_{SH}$$

It is also obvious from the Fig. P6.21 circuit that the applied voltage is dropped in part across the *pn* junction and in part across  $R_S$ . Since  $I$  is the current flowing through  $R_S$ ,

$$V_A = V_J + IR_S$$

(b)-(e) A single MATLAB program, listed below and included on the instructor's disk, was constructed to perform the required computations in parts (b)-(e) of the problem. Menus provided in the program allow the user to obtain the graphical solutions associated with a given part of the problem. Sample program output is included after the program listing.

MATLAB program script...

```
%GENERALIZED DIODE I-V CHARACTERISTICS
%Initialization
clear; close
p=menu('CHOOSE THE TYPE OF PLOTS', 'Semilog', 'Linear');
%Model Parameters
s=menu('CHOOSE PARAMETER INPUT', 'Basic Parameter List', ...
'I01 and I02 computed', 'Arbitrary Model Parameters');
I01=1.0e-13; I02=1.0e-9;
n1=1; n2=2;
RS=1; RSH=1.0e12;
if s==2, I00;
elseif s==3,
AMP=input('Input in order inside [ ], I01,I02,n1,n2,RS,RSH... ');
I01=AMP(1); I02=AMP(2);
n1=AMP(3); n2=AMP(4);
RS=AMP(5); RSH=AMP(6);
else
end
jj=menu('CHOOSE THE PARAMETER TO BE VARIED', ...
'None', 'RSH', 'RS', 'I02', 'I01');
if jj==1, j=1;
else j=4;
end
for ii=1:j,
    %Computation Proper
    VJ=linspace(0.01,1.00);
    kT=0.0259;
```

```

I=I01*(exp(VJ/(n1*kT))-1)+I02*(exp(VJ/(n2*kT))-1)+VJ/RSH;
VA=VJ+I*RS;

%Plotting Result
if p==1,
semilogy(VA,I)
axis([0, 1, 1.0e-10, 1.0e-2]); grid on
xlabel('VA (volts)'); ylabel('I (amps)')
hold on
else
plot(VA,I);
axis([0,1,0,1.0e-2]); grid on
xlabel('VA (volts)'); ylabel('I (amps)')
hold on
end

%Resetting the variable parameter
if jj==2, RSH=RSH*1.0e-3;
elseif jj==3, RS=RS*10;
else
if jj==4, I02=I02*1.0e-1;
elseif jj==5, I01=I01*1.0e1;
else
end
end
end

```

*Subprogram I00 (Required for part d)*

```

%IO1 and IO2 Calculation from first principles
%Constants and Parameters
q=1.6e-19;
e0=8.85e-14;
kT=0.0259;
ni=1.0e10;
KS=11.8;
EG=1.12;

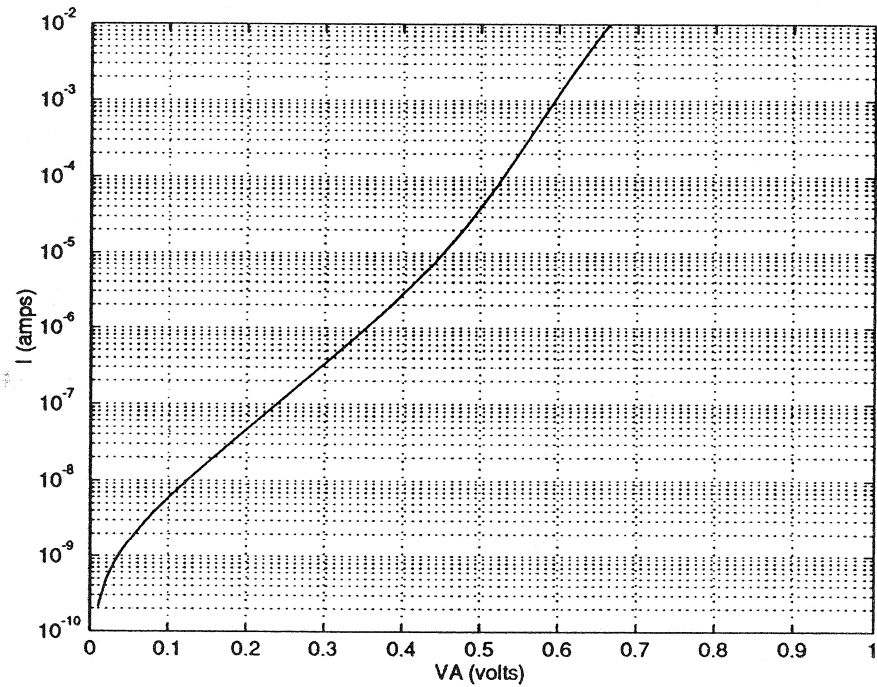
%Parameters
A=1.0e-2;
NA=1.0e15;
μn=1345;
tau=1.0e-6;

%Computed Constants
Vbi=EG/2+kT*log(NA/ni);
VA0=Vbi/4;
W0=sqrt(2*KS*e0/(q*NA)*(Vbi-VA0));

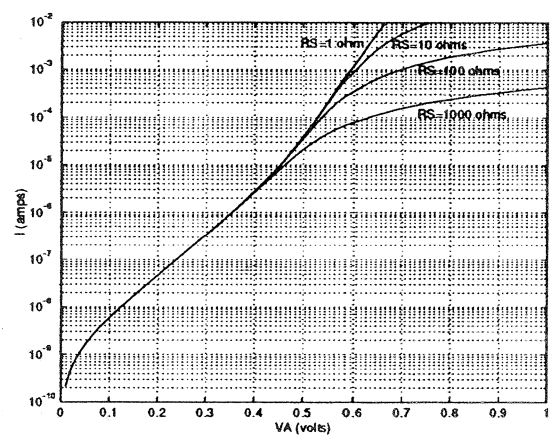
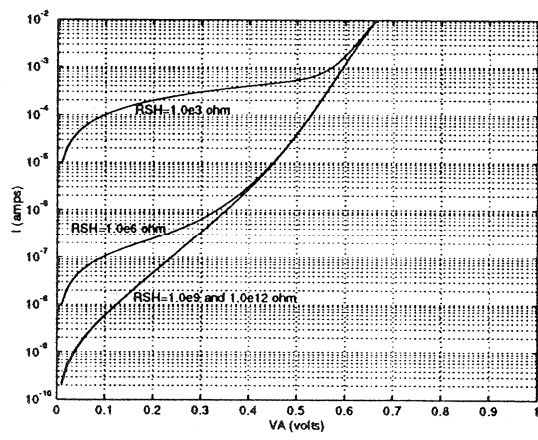
%Desired Quantities
I01=q*A*(ni^2/NA)*sqrt(kT*μn/tau)
I02=(q*A*ni*W0/tau)*(kT/(Vbi-VA0))

```

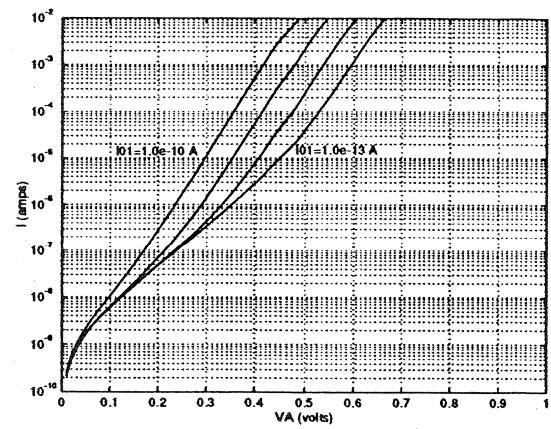
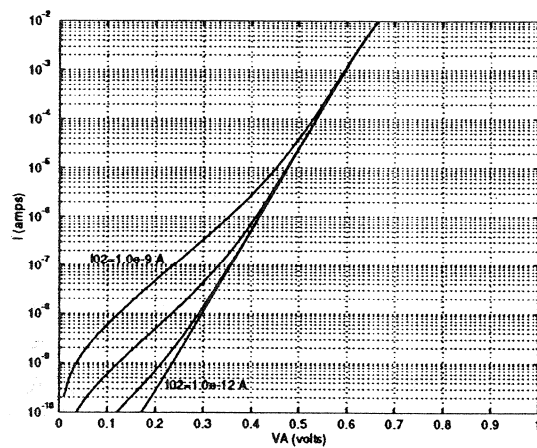
(b) -----



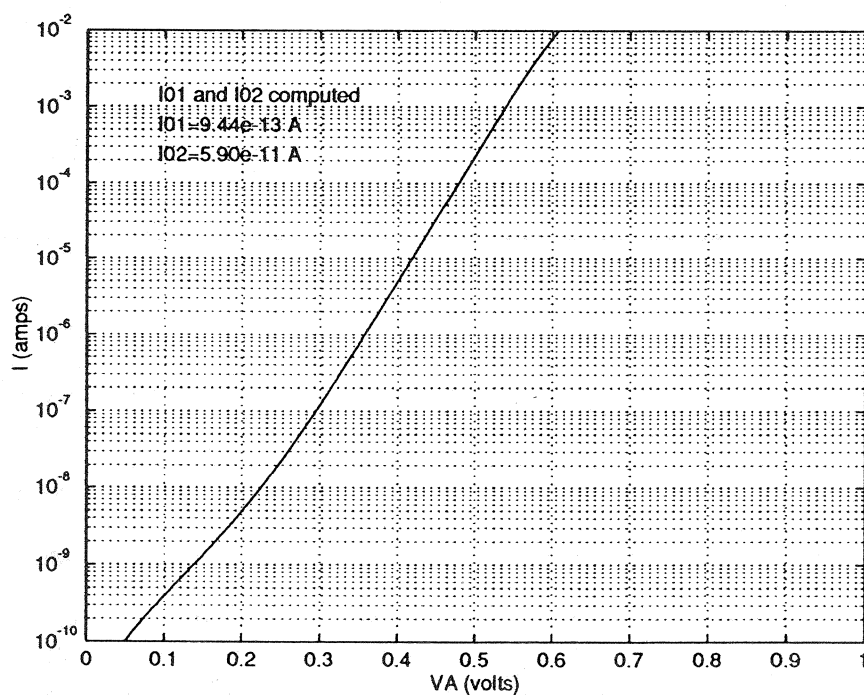
(c) -----

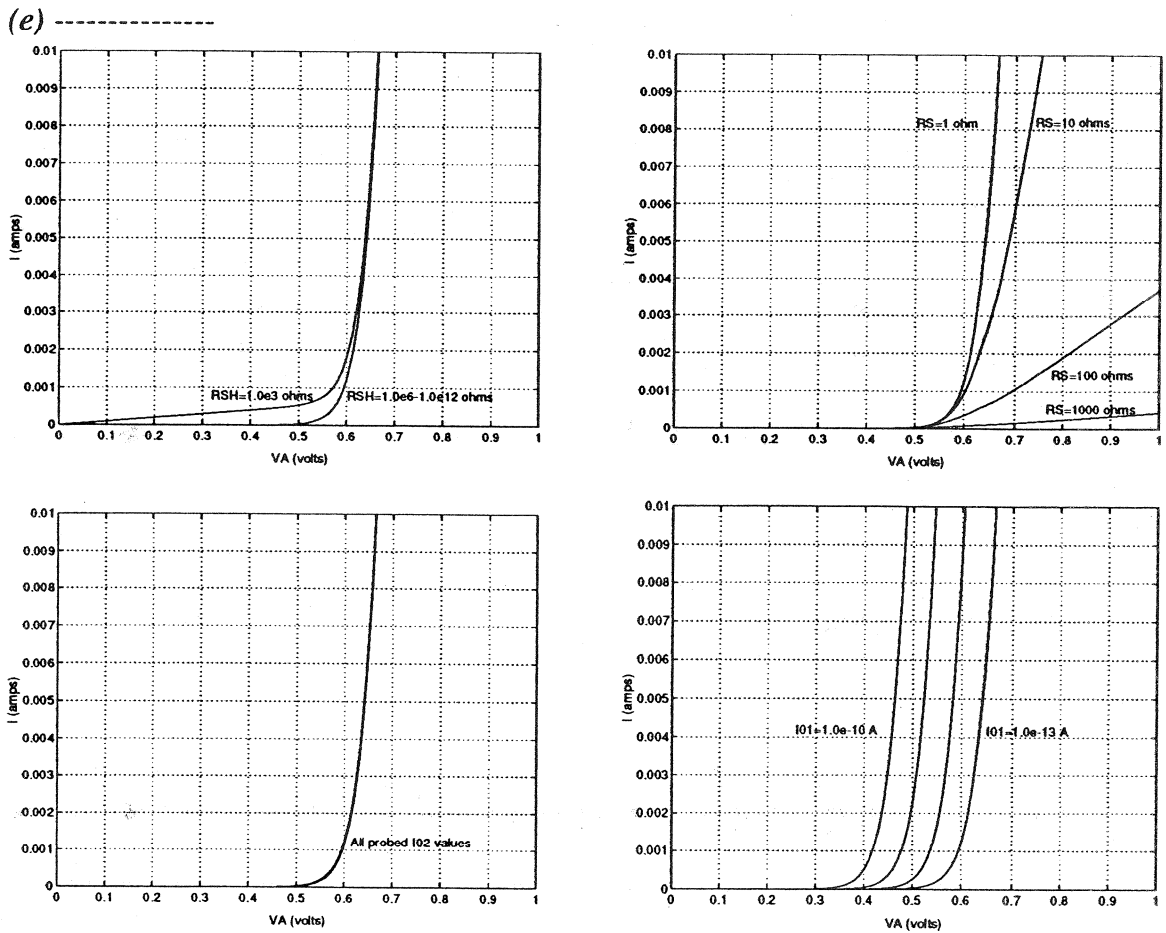


(c) (Continued)



(d) -----





**Comparison:** The same results presented employing semilog plots in part (c) and linear plots in part (e) provide a decidedly different view of how a parameter affects the observed characteristics. The effect of varying  $I_{02}$  over three orders of magnitude is not observable on the linear plot (which emphasizes the higher current levels) but is clearly visible on the semilog plot. On the other hand, the effect of the series resistance is much more dramatic when viewed on a linear scale. Although the semilog plots tend to be more informative, the comparative results here suggest that it would be worthwhile to observe the forward bias  $I$ - $V$  curves on both a semilog and linear scale when evaluating the characteristics.

(f) Part (b) confirms the general viability of the computational approach, yielding results that correspond very closely to experimentally observed characteristics. Part (d) confirms that a "first principle" computation of the  $I_0$ 's yields similar results. Parts (c) and (e) illustrate how common nonidealities affect the observed forward bias  $I$ - $V$  characteristics. Since an examination of the  $I$ - $V$  characteristics is often made to deduce information about an exploratory or defective device, the information provided has significant practical utility.

## 6.22

We make the following observations:

- (1)  $\Delta p_n$  must = 0 for  $x_b \leq x \leq x_c$  because  $\tau_p = 0$ . This yields the boundary condition  $\Delta p_n = 0$  at  $x = x_b$ .
- (2) Because we have a  $p^+ - n$  diode, we need only deal with the  $n$ -side of the junction in establishing an expression for  $I$ . Moreover, the depletion width is all but totally on the  $n$ -side of the junction given a  $p^+ - n$  diode (i.e.,  $x_n \approx W$ ).
- (3) Because  $\tau_p = \infty$  for  $0 \leq x \leq x_b$ , there will be no  $I_{R-G}$  current. ( $\tau_p = \infty$  implies that there are no R-G centers.) Thus, we need only develop an expression for the diffusion current flowing in the diode.

Let us proceed with the derivation. Since we are interested in the static state,  $\partial \Delta p_n / \partial t = 0$ . Also,  $G_L = 0$  (no light) and  $\Delta p_n / \tau_p \rightarrow 0$  because  $\tau_p = \infty$ . Thus the minority carrier diffusion equation reduces to the form

$$d^2 \Delta p_n / dx^2 = 0 \quad \dots W \leq x \leq x_b$$

subject to the boundary conditions

$$\Delta p_n(x_b) = 0 \quad \text{and} \quad \Delta p_n(W) = (n_i^2 / N_D) (e^{qV_A/kT} - 1)$$

The general (narrow-base type) solution is

$$\Delta p_n(x) = A_1 + A_2 x$$

Applying the boundary conditions

$$0 = A_1 + A_2 x_b \quad \text{and} \quad \Delta p_n(W) = A_1 + A_2 W$$

giving

$$\Delta p_n(W) = -A_2(x_b - W) \quad \text{or} \quad A_2 = -\Delta p_n(W)/(x_b - W)$$

and

$$A_1 = -A_2 x_b = \Delta p_n(W) \frac{x_b}{x_b - W}$$

Thus  $\Delta p_n(x) = \Delta p_n(W) \left( \frac{x_b - x}{x_b - W} \right) = \frac{n_i^2}{N_D} \left( \frac{x_b - x}{x_b - W} \right) (e^{qV_A/kT} - 1) \quad \dots W \leq x \leq x_b$

$$J_P \equiv -qD_P \frac{d\Delta p_n}{dx} = q \frac{n_i^2}{N_D} \left( \frac{D_P}{x_b - W} \right) (e^{qV_A/kT} - 1)$$

and

$$I \equiv AJ_P = qA \frac{n_i^2}{N_D} \left( \frac{D_P}{x_b - W} \right) (e^{qV_A/kT} - 1)$$

The foregoing result is identical to the limiting-case narrow-base result discussed in Subsection 6.3.2.  $x_b - W$  is equivalent to the  $x_c'$  introduced in the cited Subsection. Note that there would be no advantage to translating the computational origin of coordinates to the depletion region edge in this problem. Also note that since  $\Delta p_n(x)$  is a linear function of  $x$ ,  $J_P$  is constant throughout the narrow-base ( $W \leq x \leq x_b$ ) region.

### 6.23

Referring to the solution to Problem 6.22, we again need consider only  $I_{\text{DIFF}}$  because  $I_{R-G} = 0$  given  $\tau_p = \infty$  in the depletion region. Likewise, the same general solution as in Prob. 6.22 applies in the  $W \leq x \leq x_b$  region.

$$\Delta p_n(x) = A_1 + A_2 x$$

Although  $\Delta p_n(x_b) \neq 0$  in the present problem, we still have

$$\Delta p_n(W) = (n_i^2/N_D)(e^{qV_A/kT} - 1) = A_1 + A_2 W$$

which allows us to write

$$\Delta p_n(x) = \Delta p_n(W) + A_2(x - W) \quad \dots W \leq x \leq x_b$$

Introducing  $x' = x - x_b$ , the solution in the  $x' > 0$  region will have the usual wide-base form since  $x_c - x_b \gg L_P$ . Specifically,

$$\Delta p_n(x') = B e^{-x'/L_P} \quad \dots x' \geq 0 \text{ or } x \geq x_b$$

Both  $\Delta p_n$  and  $J_P \propto d\Delta p_n/dx$  must be continuous at  $x = x_b$ . The continuity requirements yield

$$\Delta p_n(W) + A_2(x_b - W) = B$$

$$A_2 = -B/L_P$$

Solving for the remaining solution constants gives

$$A_2 = -\frac{\Delta p_n(W)}{[L_P + (x_b - W)]}$$

$$B = \frac{\Delta p_n(W) L_P}{[L_P + (x_b - W)]}$$

Therefore

$$\Delta p_n(x) = \Delta p_n(W) \left[ 1 - \frac{x-W}{L_P + (x_b-W)} \right] \quad \dots W \leq x \leq x_b$$

$$\Delta p_n(x') = \frac{\Delta p_n(W) L_P}{[L_P + (x_b-W)]} e^{-x'/L_P} \quad \dots x' > 0$$

and

$$J_P(x) \equiv -qD_P \frac{d\Delta p_n}{dx} = q \frac{n_i^2}{N_D} \left( \frac{D_P}{L_P + (x_b-W)} \right) (e^{qV_A/kT} - 1) \quad \dots W \leq x \leq x_b$$

$$J_P(x') \equiv -qD_P \frac{d\Delta p_n}{dx'} = q \frac{n_i^2}{N_D} \left( \frac{D_P}{L_P + (x_b-W)} \right) (e^{qV_A/kT} - 1) e^{-x'/L_P} \quad \dots x' > 0$$

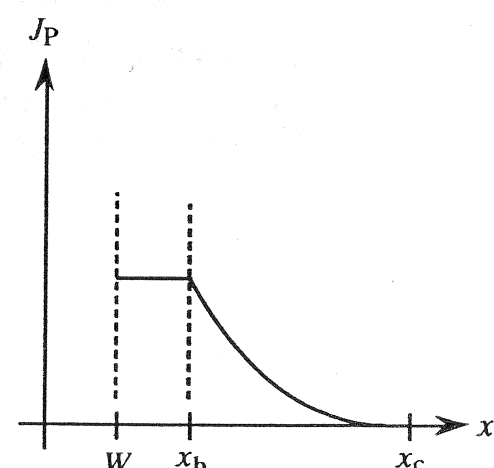
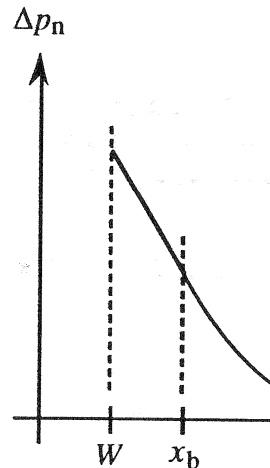
Finally,

$$I = AJ_P(x=W) = AJ_P(x'=0)$$

or

$$I = qA \frac{n_i^2}{N_D} \left( \frac{D_P}{L_P + (x_b-W)} \right) (e^{qV_A/kT} - 1)$$

Note that  $\Delta p_n$  and  $J_P$  exhibit the positional dependence sketched below.



6.24

- (a)  $V_{bi} \approx 0.92$  V for a  $p^+-n$  junction ... See Fig. E5.1.
- (b)  $V_{BR} \approx 55$  V given  $N_D = 10^{16}/\text{cm}^3$  ... See Fig. 6.11.

(c)  $W \approx x_n = \left[ \frac{2K_S \epsilon_0}{qN_D} (V_{bi} - V_A) \right]^{1/2} \stackrel{\text{set}}{=} x_b$

$$x_b^2 = \frac{2K_S \epsilon_0}{qN_D} (V_{bi} - V_A)$$

$$V_A = V_{bi} - \frac{qN_D x_b^2}{2K_S \epsilon_0} = 0.92 - \frac{(1.6 \times 10^{-19})(10^{16})(2 \times 10^{-4})^2}{(2)(11.8)(8.85 \times 10^{-14})}$$

$$= -29.7 \text{ V}$$

(d) Per Eq. (3.33a),  $\tau_p \propto 1/N_T$ . Thus,  $\tau_{p1}/\tau_{p2} = N_{T2}/N_{T1} = 100$ .

(e) There are two solution regions.

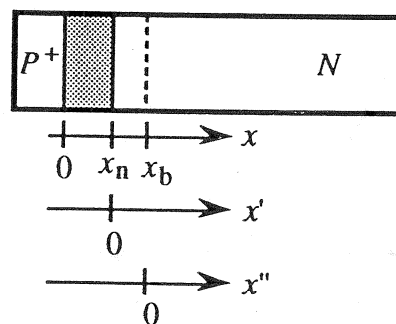
*Bias region #1* ...  $29.7 \text{ V} \leq |V_A| < V_{BR}$  ( $x_n \geq x_b$ )

If  $x_n \geq x_b$ , the quasineutral  $n$ -region is totally confined to the  $N_T = N_{T2}$  or  $\tau_p = \tau_{p2}$  portion of the  $n$ -side. The situation is identical to that for a standard "ideal" diode and we can just write down the usual  $p^+-n$  diode result.

$$I_{\text{DIFF}} = -qA \frac{D_P n_i^2}{L_{P2} N_D} \quad \dots L_{P2} = \sqrt{D_P \tau_{p2}}$$

*Bias region #2* ...  $0 \leq |V_A| \leq 29.7 \text{ V}$  ( $x_n < x_b$ )

If  $x_n < x_b$ , then there are two spatial  $n$ -regions,  $x_n \leq x \leq x_b$  and  $x \geq x_b$ , as pictured below, that must be handled separately. Note the definition of the  $x'$  and  $x''$  coordinates.



$\underline{\text{For } x_n \leq x \leq x_b}$	$\underline{\text{For } x > x_b}$	
Solve $\Rightarrow$	$0 = \frac{d^2 \Delta p_n}{dx'^2}$ (The recombination term is neglected because $L_{P1} \gg x_b$ .)	$0 = D_P \frac{d^2 \Delta p_n}{dx''^2} - \frac{\Delta p_n}{\tau_{p2}}$

Gen. sol. $\Rightarrow$	$\Delta p_{n1}(x') = A_1 + A_2 x'$ (Narrow-base diode sol.)	$\Delta p_{n2}(x'') = B_1 e^{-x''/L_{P2}} + B_2 e^{x''/L_{P2}}$ (Wide-base diode sol. $L_{P2} = \sqrt{D_P \tau_{p2}}$ )
-------------------------	--	--

B.C. $\Rightarrow$	$\Delta p_{n1}(0) = \frac{n_i^2}{N_D} (e^{qV_A/kT} - 1)$	$\Delta p_{n2}(\infty) = 0$
--------------------	--	-----------------------------

Applying the available boundary conditions yields

$$\Delta p_{n1}(x') = \Delta p_{n1}(0) + A_2 x' \quad \dots 0 \leq x' \leq x_b - x_n$$

$$\Delta p_{n2}(x'') = B_1 e^{-x''/L_{P2}} \quad \dots x'' \geq 0$$

Both  $\Delta p_n$  and  $d\Delta p_n/dx$  must be continuous at  $x = x_b$ . This requires...

$$\Delta p_{n1}(x' = x_b - x_n) = \Delta p_{n2}(x'' = 0)$$

$$\left. \frac{d\Delta p_{n1}}{dx'} \right|_{x' = x_b - x_n} = \left. \frac{d\Delta p_{n2}}{dx''} \right|_{x'' = 0}$$

or

$$\Delta p_n(0) + A_2(x_b - x_n) = B_1$$

$$A_2 = -B_1/L_{P2}$$

Solving for the constants...

$$\Delta p_{n1}(0) = B_1 + B_1 \left( \frac{x_b - x_n}{L_{P2}} \right) \quad \text{or} \quad B_1 = \frac{\Delta p_{n1}(0) L_{P2}}{L_{P2} + (x_b - x_n)}$$

and

$$A_2 = -\frac{\Delta p_{n1}(0)}{L_{P2} + (x_b - x_n)}$$

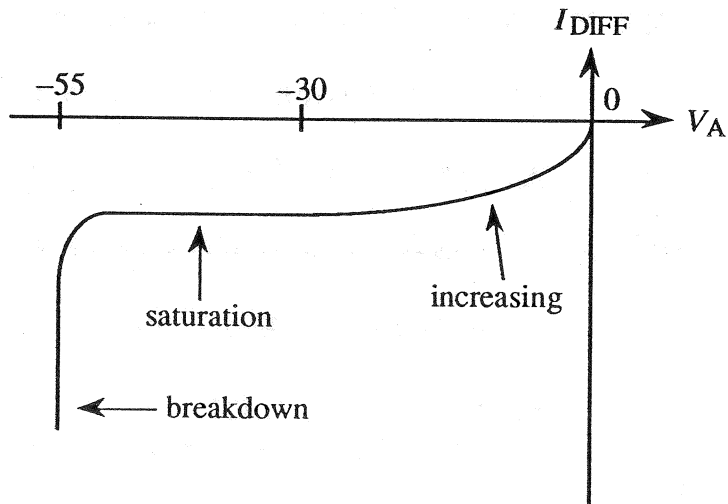
Substituting back into the  $\Delta p_n(x')$  solution then yields

$$\Delta p_{n1}(x') = \Delta p_{n1}(0) \left[ 1 - \frac{x'}{L_{P2} + (x_b - x_n)} \right] \quad \dots 0 \leq x' \leq x_b - x_n$$

and finally

$$I_{\text{DIFF}} = -qAD_P \frac{d\Delta p_{n1}}{dx'} \Big|_{x'=0} = qA \left( \frac{D_P}{L_{P2} + (x_b - x_n)} \right) \frac{n_i^2}{N_D} \left( e^{qV_A/kT} - 1 \right)$$

The above solution is rather interesting in that the reverse bias  $I_{\text{DIFF}}$  does not saturate. Because  $x_b - x_n$  decreases with increasing reverse bias and vanishes at the end of the biasing region (at  $V_A = -29.7V$ ),  $I_{\text{DIFF}}$  systematically increases in magnitude with increasing reverse bias. The general form of the predicted reverse bias characteristics, taking into account both biasing regions, is sketched below.



(f) Here again there are two solution regions corresponding to whether  $x_n < x_b$  or  $x_n > x_b$ .

*Bias region #1...0 \leq |V\_A| \leq 29.7V (x\_n < x\_b)*

Here the depletion region lies totally in the denuded zone and

$$I_{R-G} = -qA \int_{-x_p=0}^{x_n=W} \frac{n_i}{2\tau_{p1}} dx = -qA \frac{n_i}{2\tau_{p1}} W$$

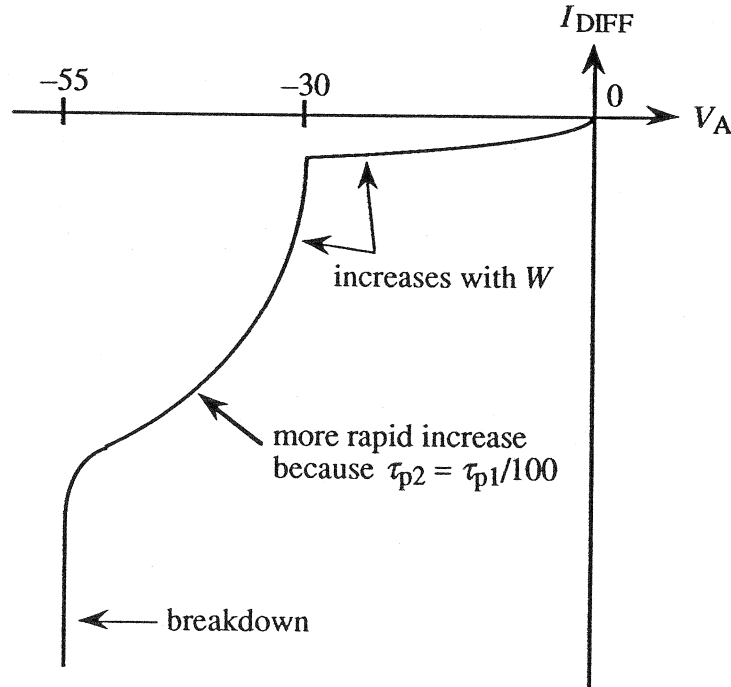
*Bias region #2* ...  $29.7V \leq |V_A| < V_{BR}$  ( $x_n \geq x_b$ )

Here the depletion region is partly in the denuded zone and partly in the region of the semiconductor with a high R-G center concentration. Nevertheless, the R-G current is readily obtained by summing the contributions from the two spatial regions.

$$I_{R-G} = -qA \left[ \int_0^{x_b} \frac{n_i}{2\tau_{p1}} dx + \int_{x_b}^{x_n=W} \frac{n_i}{2\tau_{p2}} dx \right]$$

$$= -qA \left[ \frac{n_i}{2\tau_{p1}} x_b + \frac{n_i}{2\tau_{p2}} (W-x_b) \right]$$

Thus we conclude



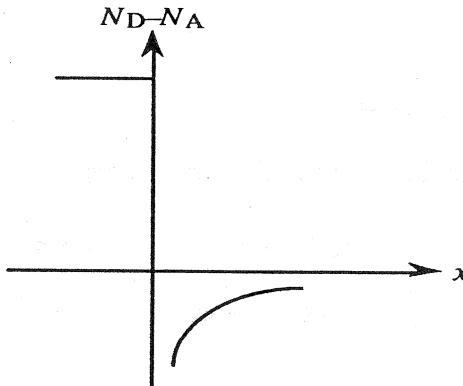


## CHAPTER 7

### 7.1

(a) The in and out movement of the majority carriers about the steady-state depletion width in response to the applied a.c. signal.

(b)



(c) *Quasistatically* is an adverb used to describe a situation where carriers or a device subject to non-steady-state conditions responds as if steady-state conditions applied at each instant of time.

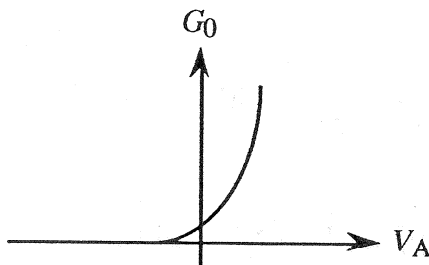
(d) *Varactor*—a contraction of *variable reactor*. A commercial device, such as a reverse-biased *pn* junction diode, where the reactance  $= 1/j\omega C$  varies as a function of the applied voltage.

(e) *Profiling*—the process of determining the doping concentration inside a device as a function of position.

(f) The low-frequency conductance of an ideal diode was noted to be (Eq. 7.15),

$$G_0 = \frac{q}{kT} (I + I_0)$$

$G_0 \propto I$  when the diode is forward biased and vanishes for reverse biases greater than a few  $kT/q$ . Also note that  $G_0 = qI_0/kT$  when  $V_A = 0$ . We conclude



- (g) The diffusion admittance arises from fluctuations in the number and position of minority carriers stored in the quasineutral regions adjacent to the depletion region.
- (h) At signal frequencies where  $\omega\tau_p \geq 1$ , the minority carriers have trouble following the a.c. signal and the resulting out-of-phase oscillations enhance the diffusion conductance at the expense of the diffusion capacitance.

## 7.2

Given

$$N_B(x) = N_D(x) = bx^m \quad \dots x > 0$$

the application of the depletion approximation yields

$$\rho \equiv qN_D = qbx^m \quad \dots 0 \leq x \leq x_n \equiv W$$

Next substituting into Poisson's equation gives

$$\frac{dE}{dx} = \frac{\rho}{K_S \epsilon_0} = \frac{qb}{K_S \epsilon_0} x^m \quad \dots 0 \leq x \leq W$$

Separating variables and solving for the electric field, we find

$$\int_{E(x)}^0 dE' = \int_x^W \frac{qb}{K_S \epsilon_0} x'^m dx'$$

or

$$-E(x) = \frac{dV}{dx} = \frac{qb}{K_S \epsilon_0} \frac{(x')^{m+1}}{m+1} \Big|_x^W = \frac{qb}{(m+1)K_S \epsilon_0} (W^{m+1} - x^{m+1})$$

Again separating variables and this time integrating across the entire depletion region, we obtain

$$\int_0^{V_{bi}-V_A} dV = \frac{qb}{(m+1)K_S \epsilon_0} \int_0^W [W^{m+1} - x^{m+1}] dx$$

or

$$V_{bi}-V_A = \frac{qb}{(m+1)K_S \epsilon_0} \left[ W^{m+1}x - \frac{x^{m+2}}{m+2} \right] \Big|_0^W$$

Note that the second term on the right hand side of the  $V_{bi}-V_A$  expression blows up when evaluated at the lower limit if  $m < -2$ . The solution likewise blows up at the upper limit if  $m = -2$ . It is for this reason that we must restrict  $m$  to values  $m > -2$ . With  $m > -2$ , we conclude

$$V_{bi}-V_A = \frac{qb}{(m+1)K_S\epsilon_0} \left[ W^{m+2} - \frac{W^{m+2}}{m+2} \right] = \frac{qb}{(m+2)K_S\epsilon_0} W^{m+2}$$

or

$$W = \left[ \frac{(m+2)(K_S\epsilon_0)}{qb} (V_{bi}-V_A) \right]^{1/(m+2)}$$

### 7.3

(a)/(b) Script of a MATLAB program yielding fully-dimensioned reverse-bias C-V curves, and a sample output to be compared with Fig. 7.3, are reproduced below. Using a computed  $V_{bi}$  consistent with the specified doping yields capacitance values that are too low. This is especially true at small applied voltages where  $|V_A|$  is comparable to  $V_{bi}$ . For example, at  $V_A = 0$ , the computed  $C_J$  is 106 pF while the observed value is approximately 123 pF. The noted discrepancy is indeed related to the result in Exercise 7.2 where a lower  $V_{bi}$ , a  $V_{bi}$  not consistent with the doping concentration, was deduced from the Fig. 7.3 experimental data. Not surprisingly, if one employs the  $V_{bi}$  deduced in Exercise 7.2 instead of the computed value (which is possible with the supplied m-file), one obtains excellent agreement with the Fig. 7.3 data. (It should be noted that even better agreement is obtained if 2 pF are added to the computed values to account for stray capacitance.)

(c) Because the depletion width at a given reverse bias shrinks with increased doping, the capacitance, which is proportional to  $1/W$ , increases with increased doping on the lightly doped side of the junction. This is readily verified by simply running the P\_07\_03.m program with different  $N_D$  inputs.

MATLAB program script...

```
% Fully-dimensioned Reverse-bias C-V curves
% appropriate for p+-n step junction diodes
%Initialization
clear; close
%Constants and Parameters
q=1.6e-19; e0=8.85e-14;
EG=1.12; kT=0.0259;
ni=1.0e10; KS=11.8;
```

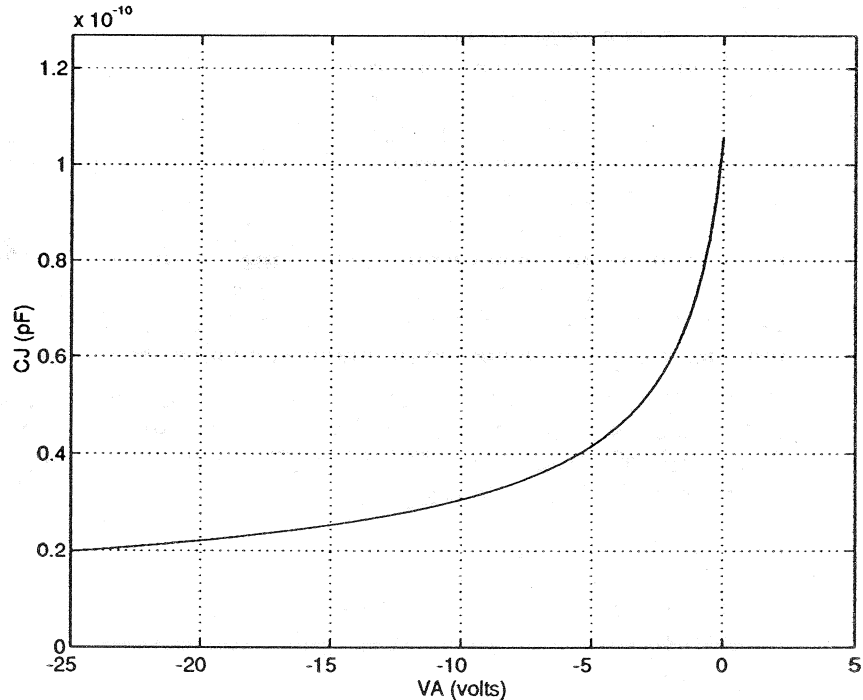
```

s=menu('CHOOSE Vbi APPROACH', 'Compute', 'Input');
A=input('Input the diode area in cm^2, A = ');
ND=input('Input the n-side (of p+-n) doping, ND = ');
VAmax=input('Input reverse-bias |VA|max, |VA|max = ');
if s==1, Vbi=EG/2+kT*log(ND/ni);
else Vbi=input('Input Vbi, Vbi = ');
end

%C-V Computation
VA=linspace(0,-VAmax);
CJ0=(KS*e0*A)/sqrt(2*KS*e0*Vbi/(q*ND));
CJ=CJ0./sqrt(1-VA/Vbi);

%Plot result
ymax=1.2*max(CJ);
plot(VA,CJ);
axis([-VAmax,5,0,ymax]); grid
xlabel('VA (volts)'); ylabel('CJ (pF)')

```



## 7.4

For an abrupt  $p^+-n$  junction, we know in general from Eq. (7.11) that

$$\frac{1}{C_J^2} = \frac{2}{qN_D K_S \epsilon_0 A^2} (V_{bi} - V_A)$$

After reducing all capacitance values in Table P7.4 by 3pF to account for the stray capacitance shunting the encapsulated diode<sup>†</sup>, a least squares fit to the corrected data employing the MATLAB polyfit function yields

$$\frac{1}{C_J^2} = (8.254 \times 10^{20}) - (1.123 \times 10^{21})V_A \quad \dots C_J \text{ in Farads}$$

We therefore conclude

$$N_D = \frac{2}{qK_S \epsilon_0 A^2 |\text{slope}|} = \frac{2}{(1.6 \times 10^{-19})(11.8)(8.85 \times 10^{-14})(6 \times 10^{-3})^2 (1.123 \times 10^{21})} \\ = 2.96 \times 10^{14}/\text{cm}^3$$

and

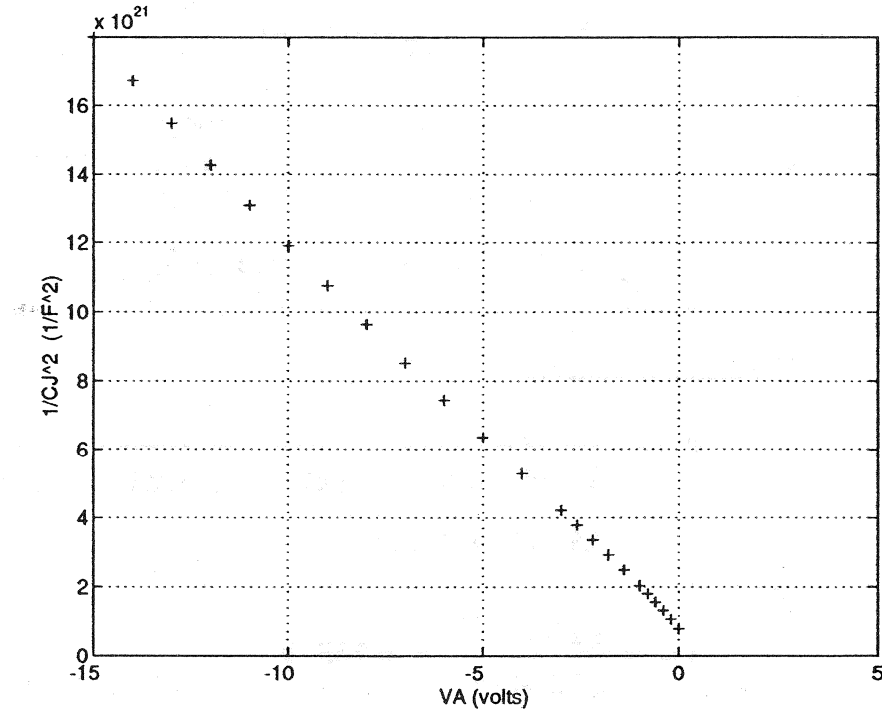
$$V_{bi} = \frac{8.254 \times 10^{20}}{1.123 \times 10^{21}} = 0.735 \text{ V}$$

Referring to Fig. E5.1, one finds the  $V_{bi}$  result here is reasonably close to the theoretically computed  $V_{bi} = 0.83\text{V}$  associated with an  $N_D \approx 3 \times 10^{14}/\text{cm}^3$   $p^+-n$  step junction.

---

<sup>†</sup> It was incorrectly stated in the first printing of the text that the data listed in Table P7.4 had already been corrected to account for the cited stray capacitance.

A plot of the corrected  $1/C_J^2$  versus  $V_A$  data, which may be used for obtaining a result by "eyeballing," is displayed below. (Also see m-file P\_07\_04.m available on the instructor's disk.)



### 7.5

For concreteness, we take the device under test to be a  $p^+-n$  junction diode, with  $N_D(x)$  the arbitrary nondegenerate donor doping on the lightly doped side of the junction. Based on the depletion approximation, the total charge in the depletion region on the  $n$ -side of the junction will be

$$Q_N = A \int_0^{x_n \approx W} \rho(x) dx = qA \int_0^W N_D(x) dx$$

Assuming the diode follows the applied a.c. signal quasistatically,

$$C_J = \frac{dQ_P}{dV_A} = -\frac{dQ_N}{dV_A} = -qA \frac{d}{dV_A} \int_0^W N_D(x) dx = -qAN_D(W) \frac{dW}{dV_A}$$

However,

$$C_J = \frac{K_S \epsilon_0 A}{W}$$

$$\frac{dC_J}{dV_A} = -\frac{K_S \epsilon_0 A}{W^2} \frac{dW}{dV_A}$$

and therefore

$$\frac{dW}{dV_A} = -\frac{W^2}{K_S \epsilon_0 A} \frac{dC_J}{dV_A} = -\frac{K_S \epsilon_0 A}{C_J^2} \frac{dC_J}{dV_A}$$

Substituting back into the generalized capacitance expression then yields

$$C_J = -qAN_D(W) \frac{dW}{dV_A} = \frac{qK_S \epsilon_0 A^2 N_D(W)}{C_J^2} \frac{dC_J}{dV_A}$$

and solving for  $N_D(W)$  gives

$$N_D(W) = \frac{1}{qK_S \epsilon_0 A^2 [(dC_J/dV_A)/C_J^3]}$$

Finally, noting

$$\frac{d}{dV_A} \left( \frac{1}{C_J^2} \right) = -\frac{2}{C_J^3} \frac{dC_J}{dV_A}$$

and realizing  $W$  is synonymous with the distance  $x$  from the junction being probed, we obtain

$$N_D(x) = \frac{2}{qK_S \epsilon_0 A^2 |d(1/C_J^2)/dV_A|}$$

where

$$x = W = \frac{K_S \epsilon_0 A}{C_J} \quad \dots \text{(from } C_J = K_S \epsilon_0 A/W\text{)}$$

## 7.6 (Solution not supplied.)

## 7.7

As deduced by combining Eqs. (7.29) and (7.30),

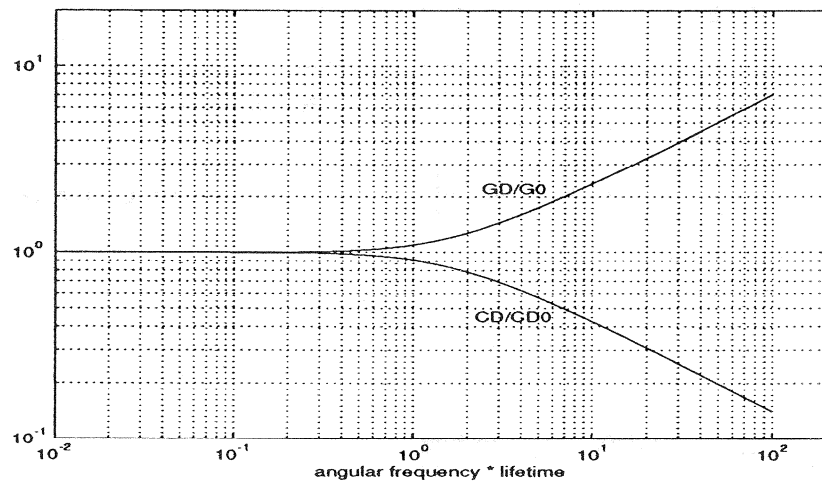
$$G_D/G_0 = \frac{1}{\sqrt{2}} (\sqrt{1 + \omega^2 \tau_p^2} + 1)^{1/2}$$

$$C_D/C_{D0} = \frac{\sqrt{2}}{\omega \tau_p} (\sqrt{1 + \omega^2 \tau_p^2} - 1)^{1/2}$$

Computations based on the above relationships and implemented using the program listed below yield an almost perfect reproduction of the text plot.

MATLAB program script...

```
% Frequency variation of the normalized diffusion
% conductance (GD/G0) and capacitance (CD/CD0)
% (reproduction of Fig. 7.10)
% Initialization
clear; close
%Computation
x=logspace(-2,2);
Gratio=sqrt(sqrt(1+x.^2)+1)./sqrt(2);
Cratio=sqrt(sqrt(1+x.^2)-1).*sqrt(2)./x;
%Plot
loglog(x,Gratio,x,Cratio);
axis([0.01,200,0.1,20]); grid
xlabel('angular frequency * lifetime')
text(2.4,2.2,'GD/G0')
text(2.2,0.45,'CD/CD0')
```



### 7.8

As deduced by combining Eqs. (7.30a) and (7.30b),

$$\omega C_D/G_D \rightarrow \omega\tau_p/2 \quad \dots \omega\tau_p \ll 1$$

As deduced from Eqs. (7.29a) and (7.29b),

$$C_D \rightarrow \frac{G_0}{\omega\sqrt{2}} \sqrt{\omega\tau_p} \quad \dots \omega\tau_p \gg 1$$

$$G_D \rightarrow \frac{G_0}{\sqrt{2}} \sqrt{\omega\tau_p} \quad \dots \omega\tau_p \gg 1$$

and

$$\omega C_D/G_D \rightarrow 1 \quad \dots \omega\tau_p \gg 1$$

In general, again referring to Eqs. (7.29),

$$\frac{\omega C_D}{G_D} = \left( \frac{\sqrt{1 + \omega^2 \tau_p^2} - 1}{\sqrt{1 + \omega^2 \tau_p^2} + 1} \right)^{1/2}$$

A plot of  $\omega C_D/G_D$  versus  $\omega\tau_p$  that is consistent with the limiting-case solutions and the script of the generating MATLAB program are displayed below. The result here provides some food for thought. Even though  $G_D$  increases and  $C_D$  decreases with increased frequency above  $\omega\tau_p = 1$ , the relative size of the real and imaginary components of the diffusion admittance approach the same value and increase at the same rate if  $\omega\tau_p \gg 1$ . Also, the result emphasizes that the diffusion conductance is the larger admittance component at low frequencies.

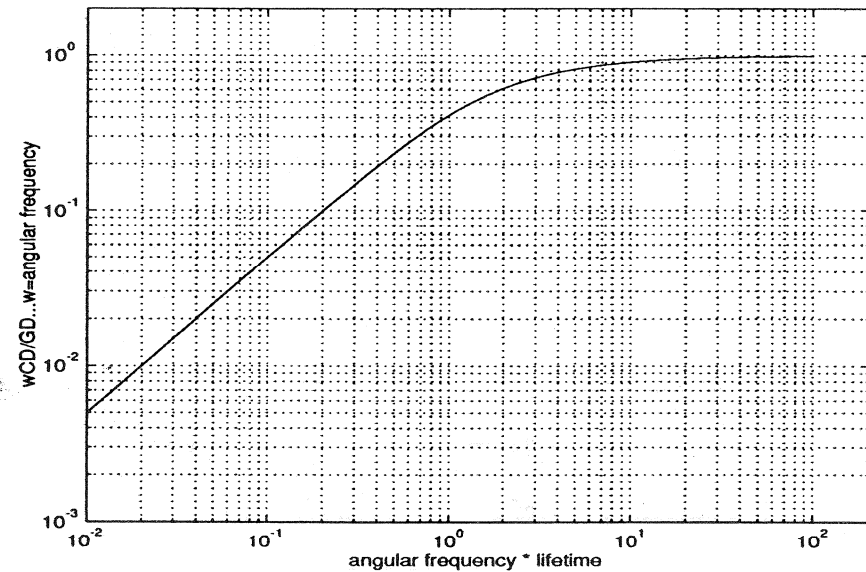
MATLAB program script...

```
% Relative size of the capacitive and conductive
% components of the diffusion admittance (wCD/GD)

% Initialization
clear; close

% Computation
x=logspace(-2,2);
ratio=sqrt((sqrt(1+x.^2)-1)./(sqrt(1+x.^2)+1));

% Plot
loglog(x,ratio);
axis([0.01,200,0.001,2]); grid
xlabel('angular frequency * lifetime')
ylabel('wCD/GD...w=angular frequency')
```



### 7.9

A table listing the computational variables and the deduced values of  $\tau_n$  is presented below. Capacitance entries in this table were established as follows:

(1) The  $C_{TOTAL} = C_J + C_D$  data spanning the voltage range from 0.5V to 0.58V were extracted from line 20 of the MATLAB program script in Exercise 7.4.

(2)  $C_J$  was computed using

$$C_J = C_{J0}/\sqrt{1 - V_A/V_{bi}} = 120/\sqrt{1 - V_A/0.7} \quad (\text{pF})$$

The values of  $C_{J0}$  and  $V_{bi}$  were noted from entries in the Exercise 7.4 program script.

(3)  $C_D = C_{TOTAL} - C_J$

$V_A$ (volts)	$C_{TOTAL}$ (pF)	$C_J$ (pF)	$C_D$ (pF)	$G_D$ (S)	$\tau_n = 2C_D/G_D$ (sec)
0.5	276	224	52	$2.00 \times 10^{-4}$	$5.20 \times 10^{-7}$
0.52	346	237	109	$3.90 \times 10^{-4}$	$5.59 \times 10^{-7}$
0.54	440	251	189	$7.15 \times 10^{-4}$	$5.29 \times 10^{-7}$
0.56	654	268	386	$1.33 \times 10^{-3}$	$5.81 \times 10^{-7}$
0.58	938	290	648	$2.28 \times 10^{-3}$	$5.68 \times 10^{-7}$

$\tau_n = 5.51 \times 10^{-7} \text{ sec}$

## CHAPTER 8

### 8.1

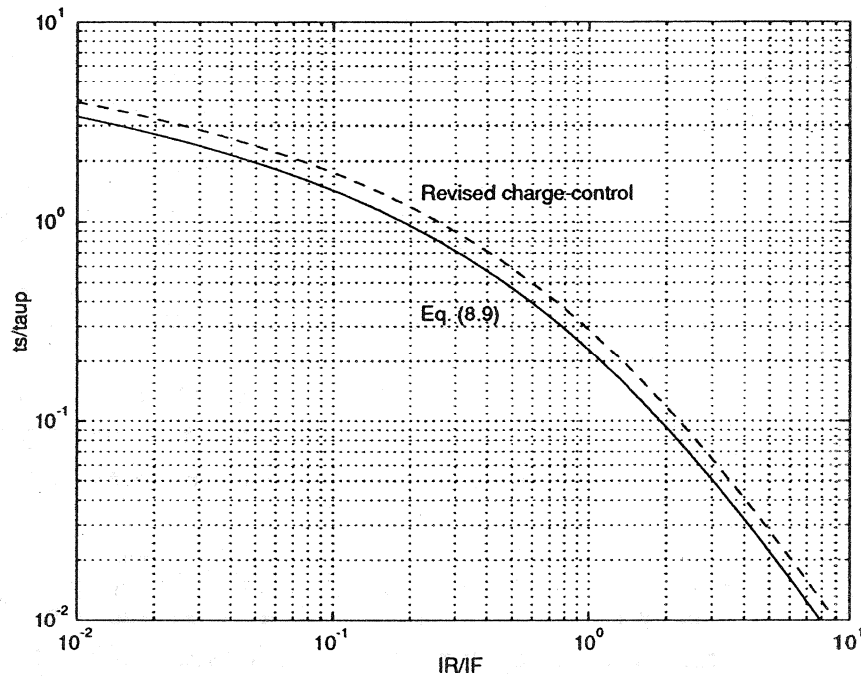
- (a) It is the time period ( $t_s$ ) during which the observed current associated with the turn-off transient remains constant at a large negative value.—See Fig. 8.1(b). The excess minority carriers stored in the quasineutral region are being removed during this time period.
- (b) With reference to the turn-off transient pictured in Fig. 8.1(b),  $t_r = t_{rr} - t_s$ , where  $t_{rr}$  is the total time for the reverse current to decay to 10% of its maximum magnitude and  $t_s$  is the storage delay time.
- (c) **Yes**. This is precisely what happens during the  $t_s$  portion of the turn-off transient. Even though there is an excess of carriers at the edges of the depletion region making  $v_A > 0$ , the external circuitry enables a reverse current flow that acts to eliminate the excess.
- (d) A delay in switching from the on- to the off-state arises because a finite amount of time is required to remove the excess minority carriers stored in the quasineutral regions on the two sides of the junction.
- (e) The excess carriers are removed by *recombination* and *reverse injection*.
- (f) **True**.  $\Delta p_n(x,t) > 0$  implies  $\Delta p_n(x_n,t) > 0$ , the necessary condition making  $v_A > 0$ .
- (g) **False**. Referring to Eq. (8.2), if  $i > 0$ , the slope of a  $p_n(x,t)$  versus  $x$  plot must be *negative* at  $x = x_n$ .
- (h) The electrical response of the step-recovery diode is special in that the  $t_r$  portion of the transient is very short compared to the storage delay time. Physically, step recovery diodes are actually a P-I-N type structure with very abrupt junctions.
- (i) **True**. Both the approximate expression (Eq. 8.8) and the more exacting expression (Eq. 8.9) for  $t_s$  vary only as the ratio of  $I_F$  and  $I_R$ . Thus, increasing both  $I_F$  and  $I_R$  by the same amount will have no effect.
- (j) **True**. During turn-on recombination obviously dominates over generation because there is a carrier excess. Thus, the inevitable loss of carriers via recombination will indeed retard the build-up of stored carriers. (This fact is confirmed mathematically by Eq. 8.10.)

### 8.2

- (a) **Reverse biased**.  $\Delta p_n(x_n,t) = p_n(x_n,t) - p_{n0} < 0$ . A carrier deficit at the edge of the depletion region indicates the junction is reverse biased.
- (b) Invoking the law of the junction,
- $$n(x_n)p(x_n) = N_D p_{n0}/2 = n_i^2/2 = n_i^2 e^{qv_A/kT}$$
- or  $v_A = (kT/q) \ln(1/2) = -0.0259 \ln 2 = -0.018 \text{ V}$
- (c) **Reverse**. Since  $d\Delta p_n/dx|_{x=x_n} = dp_n/dx|_{x=x_n} > 0$ , it follows from Eq. (8.2) that  $i < 0$ .

### 8.3

A comparison of the plot displayed below and Fig. 8.6 indicates the revised charge-control expression is indeed a significant improvement. The improvement is clearly greatest at the largest  $I_R/I_F$  values.



MATLAB program script...

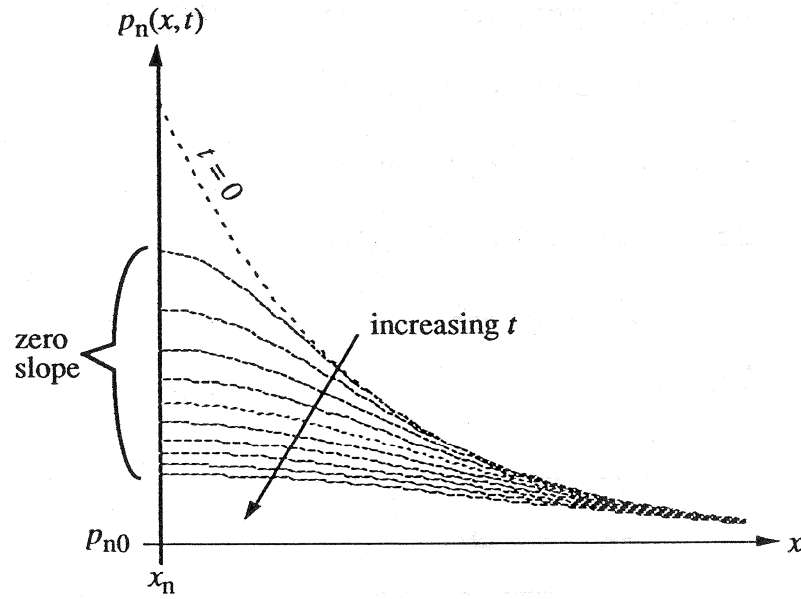
```
% Comparison of the ts/taup versus IR/IF computed
% using Eq.(8.9) and the revised charge control expression
%Initialization
clear; close

%ts/taup calculation
Iratio=logspace(-2,1); %Iratio=IR/IF
%Revised charge control expression
x=1./Iratio;
ts1=log((1+x).^2./(1+2.*x));
%Equation (8.9)
ts2=erfinv(1./(1+Iratio)).^2;

%Plotting results
loglog(Iratio,ts1,'--g')
axis([1.0e-2,10,1.0e-2,10]); grid
hold on
loglog(Iratio,ts2)
xlabel('IR/IF'); ylabel('ts/taup')
text(0.22,1.4,'Revised charge-control');
text(0.22,0.35,'Eq. (8.9)')
hold off
```

### 8.4

(a) Because the diode is open circuited,  $i = 0$ . Thus, based on Eq. (8.2), the slope of all the  $p_n(x,t)$  versus  $x$  curves evaluated at  $x = x_n$  should be zero.



(b) With  $i = 0$ , the general equation for the stored hole charge reduces to

$$\frac{dQ_p}{dt} = -\frac{Q_p}{\tau_p}$$

The general solution is

$$Q_p(t) = Q_p(0^+) e^{-t/\tau_p}$$

where paralleling the analysis in the text

$$Q_p(0^+) = I_F \tau_p$$

Thus

$$Q_p(t) = I_F \tau_p e^{-t/\tau_p}$$

(c) If the charge is assumed to decay quasistatically, then, referring to Eq. (8.15),

$$Q_P(t) = I_0 \tau_p (e^{qv_A/kT} - 1) \approx I_0 \tau_p e^{qv_A/kT}$$

Equating the part (b) and (c) expressions for  $Q_P(t)$  gives

$$I_F \tau_p e^{-t/\tau_p} = I_0 \tau_p e^{qv_A/kT}$$

or

$$e^{qv_A/kT} = (I_F/I_0) e^{-t/\tau_p}$$

But from the statement of the problem

$$I_F/I_0 \approx e^{qV_{ON}/kT}$$

Therefore

$$e^{qv_A/kT} = e^{qV_{ON}/kT} e^{-t/\tau_p}$$

or

$$v_A(t) = V_{ON} - \frac{kT}{q} \frac{t}{\tau_p}$$

(d) The part (c) result suggests a very simple way of determining  $\tau_p$  (known as the Open-Circuit Decay Method). After forward biasing the diode, one open-circuits the device and monitors the voltage drop across the diode as a function of time. Provided the decay follows the ideal form,  $\tau_p$  is readily determined from the slope of the data.

## 8.5

Since under steady state conditions

$$I_F = I_0 (e^{qV_{ON}/kT} - 1) \cong I_0 e^{qV_{ON}/kT}$$

$$V_{ON} \cong \frac{kT}{q} \ln\left(\frac{I_F}{I_0}\right) = 0.0259 \ln\left(\frac{10^{-3}}{10^{-15}}\right) = 0.716 \text{ V}$$

Next, solving Eq. (8.16) for  $t$ , one obtains in general

$$t = -\tau_p \ln[1 - (I_0/I_F)(e^{qv_A/kT} - 1)] \cong -\tau_p \ln[1 - e^{qv_A/kT}/e^{qV_{ON}/kT}]$$

or

$$t = -\tau_p \ln[1 - e^{q(v_A - V_{ON})/kT}]$$

Corresponding to  $v_A = 0.9V_{ON}$ ,

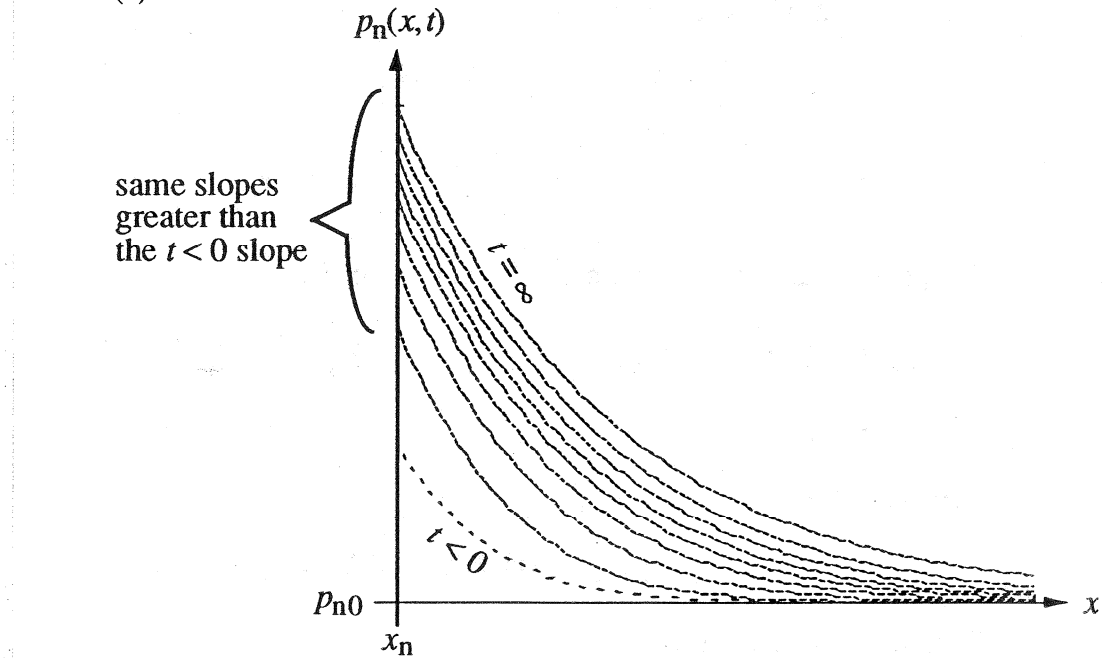
$$t_{90\%} = -(10^{-6}) \ln[1 - e^{-(0.1)(0.716)/(0.0259)}] = 65.1 \text{ nsec}$$

To reach  $v_A = 0.95V_{ON}$ ,

$$t_{95\%} = -(10^{-6}) \ln[1 - e^{-(0.05)(0.716)/(0.0259)}] = 289 \text{ nsec}$$

Note that the 90%–95% portion of the transient takes much longer than the 0–90% portion of the transient. This property of the turn-on transient was noted at the end of Section 8.2.

8.6  
(a)



(b) Here for  $t > 0$ ,

$$\frac{dQ_P}{dt} = I_{F2} - \frac{Q_P}{\tau_p}$$

$$\int_{Q_P(0^+)}^{Q_P(t)} \frac{dQ_P}{I_{F2} - Q_P/\tau_p} = t$$

$$t = -\tau_p \ln \left( I_{F2} - \frac{Q_P}{\tau_p} \right) \Big|_{Q_P(0^+) = I_{F1}\tau_p}^{Q_P(t)} = -\tau_p \ln \left( \frac{I_{F2} - Q_P/\tau_p}{I_{F2} - I_{F1}} \right)$$

Thus

$$I_{F2} - \frac{Q_P}{\tau_p} = (I_{F2} - I_{F1}) e^{-t/\tau_p}$$

and

$$Q_P(t) = I_{F2}\tau_p - (I_{F2} - I_{F1})\tau_p e^{-t/\tau_p}$$

Invoking the quasistatic assumption (Eq. 8.15), we can also write

$$Q_P(t) = I_0 \tau_p (e^{qv_A/kT} - 1)$$

Therefore, equating the  $Q_P(t)$  relationships,

$$e^{qv_A/kT} - 1 = \frac{I_{F2}}{I_0} - \frac{(I_{F2} - I_{F1})}{I_0} e^{-t/\tau_p}$$

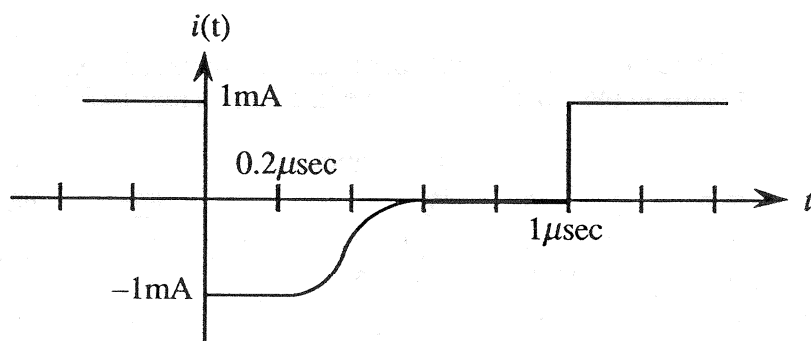
or

$$v_A(t) = \frac{kT}{q} \ln \left[ 1 + \frac{I_{F2}}{I_0} - \frac{(I_{F2} - I_{F1})}{I_0} e^{-t/\tau_p} \right]$$

Note as a check that the foregoing expression reduces to Eq. (8.16) if  $I_{F1} \rightarrow 0$  and  $I_{F2} \rightarrow I_F$ .

### 8.7

(a) We note using Fig. 8.6 that  $t_s/\tau_p \cong 0.22$  when  $I_R/I_F = 1$ . Thus  $t_s = 0.22\mu\text{sec}$ , or the diode becomes reverse biased before it is pulsed back to the ON condition. Based on the above information, we conclude



(b) Since pulsing is occurring from reverse bias, we can assume by analogy with the text turn-on development that the pulsing effectively occurs from  $i = 0$  with  $Q_P(1\mu\text{sec}) = 0$ . The situation here is completely analogous—all but identical—to the turn-on situation considered in Section 8.2, except  $t$  is replaced by  $t - 1\mu\text{sec}$ . Consequently, the required expression is just Eq. (8.16) with the  $t$  in  $\exp(-t/\tau_p)$  replaced by  $t - 1\mu\text{sec}$

## 8.8

### (a) In the CPG program

$$yon(1) = \Delta p_n(0,t)/\Delta p_{n\max}$$

Thus

$$yon(1) = \frac{e^{qv_A/kT} - 1}{e^{qV_{ON}/kT} - 1}$$

and

$$\frac{v_A}{V_{ON}} = \left( \frac{kT/q}{V_{ON}} \right) \ln \left[ 1 + yon(1) \left( e^{qV_{ON}/kT} - 1 \right) \right]$$

The desired  $v_A/V_{ON}$  values can be obtained by inserting the following five lines into the last segment of the CPG program.

*Place before* for i=1:j,  
 $V_{ON}=0.5;$   
 $vrel=[];$  %vrel=vA/VON  
 $kT=0.0259;$

*Place after*  $yon=(A-B)/2;$   
 $vj=(kT/VON)*log(1+yon(1)*(exp(VON/kT)-1));$   
 $vrel=[vrel,vj];$

After the program is run, vrel is read out from the Command window.

### (b) Appropriately modifying Eq. (8.16),

$$\frac{v_A}{V_{ON}} = \left( \frac{kT/q}{V_{ON}} \right) \ln \left[ 1 + \left( 1 - e^{-t/\tau_p} \right) \left( e^{qV_{ON}/kT} - 1 \right) \right]$$

The computational results based on the above relationship are recorded along with the exact results in the table below. Note in all cases that  $v_A/V_{ON}(\text{exact}) > v_A/V_{ON}(\text{quasistatic})$ .

$t/\tau_p$	exact $v_A/V_{ON}$	quasistatic $v_A/V_{ON}$	$t/\tau_p$	exact $v_A/V_{ON}$	quasistatic $v_A/V_{ON}$
0.1	0.9449	0.8782	1.1	0.9923	0.9790
0.2	0.9612	0.9115	1.2	0.9933	0.9814
0.3	0.9701	0.9301	1.3	0.9941	0.9835
0.4	0.9760	0.9425	1.4	0.9949	0.9853
0.5	0.9802	0.9517	1.5	0.9955	0.9869
0.6	0.9835	0.9588	1.6	0.9960	0.9883
0.7	0.9860	0.9644	1.7	0.9965	0.9896
0.8	0.9881	0.9691	1.8	0.9969	0.9906
0.9	0.9897	0.9730	1.9	0.9973	0.9916
1.0	0.9911	0.9762	2.0	0.9976	0.9925

## **CHAPTER 10**

### 10.1

- (a) Common base.
- (b) Common emitter.
- (c) Saturation, active, inverted, and cutoff.
- (d) The buried layer serves as a low-resistance path between the active collector region of the BJT and the top-side collector contact.
- (e)  $N_{AE} \gg N_{DB} > N_{AC}$
- (f)  $W$  in both cases.
- (g) The width of the base is less than, typically much less than, the minority carrier diffusion length in the base.
- (h) The narrow nature of the base couples the current flow across the E-B and C-B junctions, a prerequisite for transistor action.
- (i) The emitter efficiency specifies the fraction of the emitter current that is associated with carrier injection from the emitter into the base.
- (j) The base transport factor is the fraction of the minority carriers injected into the base that successfully diffuse across the quasineutral width of the base and enter the collector.

### 10.2

#### (a) *pnp*

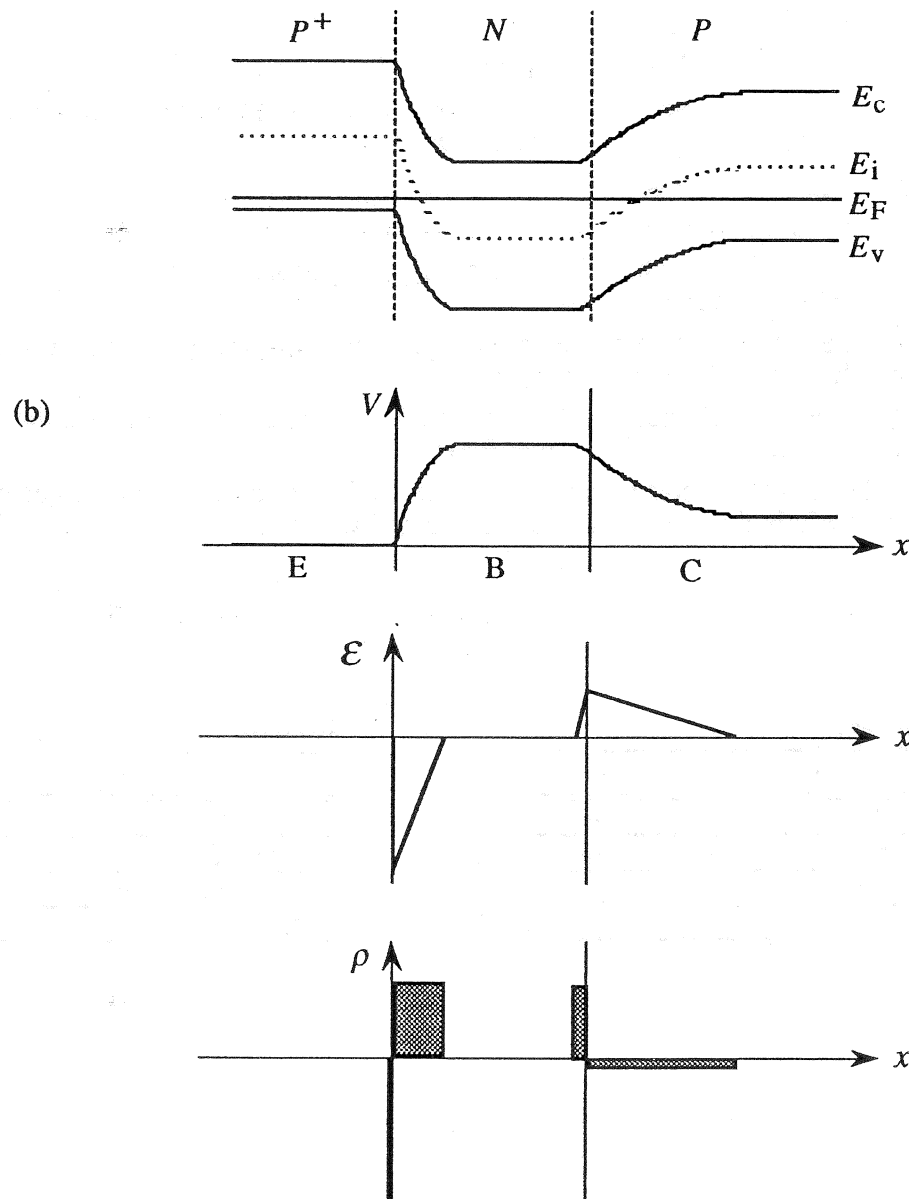
Mode	$V_{EB}$	$V_{CB}$
Active	+	-
Inverted	-	+
Saturation	+	+
Cutoff	-	-

#### (b) *npn*

Mode	$V_{BE}$	$V_{BC}$
Active	+	-
Inverted	-	+
Saturation	+	+
Cutoff	-	-

### 10.3

(a) For the given doping concentrations, one computes  $E_F - E_i = -0.459\text{eV}$ ,  $0.298\text{eV}$ , and  $-0.239\text{eV}$  respectively in the emitter, base, and collector. Also, with  $N_{AE} \gg N_{DB}$ , the E-B depletion width will lie almost exclusively in the base. Likewise, the majority of the C-B depletion width will lie in the collector. The diagram produced by the BJT\_Eband program is displayed below.



$$(c) \quad \Delta V_{CE} = (1/q)[(E_i - E_F)_{\text{emitter}} - (E_i - E_F)_{\text{collector}}] \\ = (kT/q)[\ln(N_{AE}/n_i) - \ln(N_{AC}/n_i)]$$

or

$$\Delta V_{CE} = (kT/q) \ln(N_{AE}/N_{AC}) = (0.0259) \ln(5 \times 10^{17}/10^{14}) = 0.221 \text{ V}$$

(d) As noted in the text (Eq. 10.3),

$$W = W_B - x_{nEB} - x_{nCB}$$

$$x_{nEB} \cong \left[ \frac{2K_S \epsilon_0}{qN_{DB}} V_{biEB} \right]^{1/2} = \left[ \frac{(2)(11.8)(8.85 \times 10^{-14})(0.757)}{(1.6 \times 10^{-19})(10^{15})} \right]^{1/2} = 9.94 \times 10^{-5} \text{ cm}$$

$$x_{nCB} = \left[ \frac{2K_S \epsilon_0}{qN_{DB}} \frac{N_{AC}}{N_{AC} + N_{DB}} V_{biCB} \right]^{1/2} = \left[ \frac{(2)(11.8)(8.85 \times 10^{-14})(10^{14})(0.537)}{(1.6 \times 10^{-19})(10^{15})(1.1 \times 10^{15})} \right]^{1/2} \\ = 2.52 \times 10^{-5} \text{ cm}$$

and therefore

$$W = 3 \times 10^{-4} - 9.94 \times 10^{-5} - 2.52 \times 10^{-5} = 1.75 \times 10^{-4} \text{ cm} = 1.75 \mu\text{m}$$

The emitter-base and collector-base built-in voltages ( $V_{biEB}$  and  $V_{biCB}$ ) were deduced from the  $E_F - E_i$  values computed in part (a).

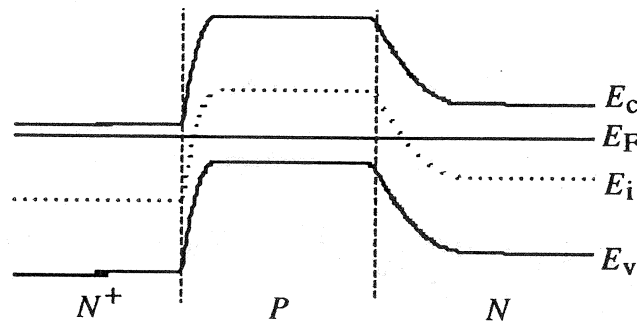
(e)

$$|\mathcal{E}|_{\max(E-B)} = \frac{qN_{DB}}{K_S \epsilon_0} x_{nEB} = \frac{(1.6 \times 10^{-19})(10^{15})(9.94 \times 10^{-5})}{(11.8)(8.85 \times 10^{-14})} = 1.52 \times 10^4 \text{ V/cm}$$

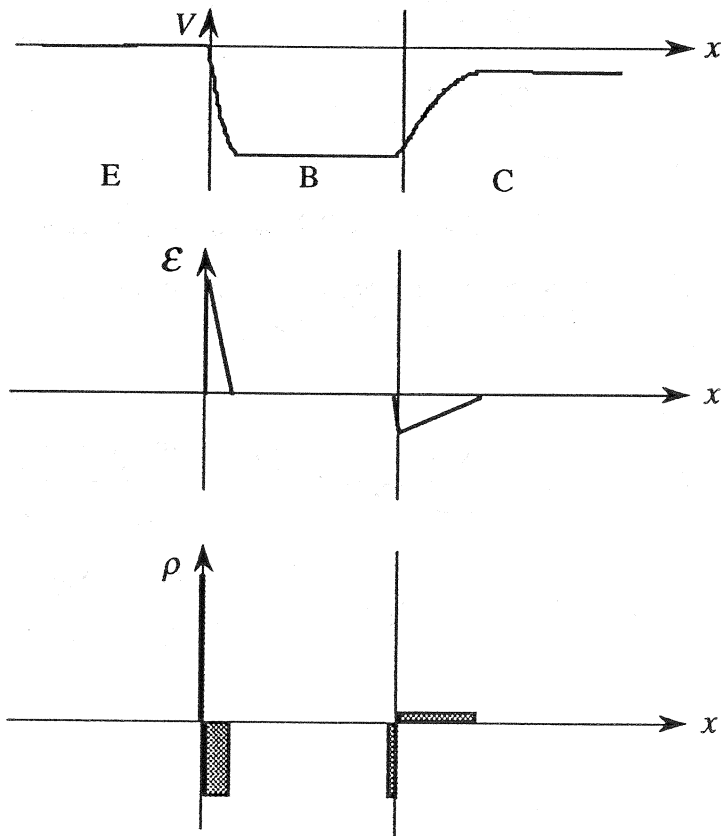
$$\mathcal{E}_{\max(C-B)} = \frac{qN_{DB}}{K_S \epsilon_0} x_{nCB} = \frac{(1.6 \times 10^{-19})(10^{15})(2.52 \times 10^{-5})}{(11.8)(8.85 \times 10^{-14})} = 3.86 \times 10^3 \text{ V/cm}$$

10.4

(a) For the given doping concentrations, one computes  $E_F - E_i = 0.477\text{eV}$ ,  $-0.358\text{eV}$ , and  $0.298\text{eV}$  respectively in the emitter, base, and collector. Also, with  $N_{DE} \gg N_{AB}$ , the E-B depletion width will lie almost exclusively in the base. Likewise, the majority of the C-B depletion width will lie in the collector. The diagram produced by the BJT\_Eband program is displayed below.



(b)



$$(c) \quad \Delta V_{CE} = (1/q)[(E_F - E_i)_{\text{collector}} - (E_F - E_i)_{\text{emitter}}] \\ = (kT/q)[\ln(N_{DC}/n_i) - \ln(N_{DE}/n_i)]$$

or

$$\Delta V_{CE} = (kT/q) \ln(N_{DC}/N_{DE}) = (0.0259) \ln(10^{15}/10^{18}) = -0.179 \text{ V}$$

(d) Analogous to Eq.(10.3) in the text,

$$W = W_B - x_{pEB} - x_{pCB}$$

$$x_{pEB} \cong \left[ \frac{2K_S \epsilon_0}{qN_{AB}} V_{biEB} \right]^{1/2} = \left[ \frac{(2)(11.8)(8.85 \times 10^{-14})(0.835)}{(1.6 \times 10^{-19})(10^{16})} \right]^{1/2} = 3.30 \times 10^{-5} \text{ cm}$$

$$x_{pCB} = \left[ \frac{2K_S \epsilon_0}{qN_{AB}} \frac{N_{DC}}{N_{DC} + N_{AB}} V_{biCB} \right]^{1/2} = \left[ \frac{(2)(11.8)(8.85 \times 10^{-14})(10^{15})(0.656)}{(1.6 \times 10^{-19})(10^{16})(1.1 \times 10^{16})} \right]^{1/2} \\ = 8.82 \times 10^{-6} \text{ cm}$$

and therefore

$$W = 2 \times 10^{-4} - 3.30 \times 10^{-5} - 8.82 \times 10^{-6} = 1.58 \times 10^{-4} \text{ cm} = 1.58 \mu\text{m}$$

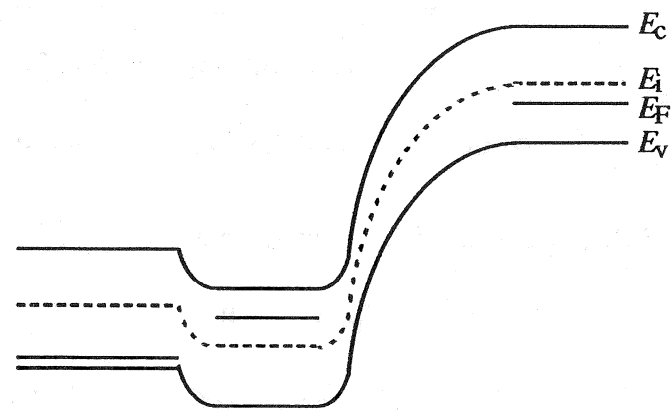
The emitter-base and collector-base built-in voltages ( $V_{biEB}$  and  $V_{biCB}$ ) were deduced from the  $E_F - E_i$  values computed in part (a).

(e)

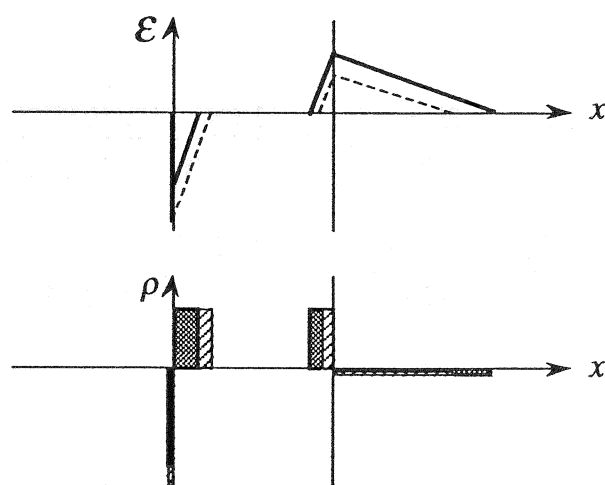
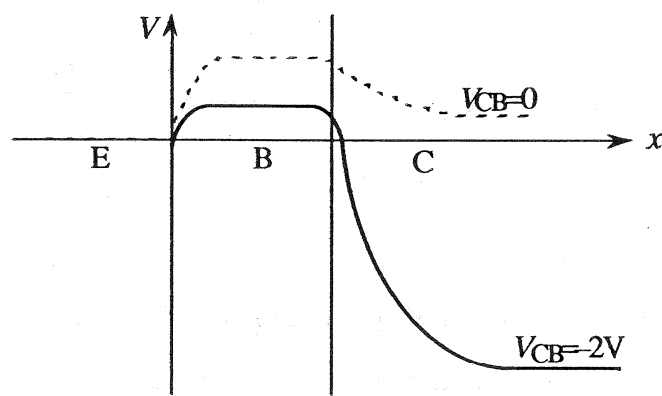
$$\mathcal{E}_{\max(E-B)} = \frac{qN_{AB}}{K_S \epsilon_0} x_{pEB} = \frac{(1.6 \times 10^{-19})(10^{16})(3.30 \times 10^{-5})}{(11.8)(8.85 \times 10^{-14})} = 5.06 \times 10^4 \text{ V/cm}$$

$$|\mathcal{E}|_{\max(C-B)} = \frac{qN_{AB}}{K_S \epsilon_0} x_{pCB} = \frac{(1.6 \times 10^{-19})(10^{16})(8.82 \times 10^{-6})}{(11.8)(8.85 \times 10^{-14})} = 1.35 \times 10^4 \text{ V/cm}$$

10.5  
(a)

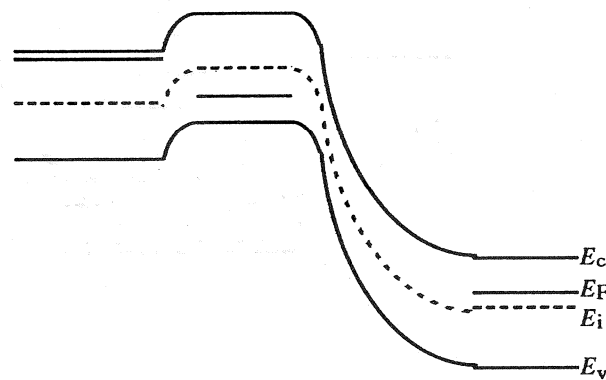


(b)

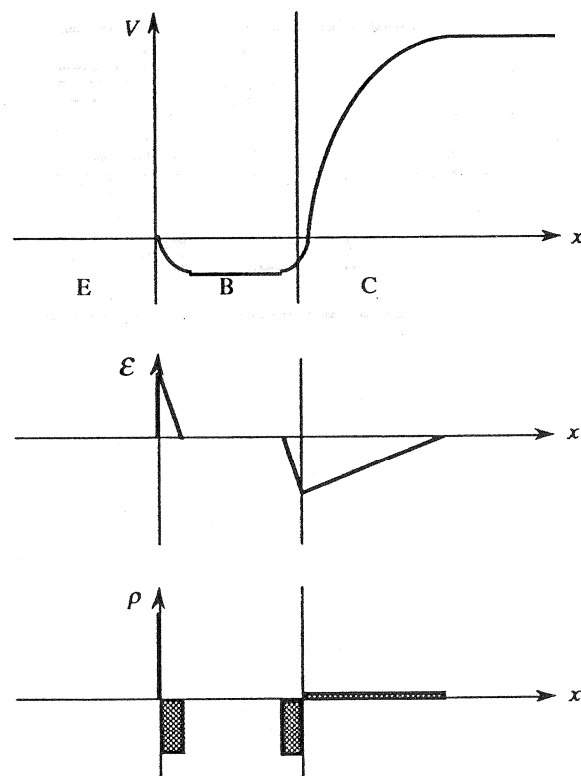


### 10.6

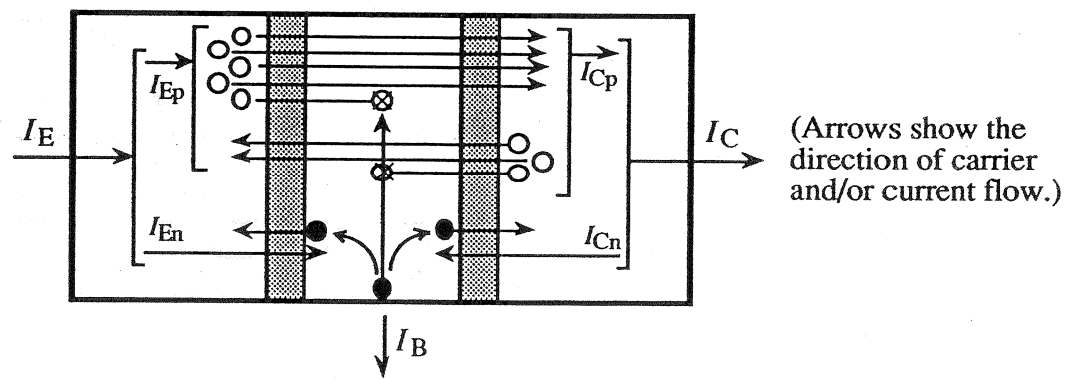
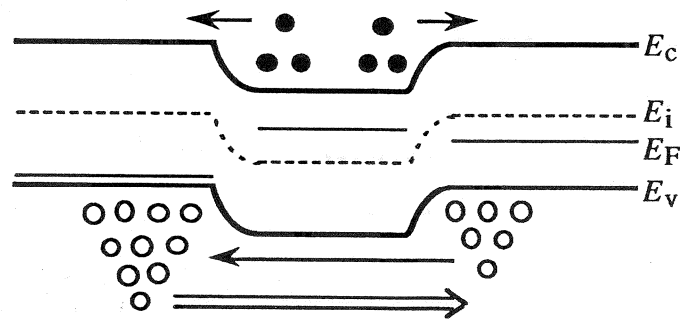
The energy band diagram for a typically doped Si *npn* transistor under equilibrium conditions was sketched in Fig. E10.1(a). Under active mode biasing in the *npn* transistor  $V_{BE} > 0$  and  $V_{BC} < 0$ . Appropriately modifying the Fig. E10.1(a) diagram to account for the applied biases, we conclude



Following the usual procedures in interpreting the energy band diagram to deduce the electrostatic variables, we conclude

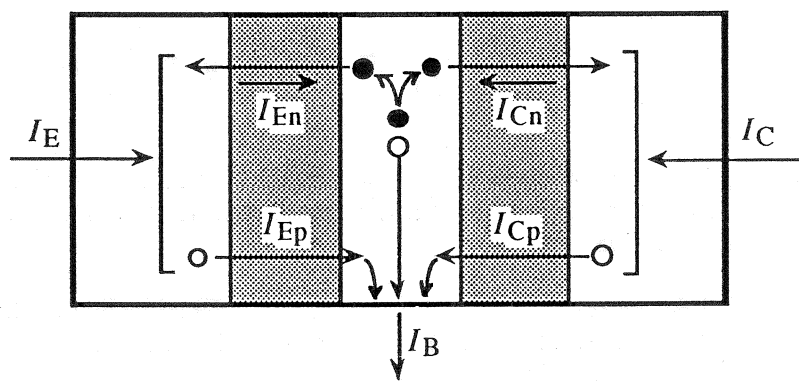
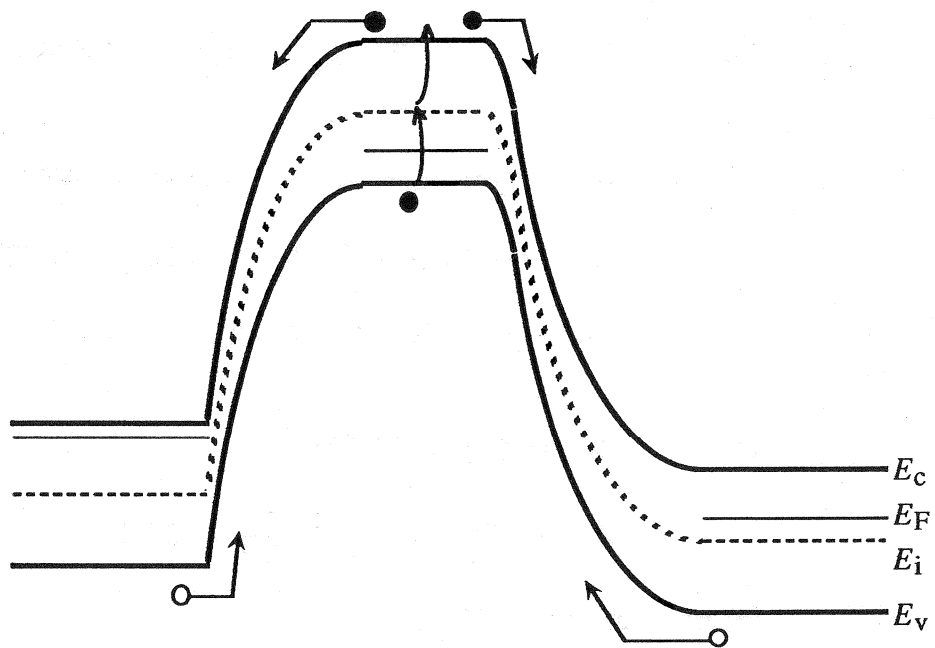


10.7



10 - 8

10.8



10-9

10.9

(a)  $\alpha_T = \frac{I_{CP}}{I_{EP}} = \frac{0.98 \text{ mA}}{1 \text{ mA}} = 0.9800$

(b)  $\gamma = \frac{I_{EP}}{I_{EP} + I_{En}} = \frac{1 \text{ mA}}{1 \text{ mA} + 0.01 \text{ mA}} = 0.9901$

(c)  $I_E = I_{EP} + I_{En} = 1 \text{ mA} + 0.01 \text{ mA} = 1.01 \text{ mA}$

$I_C = I_{CP} + I_{Cn} = 0.98 \text{ mA} + 0.1 \mu\text{A} = 0.9801 \text{ mA}$

$I_B = I_E - I_C = 1.01 \text{ mA} - 0.9801 \text{ mA} = 29.9 \mu\text{A}$

(d)  $\alpha_{dc} = \gamma \alpha_T = 0.9703$

$\beta_{dc} = \frac{\alpha_{dc}}{1 - \alpha_{dc}} = \frac{0.9703}{1 - 0.9703} = 32.7$

(e) As given by Eq. (10.12),

$I_{CB0} = I_{Cn} = 0.1 \mu\text{A}$

Likewise, Eq. (10.17) states

$I_{CE0} = \frac{I_{CB0}}{1 - \alpha_{dc}} = \frac{0.1 \mu\text{A}}{1 - 0.9703} = 3.37 \mu\text{A}$

(f) The  $I_{CP}$  increase while  $I_{EP}$  remains fixed indicates that the base transport factor has been improved. An increase in  $\alpha_T$  in turn leads to an increase in  $\alpha_{dc} = \gamma \alpha_T$  and therefore to an **increase in  $\beta_{dc}$** .

(g) An increase in  $I_{En}$  while  $I_{EP}$  remains fixed indicates that the emitter efficiency has been degraded. A decrease in  $\gamma$  in turn leads to a decrease in  $\alpha_{dc} = \gamma \alpha_T$  and therefore to a **decrease in  $\beta_{dc}$** .

10.10

(a)  $\alpha_T = \frac{I_{Cn}}{I_{En}} = \frac{99 \mu A}{100 \mu A} = 0.9900$

(b)  $\gamma = \frac{I_{En}}{I_{En} + I_{Ep}} = \frac{100 \mu A}{100 \mu A + 1 \mu A} = 0.9901$

(c)  $I_E = I_{En} + I_{Ep} = 100 \mu A + 1 \mu A = 101 \mu A$

$I_C = I_{Cn} + I_{Cp} = 99 \mu A + 0.1 \mu A = 99.1 \mu A$

$I_B = I_E - I_C = 101 \mu A - 99.1 \mu A = 1.9 \mu A$

(d)  $\alpha_{dc} = \gamma \alpha_T = 0.9802$

$\beta_{dc} = \frac{\alpha_{dc}}{1 - \alpha_{dc}} = \frac{0.9802}{1 - 0.9802} = 49.5$

(e) Analogous to Eq. (10.12),

$I_{CB0} = I_{Cp} = 0.1 \mu A$

Likewise, analogous to Eq. (10.17),

$I_{CE0} = \frac{I_{CB0}}{1 - \alpha_{dc}} = \frac{0.1 \mu A}{1 - 0.9802} = 5.05 \mu A$

(f) The  $I_{Cn}$  increase while  $I_{En}$  remains fixed indicates that the base transport factor has been improved. An increase in  $\alpha_T$  in turn leads to an increase in  $\alpha_{dc} = \gamma \alpha_T$  and therefore to an **increase in  $\beta_{dc}$** .

(g) An increase in  $I_{Ep}$  while  $I_{En}$  remains fixed indicates that the emitter efficiency has been degraded. A decrease in  $\gamma$  in turn leads to a decrease in  $\alpha_{dc} = \gamma \alpha_T$  and therefore to a **decrease in  $\beta_{dc}$** .

### 10.11

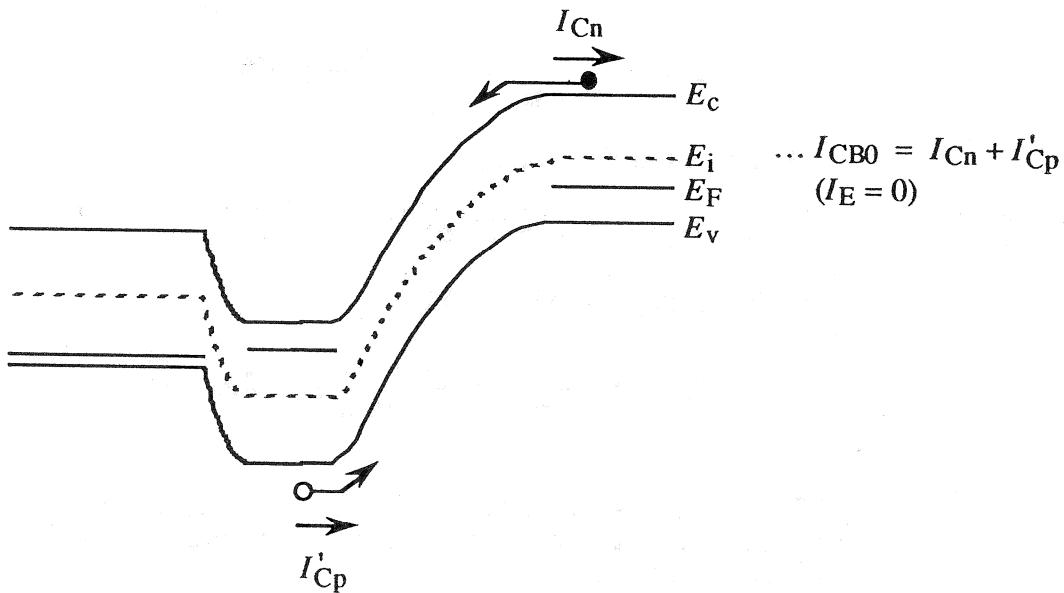
As pictured below, there will indeed be some minority carrier holes in the base that wander into the C-B depletion region and thereby contribute to  $I_{CB0}$ . However, because the base is very narrow, the quasineutral region generation that sustains the hole current is expected to be small, and the hole current itself is therefore expected to be negligible compared to  $I_{Cn}$ . Quantitatively, employing an analysis similar to that in Exercise 6.4,

$$I_{Cn} = q(AL_C) \left( \frac{n_i^2 / N_{AC}}{\tau_C} \right) = qA \frac{n_i^2}{N_{AC}} \frac{D_C}{L_C}$$

and

$$I'_{Cp} < q(AW) \left( \frac{n_i^2 / N_{DB}}{\tau_B} \right) = qA \frac{n_i^2}{N_{DB}} \frac{D_B}{L_B} \frac{W}{L_B}$$

where the B and C subscripts refer to parameters in the base and collector, respectively. Since  $N_{DB} > N_{AC}$  and  $W/L_B \ll 1$ , and assuming  $D_C/L_C \sim D_B/L_B$ , we again conclude  $I'_{Cp} \ll I_{Cn}$ .

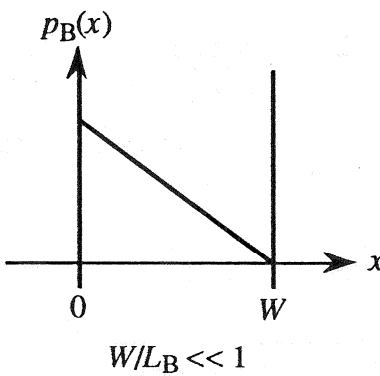


## CHAPTER 11

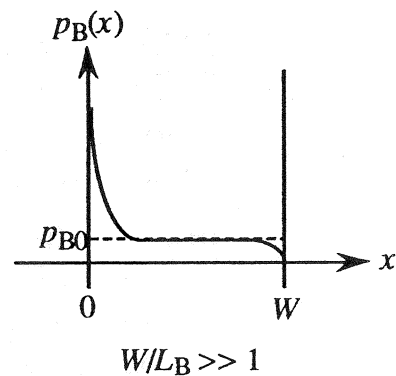
### 11.1

(a) The E, B, and C dopings are assumed to be nondegenerate and constant throughout a given region. The quasineutral widths of the emitter and collector are assumed to be much greater than the minority carrier diffusion lengths in the respective regions.

(b)

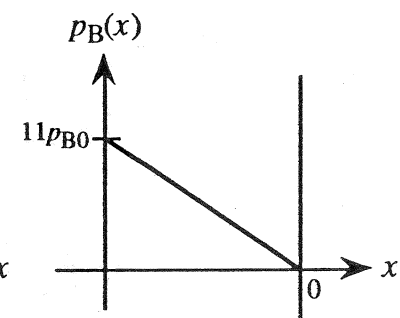
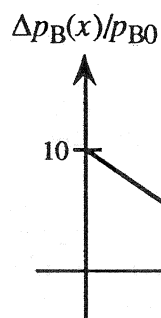
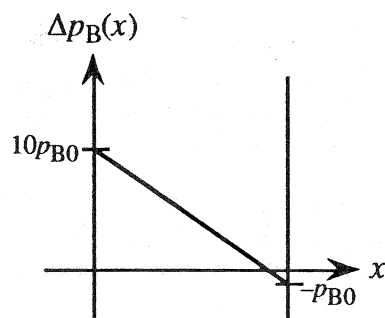


$$W/L_B \ll 1$$



$$W/L_B \gg 1$$

(c)



(d)  $\gamma$ ,  $\alpha_T$ , and  $\alpha_{dc}$  are all typically slightly less than unity.  $\beta_{dc} \sim 100$  to 1000.

(e) The desired equation is simply obtained by subtracting Eq. (11.47b) from Eq. (11.47a).

$$I_B = I_E - I_C = (1-\alpha_F)I_{F0}(e^{qV_{EB}/kT} - 1) + (1-\alpha_R)I_{R0}(e^{qV_{CB}/kT} - 1)$$

(f) As noted in Eq. (11.46)

$$\alpha_F I_{F0} = \alpha_R I_{R0}$$

Thus

$$I_{R0} = \alpha_F I_{F0}/\alpha_R = (0.9944)(4.749 \times 10^{-15})/(0.4286) = 1.102 \times 10^{-14} \text{ A}$$

(g) The quasi-linear slope at low  $V_{EC}$  is caused by base width modulation. The sharp upward curvature when  $V_{EC} \rightarrow V_{CE0}$  is caused by carrier multiplication and feedback.

(h) Yes, it is possible. Even though  $V_{CB0}$  may be punch-through limited, the voltage where  $M \rightarrow 1/\alpha_{dc}$  may be less than the  $V_{CB0}$  due to punch-through.

(i) "Current crowding" is caused by the voltage drop associated with the base current flowing laterally across the face of the emitter.

(j) ...The drift-enhanced transport of carriers across the base decreases the transit time, thereby reduces recombination in the base, which ultimately increases  $\alpha_T$  and the current gains.

...The built-in  $E$ -field and attendant decrease in the carrier transit times across the base lead to an improved high-frequency response.

(k) A Gummel plot is a simultaneous semilog plot of  $I_B$  and  $I_C$  as a function of the input voltage  $V_{EB}$ .

(l) The fall-off in  $\beta_{dc}$  at low  $I_C$  is due to an increasingly important  $I_{R-G}$  component in  $I_B$  as  $I_C(V_{EB})$  is reduced. The fall-off in  $\beta_{dc}$  at high  $I_C$  levels is caused by high-level injection in the collector, current crowding, and/or series resistance.

(m) No ...A totally poly-Si emitter would be essentially the same (function the same) as a totally crystalline-Si emitter.—The minority carrier distribution in a totally poly-Si emitter would be similar to Fig. 11.18(a). (Actually, a totally poly-Si emitter would undoubtedly lead to a poor E-B interface and a poorly operating BJT.)

(n) In general, "heterojunction" refers to a junction between two dissimilar materials. With reference to the HBT, however, a "heterojunction" is understood to be a junction between two dissimilar semiconductors.

(o) In a standard BJT the device is fabricated in a single semiconductor and  $N_E \gg N_B$ . In HBTs the emitter is a wider band gap semiconductor and the base is the heaviest doped of the transistor regions ( $N_E \ll N_B \gg N_C$ ).

## 11.2

(a)  $\gamma = \frac{I_{Ep}}{I_{Ep} + I_{En}} = \frac{I_I}{1.001I_I} = 0.9990$

(b)  $\alpha_T = \frac{I_{Cp}}{I_{Ep}} = \frac{0.999I_I}{I_I} = 0.9990$

(c)  $\alpha_{dc} = \gamma\alpha_T = 0.9980$

$$\beta_{dc} = \frac{\alpha_{dc}}{1 - \alpha_{dc}} = 499$$

(d) There are two possible solution approaches:

Approach #1...

$$I_E = I_{Ep} + I_{En} = 1.001I_I$$

$$I_C = I_{Cp} + I_{Cn} = 0.999I_I + 10^{-6}I_I$$

$$I_B = I_E - I_C = (1.999 \times 10^{-3})I_I$$

Approach #2...

$$I_{B1} = I_{En} = 0.001I_I$$

$$I_{B2} = I_{Ep} - I_{Cn} = 0.001I_I$$

$$I_{B3} = -I_{Cn} = -(10^{-6})I_I$$

$$I_B = I_{B1} + I_{B2} + I_{B3} = (1.999 \times 10^{-3})I_I$$

Note:  $I_{Cn}$  was incorrectly shown on Fig. P11.2 as a negative current in the first printing.

(e) Yes. All currents on the figure are constant across the depletion regions. This implies (see the Depletion Region Considerations in Subsection 6.1.2) that recombination-generation is negligible in these regions.

## 11.3

Provided the direction of positive current flow for  $I_E$ ,  $I_C$ , and  $I_B$  are as defined in Fig. 10.2(b), the equations in Subsection 11.1.1 and 11.1.2 can be appropriately modified for an *npn* BJT by simply making the following substitutions:

$n_E \rightarrow p_E$	$I_{Ep} \rightarrow I_{En}; I_{En} \rightarrow I_{Ep}$
$p_B \rightarrow n_B$	$I_{Cp} \rightarrow I_{Cn}; I_{Cn} \rightarrow I_{Cp}$
$n_C \rightarrow p_C$	$V_{EB} \rightarrow V_{BE}; V_{CB} \rightarrow V_{BC}$

### 11.4

The desired sample computational results along with the generation program (m-file P\_11\_04.m), are reproduced below. Note: The assumed device area,  $A = 10^{-4} \text{ cm}^2$ , was omitted in the first printing.

- (a)  $\cosh(W/L_P) = 1.0018$   
 $\sinh(W/L_P) = 5.9559 \times 10^{-2}$   
 $W/L_P = 5.9524 \times 10^{-2}$
- (b)  $I_{Ep} = 4.9473 \times 10^{-3} \text{ A}$   
 $I_{En} = 7.2194 \times 10^{-6} \text{ A}$   
 $I_{Cp} = 4.9386 \times 10^{-3} \text{ A}$   
 $I_{Cn} = 9.4373 \times 10^{-15} \text{ A}$
- (c)  $I_E = 4.9545 \times 10^{-3} \text{ A}$   
 $I_C = 4.9386 \times 10^{-3} \text{ A}$   
 $I_B = 1.5971 \times 10^{-5} \text{ A}$
- (d)  $I_{B1} = 7.2194 \times 10^{-6} \text{ A}$   
 $I_{B2} = 8.7515 \times 10^{-6} \text{ A}$   
 $I_{B3} = -9.4373 \times 10^{-15} \text{ A}$
- (e)  $\gamma = 0.99854$   
 $\alpha_T = 0.99823$   
 $\alpha_{dc} = 0.99678$   
 $\beta_{dc} = 309.22$

#### MATLAB program script...

```
%Sample Ideal-Transistor Computations...Problem 11.4  
%Initialization  
clear; format compact  
format short e  
  
%Parameters and constants  
NE=1.0e18; NB=1.0e16; NC=1.0e15;  
μE=263; μB=437; μC=1345;  
DE=6.81; DB=11.3; DC=34.8;  
tauE=1.0e-7; tauB=1.0e-6; tauC=1.0e-6;  
LE=8.25e-4; LB=3.36e-3; LC=5.90e-3;  
WB=2.0e-4;
```

```

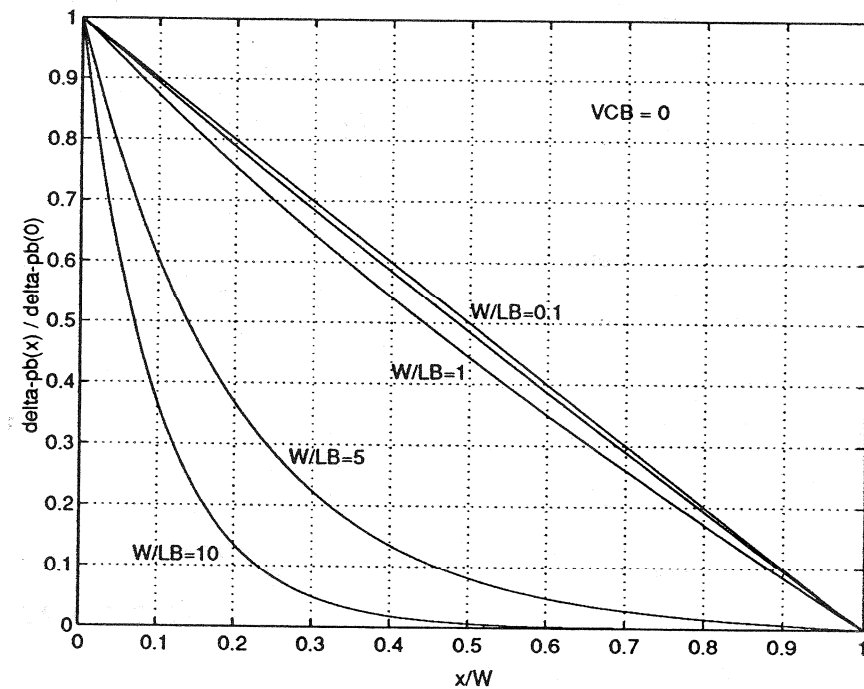
VEB=0.7;
VCB=-5;
W=WB;
A=1.0e-4;
q=1.6e-19;
ni=1.0e10;
kT=0.0259;

%Computations
    %Part (a)
c=cosh (W/LB)
s=sinh (W/LB)
r=W/LB
    %Part (b)
nE0=ni^2/NE;
pB0=ni^2/NB;
nC0=ni^2/NC;
IEp=q*A*DB*pB0/LB*(c/s*(exp(VEB/kT)-1)-1/s*(exp(VCB/kT)-1))
IEn=q*A*DE/LE*nE0*(exp(VEB/kT)-1)
ICp=q*A*DB*pB0/LB*(1/s*(exp(VEB/kT)-1)-c/s*(exp(VCB/kT)-1))
ICn=-q*A*DC/LC*nC0*(exp(VCB/kT)-1)
    %Part (c)
IE=IEp+IEn
IC=ICp+ICn
IB=IE-IC
    %Part (d)
IB1=IEn
IB2=IEp-ICp
IB3=-ICn
    %Part (e)
gamma=IEp/(IEp+IEn)
aT=ICp/IEp
adc=gamma*aT
Bdc=adc/(1-adc)

```

### 11.5

The plot displayed on the next page illustrates how the minority carrier distribution in the base of a BJT varies with  $W/L_B$ . The plot is consistent with the fact that we expect a linear distribution when  $W/L_B \ll 1$  and an exponentially decaying distribution when  $W/L_B \gg 1$ . It is perhaps somewhat surprising, however, that  $W/L_B$  values as large as unity yield a nearly linear distribution.



### MATLAB program script...

```
%Minority Carrier Distribution in the base of a BJT
%Variation with W/LB

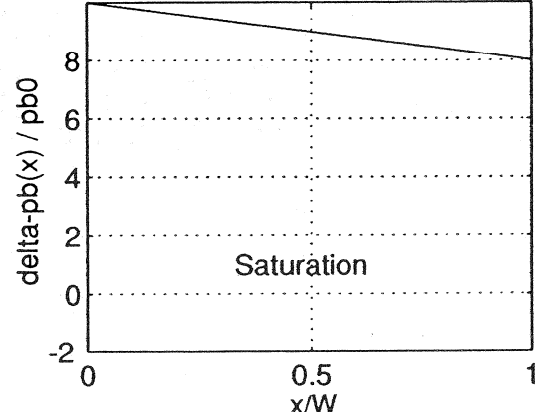
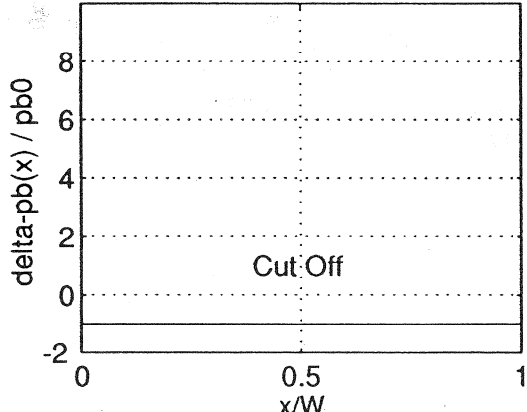
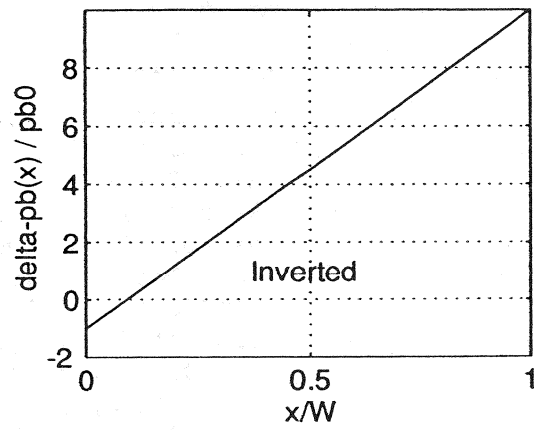
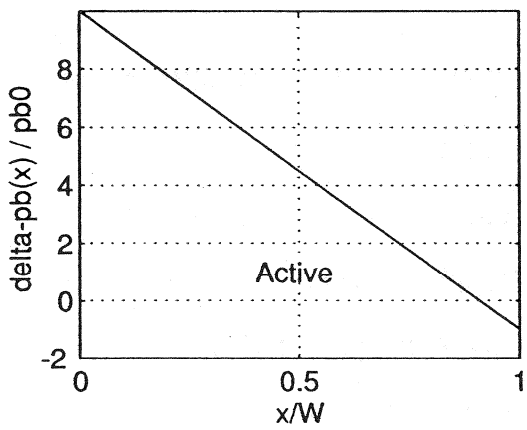
%Initialization
clear; close

%Δpb(x)/Δpb(0) vs. x/W (VCB=0) calculation
%Let r=W/LB, z=x/W, Δpbr=Δpb(x)/Δpb(0)
r=[10 5 1 0.5 0.1];
z=linspace(0,1);
for i=1:5,
    Δpbr(i,:)=sinh(r(i).* (1-z))./sinh(r(i));
end

%Plotting result
plot(z,Δpbr);
axis([0 1 0 1]);
grid
xlabel('x/W'); ylabel('delta-pb(x) / delta-pb(0)');
text(0.65,0.85,'VCB = 0');
text(0.5,0.52,'W/LB=0.1'); text(0.4,0.42,'W/LB=1');
text(0.27,0.28,'W/LB=5'); text(0.07,0.12,'W/LB=10');
```

### 11.6

"Demonstration plots" illustrating the general nature of the minority carrier distribution in a base of a BJT corresponding to the four biasing modes are displayed below. There also follows a listing of the MATLAB m-file used to produce the plots.

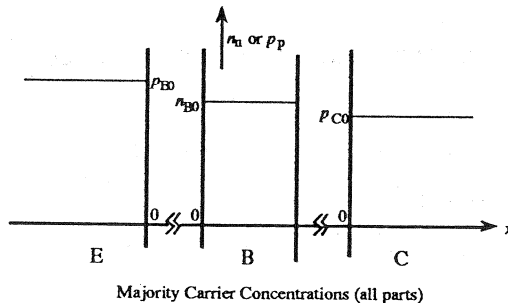


### MATLAB program script...

```
%BJT Biasing Modes Illustration
%Initialization
clear; close
% $\Delta p_b(x)/pb_0$  vs.  $x/W$  calculation
%Let  $r=W/LB$ ,  $z=x/W$ , and  $\Delta p_{br}=\Delta p_b(x)/pb_0$ 
r=0.1;
z=linspace(0,1);
A=[10 -1 -1 10];
B=[-1 10 -1 8];
Apbr=A'*sinh(r*(1-z))/sinh(r) + B'*sinh(r*z)/sinh(r);
%Constructing Plots
    subplot(2,2,1); plot(z,Apbr(1,:));
axis([0 1 -2 10]); grid
xlabel('x/W'); ylabel('delta-pb(x) / pb0');
text(0.4,1,'Active');
    subplot(2,2,2); plot(z,Apbr(2,:));
axis([0 1 -2 10]); grid
xlabel('x/W'); ylabel('delta-pb(x) / pb0');
text(0.37,1,'Inverted');
    subplot(2,2,3); plot(z,Apbr(3,:));
axis([0 1 -2 10]); grid
xlabel('x/W'); ylabel('delta-pb(x) / pb0');
text(0.39,1,'Cut Off');
    subplot(2,2,4); plot(z,Apbr(4,:));
axis([0 1 -2 10]); grid
xlabel('x/W'); ylabel('delta-pb(x) / pb0');
text(0.33,1,'Saturation');
```

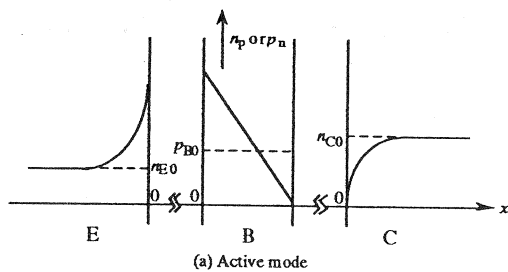
### 11.7

**Majority carriers...** Assuming low-level injection, the majority carrier concentrations will be essentially unperturbed from their equilibrium values in all cases. Thus the majority carrier sketches will all be the same, with the solid carrier-distribution lines lying on top of the dashed equilibrium values in the three device regions.

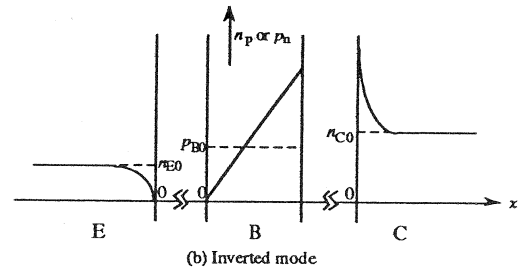


Majority Carrier Concentrations (all parts)

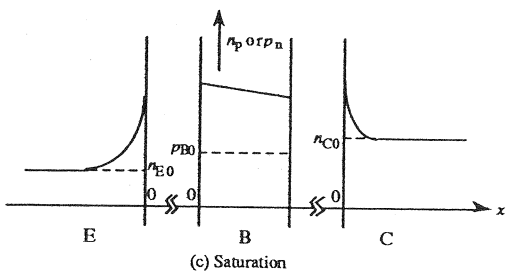
**Minority carriers...** With  $W \ll L_B$ , the minority carrier concentration will vary linearly with position in the base under all biasing conditions. In the emitter and collector regions the carrier concentrations will decay exponentially with distance from the edges of the respective E-B and C-B depletion regions. The carrier concentrations will be greater than the equilibrium values when the applied biases are positive and less than the equilibrium values when the applied biases are negative. The distributions are concluded to be of the general form pictured below. Note that  $p_B(x)$  in the base is approximately zero everywhere under cutoff biasing if  $|V_{EB}|$  and  $|V_{CB}|$  are greater than a few  $kT/q$  volts.



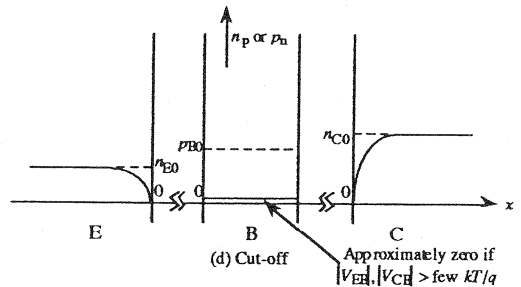
(a) Active mode



(b) Inverted mode



(c) Saturation



Approximately zero if  $|V_{EB}|, |V_{CB}| > \text{few } kT/q$

## 11.8

- (a)  $V_{EB} < 0$ . The E-B junction is concluded to be reverse biased because both  $\Delta n_E/n_{E0}$  and  $\Delta p_B/p_{B0}$  are less than zero at the edges of the E-B depletion region.
- (b)  $V_{CB} > 0$ . The C-B junction is concluded to be forward biased because both  $\Delta p_B/p_{B0}$  and  $\Delta n_C/n_{C0}$  are greater than zero at the edges of the C-B depletion region.
- (c) The boundary condition at the base edge of the C-B depletion region (Eq. 11.4b) requires

$$\Delta p_B(W) = p_{B0}(e^{qV_{CB}/kT} - 1)$$

Thus

$$\Delta p_B(W)/p_{B0} = e^{qV_{CB}/kT} - 1 = 10$$

and assuming room temperature operation

$$V_{CB} = (kT/q) \ln(11) = (0.0259) \ln(11) = 0.062 \text{ V}$$

### (d) **Inverted**

- (e) For an *npn* BJT,  $n_E \rightarrow p_E$ ,  $p_B \rightarrow n_B$ , and  $n_C \rightarrow p_C$ . However, little else changes. The E-B junction would still be reverse biased, the C-B junction forward biased, and the BJT operated in the inverted mode with  $V_{BC} = 0.062$  V. (Note that  $V_{BC}$  replaces  $V_{CB}$ .)

### 11.9

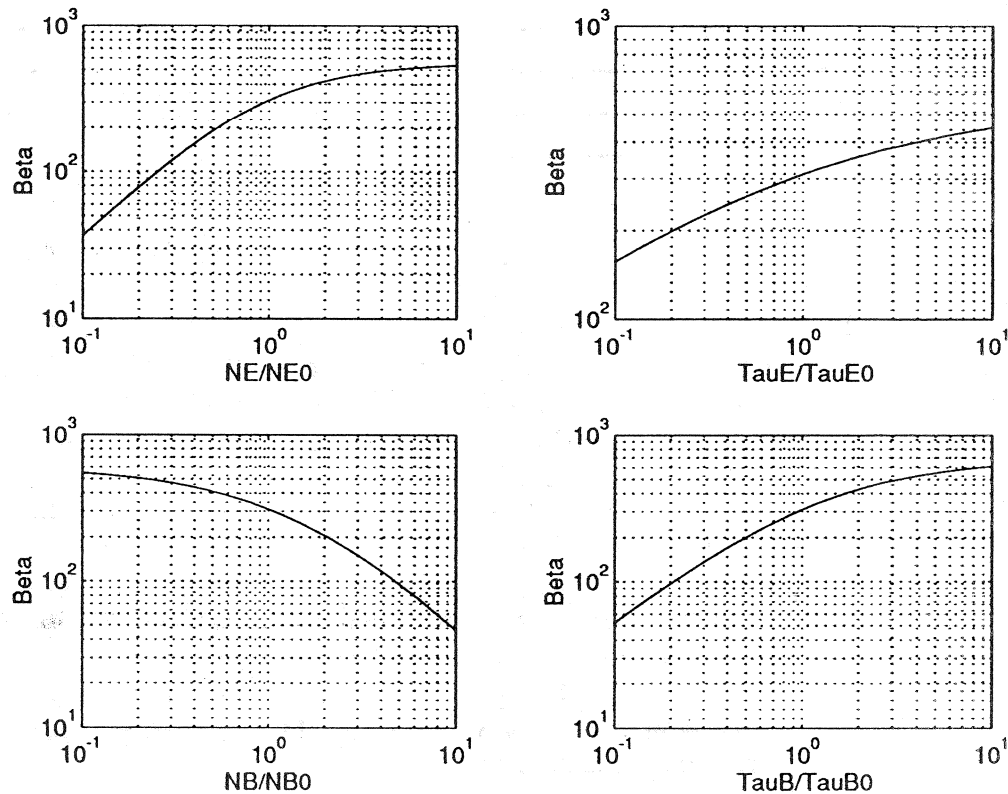
Change	Effect on $\gamma$	Effect on $\alpha_T$	Effect on $\beta_{dc}$
Increase $W_B$	Decreases	Decreases	Decreases
Increase $\tau_B$	No Effect (if $W \ll L_B$ )	Increases	Increases
Increase $N_B$	Decreases	Decreases	Decreases
Increase $\tau_E$	Increases	No Effect	Increases
Increase $N_E$	Increases	Essentially No Effect	Increases

*Explanations:*

- (1) In all cases, the effect on  $\beta_{dc}$  is determined by noting the effect on  $\gamma$  and  $\alpha_T$ . Specifically,  $\beta_{dc}$  exhibits the same modification as  $\alpha_{dc}$ , and  $\alpha_{dc} = \gamma\alpha_T$ . Thus, if the  $\gamma\alpha_T$  product decreases, then  $\beta_{dc}$  decreases; if the  $\gamma\alpha_T$  product increases,  $\beta_{dc}$  increases.
- (2) Assuming increasing  $W_B$  likewise increases  $W$ , the effect of increasing  $W_B$  on  $\gamma$  and  $\alpha_T$  is obvious by inspecting Eqs. (11.41) and (11.42), respectively.
- (3) Since  $L_B = (D_B \tau_B)^{1/2}$ , increasing  $\tau_B$  increases  $L_B$ , which in turn increases  $\alpha_T$ . In a typical BJT,  $W \ll L_B$  and from Eq. (11.41) we conclude increasing  $\tau_B$  has no effect on  $\gamma$ . However, if  $W$  is allowed to be arbitrary, then per Eq. (11.31) increasing  $\tau_B$  increases  $L_B$ , which decreases the sinh/cosh term and thereby increases  $\gamma$ .
- (4) Inspecting Eq. (11.41) it is obvious  $\gamma$  decreases if  $N_B$  increases. Noting that the mobility decreases if  $N_B$  increases and given  $L_B = (D_B \tau_B)^{1/2} = [(kT/q)\mu_B \tau_B]^{1/2}$ , it follows that  $\alpha_T$  also decreases if  $N_B$  increases.
- (5) Since  $L_E = (D_E \tau_E)^{1/2}$ , an increase in  $\tau_E$  leads to an increase in  $L_E$ , which in turn leads to an increase in  $\gamma$  as is obvious from Eq. (11.41). The  $\tau_E$  parameter has no effect on transport through the base and  $\alpha_T$ .
- (6) It is obvious from an inspection of Eqs. (11.41) and (11.42) that  $\gamma$  increases with increasing  $N_E$  and that  $N_E$  does not explicitly affect  $\alpha_T$ . Changing  $N_E$  will slightly change the  $V_{bi}$  across the emitter-base junction and thereby affect the emitter-base depletion width. The net effect on  $\alpha_T$ , however, should typically be small.

### 11.10

The requested plots and the generating program are reproduced below. The graphical results here are indeed consistent with the answers to Problem 11.9.— $\beta_{dc}$  increases with increasing  $N_E$ ,  $\tau_E$ , and  $\tau_B$ .  $\beta_{dc}$  decreases with increasing  $N_B$ .



MATLAB program script...

```
%Problem 11.10...Beta Calculation  
%Initialization  
clear; close  
%Reference Values and Constants  
NE0=1.0e18;  
TauE0=1.0e-7;  
NB0=1.0e16;  
TauB0=1.0e-6;  
WB=2.0e-4;  
kT=0.0259;
```

```

W=WB;

%Mobility Fit Parameters
NDref=1.3e17; NAref=2.35e17;
μnmin=92; μpmin=54.3;
μn0=1268; μp0=406.9;
an=0.91; ap=0.88;

%Beta vs. NE/NE0
%Base Parameters
NB=NBO;
μB=μpmin+μp0./ (1+(NB./NAref).^ap);
DB=kT.*μB;
TauB=TauB0;
LB=sqrt(DB.*TauB);

%Emitter Parameters
NE=logspace(log10(0.1*NE0),log10(10*NE0));
μE=μnmin+μn0./ (1+(NE./NDref).^an);
DE=kT.*μE;
TauE=TauE0;
LE=sqrt(DE.*TauE);

%Beta Calculation
Y=1 ./((DE./DB).* (NB./NE).* (W./LE)+(0.5).* (W./LB).^2);
X=NE./NE0;
%Plotting
subplot(2,2,1); loglog(X,Y); grid
xlabel('NE/NE0'); ylabel('Beta');

%Beta vs. TauE/TauE0
%Revised Emitter Parameters
NE=NE0;
μE=μnmin+μn0./ (1+(NE./NDref).^an);
DE=kT.*μE;
TauE=logspace(log10(0.1*TauE0),log10(10*TauE0));
LE=sqrt(DE.*TauE);

%Beta Calculation
Y=1 ./((DE./DB).* (NB./NE).* (W./LE)+(0.5).* (W./LB).^2);
X=TauE/TauE0;
%Plotting
subplot(2,2,2); loglog(X,Y); grid
xlabel('TauE/TauE0'); ylabel('Beta');

%Beta vs. NB/NBO
%Emitter Parameters
%NE, μE, and DE same as prior calculation
TauE=TauE0;
LE=sqrt(DE.*TauE);

```

```

%Base Parameters
NB=logspace(log10(0.1*NBO),log10(10*NBO));
μB=μpmin+μp0./(1+(NB./NAreff).^ap);
DB=kT.*μB;
TauB=TauB0;
LB=sqrt(DB.*TauB);
%Beta Calculation
Y=1 ./(DE./DB).* (NB./NE).* (W./LE)+(0.5).* (W./LB).^2;
X=NB/NBO;
%Plotting
subplot(2,2,3); loglog(X,Y); grid
xlabel('NB/NBO'); ylabel('Beta')

%Beta vs. TauB/TauB0
%Revised Base Parameters
NB=NBO;
μB=μpmin+μp0./(1+(NB./NAreff).^ap);
DB=kT.*μB;
TauB=logspace(log10(0.1*TauB0),log10(10*TauB0));
LB=sqrt(DB.*TauB);
%Beta Calculation
Y=1 ./(DE./DB).* (NB./NE).* (W./LE)+(0.5).* (W./LB).^2;
X=TauB/TauB0;
%Plotting
subplot(2,2,4); loglog(X,Y); grid
xlabel('TauB/TauB0'); ylabel('Beta')

```

### 11.11

(a) Like in the standard ideal-transistor analysis, the general solution for  $\Delta n_E(x'')$  is

$$\Delta n_E(x'') = A_1 e^{-x''/L_E} + A_2 e^{x''/L_E}$$

However, because of the finite width of the emitter,  $A_2 \neq 0$ . Rather

$$\Delta n_E(x''=0) = n_{E0}(e^{qV_{EB}/kT} - 1) = A_1 + A_2$$

$$\Delta n_E(x''=W_E) = 0 = A_1 e^{-W_E/L_E} + A_2 e^{W_E/L_E}$$

Solving for  $A_1$  and  $A_2$  yields

$$A_1 = \frac{\Delta n_E(0) e^{W_E/L_E}}{e^{W_E/L_E} - e^{-W_E/L_E}} \quad \text{and} \quad A_2 = -\frac{\Delta n_E(0) e^{-W_E/L_E}}{e^{W_E/L_E} - e^{-W_E/L_E}}$$

Substituting back into the general solution then gives

$$\Delta n_E(x'') = \Delta n_E(0) \left[ \frac{e^{(W_E-x'')/L_E} - e^{-(W_E-x'')/L_E}}{e^{W_E/L_E} - e^{-W_E/L_E}} \right]$$

or

$$\boxed{\Delta n_E(x'') = n_{E0} \frac{\sinh[(W_E-x'')/L_E]}{\sinh(W_E/L_E)} (e^{qV_{EB}/kT} - 1)}$$

Applying Eq. (11.7), we obtain the revised  $I_{En}$  expression

$$\boxed{I_{En} = qA \frac{D_E}{L_E} n_{E0} \frac{\cosh(W_E/L_E)}{\sinh(W_E/L_E)} (e^{qV_{EB}/kT} - 1)}$$

(b) Relative to the standard result (Eq. 11.20), the finite width of the emitter leads to the modification

$$n_{E0} \rightarrow n_{E0} \frac{\cosh(W_E/L_E)}{\sinh(W_E/L_E)}$$

or equivalently, since  $n_{E0} = n_i^2/N_E$ ,

$$\frac{1}{N_E} \rightarrow \frac{1}{N_E} \frac{\cosh(W_E/L_E)}{\sinh(W_E/L_E)}$$

Revised expressions for the performance parameters analogous to Eqs. (11.31)–(11.34) are therefore obtained by simply making the above noted substitution. Specifically,

$$\boxed{\left( \frac{D_E}{D_B} \frac{L_B}{L_E} \frac{N_B}{N_E} \right) \rightarrow \left( \frac{D_E}{D_B} \frac{L_B}{L_E} \frac{N_B}{N_E} \right) \frac{\cosh(W_E/L_E)}{\sinh(W_E/L_E)}}$$

in the  $\gamma$ ,  $\alpha_{dc}$ , and  $\beta_{dc}$  expressions.  $\alpha_T$  remains unchanged.

(c) With  $W_E/L_E \ll 1$ ,

$$\frac{\cosh(W_E/L_E)}{\sinh(W_E/L_E)} \approx \frac{L_E}{W_E}$$

and  $L_E$  in the Eq. (11.41)–(11.44) expressions is to first order simply replaced by  $W_E$ . This yields, for example,

$$\boxed{\gamma = \frac{1}{1 + \frac{D_E N_B}{D_B N_E} \frac{W}{W_E}}}$$

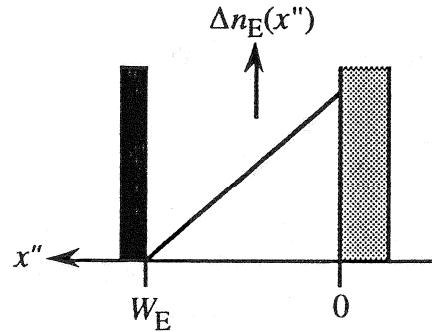
A similar modification applies to  $\alpha_{dc}$  and  $\beta_{dc}$ . Being independent of  $L_E$ , the  $\alpha_T$  expression remains unchanged.

(d) A systematic decrease in  $W_E$  obviously causes a monotonic decrease in  $\gamma$  and a corresponding decrease in  $\beta_{dc}$ . Reducing the width of the emitter has the negative effect of degrading the gain of the BJT (which is the point of the problem).

(e) If  $W_E \ll L_E$  the part (a) result simplifies to

$$\Delta n_E(x'') = \Delta n_E(0) \left(1 - \frac{x''}{W_E}\right)$$

or one obtains a linear distribution analogous to the situation in the base. Moreover, since the emitter is forward biased under active mode biasing,  $\Delta n_E(0) > 0$ . Thus we conclude



11.12

**"Diode" Configuration (a)...**

(a) Note that  $I = I_E$ ,  $V_{EB} = V_A$ , and  $I_C = 0$  for the given circuit configuration. Since  $I_C = 0$ , it follows from Eq. (11.47b) that

$$\alpha_F I_{F0} (e^{qV_{EB}/kT} - 1) = I_{R0} (e^{qV_{CB}/kT} - 1)$$

or

$$(e^{qV_{CB}/kT} - 1) = (\alpha_F I_{F0}/I_{R0})(e^{qV_{EB}/kT} - 1)$$

and

$$I = I_E = I_{F0} (e^{qV_{EB}/kT} - 1) - (\alpha_R I_{R0})(\alpha_F I_{F0}/I_{R0})(e^{qV_{EB}/kT} - 1)$$

Therefore

$$I = (1 - \alpha_R \alpha_F) I_{F0} (e^{qV_A/kT} - 1)$$

(b)  $\Delta p_B(0)/p_{B0} = (e^{qV_{EB}/kT} - 1) = (e^{qV_A/kT} - 1)$

$$\Delta p_B(W)/p_{B0} = (e^{qV_{CB}/kT} - 1) = (\alpha_F I_{F0}/I_{R0})(e^{qV_A/kT} - 1)$$

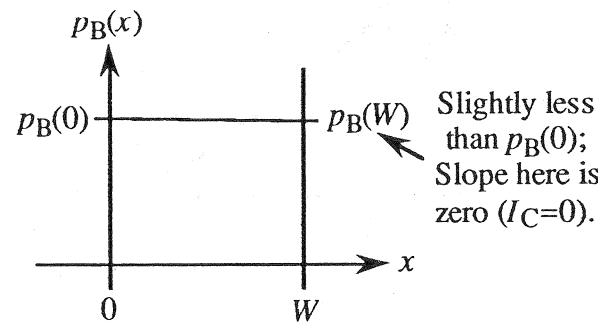
(c) Simplifying

$$\Delta p_B(0)/p_{B0} = (e^{qV_A/kT} - 1)$$

$$\Delta p_B(W)/p_{B0} = \alpha (e^{qV_A/kT} - 1)$$

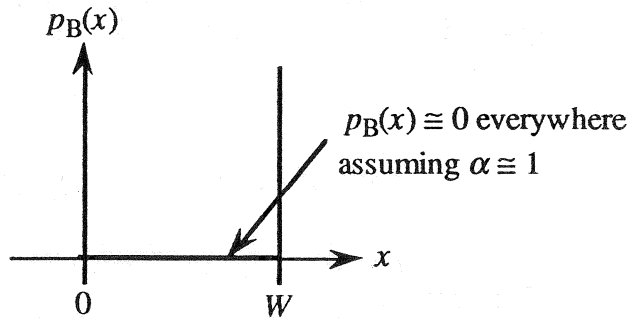
(d) If  $V_A \gg kT/q$ ,

$$p_B(0) = p_{B0} e^{qV_A/kT} \quad \text{and} \quad p_B(W) \equiv \alpha p_{B0} e^{qV_A/kT}$$



(e) If  $-V_A \gg kT/q$ ,

$$p_B(0) \cong 0 \quad \text{and} \quad p_B(W) \cong (1-\alpha)p_{B0} \cong 0$$



**"Diode" Configuration (b)...**

(a) For the given circuit configuration,  $V_{EB} = V_A$ ,  $V_{CB} = 0$ , and  $I = I_E$ . It therefore follows from Eq. (11.47a) that

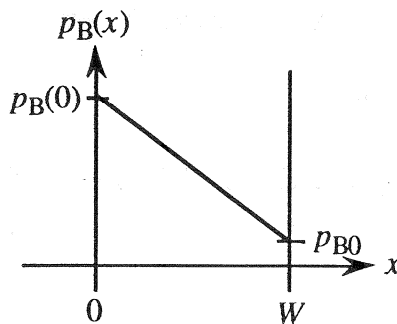
$$I = I_{F0} (e^{qV_A/kT} - 1)$$

(b)  $\Delta p_B(0)/p_{B0} = (e^{qV_{EB}/kT} - 1) = (e^{qV_A/kT} - 1)$

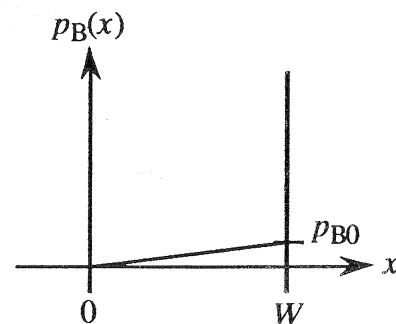
$$\Delta p_B(W)/p_{B0} = (e^{qV_{CB}/kT} - 1) = 0$$

(c) There is no further simplification of the part (b) result.

(d)



(e)



**"Diode" Configuration (c)...**

(a)/(b) For the given configuration,  $V_{EB} - V_{CB} = V_A$  and  $I = I_E = I_C$ . Equating the Ebers-Moll relationships for  $I_E$  and  $I_C$  yields

$$(1-\alpha_F) I_{F0} (e^{qV_{EB}/kT} - 1) = -(1-\alpha_R) I_{R0} (e^{qV_{CB}/kT} - 1)$$

or

$$(e^{qV_{EB}/kT} - 1) = -\xi (e^{qV_{CB}/kT} - 1) \quad \dots \xi \equiv \frac{(1-\alpha_R)I_{R0}}{(1-\alpha_F)I_{F0}}$$

Next noting

$$(e^{qV_{EB}/kT} - 1) = (e^{qV_A/kT} e^{qV_{CB}/kT} - 1) = e^{qV_A/kT} (e^{qV_{CB}/kT} - 1) + (e^{qV_A/kT} - 1)$$

Thus

$$(e^{qV_A/kT} + \xi) (e^{qV_{CB}/kT} - 1) = - (e^{qV_A/kT} - 1)$$

or

$$(e^{qV_{CB}/kT} - 1) = - \frac{(e^{qV_A/kT} - 1)}{(e^{qV_A/kT} + \xi)} = \frac{\Delta p_B(W)}{p_{B0}}$$

and

|-----Part (b) Answer

$$(e^{qV_{EB}/kT} - 1) = \frac{\xi (e^{qV_A/kT} - 1)}{(e^{qV_A/kT} + \xi)} = \frac{\Delta p_B(0)}{p_{B0}}$$

Finally, substituting into Eq. (11.47a) and simplifying

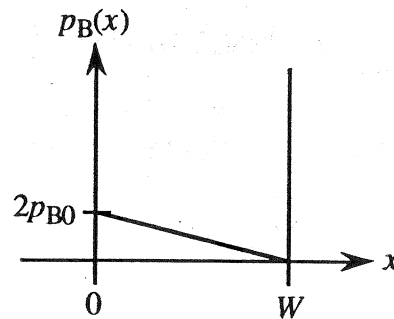
$$I = \frac{(1-\alpha_R)\alpha_F I_{R0} I_{F0} (e^{qV_A/kT} - 1)}{(1-\alpha_F) I_{F0} e^{qV_A/kT} + (1-\alpha_R) I_{R0}}$$

(c) Under the given simplifications,  $\xi \rightarrow 1$  and

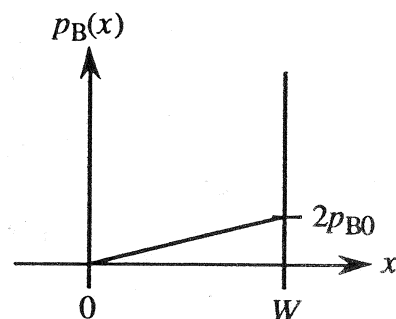
$$\frac{\Delta p_B(0)}{p_{B0}} = - \frac{\Delta p_B(W)}{p_{B0}} = \frac{e^{qV_A/kT} - 1}{e^{qV_A/kT} + 1}$$

(d)/(e) If  $V_A \gg kT/q$ ,  $\Delta p_B(0)/p_{B0} = -\Delta p_B(W)/p_{B0} = 1$  or  $p_B(0) = 2p_{B0}$  and  $p_B(W) = 0$ .  
If  $-V_A \gg kT/q$ ,  $\Delta p_B(0)/p_{B0} = -\Delta p_B(W)/p_{B0} = -1$  or  $p_B(0) = 0$  and  $p_B(W) = 2p_{B0}$ .

(d)



(e)



*“Diode” Configuration (d)...*

(a) For the given connection,  $I = I_B$  and  $V_{EB} = V_{CB} = V_A$ . In general, employing Eqs. (11.47a) and (11.47b),

$$I_B = I_E - I_C = (1-\alpha_F) I_{F0} (e^{qV_{EB}/kT_0} - 1) + (1-\alpha_R) I_{R0} (e^{qV_{CB}/kT_0} - 1)$$

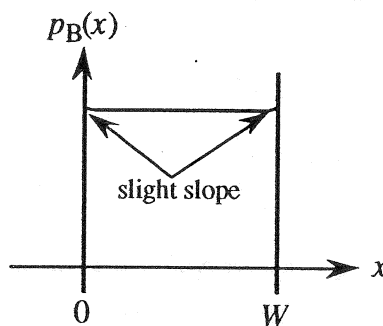
Thus

$$I = [(1-\alpha_F) I_{F0} + (1-\alpha_R) I_{R0}] (e^{qV_A/kT_0} - 1)$$

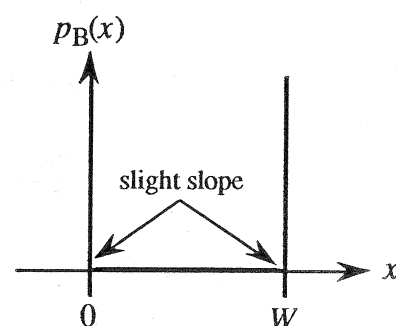
(b)  $\Delta p_B(0)/p_{B0} = \Delta p_B(W)/p_{B0} = (e^{qV_A/kT_0} - 1)$

(c) There is no further simplification of the part (b) result.

(d)



(e)



**"Diode" Configuration (e)...**

(a) Here  $I = -I_C$ ,  $V_{CB} = V_A$ , and  $I_E = 0$ . Since  $I_E = 0$ , it follows from Eq. (11.47a) that

$$I_{F0}(e^{qV_{EB}/kT_0} - 1) = \alpha_R I_{R0}(e^{qV_{CB}/kT_0} - 1)$$

or

$$(e^{qV_{EB}/kT_0} - 1) = (\alpha_R I_{R0}/I_{F0})(e^{qV_{CB}/kT_0} - 1)$$

and

$$I = -I_C = -(\alpha_F I_{F0})(\alpha_R I_{R0}/I_{F0})(e^{qV_{CB}/kT_0} - 1) + I_{R0}(e^{qV_{CB}/kT_0} - 1)$$

Therefore

$$I = (1 - \alpha_R \alpha_F) I_{R0} (e^{qV_A/kT_0} - 1)$$

(b)  $\Delta p_B(0)/p_{B0} = (e^{qV_{EB}/kT_0} - 1) = (\alpha_R I_{R0}/I_{F0})(e^{qV_A/kT_0} - 1)$

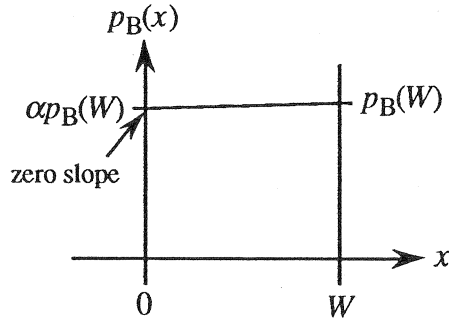
$$\Delta p_B(W)/p_{B0} = (e^{qV_{CB}/kT_0} - 1) = (e^{qV_A/kT_0} - 1)$$

(c) Simplifying

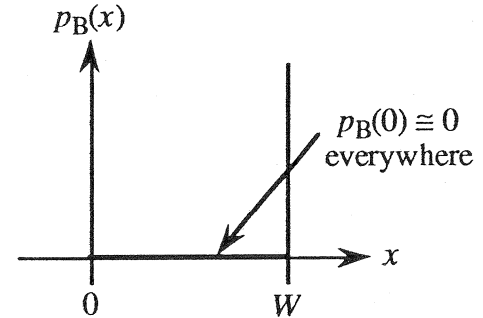
$$\Delta p_B(0)/p_{B0} = \alpha (e^{qV_A/kT_0} - 1)$$

$$\Delta p_B(W)/p_{B0} = (e^{qV_A/kT_0} - 1)$$

(d)



(e)



**"Diode" Configuration (f)...**

(a) Here  $V_{EB} = 0$ ,  $V_{CB} = V_A$ , and  $I = -I_C$ . It therefore follows from Eq. (11.47b) that

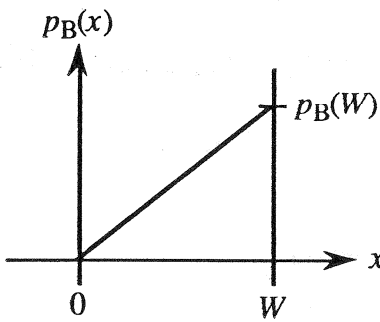
$$I = I_{R0} (e^{qV_A/kT} - 1)$$

(b)  $\Delta p_B(0)/p_{B0} = (e^{qV_{EB}/kT} - 1) = 0$

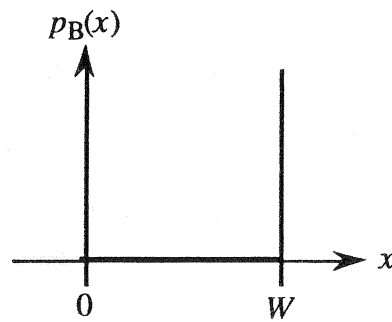
$$\Delta p_B(W)/p_{B0} = (e^{qV_{CB}/kT} - 1) = (e^{qV_A/kT} - 1)$$

(c) There is no further simplification of the part (b) result.

(d)

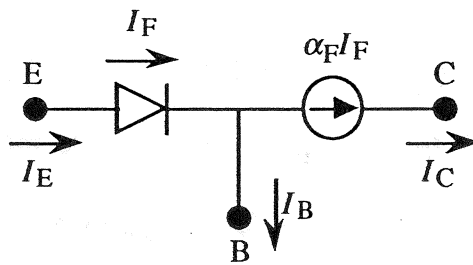


(e)



### 11.13

(a) Since  $V_{CB} = 0$  at the active-mode/saturation-mode boundary, it follows that  $I_R = 0$ . The two Ebers-Moll circuit elements involving  $I_R$  therefore vanish yielding the following simplified circuit.



(b) As deduced from the part (a) circuit,

$$I_B = I_E - I_C = I_F - \alpha_F I_F = (1 - \alpha_F) I_{F0} (e^{qV_{EB}/kT} - 1)$$

but

$$V_{EC} = V_{EB} - V_{CB} = V_{EB} \quad (V_{CB} = 0)$$

Thus

$$I_B = (1 - \alpha_F) I_{F0} (e^{qV_{EC}/kT} - 1)$$

and

$$V_{EC} = \frac{kT}{q} \ln \left[ 1 + \frac{I_B}{(1 - \alpha_F) I_{F0}} \right]$$

### 11.14

(a) Solving Eq. (11.47a) for  $\exp(qV_{EB}/kT) - 1$ , one obtains

$$e^{qV_{EB}/kT} - 1 = \frac{I_E + \alpha_R I_{R0}(e^{qV_{CB}/kT} - 1)}{I_{F0}}$$

Substituting the  $\exp(qV_{EB}/kT) - 1$  expression into Eq. (11.47b) then yields

$$I_C = \alpha_F I_E + \alpha_F \alpha_R I_{R0}(e^{qV_{CB}/kT} - 1) - I_{R0}(e^{qV_{CB}/kT} - 1)$$

or

$$I_C = \alpha_F I_E - (1 - \alpha_F \alpha_R) I_{R0}(e^{qV_{CB}/kT} - 1) \quad \Leftarrow \text{desired equation}$$

(b) Making use of Eqs. (11.47a) and (11.47b), we can write

$$I_B = I_E - I_C = (1 - \alpha_F) I_{F0}(e^{qV_{EB}/kT} - 1) + (1 - \alpha_R) I_{R0}(e^{qV_{CB}/kT} - 1)$$

Now

$$V_{CB} = V_{CE} + V_{EB} = V_{EB} - V_{EC}$$

and therefore

$$I_B = (1 - \alpha_F) I_{F0} e^{qV_{EB}/kT} - (1 - \alpha_F) I_{F0} + (1 - \alpha_R) I_{R0} e^{qV_{EB}/kT} e^{-qV_{EC}/kT} - (1 - \alpha_R) I_{R0}$$

or rearranging to obtain the desired equation

$$I_B = [(1 - \alpha_F) I_{F0} + (1 - \alpha_R) I_{R0} e^{-qV_{EC}/kT}] e^{qV_{EB}/kT} - [(1 - \alpha_F) I_{F0} + (1 - \alpha_R) I_{R0}]$$

(c) Eq. (11.47b) can be rewritten

$$\begin{aligned} I_C &= \alpha_F I_{F0} e^{qV_{EB}/kT} - \alpha_F I_{F0} - I_{R0} e^{qV_{EB}/kT} e^{-qV_{EC}/kT} + I_{R0} \\ &= (\alpha_F I_{F0} - I_{R0} e^{-qV_{EC}/kT}) e^{qV_{EB}/kT} + I_{R0} - \alpha_F I_{F0} \end{aligned}$$

Referring to the  $I_B$  solution in part (b), we note

$$e^{qV_{EB}/kT} = \frac{I_B + (1 - \alpha_F) I_{F0} + (1 - \alpha_R) I_{R0}}{(1 - \alpha_F) I_{F0} + (1 - \alpha_R) I_{R0} e^{-qV_{EC}/kT}}$$

which when substituted into the  $I_C$  expression yields

$$I_C = \frac{(\alpha_F I_{F0} - I_{R0} e^{-qV_{EC}/kT}) [I_B + (1 - \alpha_F) I_{F0} + (1 - \alpha_R) I_{R0}]}{(1 - \alpha_F) I_{F0} + (1 - \alpha_R) I_{R0} e^{-qV_{EC}/kT}} + I_{R0} - \alpha_F I_{F0}$$

### 11.15

(a) As recorded in Exercise 11.7, the general relationship for the common emitter input characteristic is

$$I_B = [(1-\alpha_F)I_{F0} + (1-\alpha_R)I_{R0}e^{-qV_{EC}/kT}]e^{qV_{EB}/kT} - [(1-\alpha_F)I_{F0} + (1-\alpha_R)I_{R0}]$$

For a routine bias of  $V_{EC} > \text{few } kT/q$  volts, the term involving  $\exp(-qV_{EC})$  will be negligible. Moreover, the second group of terms is typically small and may be completely ignored for  $V_{EB}$  biases normally encountered in practice. Thus the  $I_B$  expression reduces to

$$I_B \approx (1-\alpha_F)I_{F0}e^{qV_{EB}/kT}$$

Using Eqs. (11.45a) and (11.46) to display the explicit parametric dependencies, one obtains

$$I_B \approx qA \left[ \frac{D_E}{L_E} n_{E0} + \frac{D_B}{L_B} p_{B0} \frac{\cosh(W/L_B) - 1}{\sinh(W/L_B)} \right] e^{qV_{EB}/kT}$$

In a standard transistor  $W \ll L_B$  and

$$\frac{\cosh(W/L_B) - 1}{\sinh(W/L_B)} \approx \frac{(1/2)(W/L_B)^2}{W/L_B} = W/2L_B$$

and

$$I_B = qA \left( \frac{D_E}{L_E} n_{E0} + \frac{1}{2} \frac{D_B}{L_B} \frac{W}{L_B} p_{B0} \right) e^{qV_{EB}/kT}$$

or

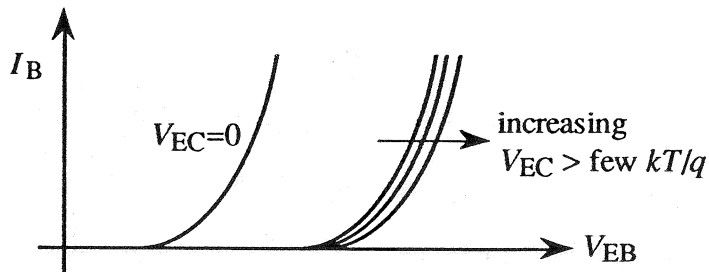
$$I_B = qA \left( \frac{D_E}{L_E} \frac{n_i^2}{N_E} + \frac{1}{2} \frac{W}{L_B} \frac{D_B}{L_B} \frac{n_i^2}{N_B} \right) e^{qV_{EB}/kT}$$

If  $D_E N_B W / D_B N_E L_E \gg (1/2)(W/L_B)^2$ , then the first term inside the parentheses in the above expression will be much greater than the second term. We conclude for the specified situation

$$I_B \approx qA \left( \frac{D_E}{L_E} \frac{n_i^2}{N_E} \right) e^{qV_{EB}/kT}$$

There is no  $W$ -dependence in the above expression. Therefore the common emitter input characteristics are expected to be relatively insensitive to base width modulation if the gain is limited by the emitter efficiency.

(b) If the gain is not limited by the emitter efficiency, then the second term in the simplified  $I_B$  expression developed in part (a) must be retained. This second term decreases with decreasing  $W$ , and  $I_B$  is therefore predicted to decrease with increasing  $V_{EC}$ . For the specified situation, the expected form of the common emitter input characteristics are as sketched below.



### 11.16

If  $V_{EB} = 0.7$  V instead of zero as assumed in Exercise 11.8, then  $x_{nEB}$  will be reduced and  $V_{CB}$  is expected to increase. Specifically, recalculating  $x_{nEB}$  and  $V_{CB}$ ,

$$x_{nEB} = \left[ \frac{2K_S \epsilon_0}{q} \frac{N_E}{N_B(N_E + N_B)} (V_{bi(EB)} - V_{EB}) \right]^{1/2}$$

$$= \left[ \frac{(2)(11.8)(8.85 \times 10^{-14})(10^{18})(0.835 - 0.7)}{(1.6 \times 10^{-19})(10^{16})(1.01 \times 10^{18})} \right]^{1/2} = 1.32 \times 10^{-5} \text{ cm}$$

$$V_{CB} = V_{bi(CB)} - \frac{(W_B - x_{nEB})^2}{\frac{2K_S \epsilon_0}{q} \frac{N_C}{N_B(N_C + N_B)}} \quad \dots \text{at punch-through}$$

$$= 0.656 - \frac{(2 \times 10^{-4} - 1.32 \times 10^{-5})^2}{\left[ \frac{(2)(11.8)(8.85 \times 10^{-14})(10^{15})}{(1.6 \times 10^{-19})(10^{16})(1.1 \times 10^{16})} \right]} = -293 \text{ V}$$

### 11.17

(a) [Transistor A]. Referring to Eq. (11.41),

$$\gamma = \frac{1}{1 + \frac{D_E N_B W}{D_B N_E L_E}}$$

In Transistor A,  $N_E \gg N_B$  and  $\gamma \rightarrow 1$ . In Transistor B,  $N_E < N_B$  and  $\gamma$  is expected to be considerably less than unity.

One might alternatively argue that  $I_{Ep} \gg I_{En}$  in Transistor A, while  $I_{En} > I_{Ep}$  in Transistor B. Since  $\gamma = I_{Ep}/(I_{Ep}+I_{En})$  in a *pnp* transistor, Transistor A clearly has the greater emitter injection efficiency.

(b) Under active mode biasing  $V_{EB} > 0$  and  $V_{CB} < 0$ . Considering the more important reverse-bias collector-base junction, there is very little incursion of the depletion region into the base in Transistor A. For Transistor B, however, most of the depletion region lies in the base because  $N_C \gg N_B$ . Thus [Transistor B] will be more sensitive to base width modulation.

(c) [Transistor A].  $V_{CB0}$  is approximately equal to  $V_{BR}$  of the C-B junction if the BJT is limited by avalanche breakdown.  $V_{BR}$  in turn is roughly inversely proportional to the doping on the lightly-doped side of the *pn* junction. In Transistor A, the collector is the lower doped with  $N_C = 10^{14}/\text{cm}^3$ ; in Transistor B, the base has the lighter doping,  $N_B = 10^{15}/\text{cm}^3$ . Since  $N_C$  of Transistor A is less than  $N_B$  of Transistor B, Transistor A will exhibit the larger  $V_{CB0}$ .

### 11.18

The following "data" was obtained by running the BJTplus program (E\_11\_10.m) with base width modulation included (but excluding carrier multiplication).

$I_B(\mu A)$	$V_{EC}(V)$	$I_C(mA)$
2.5	40.9	0.807
2.5	101.2	1.089
5.0	40.9	1.614
5.0	101.2	2.177
7.5	40.9	2.421
7.5	101.2	3.266
10.0	40.9	3.228
10.0	101.2	4.354

Seeking to fit the data with the relationship

$$I_C = B(V_{EC} - V_\epsilon)I_B$$

one computes

$$B = \frac{I_{C2} - I_{C1}}{I_B(V_{EC2} - V_{EC1})}$$

and

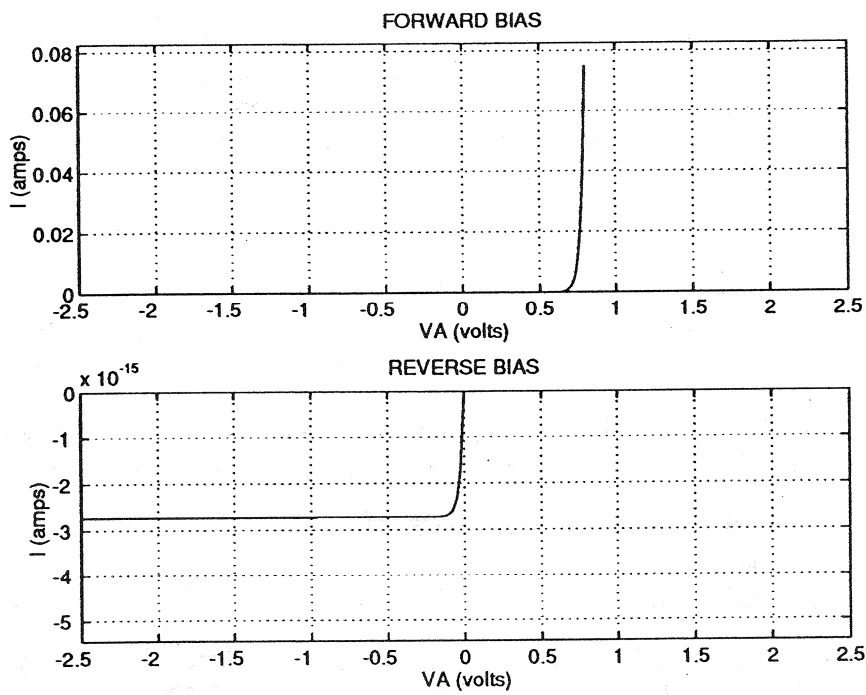
$$V_\epsilon = V_{EC2} - \frac{I_{C2}}{B I_B}$$

The same answer,  $B = 1.87/V$  and  $V_\epsilon = -132V$  is obtained employing all four data sets; i.e., for the given device

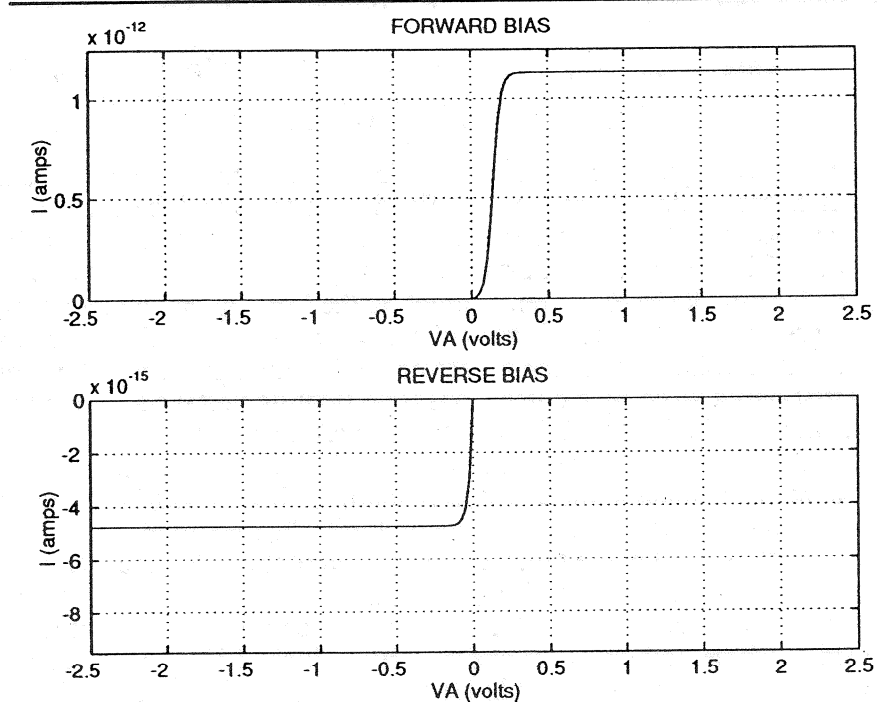
$$I_C = (1.87I_B)(V_{EC} + 132) \quad \dots V_{EC} \text{ in volts; } I_B, I_C \text{ in amps}$$

### 11.19

- (a) Basically, one obtains the same "ideal diode" type characteristic for all of the "diode" connections EXCEPT for the floating-base (c)-connection. The (c)-connection exhibits a reverse-bias type characteristic under both reverse and forward biasing. Representative print-outs of the  $I$ - $V$  characteristics generated by the P\_11\_19a.m program (included on the Instructor's disk) are reproduced on the next page.



Configuration (a)



Configuration (c)

(b) Generation of the  $I$ - $V$  characteristics with base-width modulation and carrier multiplication included is considerably more challenging than initially envisioned by the author. This is especially true of the floating terminal connections (connections a, c, e). For one, it is necessary to associate separate carrier multiplication factors with the E-B and C-B junctions. If  $V_{EB0}$  and  $V_{CB0}$  are the avalanche breakdown voltages of the E-B and C-B junctions respectively, then  $MF = 1/[1-(|V_A|/V_{EB0})^m]$  is associated with carrier multiplication in the E-B junction under reverse bias conditions and  $MR = 1/[1-(|V_A|/V_{CB0})^m]$  is associated with carrier multiplication in the C-B junction. In the computations, carrier multiplication is included by replacing  $I_{F0}$  by  $MF*I_{F0}$  and  $I_{R0}$  by  $MR*I_{R0}$ . (Note, however, that  $\alpha_F I_{F0}$  and  $\alpha_R I_{R0}$  are NOT multiplied by the  $M$ -factor.) Since base width modulation and carrier multiplication has little effect on the  $V_A > 0$  characteristics (except for the (c)-connection), only the reverse bias characteristics are included in the revised computations (except for the (c)-connection).

The voltages required for the computations are straightforward in cases where two of the terminals are shorted together. Specifically, in these cases one has

- case (b) ...  $V_{EB} = V_A; V_{CB} = 0$
- case (d) ...  $V_{EB} = V_A; V_{CB} = V_A$
- case (f) ...  $V_{EB} = 0; V_{CB} = V_A$

In connections (a) and (e) the voltage across the open junction floats up or down to assure that no current flows across this junction. The voltage across the open junction can be determined from the part (b) answers to Problem 11.12. Specifically, we find

- case (a) ...  $V_{EB} = V_A; V_{CB} = (kT/q) \ln[1 + (\alpha_F I_{F0}/I_{R0})(e^{qV_A/kT} - 1)]$
- case (e) ...  $V_{EB} = (kT/q) \ln[1 + (\alpha_R I_{R0}/I_{F0})(e^{qV_A/kT} - 1)]; V_{CB} = V_A$

The floating voltages pose somewhat of a computational problem. The Ebers-Moll parameters are needed to compute the floating voltage, and the computation of the Ebers-Moll parameters in turn depend on the floating voltage when base-width modulation is included. This is handled in the calculations by first computing the Ebers-Moll parameters ignoring base-width modulation, computing the floating voltage, redoing the Ebers-Moll parameters computation with base-width modulation included and employing the first-guess floating voltage, and then repeating the iteration procedure if necessary. It was found that only two complete iterations (two floating voltage and two base-width included computations of the Ebers-Moll parameters) was necessary.

As a final point relative to the applied voltages, please note that the avalanche breakdown in the E-B junction limits the maximum applied voltage in cases (a), (b) and (d). Avalanche breakdown in the C-B junction limits the maximum applied voltage in cases (e) and (f). With  $N_B > N_C$ , the breakdown voltage of the E-B junction is of course lower than the breakdown voltage of the C-B junction.

The (c)-connection poses the most serious computational problems. It is the only connection where both negative and positive values of  $V_A$  must be considered. Also, with the base floating, there is a built-in feedback effect as described in Subsection 11.2.4. One

therefore expects the reverse and forward limiting voltages to be somewhat less than the respective avalanche breakdown voltages. Finally, the junction voltages are coupled, with  $V_{EB} - V_{CB} = V_A$ . Note from the (c)-connection analysis in Problem 11.12 that

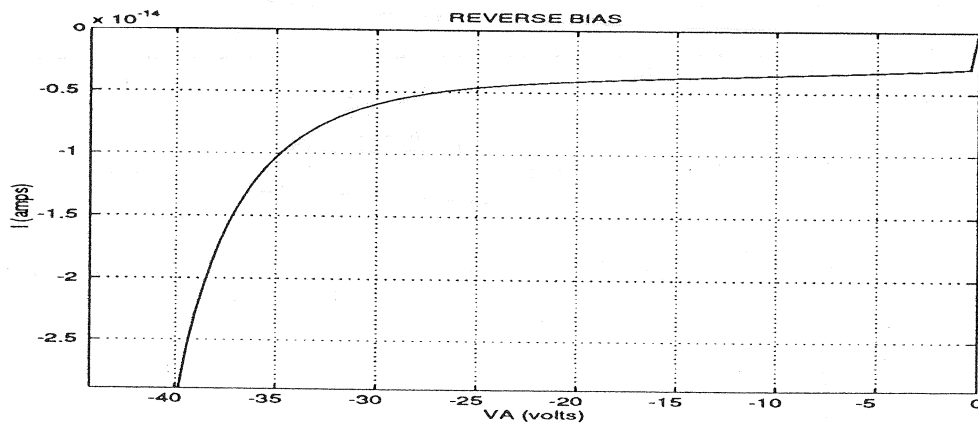
$$(e^{qV_{EB}/kT} - 1) = (e^{qV_{CB}/kT} e^{qV_A/kT} - 1) = -\frac{(1-\alpha_R)I_{R0}}{(1-\alpha_F)I_{F0}} (e^{qV_{CB}/kT} - 1)$$

and upon solving for  $V_{CB}$ ,

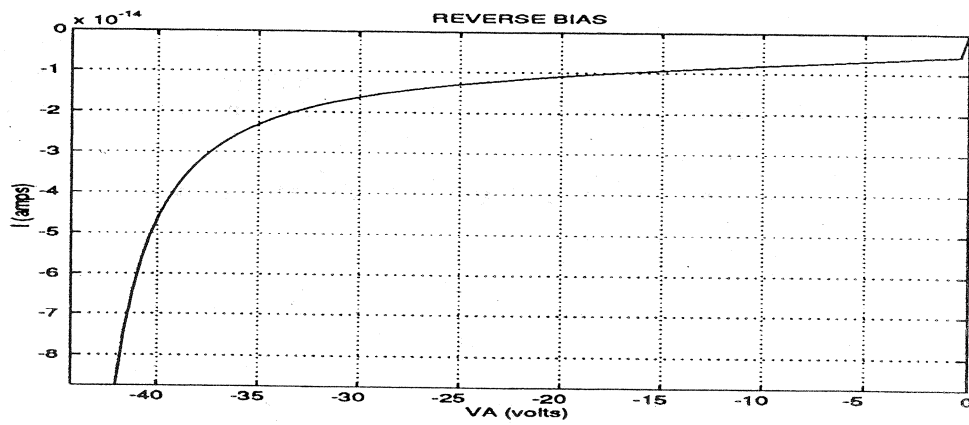
$$V_{CB} = \frac{kT}{q} \ln \left[ \frac{1 + \frac{(1-\alpha_R)I_{R0}}{(1-\alpha_F)I_{F0}}}{e^{qV_A/kT} + \frac{(1-\alpha_R)I_{R0}}{(1-\alpha_F)I_{F0}}} \right]$$

Again, it is necessary to perform an iteration to determine the junction voltages and the Ebers-Moll parameters. Some additional care must be taken in handling  $\exp(qV_A/kT)$  for forward biases. Unless the  $V_{CB}$  expression is modified, the exponential will exceed the largest value handled by the MATLAB program. When this happens, the exponential is artificially set equal to  $\infty$ , leading to erroneous results.

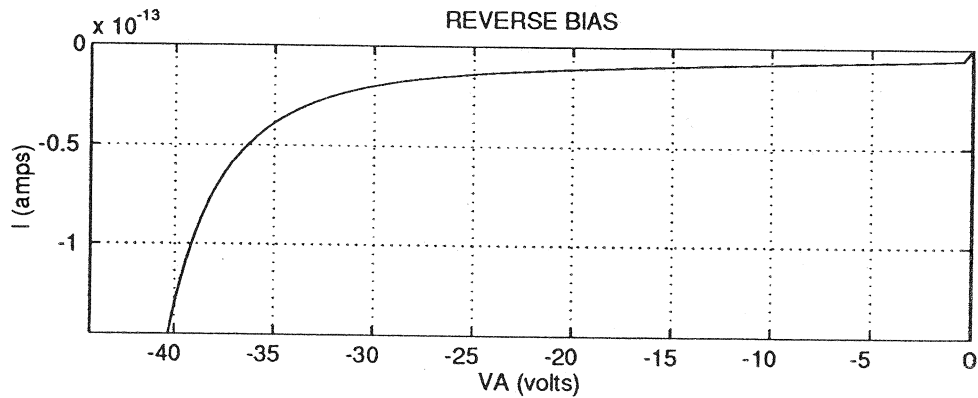
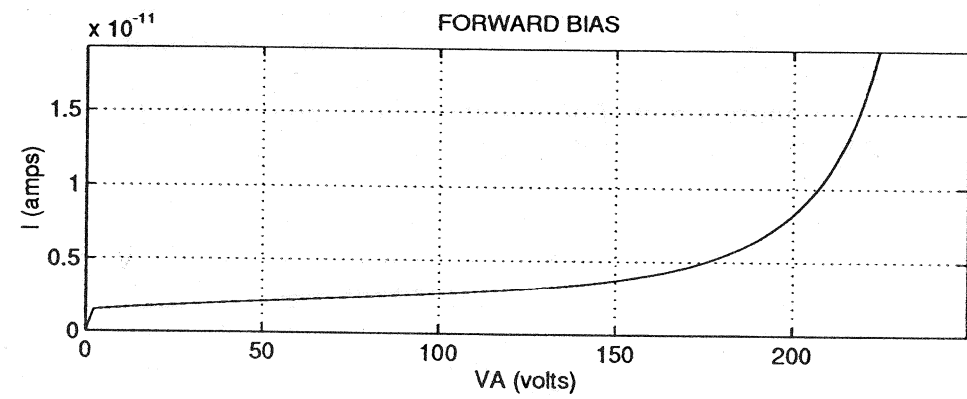
Print-outs of the  $I$ - $V$  characteristics generated by the P\_11\_19b.m program (included on the Instructor's disk) are displayed below.



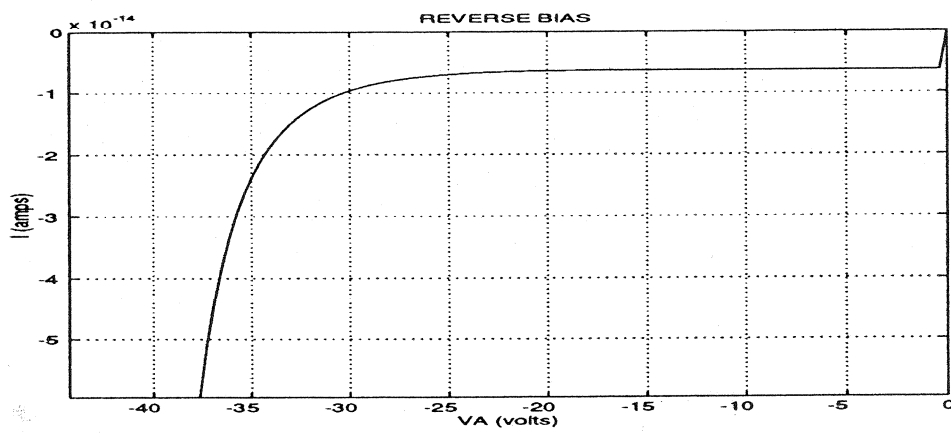
Conf. (a)



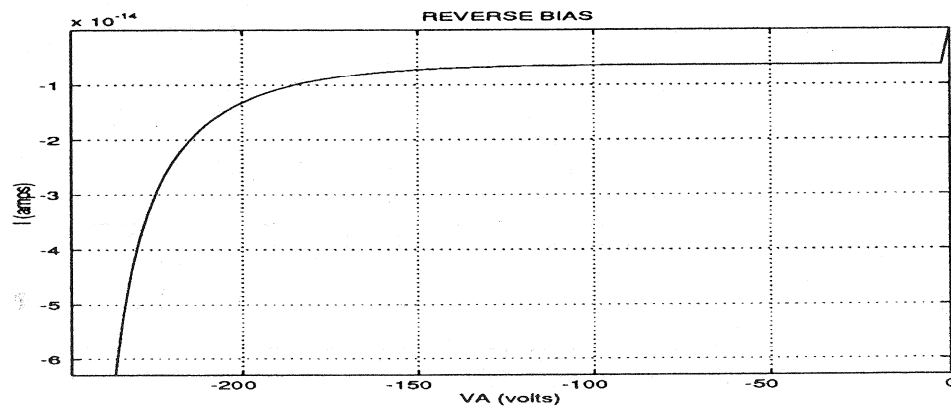
Conf. (b)



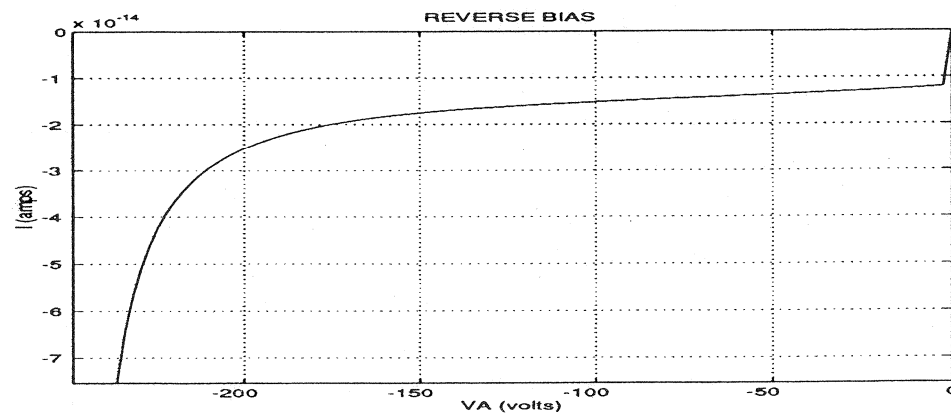
Conf. (c)



Conf. (d)



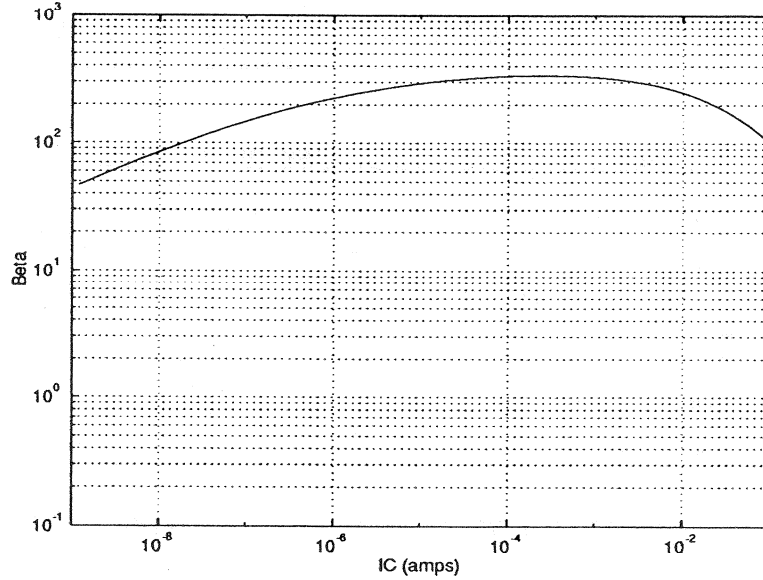
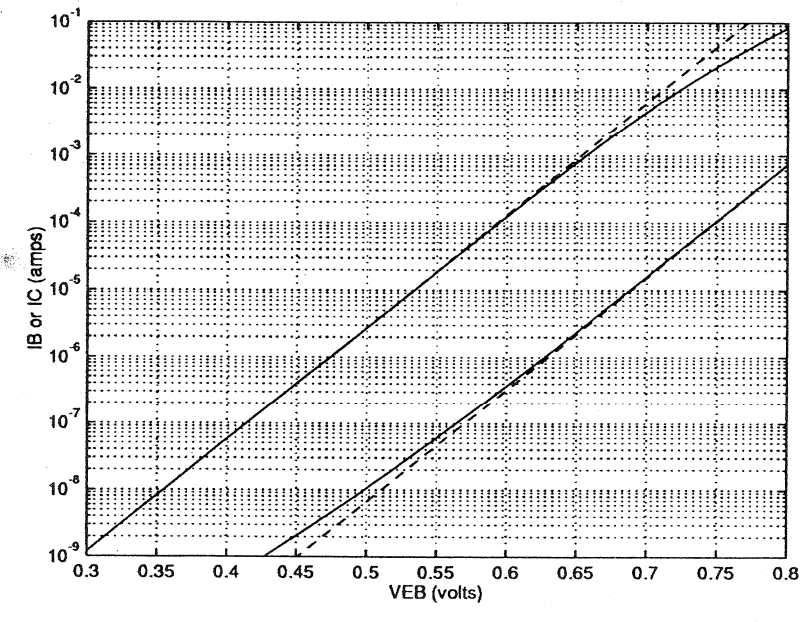
Conf. (e)



Conf. (f)

11.20

(a)/(b) The Gummel and gain plots produced per the instructions in the problem statement are displayed below. The plot-generating MATLAB program is listed after the plots. Although hardly perfect, the gain plot is a credible match to the experimental data presented in Fig. 11.16.



### MATLAB program script...

```
%Gummel and Gain Plots...Problem 11.20
%(Note: subprogram BJT0 is a runtime requirement.)
%Initialization
clear; close
%Input Constant and Material Parameters
BJT0
n2=1.5;
I02=1.0e-14;
VHi=0.75;
%Calculation of IB and IC
VEB=linspace(0.3, 0.85);
IBideal=IF0.* (1-aF).* (exp(VEB./kT)-1);
IRG=I02.* (exp(VEB/(n2*kT))-1);
IB=IBideal+IRG;
ICideal=aF.* IRO.* (exp(VEB./kT)-1);
IC=ICideal./(1+exp((VEB-VHi)./(2*kT)));
%Gummel Plot
semilogy(VEB,IBideal,:w',VEB,ICideal,:w');
axis([.3,.8,1.0e-9,1.0e-1])
hold on
semilogy(VEB,IB,'-m',VEB,IC,'-c'); grid;
xlabel('VEB (volts)'); ylabel('IB or IC (amps)')
hold off
pause
%Gain Plot
Beta=IC./IB;
loglog(IC,Beta)
axis([1.0e-9,1.0e-1,1.0e-1,1.0e3]); grid
xlabel('IC (amps)'); ylabel('Beta')
```

### 11.21

The primary cause of the increase in  $\beta_{dc}$  with increasing  $V_{EC}$  is *base-width modulation*. As noted in the text, increasing  $V_{EC}$  increases the width of the C-B depletion region in the base, which in turn decreases  $W$  and hence increases  $\beta_{dc}$ . The observed  $I_C$  of course increases with  $\beta_{dc}$  per Eq. (11.50).

#### Supplemental Observation #1

The same device was used to produce Figs. 11.5(d) and P11.21. The BJTplus program results displayed in Exercise 11.10 provide a reasonable match to the Fig. 11.5(d) data, and should therefore be applicable to the Fig. P11.21 data. In Prob. 11.18 we found the linear region of the Exercise 11.10 characteristics could be accurately fit by the relationship

$$I_C = (1.87I_B)(V_{EC}+132) \quad \dots V_{EC} \text{ in volts; } I_B, I_C \text{ in amps}$$

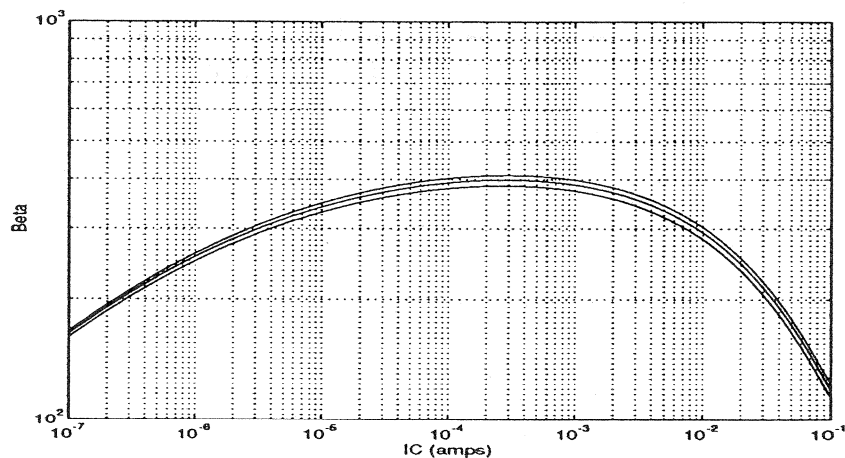
or for the given device,

$$\beta_{dc} = I_C/I_B = 1.87(V_{EC}+132)$$

One computes  $\beta_{dc} = 256, 266$ , and  $275$  if respectively  $V_{EC} = 5V, 10V$ , and  $15V$ . The cited  $\beta_{dc}$  fit is only good of course for  $I_C$  values in the low mA range, but does exhibit the correct general dependence.

#### Supplemental Observation #2

The MATLAB program developed for Prob. 11.20 can be readily revised to produce a plot similar to Fig. P11.21. The plot one obtains is reproduced below. The revised program is included on the Instructor's disk as m-file P\_11\_21.m. Note that the predicted variation is somewhat smaller than that observed experimentally.



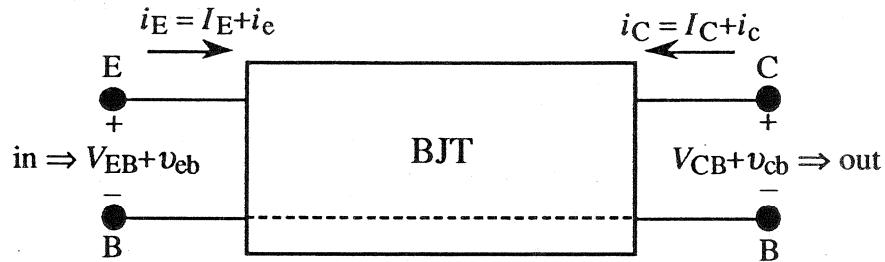
## CHAPTER 12

### 12.1

- (a) Under the quasistatic assumption the carriers and hence the device under analysis are assumed to respond to a time-varying signal as if it were a d.c. bias. In the derivation of the generalized two-port model, one specifically equates the total time-varying terminal currents ( $i_B, i_C$ ) to the d.c. currents that would exist under equivalent biasing conditions.
- (b) Two separate definitions are necessary because, contrary to the polarities assumed in the development of the generalized small-signal model, the  $I_B$  and  $I_C$  currents were previously taken to be positive flowing *out* of the base and the collector terminals in a *pnp* BJT. (As noted in Section 10.1, the direction of positive current was so chosen to avoid unnecessary complications, serious sign-related difficulties, in the physical description of current flow inside the BJT when operated in the standard amplifying mode.)
- (c) The Hybrid-Pi model gets its name from the  $\pi$ -like arrangement of circuit elements with "hybrid" (a combination of conductance and resistance) units.
- (d) Names (see the first paragraph in Subsection 12.1.2):
- $g_m$ ...transconductance
  - $r_o$ ...output resistance
  - $r_\pi$ ...input resistance
  - $r_\mu$ ...feedthrough resistance
- (e) The capacitors model the collector-base and emitter-base *pn* junction capacitances which cannot be neglected at higher frequencies.
- (f) The minority carrier concentration in the base continues to increase as pictured in plot (iii) of Fig. 12.4(d) until a maximum build-up consistent with the applied biases is attained. The base current varies as  $Q_B/\tau_B$  and therefore also continues to increase toward a saturating maximum value. (In the quantitative analysis,  $i_B$  increases from  $I_{CC}\tau_t$  at the start of saturation to a saturating value of  $I_{BB}\tau_B$ .) Once saturation biased,  $i_C$  remains essentially constant at  $i_C \equiv I_{CC} = V_{CC}/R_L$ .
- (g) In words, the *base transit time* is the average time taken by minority carriers to diffuse across the quasineutral base. Mathematically (see Eq. 12.22),  $\tau_t = W^2/2D_B$ .
- (h)  $\beta_{dc} = I_C/I_B = \tau_B/\tau_t$
- (i) An  $i_B < 0$  aids the withdrawal of stored charge from the quasineutral base, which in turn reduces both the storage delay time and the fall time.
- (j) A Schottky diode clamp is a circuit arrangement where a Schottky diode is connected between the collector and base of a BJT as pictured in Fig. 12.7(a). The Schottky diode conducts at a lower forward bias than a *pn* junction and therefore minimizes the forward (saturation-mode) bias that is applied to the BJT under turn-on conditions. This reduces the stored charge and speeds up the turn-off transient. (Also see Subsection 12.2.4.)

## 12.2

The BJT viewed as a two-port network and connected in the common-base configuration is pictured below.



Invoking the quasistatic assumption we can write

$$i_E(V_{EB} + v_{eb}, V_{CB} + v_{cb}) \cong I_E(V_{EB} + v_{eb}, V_{CB} + v_{cb}) = I_E(V_{EB}, V_{CB}) + i_e$$

$$i_C(V_{EB} + v_{eb}, V_{CB} + v_{cb}) \cong I_C(V_{EB} + v_{eb}, V_{CB} + v_{cb}) = I_C(V_{EB}, V_{CB}) + i_c$$

or

$$i_e = I_E(V_{EB} + v_{eb}, V_{CB} + v_{cb}) - I_E(V_{EB}, V_{CB})$$

$$i_c = I_C(V_{EB} + v_{eb}, V_{CB} + v_{cb}) - I_C(V_{EB}, V_{CB})$$

Next performing a Taylor series expansion of the first term on the right-hand side of the above equations, and keeping only first order terms, we obtain

$$I_E(V_{EB} + v_{eb}, V_{CB} + v_{cb}) = I_E(V_{EB}, V_{CB}) + \left. \frac{\partial I_E}{\partial V_{EB}} \right|_{V_{CB}} v_{eb} + \left. \frac{\partial I_E}{\partial V_{CB}} \right|_{V_{EB}} v_{cb}$$

$$I_C(V_{EB} + v_{eb}, V_{CB} + v_{cb}) = I_C(V_{EB}, V_{CB}) + \left. \frac{\partial I_C}{\partial V_{EB}} \right|_{V_{CB}} v_{eb} + \left. \frac{\partial I_C}{\partial V_{CB}} \right|_{V_{EB}} v_{cb}$$

which when substituted into the preceding equations gives

$$i_e = \left. \frac{\partial I_E}{\partial V_{EB}} \right|_{V_{CB}} v_{eb} + \left. \frac{\partial I_E}{\partial V_{CB}} \right|_{V_{EB}} v_{cb}$$

$$i_c = \left. \frac{\partial I_C}{\partial V_{EB}} \right|_{V_{CB}} v_{eb} + \left. \frac{\partial I_C}{\partial V_{CB}} \right|_{V_{EB}} v_{cb}$$

If the direction of positive current flow is as defined in Fig. 10.2 (+ $I_E$  out and + $I_C$  in for an *npn* BJT, + $I_E$  in and + $I_C$  out for a *pnp* BJT), then introducing

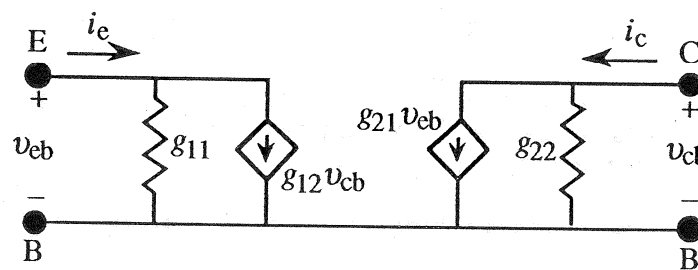
$g_{11} \equiv \left. \frac{\partial I_E}{\partial V_{BE}} \right _{V_{BC}} = \left. \frac{\partial I_E}{\partial V_{EB}} \right _{V_{CB}}$ <div style="text-align: center; margin-top: -10px;"> <math>\uparrow</math>  <i>npn</i>  +<math>I_E</math> out         </div>	$g_{12} \equiv \left. \frac{\partial I_E}{\partial V_{BC}} \right _{V_{BE}} = \left. \frac{\partial I_E}{\partial V_{CB}} \right _{V_{EB}}$ <div style="text-align: center; margin-top: -10px;"> <math>\uparrow</math>  <i>pnp</i>  +<math>I_E</math> in         </div>
$g_{21} \equiv \left. \frac{\partial I_C}{\partial V_{EB}} \right _{V_{CB}} = \left. \frac{\partial I_C}{\partial V_{BE}} \right _{V_{BC}}$ <div style="text-align: center; margin-top: -10px;"> <math>\uparrow</math>  <i>npn</i>  +<math>I_C</math> in         </div>	$g_{22} \equiv \left. \frac{\partial I_C}{\partial V_{BC}} \right _{V_{EB}} = \left. \frac{\partial I_C}{\partial V_{CB}} \right _{V_{BE}}$ <div style="text-align: center; margin-top: -10px;"> <math>\uparrow</math>  <i>pnp</i>  +<math>I_C</math> out         </div>

yield the emitter and collector a.c. current node equations

$$i_e = g_{11}v_{eb} + g_{12}v_{cb}$$

$$i_c = g_{21}v_{eb} + g_{22}v_{cb}$$

The low-frequency small-signal equivalent circuit characterizing the a.c. response of the BJT connected in the common base configuration is therefore concluded to be



### 12.3

From an inspection of Fig. 11.5(d), one concludes  $I_C \approx 1.1$  mA at the specified operating point. Given the BJT is to be modeled using the simplified equivalent circuit of Fig. 12.2(a), and assuming  $T = 300$  K, one computes (referring to Eqs. 12.9),

$$g_m = \frac{qI_C}{kT} = \frac{1.1 \times 10^{-3}}{0.0259} = 4.25 \times 10^{-2} \text{ S}$$

$$r_\pi = \frac{kT/q}{I_B} = \frac{0.0259}{5 \times 10^{-6}} = 5.18 \times 10^3 \Omega$$

### 12.4

The node equations appropriate for the B and C terminals in the Hybrid-Pi model (Fig. 12.2b) assume the form

$$i_b = v_{be}/r_\pi + v_{bc}/r_\mu$$

$$i_c = g_m v_{be} + v_{cb}/r_\mu + v_{ce}/r_o$$

But  $v_{bc} = -v_{cb} = v_{be} - v_{ce}$ . Thus

$$i_b = v_{be} \left( \frac{1}{r_\pi} + \frac{1}{r_\mu} \right) - v_{ce} \left( \frac{1}{r_\mu} \right)$$

$$i_c = v_{be} \left( g_m - \frac{1}{r_\mu} \right) + v_{ce} \left( \frac{1}{r_\mu} + \frac{1}{r_o} \right)$$

A comparison of the preceding equations with text Eqs. (12.6) leads to the conclusion

$$g_{11} = \frac{1}{r_\pi} + \frac{1}{r_\mu} \quad g_{12} = -\frac{1}{r_\mu}$$

$$g_{21} = g_m - \frac{1}{r_\mu} \quad g_{22} = \frac{1}{r_\mu} + \frac{1}{r_o}$$

Clearly  $r_\mu = -1/g_{12}$ . Moreover, substituting  $1/r_\mu = -g_{12}$  into the other three expressions allows us to solve for the remaining Hybrid-Pi parameters in terms of the generalized model parameters. Specifically,

$$r_\pi = 1/(g_{11} + g_{12}) \quad r_\mu = -1/g_{12}$$

$$g_m = g_{21} - g_{12} \quad r_o = 1/(g_{22} + g_{12})$$

Although in a somewhat different order, the preceding are Eqs. (12.10).

## 12.5

Computations were first performed to determine the  $V_{EB}$  values required to obtain an  $I_C = 1$  mA with and without accounting for base width modulation. These  $V_{EB}$  voltages were then incorporated directly into the final program (P\_12\_05.m on the Instructor's disk). In the MATLAB program, the user is asked whether he/she wishes to input  $V_{EB}$  and  $V_{EC}$  or to use the preset values. The small incremental voltage deviations from the d.c. voltage values used in approximating the partial derivatives appearing in Eqs. (12.5) were varied until a factor of two change in the incremental values led to no change to five significant places in the computed  $g_{ij}$  parameters. The  $g_{ij}$  parameters were in turn used to compute the Hybrid-Pi parameters employing Eqs. (12.10).

Sample results with and without accounting for base width modulation are tabulated below. In both cases there is at most a third-place difference between the  $g_m$  and  $r_\pi$  computed from first principles and the  $g_m$  and  $r_\pi$  computed using Eqs. (12.9). As expected,  $g_{12}$  and  $g_{22}$  are approximately zero when base width modulation is assumed to be negligible, and therefore  $r_o$  and  $r_\mu$  become infinite. Finite values are obtained for  $r_o$  and  $r_\mu$  when base width modulation is included. Note that base width modulation has little effect on  $g_m$  but leads to a significant increase in  $r_\pi$ . An increase in  $\beta_{dc} \equiv g_m r_\pi$  is of course expected when base width modulation is included.

### *No base-width modulation*

$$g_m = 3.8685 \times 10^{-2} \text{ S}$$

$$r_o = \infty$$

$$r_\pi = 4.5960 \times 10^3 \Omega$$

$$r_\mu = \infty$$

---

$$g_m = 3.8612 \times 10^{-2} \text{ S} \quad \dots \text{using Eq. (12.9)}$$

$$r_\pi = 4.6047 \times 10^3 \Omega$$

$$V_{EB} = 0.67416 \text{ V}$$

$$V_{EC} = 10 \text{ V}$$

$$I_C = 1.0000 \text{ mA}$$

### *With base-width modulation included*

$$g_m = 3.8510 \times 10^{-2} \text{ S}$$

$$r_o = 1.4932 \times 10^5 \Omega$$

$$r_\pi = 5.9530 \times 10^3 \Omega$$

$$r_\mu = 7.5141 \times 10^7 \Omega$$

---

$$g_m = 3.8611 \times 10^{-2} \text{ S} \quad \dots \text{using Eq. (12.9)}$$

$$r_\pi = 5.9761 \times 10^3 \Omega$$

$$V_{EB} = 0.66961 \text{ V}$$

$$V_{EC} = 10 \text{ V}$$

$$I_C = 1.0000 \text{ mA}$$

### MATLAB program script...

```
%Computation of the Hybrid Pi Parameters (Problem 12.5)
%Initialization
clear; close
format compact; format short e
bw=input('Include base-width modulation? 1-Yes, 2-No...');
s=input('Manually input VEB and VEC? 1-Yes, 2-No...');

%Input Eber-Moll Parameters
BJT0

%Voltages used in Calculation
VbiE=kT*log(NE*NB/ni^2);
VbiC=kT*log(NC*NB/ni^2);
if s==1,
    VEB0=input('Input VEB in volts, VEB = ');
    VEC0=input('Input VEC in volts, VEC = ');
else
    VEC0=10
    if bw==1, VEB0=0.669606
    else      VEB0=0.674162
end; end

%iB and iC Calculations
VEB=VEB0;
VEC=VEC0;
iB=[];
iC=[];
for i=1:5,
    if bw==1,
        VCB=VEB-VEC;
        BJTmod
    else
        end
    IB0=(1-aF).*IF0+(1-aR).*IRO;
    IB1=(1-aF).*IF0+(1-aR).*IRO.*exp(-VEC/kT);
    IB=(IB1.*exp(VEB/kT)-IB0);
    IC=((aF.*IF0-IRO.*exp(-VEC/kT)).*(IB+IB0)./(IB1+IRO-aF.*IRO));
    %Reset Voltages
    if i==1, VEB=VEB0-0.0001; else; end
    if i==2, VEB=VEB0+0.0001; else; end
    if i==3, VEB=VEB0; VEC= VEC0-0.01; else; end
    if i==4, VEC=VEC0+0.01; else; end
    iB=[iB,IB];
    iC=[iC,IC];
end
```

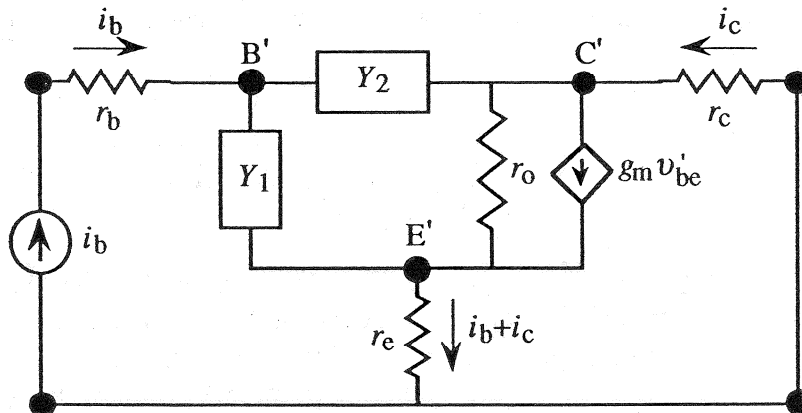
```

%Compute Generalized Two-Port Model Parameters
g11=(iB(3)-iB(2))/0.0002;
g12=(iB(5)-iB(4))/0.02;
g21=(iC(3)-iC(2))/0.0002;
g22=(iC(5)-iC(4))/0.02;
fprintf('nHybrid-Pi Model Parameters\n')
gm=g21-g12
if g22+g12==0    ro=inf
else              ro=1/(g22+g12)
end
rpi=1/(g11+g12)
if g12==0, rmu=inf
else,      rmu=-1/g12
end
fprintf('ngm and rpi computed using Eqs. (12.9)\n')
gm=iC(1)/0.0259
rpi=0.0259/iB(1)

```

### 12.6

(a) The high-frequency equivalent circuit of Fig. 12.2(c) with  $v_{ce} = 0$  can be manipulated into the form



where

$$Y_1 = \frac{1}{r_\pi} + j\omega C_{eb}$$

$$Y_2 = \frac{1}{r_\mu} + j\omega C_{cb}$$

Combining node and loop analysis we note

$$i_b = Y_1 v_{be}' - Y_2 v_{cb}' \quad (1)$$

$$i_c = g_m v_{be}' + Y_2 v_{cb}' + v_{ce}' / r_o \quad (2)$$

$$i_c r_c + v_{ce}' + (i_b + i_c) r_e = 0 \quad (3)$$

$$v_{be}' - v_{ce}' + v_{cb}' = 0 \quad (4)$$

Eq. (4) is used to eliminate  $v_{cb}'$  in Eqs. (1) and (2). Eqs. (1) and (2) are then combined to eliminate  $v_{be}'$ . Next Eqs. (3) is used to eliminate  $v_{ce}'$ . Finally, the  $i_c/i_b$  ration is formed giving

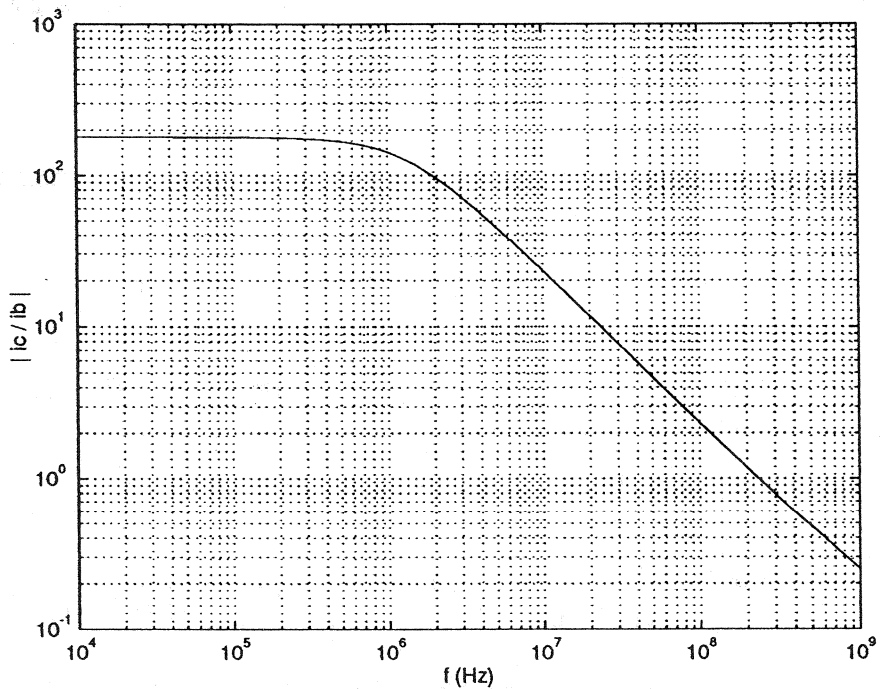
$$\boxed{\frac{i_c}{i_b} = \frac{\left(Y_2 + \frac{1}{r_o}\right)r_e + \left(\frac{g_m - Y_2}{Y_1 + Y_2}\right)(Y_2 r_e - 1)}{\left(\frac{Y_2 - g_m}{Y_1 + Y_2}\right)(r_e + r_c)Y_2 - \left(Y_2 + \frac{1}{r_o}\right)(r_e + r_c) - 1}}$$

(b) With  $r_e = 0$  as given in the list of parameters, the  $i_c/i_b$  ratio simplifies to

$$\frac{i_c}{i_b} = \frac{\frac{(Y_2 - g_m)}{(Y_1 + Y_2)}}{\frac{(Y_2 - g_m)}{(Y_1 + Y_2)}r_c Y_2 - \left(Y_2 + \frac{1}{r_o}\right)r_c - 1}$$

Using the MATLAB program to compute  $|i_c/i_b|$  versus frequency, one determines an  $f_T = 235$  MHz. Data sheets list the  $f_T$  of the 2N3906 *pnp* BJT to be approximately 200 MHz. (It should be noted that the Electronics Workbench software program was used to determine the d.c. operating point that produced an  $I_C = 1$  mA. The series resistances listed in the problem statement were those quoted by the EW program. Zero-bias capacitance values employed in computing the Hybrid-Pi parameters were also extracted from the Electronics Workbench program.)

A plot of  $|i_c/i_b|$  versus frequency, and the MATLAB m-file constructed to generate the plot and determine  $f_T$ , are reproduced on the next page.



### MATLAB program script...

```
%Problem 12.6...fT determination
%Initialization
clear; close
%Parameters
gm=3.86e-2;
rpi=4.65e3;
ro=2.00e4;
rmu=3.59e6;
Ceb=23.6e-12;
Ccb=2.32e-12;
rb=10;
rc=2.8;
re=0;
%|ic/ib| vs. frequency
f=logspace(4,9,200);
w=2.*pi.*f;
Y1=1/rpi+j.*w.*Ceb;
Y2=1/rmu+j.*w.*Ccb;
R=(Y2-gm)./(Y1+Y2);
Den=R.*rc.*Y2 - (Y2+1/ro).*rc - 1;
beta=abs(R./Den); %beta=|ic/ib|
%Plot
loglog(f,beta); grid
xlabel('f (Hz)'); ylabel('| ic / ib |')
```

### 12.7

The Eqs. (6.68)/(6.69) solution for the  $I_{\text{DIFF}}$  flowing in a narrow base diode is

$$I_{\text{DIFF}} = qA \frac{D_P}{L_P} \frac{n_i^2}{N_D} \frac{\cosh(x_c'/L_P)}{\sinh(x_c'/L_P)} (e^{qV_A/kT} - 1)$$

For application to a BJT we make the symbol replacements...  $D_P \rightarrow D_B$ ,  $L_P \rightarrow L_B$ ,  $N_D \rightarrow N_B$ ,  $x_c' \rightarrow W$ , and  $V_A \rightarrow V_{EB}$ . Then

$$I_{\text{DIFF}} = qA \frac{D_B}{L_B} \frac{n_i^2}{N_B} \frac{\cosh(W/L_B)}{\sinh(W/L_B)} (e^{qV_{EB}/kT} - 1)$$

Since  $W/L_B \ll 1$  in a standard transistor, the cosh/sinh factor can be expanded as noted in the problem statement to obtain

$$\frac{\cosh(W/L_B)}{\sinh(W/L_B)} \equiv \frac{L_B}{W} \left[ 1 + \frac{1}{3} \left( \frac{W}{L_B} \right)^2 \right] \quad \dots W/L_B \ll 1$$

and

$$I_{\text{DIFF}} \equiv \left( qA \frac{D_B}{W} \frac{n_i^2}{N_B} \right) \left[ 1 + \frac{1}{3} \left( \frac{W}{L_B} \right)^2 \right] (e^{qV_{EB}/kT} - 1)$$

Introducing the substitutions cited in Subsection 7.3.2, that is,

$$\left( \frac{W}{L_B} \right)^2 = \frac{W^2}{D_B \tau_B} \Rightarrow \frac{W^2}{D_B \tau_B} (1 + j\omega \tau_B)$$

and

$$(e^{qV_{EB}/kT} - 1) \Rightarrow (qv_{eb}/kT) e^{qV_{EB}/kT}$$

yields the corresponding a.c. relationship

$$i_{\text{diff}} \equiv \left( qA \frac{D_B}{W} \frac{n_i^2}{N_B} \right) \left( 1 + \frac{1}{3} \frac{W^2}{D_B \tau_B} + j\omega \frac{W^2}{3D_B} \right) \left( \frac{qv_{eb}}{kT} \right) e^{qV_{EB}/kT}$$

Finally, by definition,

$$Y_D = G_D + j\omega C_D = i_{\text{diff}}/v_{eb}$$

and therefore

$$C_D = \left( \frac{W^2/3D_B}{kT/q} \right) \left( qA \frac{D_B}{W} \frac{n_i^2}{N_B} \right) e^{qV_{EB}/kT} = \frac{2}{3} \left( \frac{\tau_t}{kT/q} \right) \left( qA \frac{D_B}{W} \frac{n_i^2}{N_B} \right) e^{qV_{EB}/kT}$$

### 12.8

The pictured "on" point in Fig. 12.3(b) lies right on the  $I_B = V_S/R_S$  line. Therefore  $I_{BB} \equiv V_S/R_S = 30\mu A$ .

Inspecting the plot we find  $I_{CC} \equiv V_{CC}/R_L = 5.0 \text{ mA}$ .

We know  $\beta_{dc} = I_C/I_B = \tau_B/\tau_t$ . Although base width modulation clearly causes  $\beta_{dc}$  to vary somewhat depending on the d.c. operating point, it is reasonable to employ a median value in obtaining the desired estimate. Specifically, using the point where the load line crosses the  $I_B = 15 \mu A$  characteristic, we obtain

$$\frac{\tau_B}{\tau_t} = \frac{I_C}{I_B} \cong \frac{(0.624)(V_{CC}/R_L)}{I_B} = \frac{(0.624)(5 \times 10^{-3})}{15 \times 10^{-6}} = 208$$

Thus

$$\frac{I_{CC}\tau_t}{I_{BB}\tau_B} \cong \frac{(5 \times 10^{-3})}{(30 \times 10^{-6})(208)} = 0.80$$

### 12.9

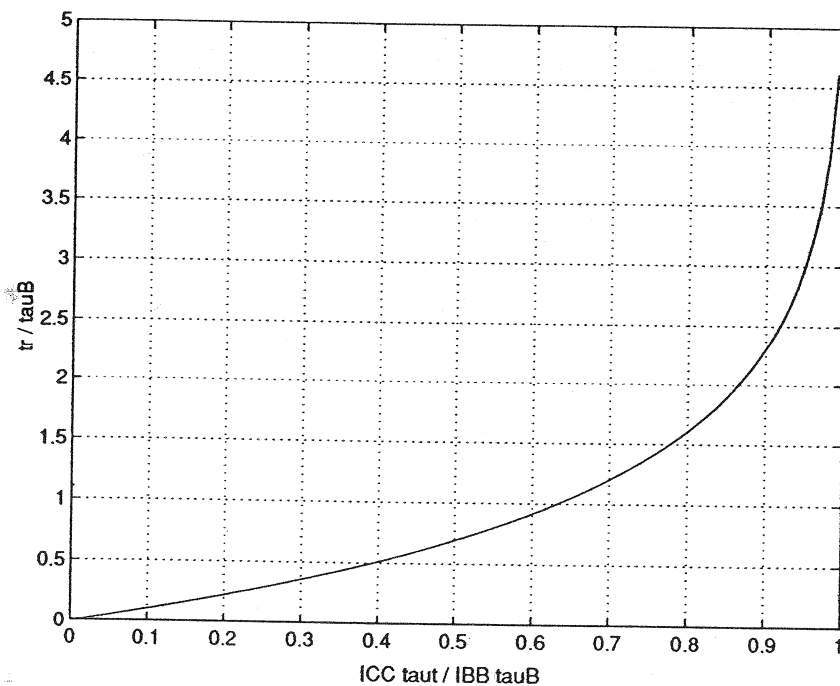
(a)/(b) The required plots and the generating MATLAB m-file are reproduced below. The computational relationships used in producing the plots were

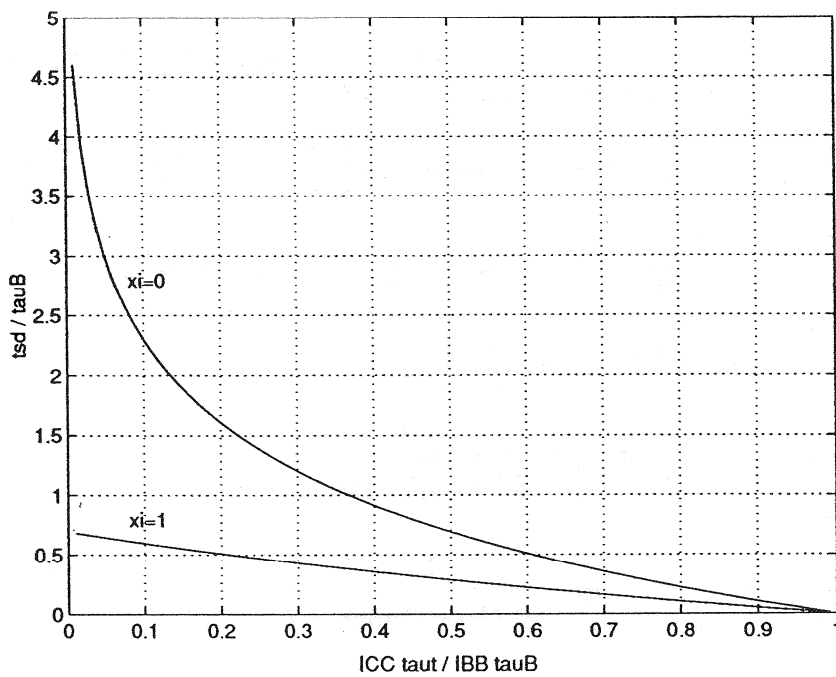
$$\frac{t_r}{\tau_B} = \ln\left(\frac{1}{1-x}\right)$$

$$\frac{t_{sd}}{\tau_B} = \begin{cases} \ln\left(\frac{1}{x}\right) & \dots \text{if } \xi = 0 \\ \ln\left(\frac{2}{1+x}\right) & \dots \text{if } \xi = 1 \end{cases}$$

where

$$x = I_{CC}\tau_t/I_{BB}\tau_B$$





MATLAB program script...

```
%Rise and Storage-Delay Time plots (Prob. 12.9)
%Initialization
clear; close
%Rise time computation
x=linspace(0.01,0.99);
rise=log(1./(1-x)); %rise=tr/tauB
plot(x,rise); grid
xlabel('ICC taut / IBB tauB'); ylabel('tr / tauB')
pause
%Storage-Delay Time computation
delay0=log(1./x); %delay0=tsd/tauB, xi=0
delay1=log(2./(1+x)); %delay1=tsd/tauB, xi=1
plot(x,delay0,x,delay1); grid
xlabel('ICC taut / IBB tauB'); ylabel('tsd / tauB')
text(0.08,2.8,'xi=0'); text(0.08,0.8,'xi=1')
```

### 12.10

(a) Let  $t_1$  be the time when  $i_C = 0.9I_{CC}$  and  $t_2$  the time when  $i_C = 0.1I_{CC}$ . Making use of Eq. (12.31b), we can then write

$$i_C(t_1) = 0.9I_{CC} = I_{BB} \frac{\tau_B}{\tau_t} [(1+\xi)e^{-t_1/\tau_B} - \xi]$$

$$i_C(t_2) = 0.1I_{CC} = I_{BB} \frac{\tau_B}{\tau_t} [(1+\xi)e^{-t_2/\tau_B} - \xi]$$

Solving for the  $t$ 's yields

$$t_1 = \tau_B \ln \left( \frac{1 + \xi}{0.9I_{CC}\tau_t/I_{BB}\tau_B + \xi} \right)$$

$$t_2 = \tau_B \ln \left( \frac{1 + \xi}{0.1I_{CC}\tau_t/I_{BB}\tau_B + \xi} \right)$$

and per the measurements-based definition

$$t_f = t_2 - t_1 = \tau_B \ln \left( \frac{0.9I_{CC}\tau_t/I_{BB}\tau_B + \xi}{0.1I_{CC}\tau_t/I_{BB}\tau_B + \xi} \right) = \tau_B \ln \left( \frac{0.9x + \xi}{0.1x + \xi} \right)$$

where  $x = I_{CC}\tau_t/I_{BB}\tau_B$

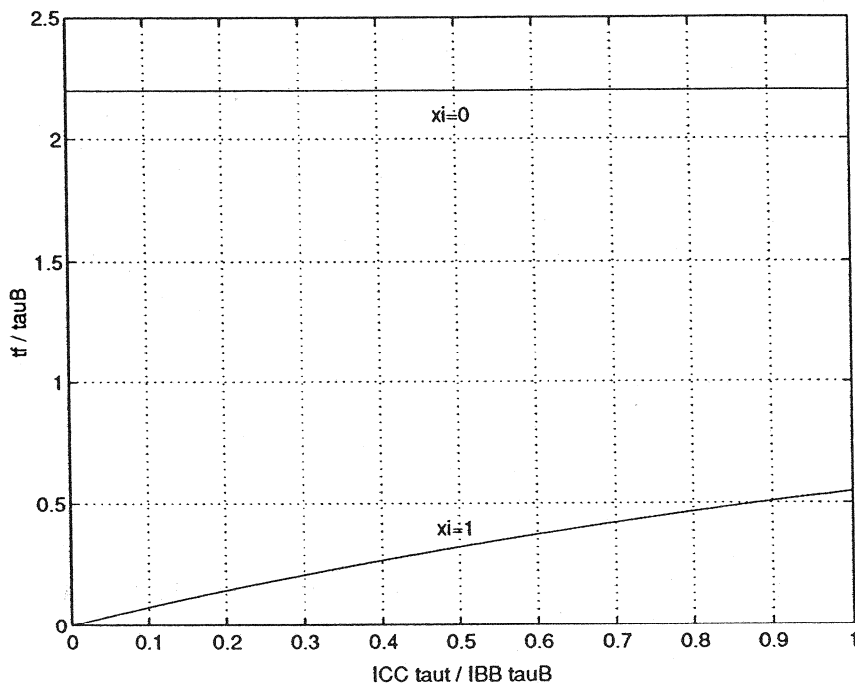
(b) With  $\xi = 0$  and  $\xi = 1$ , the part (a) relationship simplifies to

$$\frac{t_f}{\tau_B} = \begin{cases} \ln 9 & \dots \text{if } \xi = 0 \\ \ln \left( \frac{0.9x + 1}{0.1x + 1} \right) & \dots \text{if } \xi = 1 \end{cases}$$

The requested  $t_f/\tau_B$  versus  $x$  plot is displayed on the next page along with the script of the MATLAB m-file used to generate the plot.

Consistent with the analysis in Subsection 12.2.3, the plotted fall times decrease when  $\xi > 0$ . This occurs because an  $i_B < 0$  aids the withdrawal of charge from the quasineutral base. If the  $x$ -ratio increases either due to an increase in  $I_{CC}$  or a decrease in  $I_{BB}$ , the charge storage is enhanced relative to the charge removal capability of the base

current. Thus, the  $t_f/\tau_B$  ratio for the  $\xi = 1$  curve increases with increasing  $x$ . When  $\xi = 0$ , the charge removal from the base occurs only by recombination and the fall-time collector current assumes the simple form,  $i_C = A \exp(-t/\tau_B)$ . Since  $t_f$  is always evaluated employing the same relative  $i_C$  values,  $i_C(t_1)/i_C(t_2) = \text{constant} = \exp(t_f/\tau_B)$ , and  $t_f/\tau_B$  is seen to be a constant independent of  $x$ .



### MATLAB program script...

```
%Fall Time (Problem 12.10)
%Initialization
clear; close
%Fall Time computations
x0=[0,1];
y0=[log(9),log(9)]; %tf/tauB when xi=0
x1=linspace(0,1);
y1=log((0.9.*x1+1)./(0.1.*x1+1)); %tf/tauB when xi=1
plot(x0,y0,x1,y1); grid
xlabel('ICC taut / IBB tauB'); ylabel('tf / tauB')
text(0.47,2.1,'xi=0'); text(0.47,0.4,'xi=1')
```



## CHAPTER 14

### 14.1

- (a) MS, Schottky, and Hot Carrier are just alternative names for a rectifying metal-semiconductor contact. Hot Carrier diodes are typically small area devices.
- (b) If  $\Phi_M = \chi$  in an ideal MS contact, the contact is borderline rectifying/ohmic independent of the semiconductor doping.
- (c)... $V_{bi}$  is computed differently.  
...In *pn* junction analyses it is common practice to take  $V = 0$  on the *p*-side of the junction. In MS work the semiconductor bulk is typically employed as the zero-voltage reference point.
- (d) Thermionic emission current — majority carrier injection over the surface potential-energy barrier.
- (e) Since  $I_{M\bullet \rightarrow S}(V_A) = I_{M\bullet \rightarrow S}(0) = -I_{S\bullet \rightarrow M}(0)$ , the  $M\bullet \rightarrow S$  component is obtained by evaluating the  $S\bullet \rightarrow M$  component at zero bias.
- (f) The diffusion capacitance and conductance arise from the fluctuation of the minority carriers stored in a quasineutral region adjacent to the depletion region. The minority carrier storage is large in a forward-biased *pn* junction diode and leads to a significant diffusion admittance. In an MS diode there is minimal minority carrier storage for operational forward biases.
- (g) There is a minimal number of stored minority carriers to be removed in going from the forward-bias “on” condition to the reverse-bias “off” condition.
- (h) It is a special circuit or fabricated-in arrangement where an MS (Schottky) diode is connected between the base and collector of a BJT. The arrangement leads to a significant reduction in the turn-off time when the BJT is used as a switch.
- (i) Ohmic contacts are usually produced in practice by heavily doping the surface region of the semiconductor immediately beneath the contact. The device structure is also routinely annealed (heated in an inert atmosphere) to minimize the contact resistance.
- (j) “Spiking” is the nonuniform penetration of Al into Si beneath an Al-Si contact. (See Fig. 14.11a.)

## 14.2

(NOTE: In the first printing, all of the semiconductors were erroneously identified as *n*-type. Combinations B, D, and F should have been labeled as  $N_A$  doped.)

For a given combination, it is first necessary to determine the nature of the contact. This requires that we compute  $\Phi_S$  using

$$\Phi_S = \chi + (E_c - E_F)_{FB} \approx \chi + E_G/2 - (E_F - E_i)_{FB}$$

$$(E_F - E_i)_{FB} = \begin{cases} kT \ln(N_D/n_i) & \dots n\text{-type} \\ -kT \ln(N_A/n_i) & \dots p\text{-type} \end{cases}$$

Combo	Mat	Type	Doping (cm <sup>-3</sup> )	$n_i$ (cm <sup>-3</sup> )	$E_F - E_i$ (eV)	$E_G/2$ (eV)	$\Phi_S$ (eV)
A	Ge	<i>n</i>	$10^{16}$	$2.5 \times 10^{13}$	0.155	0.33	4.18
B	Ge	<i>p</i>	$10^{15}$	$2.5 \times 10^{13}$	-0.096	0.33	4.43
C	Si	<i>n</i>	$10^{15}$	$10^{10}$	0.298	0.56	4.29
D	Si	<i>p</i>	$10^{16}$	$10^{10}$	-0.358	0.56	4.95
E	GaAs	<i>n</i>	$10^{16}$	$2.25 \times 10^6$	0.575	0.71	4.21
F	GaAs	<i>p</i>	$10^{17}$	$2.25 \times 10^6$	-0.635	0.71	5.42

Noting the semiconductor type and whether  $\Phi_M > \Phi_S$  or  $\Phi_M < \Phi_S$ , the ideal nature of the contact is deduced by referring to Table 14.1.

Combo	Type	$\Phi_M ? \Phi_S$	ideal nature	Part (a) diagram similar to	Part (b) argument similar to that in
A	<i>n</i>	$\Phi_M > \Phi_S$	Rectifying	Fig. 14.2(b)	Section 14.1
B	<i>p</i>	$\Phi_M > \Phi_S$	Ohmic	Fig. (b), Exer. 14.1	Exercise 14.1
C	<i>n</i>	$\Phi_M < \Phi_S$	Ohmic	Fig. 14.2(d)	Section 14.1
D	<i>p</i>	$\Phi_M < \Phi_S$	Rectifying	Fig. (a), Exer. 14.1	Exercise 14.1
E	<i>n</i>	$\Phi_M > \Phi_S$	Rectifying	Fig. 14.2(b)	Section 14.1
F	<i>p</i>	$\Phi_M < \Phi_S$	Rectifying	Fig. (a), Exer. 14.1	Exercise 14.1

### 14.3

$$(a) \Phi_B = \Phi_M - \chi = 5.10 - 4.03 = 1.07 \text{ eV}$$

$$\begin{aligned} (b) (E_c - E_F)_{FB} &\equiv E_G/2 - (E_F - E_i)_{FB} = E_G/2 - kT \ln(N_D/n_i) \\ &= 0.56 - (0.0259)\ln(10^{15}/10^{10}) \\ &= 0.26 \text{ eV} \end{aligned}$$

$$V_{bi} = \frac{1}{q} [\Phi_M - (E_c - E_F)_{FB}] = 1.07 - 0.26 = 0.81 \text{ V}$$

(c)  $V_A = 0$  under equilibrium conditions and

$$W = \left[ \frac{2K_S \epsilon_0}{qN_D} V_{bi} \right]^{1/2} = \left[ \frac{2(11.8)(8.85 \times 10^{-14})(0.81)}{(1.6 \times 10^{-19})(10^{15})} \right]^{1/2} = 1.03 \times 10^{-4} \text{ cm}$$

$$(d) |\mathcal{E}_{max} = |\mathcal{E}_{x=0}| = \frac{qN_D}{K_S \epsilon_0} W = \frac{(1.6 \times 10^{-19})(10^{15})(1.03 \times 10^{-4})}{(11.8)(8.85 \times 10^{-14})} = 1.58 \times 10^4 \text{ V/cm}$$

### 14.4

The computations were performed employing Eq. (14.12) with  $V_A = 0$ , Eq. (14.3), and

$$(E_c - E_F)_{FB} \equiv E_G/2 - kT \ln(N_D/n_i)$$

The resultant plot and associated MATLAB m-file are displayed below.

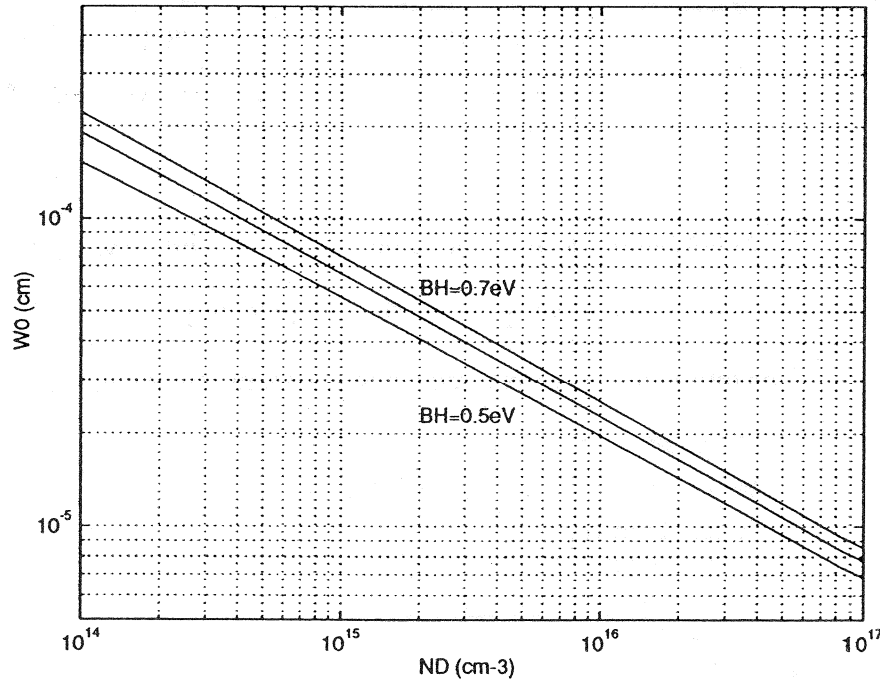
MATLAB program script...

```
%Equilibrium Depletion Width (Problem 14.4)
%Initialization
clear; close
%Constants and Parameters
q=1.6e-19;
e0=8.85e-14;
kT=0.0259;
```

```

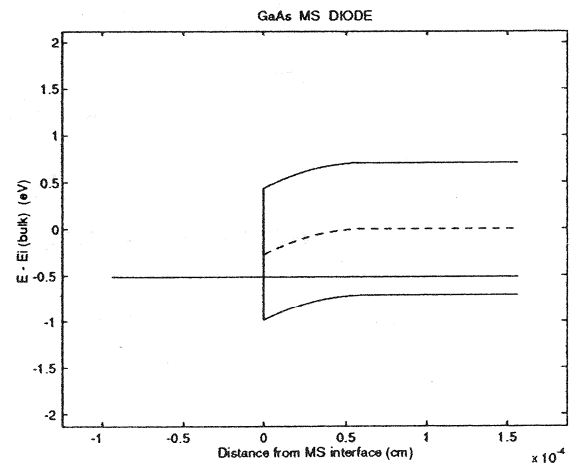
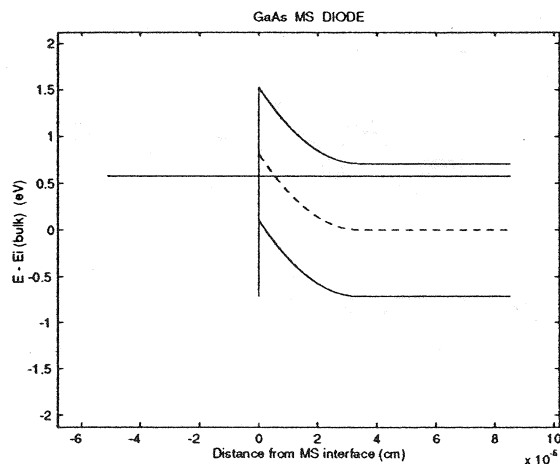
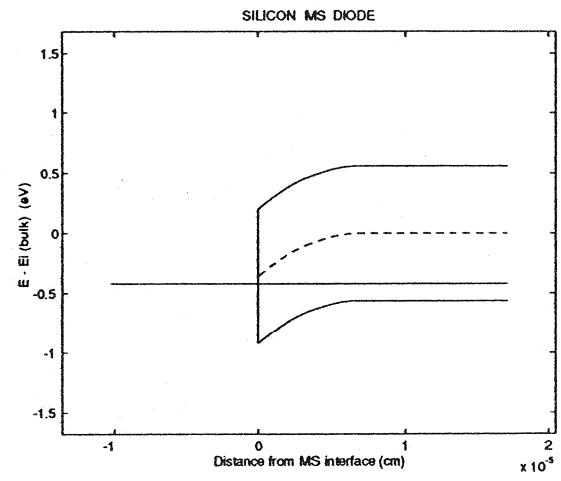
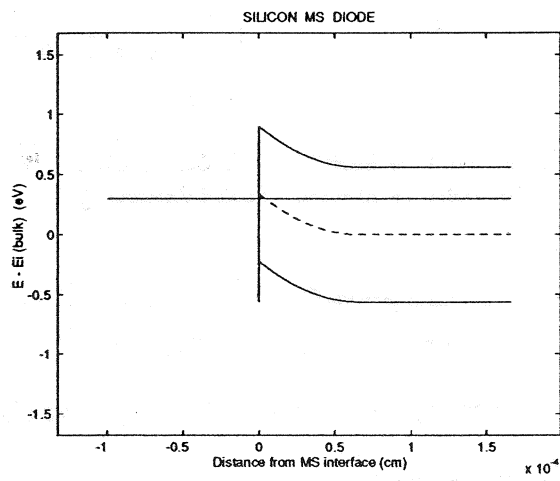
EG=1.12;
ni=1.0e10;
KS=11.8;
BH=[0.5,0.6,0.7]; %Barrier Height
ND=logspace(14,17);
%Depletion Width Calculation
ECF=EG/2-kT*log(ND./ni);
W0=[];
for i=1:3,
    Vbi=BH(i)-ECF;
    W=sqrt((2*KS*e0.*Vbi)./(q.*ND));
    W0=[W0;W];
end
%Plot result
loglog(ND,W0);
axis([1.0e14,1.0e17,5e-6,5e-4]); grid
xlabel('ND (cm-3)'); ylabel('W0 (cm)')
text(2e15,2.3e-5,'BH=0.5eV')
text(2e15,6e-5,'BH=0.7eV')

```



### 14.5

(a)/(b)/(c) A sample MATLAB program that generates MS diode energy band diagrams (equilibrium, 300 K) is included on the instructor's disk as m-file P\_14\_05.m. The program can generate both *n*- and *p*-type Si diagrams plus *n*- and *p*-type GaAs diagrams. Sample plots are displayed below.



### 14.6

Substituting Eq. (14.17) into Eq. (14.16) gives

$$\begin{aligned} I_{S\bullet \rightarrow M} &= -qA \left( \frac{4\pi k T m_n^{*2}}{h^3} \right) e^{(E_F - E_C)/kT} \int_{-\infty}^{-v_{\min}} v_x e^{-(m_n^*/2kT)v_x^2} dv_x \\ &= qA \left( \frac{4\pi k T m_n^{*2}}{h^3} \right) e^{(E_F - E_C)/kT} \int_{v_{\min}}^{\infty} v_x e^{-(m_n^*/2kT)v_x^2} dv_x \end{aligned}$$

where the second form of the above equation is obtained by interchanging the limits on the integral and changing variables from  $v_x$  to  $-v_x$ . Next evaluating the integral yields

$$\int_{v_{\min}}^{\infty} v_x e^{-(m_n^*/2kT)v_x^2} dv_x = - \left( \frac{kT}{m_n^*} \right) e^{-(m_n^*/2kT)v_x^2} \Big|_{v_{\min}}^{\infty} = \left( \frac{kT}{m_n^*} \right) e^{-(m_n^*/2kT)v_{\min}^2}$$

Thus, noting from Eq. (14.14) that  $v_{\min}^2 = (2q/m_n^*)(V_{bi} - V_A)$ , we obtain

$$I_{S\bullet \rightarrow M} = qA \left( \frac{4\pi k^2 T^2 m_n^*}{h^3} \right) e^{(E_F - E_C)/kT} e^{-q(V_{bi} - V_A)/kT}$$

But

$$qV_{bi}/kT = \Phi_B/kT + (E_F - E_C)/kT$$

and

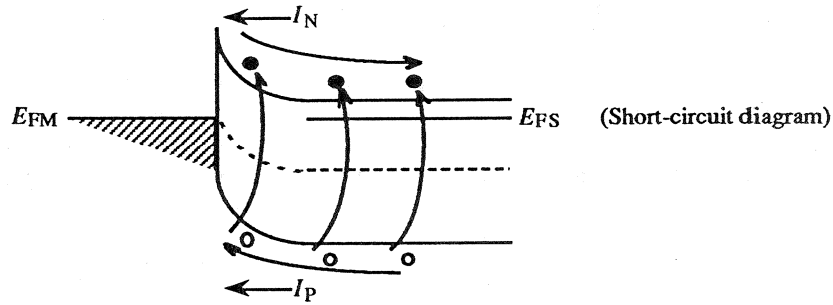
$$qA \left( \frac{4\pi k^2 T^2 m_n^*}{h^3} \right) = A \left( \frac{m_n^*}{m_0} \right) \left( \frac{4\pi q m_0 k^2}{h^3} \right) T^2 = A \mathcal{A}^* T^2$$

leading to the conclusion

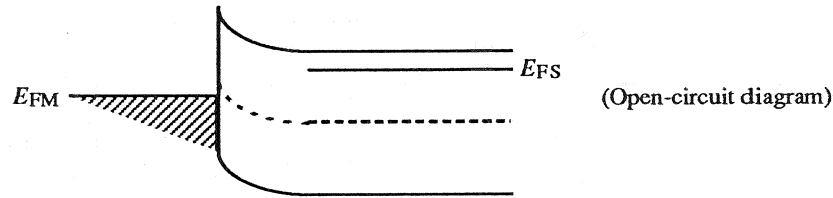
$$I_{S\bullet \rightarrow M} = A \mathcal{A}^* T^2 e^{-\Phi_B/kT} e^{qV_A/kT}$$

14.7

(a) With positive current flow as defined in Fig. 14.3(a), the short-circuit photocurrent is negative. (Note that  $E_{FM} = E_{FS}$  in the energy band diagram because the device is short-circuited. However, both  $F_N$  and  $F_P$  deviate from  $E_{FS}$  near the M-S interface.)



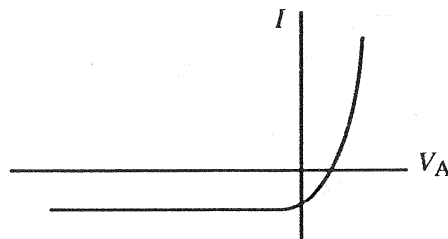
(b) A forward bias must be developed under open-circuit conditions so that the negative-going photocurrent is precisely balanced by a positive-going thermionic emission current.



(c) Paralleling the approach presented in Subsection 9.2.1, the photocurrent ( $I_L$ ) will be equal to  $-q$  times the electron-hole pairs photogenerated per second in the volume  $A(W + L_p)$ , or

$$I_L = -qA(W + L_p)G_L$$

(d) The  $I$ - $V$  sketch should be similar to one of the  $G_0 \neq 0$  curves in Fig. 9.3; i.e., a constant value is subtracted from the dark  $I$ - $V$  characteristic to obtain the light-on characteristic. Consistent with the part (a) and (b) answers,  $I < 0$  if the device is short-circuited ( $V_A = 0$ ) and  $V > 0$  if the device is open circuited ( $I = 0$ ).



### 14.8

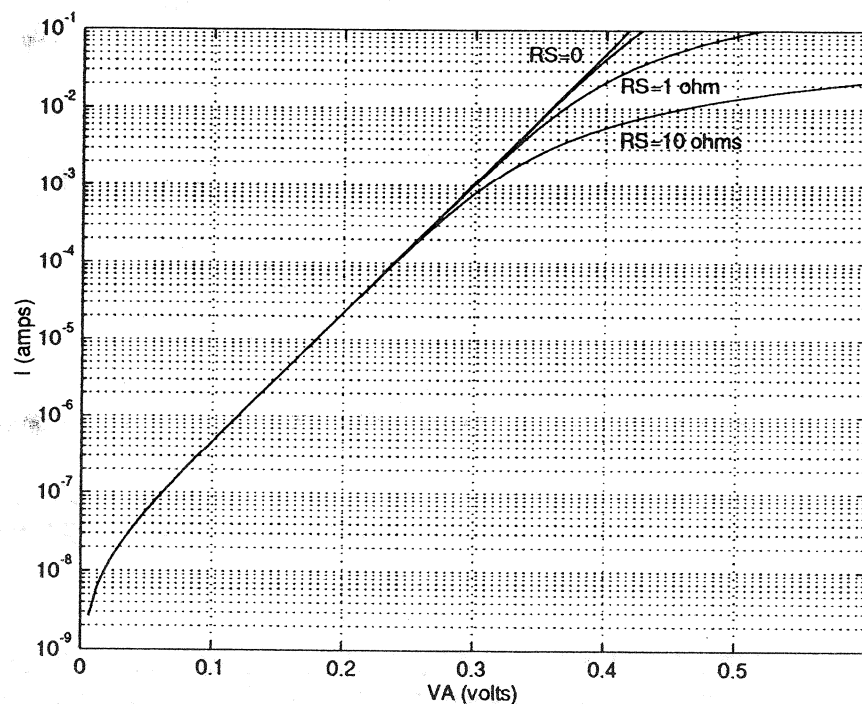
When the series resistance cannot be ignored, Eq. (14.24) assumes the modified form

$$I = I_s(e^{qV_J/kT} - 1)$$

where

$$V_J = V_A - IR_S \quad \text{or} \quad V_A = V_J + IR_S$$

The  $I$ - $V$  relationships here are totally analogous to the high-current  $pn$  junction relationships presented in Subsection 6.2.4. In performing computations, it is convenient to first choose a value for  $V_J$ , compute  $I$ , and then compute  $V_A$ . The requested  $I$ - $V$  characteristics illustrating the effect of the series resistance are reproduced below.



MATLAB program script...

```
%Effect of RS on MS diode I-V Characteristics
%Initialization
clear; close
%Constants and Parameters
kT=0.0259;
```

```

IS=1.0e-8;
RS=[0,0.1,1.0,10];
VJ=linspace(0,0.6);
%Calculate I versus VA
I=IS.*exp(VJ/kT)-1;
VA=[];
for i=1:4,
VA=[VA;VJ+I.*RS(i)];
end
%Plot result
semilogy(VA,I,'w');
axis([0,0.6,1.0e-9,1.0e-1]); grid
xlabel('VA (volts)'); ylabel('I (amps)')
text(0.34,5.0e-2,'RS=0'); text(0.41,2.0e-2,'RS=1 ohm')
text(0.41,4.0e-3,'RS=10 ohms')

```

### 14.9

For a  $p^+-n$  junction...

$$I_{\text{DIFF}} = I_0(e^{qV_A/kT} - 1) = qA \frac{D_P}{L_P} \frac{n_i^2}{N_D} (e^{qV_A/kT} - 1)$$

and employing Eqs. (14.24/14.25),

$$I_{\text{TE}} = I_s(e^{qV_A/kT} - 1) = A \alpha * T^2 e^{-\Phi_B/kT} (e^{qV_A/kT} - 1)$$

Thus noting

$$\frac{D_P}{L_P} = \sqrt{\frac{D_P}{\tau_p}} = \sqrt{\frac{(kT/q)\mu_p}{\tau_p}}$$

$$\frac{I_{\text{DIFF}}}{I_{\text{TE}}} = \frac{I_0}{I_s} = \frac{qA \frac{D_P}{L_P} \frac{n_i^2}{N_D}}{A \alpha * T^2 e^{-\Phi_B/kT}} = \frac{q \sqrt{\frac{(kT/q)\mu_p}{\tau_p}} \frac{n_i^2}{N_D}}{\alpha * T^2 e^{-\Phi_B/kT}}$$

$$= \frac{(1.6 \times 10^{-19}) \left[ \frac{(0.0259)(437)}{(10^{-6})} \right]^{1/2} \left( \frac{10^{20}}{10^{16}} \right)}{(140)(300)^2 e^{-(0.72)/(0.0259)}} = 5.05 \times 10^{-7}$$

### 14.10

(a)/(b) The computational results for parts (a) and (b) and the associated MATLAB m-file are included after the part (c) comments. The primary relationships employed in the computations were:

*For part (a)...*

$$\Delta\Phi_B = \left( \frac{q|\mathcal{E}_S|}{4\pi K_S \epsilon_0} \right)^{1/2} \quad \dots (\Delta\Phi_B \text{ in eV})$$

$$|\mathcal{E}_S| = \frac{qN_D}{K_S \epsilon_0} W = \left[ \frac{2qN_D}{K_S \epsilon_0} (V_{bi} - V_A) \right]^{1/2}$$

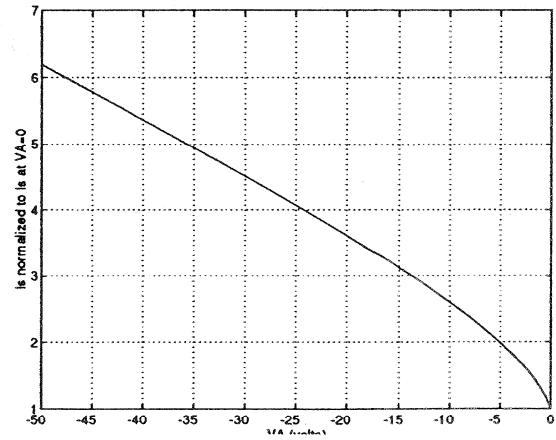
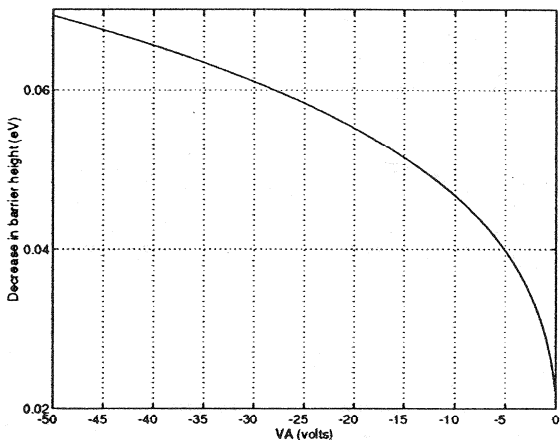
$$V_{bi} = \frac{1}{q} [\Phi_B - (E_c - E_F)_{FB}]$$

$$(E_c - E_F)_{FB} \approx E_G/2 - (E_F - E_i)_{FB} = E_G/2 - kT \ln(N_D/n_i)$$

*For part (b)...*

$$\frac{I_s(V_A)}{I_s(V_A=0)} = \frac{e^{-\Phi_B(V_A)/kT}}{e^{-\Phi_B(0)/kT}} = e^{[\Phi_B(0) - \Phi_B(V_A)]/kT} = e^{[\Delta\Phi_B(V_A) - \Delta\Phi_B(0)]/kT}$$

(c) The  $\Delta\Phi_B$ (eV) versus  $V_A$  plot shows that the change in  $\Delta\Phi_B$  tends to be quite small, only 0.047 eV corresponding to a  $\Delta V_A = 50$ V in the given calculation. However, because  $I_s$  depends exponentially on the barrier height, the effect of a small  $\Delta\Phi_B$  change on  $I_s$  is very significant.—  $I_s$  changes by more than a factor of 6 over the examined voltage range!



**MATLAB program script...**

```
%Schottky Barrier Lowering Computation
%Initialization
clear; close
%Constants and Parameters
q=1.6e-19;
e0=8.85e-14;
kT=0.0259;
KS=11.8;
EG=1.12;
ni=1.0e10;
ND=1.0e16;
BH=0.72; %BH=barrier height in eV
%Computation of ΔBH
VA=linspace(-50,0);
ECF=EG/2-kT*log(ND/ni);
Vbi=BH-ECF;
ES=sqrt((2*q*ND) / (KS*e0).* (Vbi-VA));
ΔBH=sqrt((q.*ES)./(4*pi*KS*e0));
plot(VA,ΔBH); grid
xlabel('VA (volts)'); ylabel('Decrease in barrier height (eV)');
pause
%Computation of Is/Is(0)
Isn=exp((ΔBH-ΔBH(100))./kT);
plot(VA,Isn); grid
xlabel('VA (volts)'); ylabel('Is normalized to Is at VA=0');
```

### 14.11

If not explicitly given in the problem statement, the device area ( $A = 1.5 \times 10^{-3} \text{ cm}^2$ ) may be obtained from Exercise 14.4. Effecting the fit employing the MATLAB program listed below, one finds:

<b>Fit Results</b>	<b>Exercise 14.4</b>
$N_D = 9.62 \times 10^{15}/\text{cm}^3$	$N_D \cong 9.7 \times 10^{15}/\text{cm}^3$
$V_{bi} = 0.613 \text{ V}$	$V_{bi} \cong 0.6 \text{ V}$
$\Phi_B = 0.816 \text{ eV}$	$\Phi_B \cong 0.8 \text{ eV}$

The fit results obviously compare very favorably with the approximate results obtained in Exercise 14.4.

**MATLAB program script...**

```
% Determination of Vbi, ND, and BH of MS diode
% employing P14.11 C-V data

%Initialization
clear; close
format compact; format short e

%Input data...Y=1/CJ2
VA= -[1.09,2.08,3.07,4.06,5.05,6.04,7.03,8.02,9.01,10];
Y=1.0e21*[0.953,1.494,2.035,2.579,3.125,3.673,4.217,... 
4.763,5.320,5.890];

%Fit
p=polyfit(VA,Y,1)
ND=2./ (1.6e-19*11.8*8.85e-14*(1.5e-3)^2*(-p(1)))
Vbi=-p(2)/p(1)

%Barrier Height Computation
EG=1.12; ni=1.0e10; kT=0.0259;
ECF=EG/2-kT*log(ND/ni);
BH=Vbi+ECF

%1/CJ2 vs. VA plot (not required)
plot(VA,Y,'+')
axis([-11,2,0,1.1*max(Y)]); grid
xlabel('VA (volts)'); ylabel('1/CJ^2 (1/F^2)')
```

### 14.12

In general the development of relationships for the electrostatic variables in a linearly graded MS diode closely parallels the uniformly doped analysis in Subsection 14.2.1. The results obtained are analogous to the linearly graded *pn* junction relationships established in Subsection 5.2.5.

(a) With  $N_D(x) = ax$  for  $x \geq 0$ , invoking the depletion approximation yields

$$\rho(x) = qax \quad \dots 0 \leq x \leq W$$

Substituting into Poisson's equation gives

$$\frac{d\mathcal{E}}{dx} = \frac{\rho}{K_S \epsilon_0} \equiv \frac{qa}{K_S \epsilon_0} x \quad \dots 0 \leq x \leq W$$

and

$$\int_{\mathcal{E}(x)}^0 d\mathcal{E}' = \frac{qa}{K_S \epsilon_0} \int_x^W x' dx'$$

or

$$\mathcal{E}(x) = -\frac{qa}{2K_S \epsilon_0} (W^2 - x^2) \quad \dots 0 \leq x \leq W$$

Turning to the electrostatic potential, we can write

$$\frac{dV}{dx} = -\mathcal{E}(x) = \frac{qa}{2K_S \epsilon_0} (W^2 - x^2)$$

and

$$\int_{V(x)}^0 dV' = \frac{qa}{2K_S \epsilon_0} \int_x^W (W^2 - x'^2) dx'$$

or

$$V(x) = -\frac{qa}{6K_S \epsilon_0} (2W^3 - 3W^2 x + x^3) \quad \dots 0 \leq x \leq W$$

Finally,  $V = -(V_{bi} - V_A)$  at  $x = 0$ , and therefore

$$-(V_{bi} - V_A) = -\frac{qa}{3K_S \epsilon_0} W^3$$

$$W = \left[ \frac{3K_S \epsilon_0}{qa} (V_{bi} - V_A) \right]^{1/3}$$

(b) Paralleling the development for the linearly graded *pn* junction in Subsection 5.2.5, the Eq. (14.3) expression for  $V_{bi}$  must be modified to read

$$V_{bi} = \frac{1}{q} [\Phi_B - (E_c - E_F)|_{x=W_0}]$$

where  $W_0$  is the depletion width when  $V_A = 0$ . Since approximate charge neutrality applies for  $x > W_0$ , it follows that

$$n|_{x=W_0} = n_i e^{[(E_F - E_i)|_{x=W_0}] / kT} \cong N_D(x=W_0) = aW_0$$

or

$$(E_c - E_F)|_{x=W_0} \cong E_G/2 - kT \ln \left( \frac{aW_0}{n_i} \right)$$

Thus, to determine  $V_{bi}$ , one must simultaneously solve the following two equations employing numerical techniques.

$$W_0 = \left[ \frac{3K_S \epsilon_0}{qa} V_{bi} \right]^{1/3}$$

$$V_{bi} = \frac{1}{q} \left[ \Phi_B - E_G/2 + kT \ln \left( \frac{aW_0}{n_i} \right) \right]$$

$$(c) \quad C_J = \frac{K_S \epsilon_0 A}{W} = \frac{K_S \epsilon_0 A}{\left[ \frac{3K_S \epsilon_0}{qa} (V_{bi} - V_A) \right]^{1/3}}$$

## CHAPTER R2

### C1

- (a) (iii) ...A wide-base diode is assumed.
- (b) (ii) ...The R-G current is the dominant current component.
- (c) (iv) ...Avalanching is the dominant process causing breakdown if  $V_{BR} > \sim 4.5$  V.
- (d) (i) ... $C_J$  varies as  $1/\sqrt{V_{bi}-V_A}$  if one has a step junction.

### C2

- (a) (i) forward biased ... $p_n(x=x_n) > p_{n0} = n_i^2/N_D$ . One has a carrier excess at the *n*-edge of the depletion region.
- (b) (ii) the same as ...Per the Eq. (6.18) boundary condition

$$\Delta p_n(x=x_n) = (n_i^2/N_D)(e^{qV_A/kT} - 1)$$

The  $n_i^2/N_D$  factor must be the same for both diodes since the minority carrier concentrations in the two diodes approach the same value as  $x \rightarrow \infty$ . Also,  $\Delta p_n(x=x_n)$  is the same for both diodes. It therefore follows that  $V_A$  must be the same for both diodes.

- (c) (i) significantly larger than ...As emphasized in Subsection 8.1.2 (see Eq. 8.2), the current flowing in an ideal diode is directly proportional to  $d\Delta p_n/dx|_{x=x_n}$ . Inspecting the figure associated with the problem, we find the magnitude of  $d\Delta p_n/dx|_{x=x_n} = dp_n/dx|_{x=x_n}$  is greater for Diode B.
- (d) (ii) roughly the same as ...If  $n_i^2/N_D$  is the same in two  $p^+-n$  Si diodes maintained at room temperature, then the  $N_D$  doping must be the same in the two diodes. Now, the  $V_{BR}$  of a  $p^+-n$  junction varies in an inverse manner with the *n*-side  $N_D$  doping. Thus, even though the  $p^+$ -side  $N_A$  doping may be different, having the same  $N_D$  doping, the diodes should exhibit roughly the same breakdown voltage.

C3

- (a) **Forward biased**. There is an *excess* of minority carriers adjacent to the edges of the depletion region.
- (b) **Yes** — low level injection does prevail. As required for low-level injection conditions to prevail, the majority carrier concentrations in the quasineutral regions are essentially unperturbed, and the minority carrier concentrations in these regions are much less than the majority carrier concentrations.
- (c) The diffusion capacitance ( $C_D$ ) results directly from the oscillation of minority carrier charge piled-up near the depletion region edges in response to an applied a.c. signal.
- (d) In going from the forward-bias “on”-state to the reverse-bias “off”-state, the store of minority carriers adjacent to the edges of the depletion region must be removed. Since this cannot be accomplished instantaneously, there is a lag time known as the storage delay time ( $t_s$ ) that is observed during the turn-off transient.

#### C4

(a-f) The required dashed-line or “no effect” answers are given in the figures on the next page. An explanation of the answers (which is not technically required) is provided below.

(a) The increase in  $N_D$  leads to two major modifications in the  $I-V$  characteristic. First, since  $V_{BR}$  is approximately proportional to  $1/N_D$ , increasing  $N_D$  by a factor of 2 decreases  $V_{BR}$  by about a factor of 2. Second, from the shape of the  $I-V$  characteristic, it is clear that the  $R-G$  current dominates in the given device. (This is also to be expected, since the characteristics were said to be derived from a Si diode maintained at room temperature.) For reverse biases greater than a few  $kT/q$  volts,

$$I_{R-G} = -\frac{qA n_i}{2\tau_0} W \quad \dots \text{Eq. (6.43)}$$

where

$$W = \left[ \frac{2K_S \epsilon_0}{qN_D} (V_{bi} - V_A) \right]^{1/2} \quad \dots \text{Eq. (5.38) for a } p^+-n$$

At biases where  $-V_A \gg V_{bi}$ ,  $W \propto 1/\sqrt{N_D}$ , and the factor of 2 increase in  $N_D$  reduces  $W$  and therefore  $I_{R-G}$  by a factor of  $\sqrt{2}$ . At small  $-V_A$ ,  $V_{bi}$ , which is slightly increased by increasing  $N_D$ , causes the decrease in  $W$  and  $I_{R-G}$  to be slightly less than  $\sqrt{2}$ .

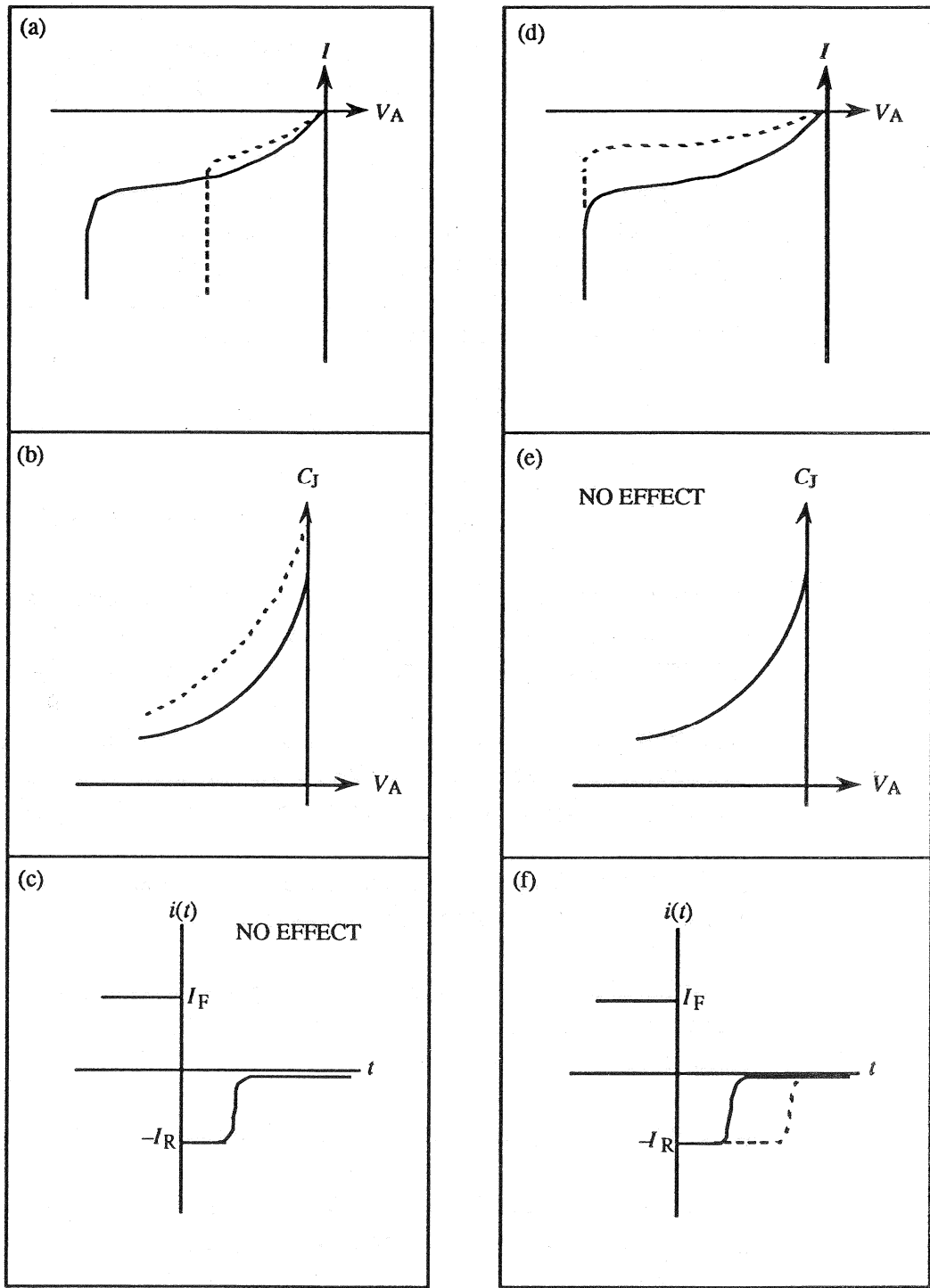
(b) Noting  $C_J = K_S \epsilon_0 A / W$ , we conclude based on the discussion in part (a) that  $C_J \propto 1/W$  will increase by a factor of  $\sqrt{2}$  if  $-V_A \gg V_{bi}$ . At small  $-V_A$ , the slight increase in  $V_{bi}$  with the increase in  $N_D$  will lead to an increase in  $C_J$  that is slightly less than  $\sqrt{2}$ .

(c) The storage delay time relationships developed and cited in Chapter 8 (Eqs. 8.8 and 8.9) are not a function of the semiconductor doping.

(d) As noted in the part (a) explanation,  $I_{R-G} \propto 1/\tau_0$  is clearly the dominant current component. Thus, increasing  $\tau_0$  by a factor of 2 will decrease the observed current by a factor of 2.

(e) The junction capacitance is not a function of the  $\tau_p$  and  $\tau_0$  carrier lifetimes.

(f)  $t_s$  as given by either Eq. (8.8) or (8.9) is directly proportional to  $\tau_p$ . Thus, increasing  $\tau_p$  by a factor of 2 causes  $t_s$  to increase by a factor of 2.



## CHAPTER 15

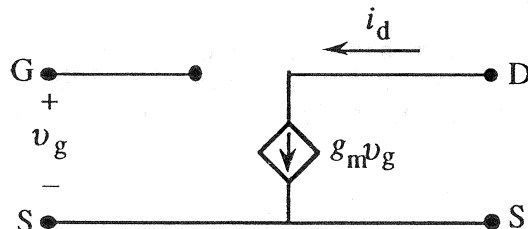
### 15.1

- (a) Field Effect...modulation of the semiconductor conductivity by an electric field applied normal to the surface of the semiconductor.
- (b) Channel...nondepleted current carrying portion of the semiconductor "bar" between the source and drain in a J-FET.
- (c) As viewed from the exterior of the device, the drain current flows *out-of* the drain contact in a *p*-channel device. Holes are the channel carriers in a *p*-channel device and by definition these must flow along the channel into the drain. The current has the same direction as the hole flow—from source to drain and out of the drain contact.
- (d) Gradual channel approximation...In this approximation it is assumed the electrostatic variables in one direction (say the *y*-direction) change slowly compared to the rate of change of the electrostatic variables in a second direction (say the *x*-direction). The *y*-direction dependence is then neglected and the electrostatic variables computed using a pseudo-one-dimensional analysis at each point *y*.
- (e) Pinch-off...complete depletion of the channel region; touching of the top and bottom depletion regions in the symmetrical J-FET.
- (f) As given by text Eqs. (15.18),

$$g_d = \left. \frac{\partial I_D}{\partial V_D} \right|_{V_G=\text{constant}} \quad \dots \text{drain conductance}$$

$$g_m = \left. \frac{\partial I_D}{\partial V_G} \right|_{V_D=\text{constant}} \quad \dots \text{transconductance}$$

- (g) In a long channel J-FET,  $I_D(V_G \text{ held constant}) \approx \text{constant}$  for  $V_D > V_{D\text{sat}}$ . Thus  $g_d \approx 0$  and the  $g_d$  conductance in Fig. 15.19(b) can be neglected in drawing the equivalent circuit.

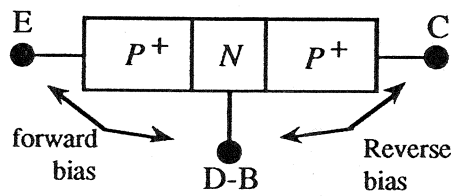


- (h) MESFET...metal semiconductor field effect transistor. D...depletion mode; E...enhancement mode.

- (i) Once  $|E_y|$  exceeds  $\sim 10^4$  V/cm, the carrier drift velocity is no longer proportional to the magnitude of the electric field as assumed in the long-channel analysis.
- (j) In the two-region theory the carrier drift velocity is set equal to  $v_{sat}$  at all points in the channel between  $y_1$  and the drain.  $y_1$  is the point in the channel where  $|E_y|$  has increased to  $v_{sat}/(\text{low-field mobility})$ .

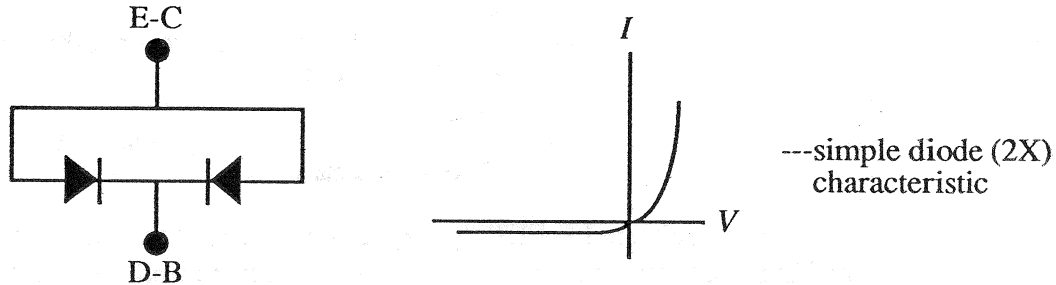
### 15.2

- (a) If  $d \ll L_P$ , the two  $pn$  junctions will be interacting like in a BJT. Moreover, the biases are equivalent to active mode biasing in a BJT.



Obviously, we are being asked for the common base output characteristics (Fig. 10.4a or Fig. 11.4d) of a bipolar junction transistor.

- (b) Since here  $d \gg L_P$ , the two  $pn$  junctions do not interact, and we simply have two diodes in parallel.



- (c) The biasing here is identical to that normally encountered in standard J-FET operation. The physical properties are also those of a J-FET. The desired characteristics are clearly just the  $I_D - V_D$  characteristics of the J-FET with  $V_D \rightarrow V_{DB}$  and  $V_G \rightarrow V_{EB}$ .

### 15.3

(a) Following the *Hint* one obtains,

$$\int_0^y I_D dy' = I_D y = 2qZ\mu_n N_D a \int_0^{V(y)} [1 - W(V')/a] dV'$$

$$y = \frac{2qZ\mu_n N_D a}{I_D} \int_0^{V(y)} [1 - W/a] dV'$$

$$= \frac{2qZ\mu_n N_D a}{I_D} \left\{ V - \frac{2}{3} (V_{bi} - V_P) \left[ \left( \frac{V + V_{bi} - V_G}{V_{bi} - V_P} \right)^{3/2} - \left( \frac{V_{bi} - V_G}{V_{bi} - V_P} \right)^{3/2} \right] \right\}$$

Note that, given the parallel development, setting  $V_D \rightarrow V$  inside the Eq. (15.9) braces yields the foregoing integration result. Eliminating  $I_D$  using Eq. (15.9) then yields

$$\frac{y}{L} = \frac{V - \frac{2}{3} (V_{bi} - V_P) \left[ \left( \frac{V + V_{bi} - V_G}{V_{bi} - V_P} \right)^{3/2} - \left( \frac{V_{bi} - V_G}{V_{bi} - V_P} \right)^{3/2} \right]}{V_D - \frac{2}{3} (V_{bi} - V_P) \left[ \left( \frac{V_D + V_{bi} - V_G}{V_{bi} - V_P} \right)^{3/2} - \left( \frac{V_{bi} - V_G}{V_{bi} - V_P} \right)^{3/2} \right]} \quad \Leftarrow \text{Answer}$$

(b) If  $V_G = 0$ ,  $V_D = 5V$ ,  $V_{bi} = 1V$  and  $V_P = -8V$ ,

$$\frac{y}{L} = \frac{V - (2/9) [(V + 1)^{3/2} - 1]}{5 - (2/9)(6^{3/2} - 1)}$$

and

$V$	$y/L$
1	0.303
2	0.546
3	0.738
4	0.888

The above data was used in constructing Fig. 15.11(c).

### 15.4

Differentiating Eq.(15.9) with respect to  $V_D$  with  $V_G$  held constant yields

$$\frac{\partial I_D}{\partial V_D} \Big|_{V_G=\text{constant}} = \frac{2qZ\mu_n N_D a}{L} \left[ 1 - \left( \frac{V_D + V_{bi} - V_G}{V_{bi} - V_P} \right)^{1/2} \right] \text{ set } 0$$

Solving we obtain

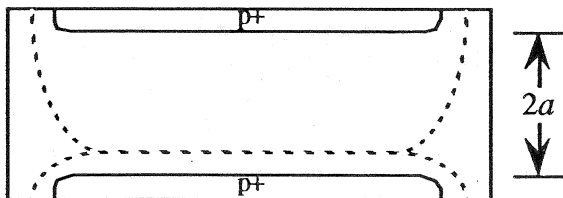
$$\left( \frac{V_{Dsat} + V_{bi} - V_G}{V_{bi} - V_P} \right)^{1/2} = 1$$

or

$$V_{Dsat} = V_G - V_P$$

### 15.5

(a)



NOTE: The bottom depletion width is the same as at equilibrium; the top depletion width is greater than  $a$ .

(b) We can state

$$2a = 2 \left[ \frac{2K_S \epsilon_0}{qN_D} (V_{bi} - V_P) \right]^{1/2} = \left[ \frac{2K_S \epsilon_0}{qN_D} (V_{bi} - V_{PT}) \right]^{1/2} + \left[ \frac{2K_S \epsilon_0}{qN_D} V_{bi} \right]^{1/2}$$

↑                      ↑                      ↑  
 normal situation    top gate            bottom gate  
 depletion width      depletion width

Thus

$$2(V_{bi} - V_P)^{1/2} = (V_{bi} - V_{PT})^{1/2} + V_{bi}^{1/2}$$

or

$$V_{PT} = V_{bi} - [2(V_{bi} - V_P)^{1/2} - V_{bi}^{1/2}]^2$$

Given  $V_{bi} = 1V$ ,  $V_P = -8V$ , one obtains

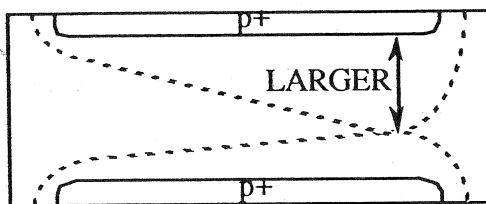
$$V_{PT} = 1 - [2\sqrt{9} - 1]^2$$

or

$$V_{PT} = -24V$$

The above answer is clearly consistent with part (a). The top depletion width needs to be wider than when the two gates are tied together, thereby necessitating a larger applied  $|V_G|$ .

(c)



Assumes  $V_{PT} < V_{GT} < 0$ .

NOTE: Although the bottom  $V_{GB} = 0$ , the bottom depletion width still contributes to the constriction of the channel.

(d) When  $V_D = V_{Dsat}$ ,  $W_T + W_B \rightarrow 2a$  and  $V(L) = V_{Dsat}$ . Also

$$W_T = \left[ \frac{2K_S \epsilon_0}{qN_D} (V_{bi} + V - V_{GT}) \right]^{1/2} \quad \dots \text{top depletion width}$$

$$W_B = \left[ \frac{2K_S \epsilon_0}{qN_D} (V_{bi} + V - V_{GB}) \right]^{1/2} \quad \dots \text{bottom depletion width}$$

Since in the problem at hand  $V_{GB} = 0$ , we obtain at pinch-off

$$2a = \left[ \frac{2K_S \epsilon_0}{qN_D} (V_{bi} + V_{Dsat} - V_{GT}) \right]^{1/2} + \left[ \frac{2K_S \epsilon_0}{qN_D} (V_{bi} + V_{Dsat}) \right]^{1/2}$$

But from part (b)...

$$2a = \left[ \frac{2K_S \epsilon_0}{qN_D} (V_{bi} - V_{PT}) \right]^{1/2} + \left[ \frac{2K_S \epsilon_0}{qN_D} V_{bi} \right]^{1/2}$$

So finally, cancelling the  $2K_S \epsilon_0 / qN_D$  factor everywhere,

$$(V_{bi} - V_{PT})^{1/2} + V_{bi}^{1/2} = (V_{bi} + V_{Dsat} - V_{GT})^{1/2} + (V_{bi} + V_{Dsat})^{1/2}$$

(e) From the part (c) answer, one can tell by inspection that  $V_{Dsat}$  for  $V_{GB} = 0$  operation will be *greater than*  $V_{Dsat}$  for  $V_{GB} = V_{GT}$  operation. The top side depletion width needs to be wider, in turn necessitating more current flow and a higher  $V_{Dsat}$  at the pinch-off point. (Alternative) Using the parameters of part (b), if  $V_{bi} = 1V$ ,  $V_P = -8V$  and  $V_{PT} = -24V$ , one concludes  $V_{Dsat} = V_G - V_P = 6V$  for  $V_{GB} = V_{GT} = -2V$  operation and  $V_{Dsat} \approx 7V$  from the part (d) result if  $V_{GT} = -2V$ . Again  $V_{Dsat}$  ( $V_{GB} = 0$  operation) is greater than  $V_{Dsat}$  ( $V_{GB} = V_{GT}$  operation). Note that the two  $V_{Dsat}$ 's are equal if  $V_{GT} = 0$ .

(f) Since the top and bottom depletion widths are not equal, the symmetry of the structure is destroyed and one must start by revising Eq.(15.3).

$$I_D = -Z \int_{W_T(y)}^{2a-W_B(y)} J_N y dx = Z \int_{W_T(y)}^{2a-W_B(y)} \left( q\mu_n N_D \frac{dV}{dy} \right) dx = qZ\mu_n N_D \frac{dV}{dy} [2a - W_B(y) - W_T(y)]$$

or

$$I_D = 2qZ\mu_n N_D a \frac{dV}{dy} \left[ 1 - \frac{W_T + W_B}{2a} \right]$$

Integrating next over the length of the channel yields,

$$I_D = \frac{2qZ\mu_n N_D a}{L} \int_0^{V_D} \left[ 1 - \frac{W_T + W_B}{2a} \right] dV \quad \dots \text{revised Eq.(15.5)}$$

Using the  $W_T$ ,  $W_B$ , and  $2a$  expressions presented in part (d), one obtains

$$\frac{W_T + W_B}{2a} = \frac{(V_{bi} + V - V_{GT})^{1/2} + (V_{bi} + V)^{1/2}}{(V_{bi} - V_{PT})^{1/2} + V_{bi}^{1/2}} \quad \dots V_{GB} = 0$$

and

$$I_D = \frac{2qZ\mu_n N_D a}{L} \int_0^{V_D} \left[ 1 - \frac{(V_{bi} + V - V_{GT})^{1/2} + (V_{bi} + V)^{1/2}}{(V_{bi} - V_{PT})^{1/2} + V_{bi}^{1/2}} \right] dV$$

Performing the integration gives the desired solution

$$I_D = \frac{2qZ\mu_n N_D a}{L} \left[ V_D - \frac{2}{3} \frac{(V_{bi} + V_D - V_{GT})^{3/2} + (V_{bi} + V_D)^{3/2} - (V_{bi} - V_{GT})^{3/2} - V_{bi}^{3/2}}{(V_{bi} - V_{PT})^{1/2} + V_{bi}^{1/2}} \right]$$

## 15.6

(a) The general  $W$ -relationship for one-sided power-law profiles was noted to be (Eq. 7.6),

$$W = \left[ \frac{(m+2)K_S \epsilon_0}{qb} (V_{bi} - V_A) \right]^{1/(m+2)}$$

For a linearly graded junction  $m = 1$  and  $b = N_0/a$ , or

$$W = \left[ \frac{3K_S \epsilon_0 a}{qN_0} (V_{bi} - V_A) \right]^{1/3}$$

(b) It should be noted first of all that

$$n \equiv N_D - N_A = N_0 \frac{x}{a} \quad \text{...in the nondepleted left-hand side of the channel } (W \leq x \leq a)$$

giving

$$J_N = J_{Ny} = q\mu_n N_0 \frac{x}{a} \mathcal{E}_y = -q\mu_n N_0 \frac{x}{a} \frac{dV}{dy} \quad \text{...in the left-hand portion of the conducting channel}$$

Neglecting the  $\mu_n$  doping dependence, we can write

$$I_D = 2Z \int_{W(y)}^a \left( q\mu_n N_0 \frac{x}{a} \frac{dV}{dy} \right) dx = 2qZ\mu_n \frac{N_0}{a} \frac{dV}{dy} \int_W^a x dx = qZ\mu_n \frac{N_0}{a} \frac{dV}{dy} (a^2 - W^2)$$

or

$$I_D = qZ\mu_n N_0 a \frac{dV}{dy} \left[ 1 - \left( \frac{W}{a} \right)^2 \right] \quad \text{...revised form of Eq.(15.3b)}$$

(The "2" appears in front of the first integral above because equal contributions are obtained from the left- and right-hand sides of the channel.) Integrating over the length of the channel then yields,

$$I_D = \frac{qZ\mu_n N_0 a}{L} \int_0^{V_D} \left[ 1 - \left( \frac{W}{a} \right)^2 \right] dV$$

But from part (a),

$$W = \left[ \frac{3K_S \epsilon_0 a}{qN_0} (V_{bi} + V - V_G) \right]^{1/3} \quad \text{where } V_A = V_G - V$$

and

$$a = \left[ \frac{3K_S \epsilon_0 a}{qN_0} (V_{bi} - V_P) \right]^{1/3}$$

so

$$\frac{W}{a} = \left( \frac{V_{bi} + V - V_G}{V_{bi} - V_P} \right)^{1/3}$$

Substituting into the  $I_D$  equation,

$$I_D = \frac{qZ\mu_n N_0 a}{L} \int_0^{V_D} \left[ 1 - \left( \frac{V_{bi} + V - V_G}{V_{bi} - V_P} \right)^{2/3} \right] dV$$

and after integrating

$$I_D = \frac{qZ\mu_n N_0 a}{L} \left\{ V_D - \frac{3}{5} (V_{bi} - V_P) \left[ \left( \frac{V_D + V_{bi} - V_G}{V_{bi} - V_P} \right)^{5/3} - \left( \frac{V_{bi} - V_G}{V_{bi} - V_P} \right)^{5/3} \right] \right\}$$

### 15.7

Noting

$$I_{D0} \equiv I_{Dsat}|_{V_G=0 \text{ and } R_S=R_D=0} = G_0 \left\{ -V_P - \frac{2}{3} (V_{bi} - V_P) \left[ 1 - \left( \frac{V_{bi}}{V_{bi} - V_P} \right)^{3/2} \right] \right\}$$

and introducing

$$V_{ref} = -V_P - \frac{2}{3} (V_{bi} - V_P) \left[ 1 - \left( \frac{V_{bi}}{V_{bi} - V_P} \right)^{3/2} \right]$$

gives

$$I_{D0} = G_0 V_{ref}$$

Using the results from Exercise 15.3 we can then write:

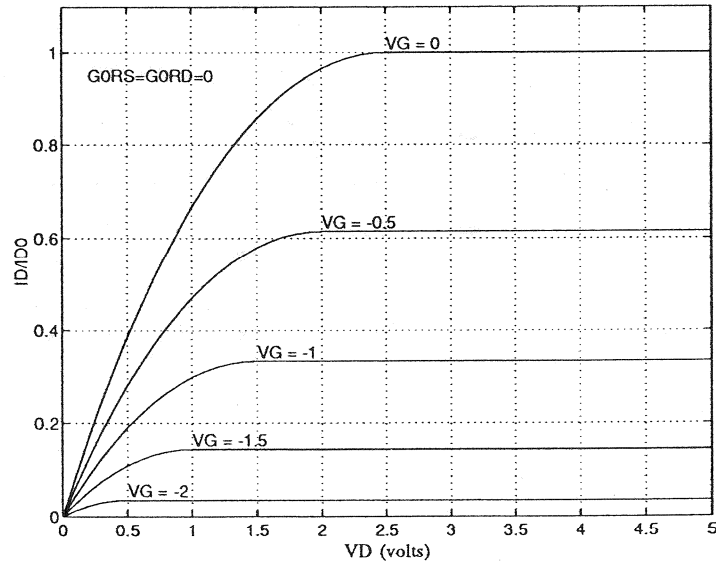
- For  $V_D \leq V_{Dsat}$

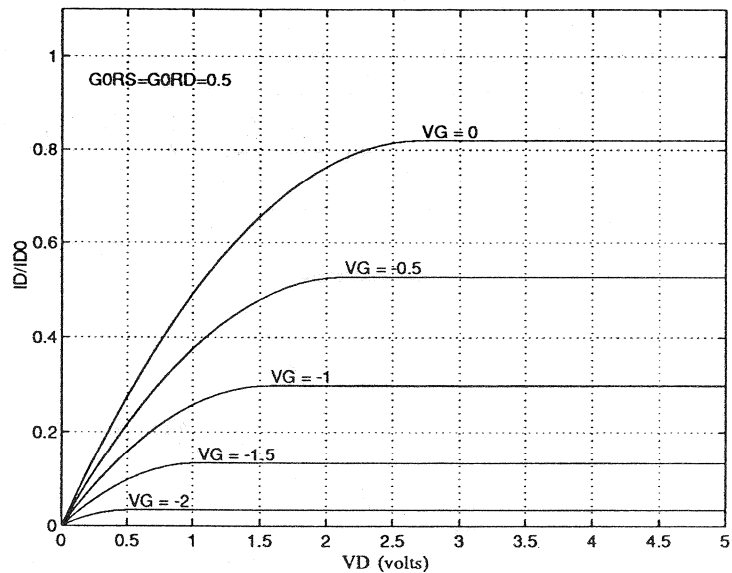
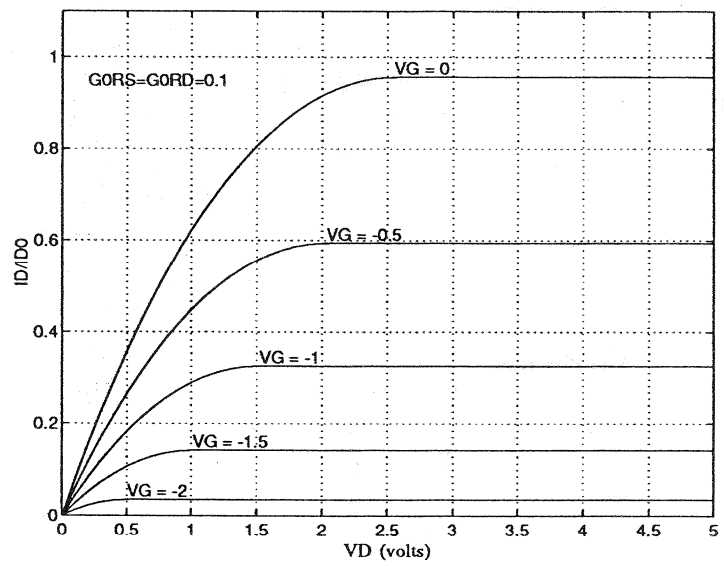
$$\frac{I_D}{I_{D0}} = \frac{V_D}{V_{ref}} - \frac{I_D}{I_{D0}} G_0(R_S + R_D) - \frac{2}{3} \left( \frac{V_{bi} - V_P}{V_{ref}} \right) \left[ \left( \frac{V_D - \frac{I_D}{I_{D0}} G_0 R_D V_{ref} + V_{bi} - V_G}{V_{bi} - V_P} \right)^{3/2} - \left( \frac{I_D G_0 R_S V_{ref} + V_{bi} - V_G}{V_{bi} - V_P} \right)^{3/2} \right]$$

- For  $V_D \geq V_{Dsat}$

$$\frac{I_{Dsat}}{I_{D0}} = \frac{V_G - V_P}{V_{ref}} - \frac{I_{Dsat}}{I_{D0}} G_0 R_S - \frac{2}{3} \left( \frac{V_{bi} - V_P}{V_{ref}} \right) \left[ 1 - \left( \frac{\frac{I_{Dsat}}{I_{D0}} G_0 R_S V_{ref} + V_{bi} - V_G}{V_{bi} - V_P} \right)^{3/2} \right]$$

The foregoing relationships can be iterated using the fzero function in MATLAB to determine  $I_D/I_{D0}$  or  $I_{Dsat}/I_{D0}$  as a function of  $V_D$  with  $V_G$  held constant at preselected values. Running the P\_05\_07.m file on the Instructor's disk yields the results reproduced below and on the next page. With  $G_0 R_S = G_0 R_D = 0$ , one obtains the same characteristics as those displayed in Fig. 15.16. Although the characteristics retain their same general shape when  $G_0 R_S = G_0 R_D > 0$ , an increase in the series resistances causes a significant decrease in  $I_{Dsat}$  and a slight increase in  $V_{Dsat}$ .





### 15.8

(a) Since the gate is shorted to the source,  $V_G = 0$ . Also,  $I = I_D$  and  $V = V_D$ . Thus, referring to Eqs.(15.9), (15.12), and (15.13),

$$G = \frac{I_D}{V_D} = G_0 \left\{ 1 - \frac{2}{3} \left( \frac{V_{bi}-V_P}{V_D} \right) \left[ \left( \frac{V_D+V_{bi}}{V_{bi}-V_P} \right)^{3/2} - \left( \frac{V_{bi}}{V_{bi}-V_P} \right)^{3/2} \right] \right\} \quad \dots 0 \leq V_D \leq V_{Dsat} = -V_P$$

and

$$G_{sat} = \frac{I_{Dsat}}{V_D} = G_0 \left\{ -\frac{V_P}{V_D} - \frac{2}{3} \left( \frac{V_{bi}-V_P}{V_D} \right) \left[ 1 - \left( \frac{V_{bi}}{V_{bi}-V_P} \right)^{3/2} \right] \right\} \quad \dots V_D \geq V_{Dsat} = -V_P$$

Likewise (utilizing Table 15.1),

$$g = \frac{dI_D}{dV_D} = g_{dV_G=0} = G_0 \left[ 1 - \left( \frac{V_D+V_{bi}}{V_{bi}-V_P} \right)^{1/2} \right] \quad \dots 0 \leq V_D \leq V_{Dsat} = -V_P$$

and

$$g_{sat} = \frac{dI_{Dsat}|_{V_G=0}}{dV_D} = 0 \quad \dots V_D \geq V_{Dsat} = -V_P$$

(b) With  $V_D = V_{Dsat}/2 = -V_P/2$

$$R = \frac{1}{G} = \frac{1}{G_0 \left\{ 1 - \frac{4}{3} \left( \frac{V_{bi}-V_P}{-V_P} \right) \left[ \left( \frac{V_{bi}-V_P/2}{V_{bi}-V_P} \right)^{3/2} - \left( \frac{V_{bi}}{V_{bi}-V_P} \right)^{3/2} \right] \right\}}$$

$$r = \frac{1}{g} = \frac{1}{G_0 \left[ 1 - \left( \frac{V_{bi}-V_P/2}{V_{bi}-V_P} \right)^{1/2} \right]}$$

$$G_0 = \frac{2qZ\mu_n N_D a}{L} = 2 (1.6 \times 10^{-19})(1248)(10^{16})(5 \times 10^{-5}) = 2.00 \times 10^{-4} \text{ S}$$

$$R = \frac{1}{(2 \times 10^{-4}) \left\{ 1 - \left( \frac{4}{3} \right) \left( \frac{3}{2} \right) \left[ \left( \frac{2}{3} \right)^{3/2} - \left( \frac{1}{3} \right)^{3/2} \right] \right\}} = 16.9 \text{ k}\Omega$$

$$r = \frac{1}{(2 \times 10^{-4}) \left[ 1 - \left( \frac{2}{3} \right)^{1/2} \right]} = 27.3 \text{ k}\Omega$$

### 15.9

(a) The same development as presented in Section 17.3.2 can be followed with the replacement of  $C_O$  with  $C_G$ .

(b) At maximum (whether one considers below or above pinch-off biasing), one can write

$$g_m \leq G_0 = \frac{2qZ\mu_n N_D a}{L}$$

Also, in general,

$$C_G = 2 \int_0^L \frac{K_S \epsilon_0 Z}{W} dy$$

Since  $a \geq W(y)$

$$C_G \geq 2 \int_0^L \frac{K_S \epsilon_0 Z}{a} dy = \frac{2K_S \epsilon_0 Z L}{a}$$

If  $g_m$  is replaced by something greater than or equal to itself, and  $C_G$  is replaced by something less than or equal to itself, then it follows that

$$f_{max} = \frac{g_m}{2\pi C_G} \leq \frac{2qZ\mu_n N_D a}{2\pi L} \cdot \frac{a}{2K_S \epsilon_0 Z L} = \frac{q\mu_n N_D a^2}{2\pi K_S \epsilon_0 L^2}$$

(c)

$$\begin{aligned} f_{max(\text{limit})} &= \frac{q\mu_n N_D a^2}{2\pi K_S \epsilon_0 L^2} = \frac{(1.6 \times 10^{-19})(1248)(10^{16})(5 \times 10^{-5})^2}{2\pi (11.8)(8.85 \times 10^{-14})(5 \times 10^{-4})^2} \\ &= 3.04 \text{ GHz} \end{aligned}$$

### 15.10

(a)/(b) With the device saturation biased and  $V_G = 0$ , we conclude from Table 15.1 that

$$g_m = G_0 \left[ 1 - \left( \frac{V_{bi}}{V_{bi} - V_p} \right)^{1/2} \right]$$

where

$$G_0 \equiv \frac{2qZ\mu_n N_D a}{L}$$

The only parameter in  $G_0$  which is temperature dependent is  $\mu_n$ . Thus

$$\frac{g_m(T)}{g_m(300K)} = \left( \frac{\mu_n(T)}{\mu_n(300K)} \right) \left( \frac{1 - [V_{bi}(T)/(V_{bi}-V_p)]^{1/2}}{1 - [V_{bi}(300K)/(V_{bi}-V_p)]^{1/2}} \right)$$

with

$$V_{bi} = (kT/q) \ln(N_A N_D / n_i^2)$$

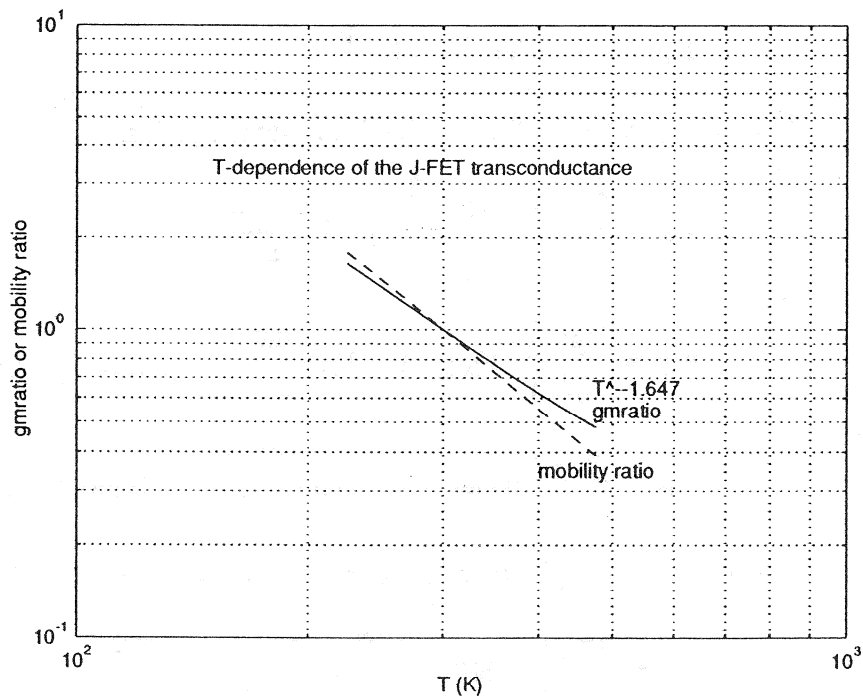
and

$$a = \left[ \frac{2K_S \epsilon_0}{qN_D} (V_{bi}-V_p) \right]^{1/2}$$

or

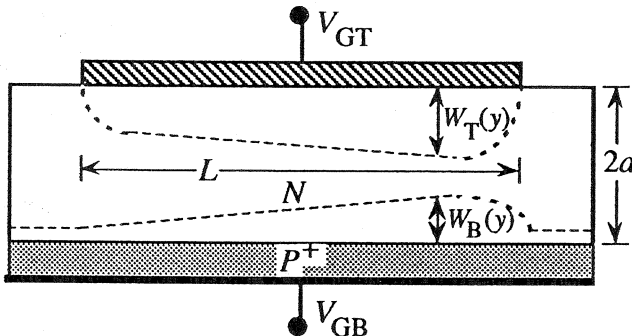
$$(V_{bi}-V_p)|_T = (V_{bi}-V_p)|_{300K} = (qN_D a^2)/(2K_S \epsilon_0)$$

The required computations for both part (a) and part (b) are performed by file P\_15\_10.m on the Instructor's disk. The  $\mu_n$  vs.  $T$  dependence was established employing the empirical-fit relationships found in Exercise 3.1 and programmed in file P\_03\_03.m. The  $n_i$  vs.  $T$  dependence was computed following the procedure outlined in Exercise 2.4(a). The resultant  $g_m(T)/g_m(300K)$  and  $\mu_n(T)/\mu_n(300K)$  plots reproduced in the following figure clearly exhibit a power-law type dependence, with a least squares fit yielding  $g_m(T)/g_m(300K) = (T/300)^{-1.647}$ . The variation of the transconductance with temperature is seen to arise primarily from the variation of the carrier mobility with temperature.



15.11

The device subject to analysis is pictured below



In the two region model the long-channel theory can be employed for drain biases below saturation. Paralleling the solution to Problem 15.5(f), let  $W_T(y)$  be the top gate (MS) depletion width and  $W_B(y)$  the bottom gate ( $p^+$ - $n$ ) depletion width. In general

$$I_D = -Z \int_{W_T(y)}^{2a-W_B(y)} J_{Ny} dx = Z \int_{W_T}^{2a-W_B} \left( q\mu_n N_D \frac{dV}{dy} \right) dx = qZ\mu_n N_D \frac{dV}{dy} [2a - W_B - W_T]$$

or

$$I_D = 2qZ\mu_n N_D a \frac{dV}{dy} \left( 1 - \frac{W_T + W_B}{2a} \right)$$

Integrating next over the length of the channel yields,

$$I_D = \frac{2qZ\mu_n N_D a}{L} \int_0^{V_D} \left( 1 - \frac{W_T + W_B}{2a} \right) dV$$

Now

$$W_T = \left[ \frac{2K_S \epsilon_0}{qN_D} (V_{biT} + V - V_{GT}) \right]^{1/2} \quad \dots \text{top depletion width}$$

$$W_B = \left[ \frac{2K_S \epsilon_0}{qN_D} (V_{biB} + V - V_{GB}) \right]^{1/2} \quad \dots \text{bottom depletion width}$$

and, given total depletion of the channel occurs when  $V_{GT} = V_P$  and  $V_D = V_{GB} = 0$ ,

$$2a = \left[ \frac{2K_S \epsilon_0}{qN_D} (V_{biT} - V_P) \right]^{1/2} + \left[ \frac{2K_S \epsilon_0}{qN_D} V_{biB} \right]^{1/2}$$

Thus

$$\frac{W_{T+B}}{2a} = \frac{(V_{biT}+V-V_{GT})^{1/2} + (V_{biB}+V-V_{GB})^{1/2}}{(V_{biT}-V_P)^{1/2} + V_{biB}^{1/2}}$$

Substituting the depletion width relationship into the  $I_D$  expression and performing the integration finally yields the desired computational relationship.

$$I_D = G_0 \left[ V_D - \frac{2}{3} \frac{(V_{biT}+V_D-V_{GT})^{3/2} + (V_{biB}+V_D-V_{GB})^{3/2} - (V_{biT}-V_{GT})^{3/2} - (V_{biB}-V_{GB})^{3/2}}{(V_{biT}-V_P)^{1/2} + V_{biB}^{1/2}} \right]$$

### 15.12

Setting  $\mu_0 \rightarrow -\mu_n$  and  $\mathcal{E} \rightarrow \mathcal{E}_y = -dV/dy$  in Eq. (15.21), and replacing  $\mu_n$  in Eq. (15.2) with the resulting  $\mu(\mathcal{E})$  expression, one obtains

$$J_{Ny} = -q \left( \frac{\mu_n}{1 + \frac{\mu_n}{v_{sat}} \frac{dV}{dy}} \right) N_D \frac{dV}{dy} \quad (15.2')$$

and

$$I_D = 2qZ \left( \frac{\mu_n}{1 + \frac{\mu_n}{v_{sat}} \frac{dV}{dy}} \right) N_D a \frac{dV}{dy} \left( 1 - \frac{W}{a} \right) \quad (15.3b')$$

or

$$I_D \left( 1 + \frac{\mu_n}{v_{sat}} \frac{dV}{dy} \right) = 2qZ \mu_n N_D a \frac{dV}{dy} \left( 1 - \frac{W}{a} \right)$$

Integrating over the length of the channel and remembering  $I_D$  is independent of  $y$ , we obtain

$$I_D \left[ \int_0^L dy + \frac{\mu_n}{v_{sat}} \int_0^{V_D} dV \right] = 2qZ \mu_n N_D a \int_0^{V_D} \left( 1 - \frac{W}{a} \right) dV$$

or

$$I_D = \frac{2qZ \mu_n N_D a}{L \left( 1 + \frac{\mu_n}{v_{sat}} \frac{V_D}{L} \right)} \int_0^{V_D} \left( 1 - \frac{W}{a} \right) dV = \frac{I_D(\text{long-channel})}{1 + \frac{\mu_n}{v_{sat}} \frac{V_D}{L}}$$

### 15.13

Since  $dV/dy = -\mathcal{E}_y$ , differentiating both sides of the Problem 15.3(a) result with respect to  $y$  yields

$$\frac{1}{L} = \frac{-\mathcal{E}_y + \mathcal{E}_y \left( \frac{V+V_{bi}-V_G}{V_{bi}-V_P} \right)^{1/2}}{V_D - \frac{2}{3}(V_{bi}-V_P) \left[ \left( \frac{V_D+V_{bi}-V_G}{V_{bi}-V_P} \right)^{3/2} - \left( \frac{V_{bi}-V_G}{V_{bi}-V_P} \right)^{3/2} \right]}$$

Next solving for  $\mathcal{E}_y$  gives

$$\mathcal{E}_{yL} = \frac{V_D - \frac{2}{3}(V_{bi}-V_P) \left[ \left( \frac{V_D+V_{bi}-V_G}{V_{bi}-V_P} \right)^{3/2} - \left( \frac{V_{bi}-V_G}{V_{bi}-V_P} \right)^{3/2} \right]}{\left( \frac{V+V_{bi}-V_G}{V_{bi}-V_P} \right)^{1/2} - 1}$$

$\mathcal{E}_y = \mathcal{E}_{sat}$  when  $V(L) = V_D = V_{Dsat}$ . Thus, substituting into the preceding equation

$$\mathcal{E}_{satL} = \frac{V_{Dsat} - \frac{2}{3}(V_{bi}-V_P) \left[ \left( \frac{V_{Dsat}+V_{bi}-V_G}{V_{bi}-V_P} \right)^{3/2} - \left( \frac{V_{bi}-V_G}{V_{bi}-V_P} \right)^{3/2} \right]}{\left( \frac{V_{Dsat}+V_{bi}-V_G}{V_{bi}-V_P} \right)^{1/2} - 1} \quad (15.26)$$

### 15.14

(a) The MATLAB m-file P\_15\_14.m found on the Instructor's disk was constructed to calculate and plot the FET  $I_D-V_D$  characteristics predicted by the two region model. Characteristics numerically identical to those in Fig. 15.23 are obtained when the short channel parameters noted in the figure caption are input into the program. This is not too surprising since a version of the file was employed in constructing Fig. 15.23.

(b) An FET with a channel length of  $L = 100\mu\text{m}$  qualifies as a long-channel device. With  $L = 100\mu\text{m}$  the computed characteristics are indeed identical to those of the long-channel characteristics pictured in Fig. 15.16.

(c) Per the definition in the problem statement, the long-channel theory begins to "fail" when  $\mathcal{E}_{satL} = -5.575\text{V}$ . Although there are a number of approaches that could be employed, the author obtained this result by simply monitoring the command window output of  $I_{Dsat}/I_{D0}$  ( $V_G=0$ ) as a function of  $L$  with  $\mathcal{E}_{sat}$  held constant at  $-10^4\text{ V/cm}$ .

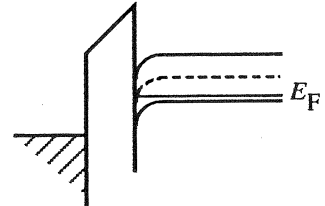
## CHAPTER 16

### 16.1

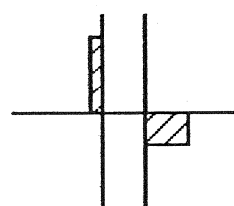
Part    Doping    Biasing Condition

(a)    *p*    depletion

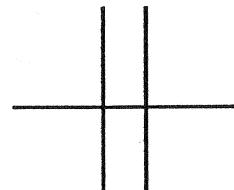
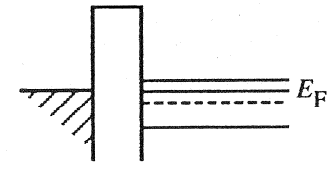
Energy Band Diagram



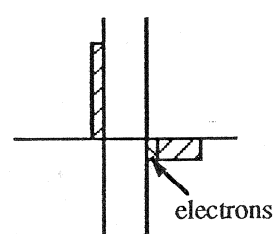
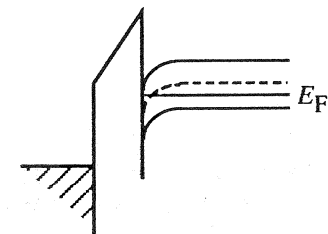
Block Charge Diagram



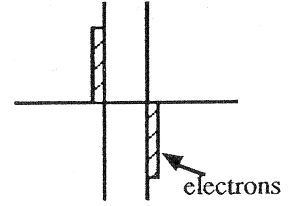
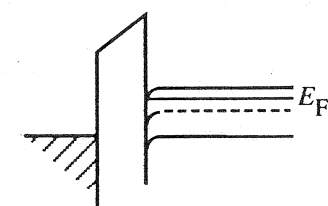
(b)    *n*    flat band



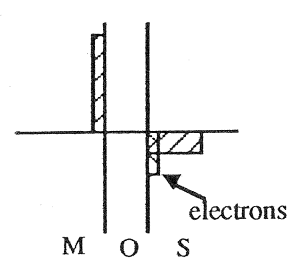
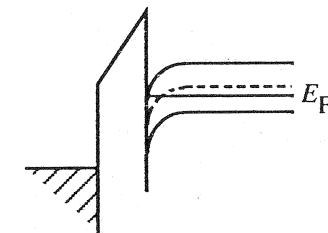
(c)    *p*    depl/inv transition



(d)    *n*    accumulation

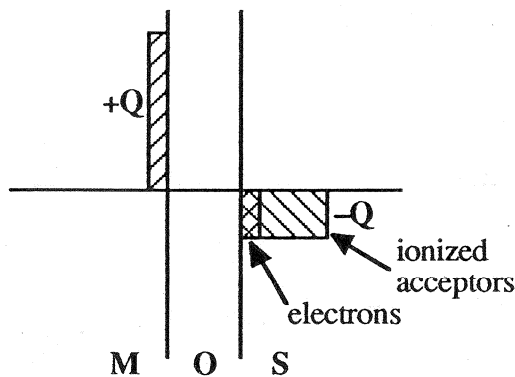


(e)    *p*    inversion

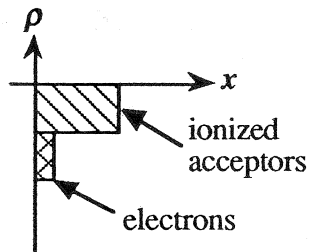


16.2

(a)



(b) The part (a) charge diagram is in agreement with the  $\rho/qN_A$  versus  $x$  plot in Fig. 16.8(c). To obtain the total charge in the semiconductor at each point one adds the separate block charges shown in part (a).



The spike near  $x = 0$  in the Fig. 16.8(c) plot simply reflects the forming inversion layer of electrons at the surface. By definition, at the onset of inversion  $n_{\text{surface}} = N_A$ . Thus, at the special  $V_T$  bias point  $\rho_s = -q(n_{\text{surface}} + N_A) = -2qN_A$ , or  $\rho/qN_A = -2$  at  $x = 0$  at the onset of inversion.

(c) Since  $\phi_F/(kT/q) = 12$ , inverting Eq.(16.8a) yields

$$N_A = n_i e^{\phi_F/(kT/q)} = 1.00 \times 10^{10} e^{12} = 1.63 \times 10^{15}/\text{cm}^3$$

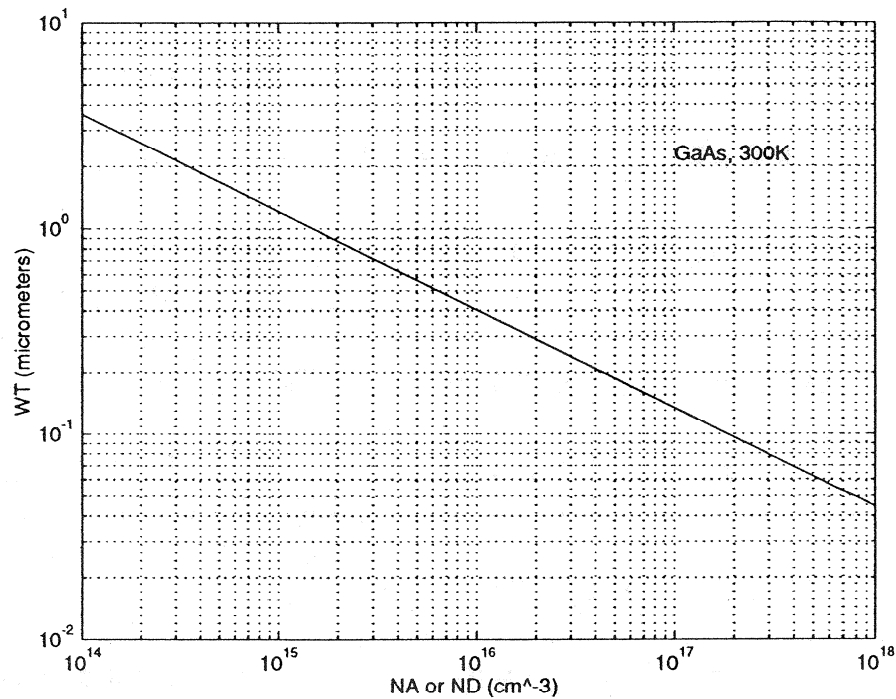
$$W_T = \left[ \frac{2K_S \epsilon_0}{qN_A} (2\phi_F) \right]^{1/2} = \left[ \frac{(2)(11.8)(8.85 \times 10^{-14})(24)(0.0259)}{(1.6 \times 10^{-19})(1.63 \times 10^{15})} \right]^{1/2} = 0.706 \mu\text{m}$$

(From Fig. 16.9 one also reads  $W_T \approx 0.7 \mu\text{m}$ .)

The above  $W_T$  is indeed consistent with the positioning of the end of the approximate charge distribution (the dashed-line distribution) in Fig. 16.8(c).

### 16.3

The required  $W_T$  versus doping plot appropriate for GaAs and the MATLAB program script that generated the plot are reproduced below.



MATLAB program script...

```
%WT versus NA or ND for GaAs at 300K
%Initialization
clear; close;
%Constants and parameters
q=1.6e-19;
e0=8.85e-14;
ni=2.25e6;
KS=12.85;
kT=0.0259;
NB=logspace(14,18); %NB = NA or ND
%WT calculation
øF=kT.*log(NB./ni);
WT=sqrt(4*KS*e0.*øF./(q.*NB));
WT=(1.0e4).*WT; %WT in micrometers
%Plotting result
loglog(NB,WT); grid
xlabel('NA or ND ( $\text{cm}^{-3}$ )');
ylabel('WT (micrometers)');
text(1.0e17,2.3,'GaAs, 300K')
```

## 16.4

(a)

$$\frac{\phi_F}{kT/q} = -\ln(N_D/n_i) = -\ln\left(\frac{10^{15}}{10^{10}}\right) = -11.51$$

$$\phi_F = -11.51 (kT/q) = -(11.51)(0.0259) = \mathbf{-0.298V}$$

(b) Using Eq.(16.16) with  $N_A \rightarrow -N_D$ ,

$$W = W_T = \left[ \frac{2K_S \epsilon_0}{-qN_D} (2\phi_F) \right]^{1/2} = \left[ \frac{(2)(11.8)(8.85 \times 10^{-14})(2)(0.298)}{(1.6 \times 10^{-19})(10^{15})} \right]^{1/2} = \mathbf{0.882 \mu m}$$

(c) Evaluating Eq.(16.12) at  $x = 0$  yields  $\mathcal{E}_S$ . Thus, with  $N_A \rightarrow -N_D$  in Eq. (16.12),

$$\mathcal{E}_S = -\frac{qN_D}{K_S \epsilon_0} W = -\frac{(1.6 \times 10^{-19})(10^{15})(0.882 \times 10^{-4})}{(11.8)(8.85 \times 10^{-14})} = \mathbf{-1.35 \times 10^4 V/cm}$$

(d) Substituting into Eq.(16.26) gives

$$\begin{aligned} V_G &= 2\phi_F + \frac{K_S}{K_O} x_0 \mathcal{E}_S && \dots \mathcal{E}_S \text{ evaluated at } \phi_S = 2\phi_F \\ &= -(2)(0.298) - \frac{(11.8)(10^{-5})(1.35 \times 10^4)}{3.9} \\ &= \mathbf{-1.00 V} \end{aligned}$$

Except for the doping type, the parameters used in this problem are identical to those assumed in constructing Fig. 16.10. Since  $\phi_S = 2\phi_F$ , the  $|V_G|$  calculated in part (d) should correspond to the depletion/inversion transition point in Fig. 16.10. Indeed, in the figure  $V_T \equiv 1V$ .

(e) The MATLAB program script yielding a computer generated computation of  $\phi_F$ ,  $W$ ,  $\mathcal{E}_S$ , and  $V_G$  is listed on the next page and included on the Instructor's disk as m-file P\_16\_04.m. Note that a normalized  $\phi_S$ ,  $\phi_S/2\phi_F$ , is taken to be one of the input variables. Also, donor dopings must be input as a negative concentration in running the program.

### MATLAB program script...

```
%Autocalculation of  $\phi_F$ , W, ES and VG
%Initialization
clear; close;
format compact
%Constants and parameters
q=1.6e-19;
e0=8.85e-14;
ni=1.0e10;
KS=11.8;
KO=3.9;
kT=0.0259;
%Input variables
xo=input('Please input xo in cm, xo = ');
N=input('Please input NA or -ND in cm^-3, N = ');
r=input('Please input  $\phi_S/2\phi_F$ ,  $\phi_S/2\phi_F =$ ');
NB=abs(N); s=N/NB;
% $\phi_F$  and WT calculation
 $\phi_F=s*kT*log(NB/ni)$ 
 $\phi_S=r^2*\phi_F;$ 
W0=sqrt(2*KS*e0* $\phi_S/(q*N)$ ); %W0 in cm
W=(1.0e4)*W0 %W in micrometers
%Surface Electric Field (ES) calculation
ES=(q*N*W0)/(KS*e0)
%VG calculation
VG= $\phi_S+KS*xo*ES/KO$ 
```

### 16.5

(a) In general we can write

$$\text{Also } V_G = \phi_S + \frac{K_S}{K_O} x_0 \mathcal{E}_S \quad \dots \text{Eq.(16.26)}$$

$$\phi_S = \frac{kT}{q} U_S \quad \dots \text{Eq.(B.2)}$$

and Eq.(B.16) evaluated at the surface gives

$$\mathcal{E}_S = \hat{U}_S \frac{kT}{q} \frac{F(U_S, U_F)}{L_D}$$

Substituting the above  $\phi_S$  and  $\mathcal{E}_S$  expressions into the general  $V_G-\phi_S$  relationship yields the desired result;

$$V_G = \frac{kT}{q} \left[ U_S + \hat{U}_S \frac{K_S x_0}{K_O L_D} F(U_S, U_F) \right]$$

(b) The required  $V_G$  versus  $U_S$  computation is performed by the MATLAB m-file listed below. Setting  $x = 0.1\mu\text{m}$  and  $N_D = 10^{15}/\text{cm}^3$  yields a plot identical to Fig. 16.10 except the entire plot is reflected through the origin of coordinates.

MATLAB program script...

```
%VG versus US Calculation
%Initialization
clear; close
format compact

%Universal and System Constants
q=1.60e-19;
e0=8.85e-14;
kT=0.0259;

%Device and Material Constants
KS=11.8;
KO=3.9;
ni=1.00e10;
LD=sqrt((KS*e0*kT)/(2*q*ni));
s=input('Employ xo=1.0e-5cm and ND=1.0e15/cm3? 1-Yes, 2-No... ');
if s==1
    Net=1.0e15;
    xo=1.0e-5;
else
    Net=input('Input the net semi doping in cm-3, ND-NA = ');
    xo=input('Input the oxide thickness in cm, xo = ');
end
N=abs(Net); sign=-Net/N;
UF=sign*log(N/ni)

%Computation Proper
US=UF-21:1:UF+21;
S=US./abs(US);
F=sqrt(exp(UF).* (exp(-US)+US-1)+exp(-UF).* (exp(US)-US-1));
VG=kT*(US+S*(KS*xo)/(KO*LD).*F);

%Plot result
plot(US,VG); grid
if s==1
    axis([-40, 10, -4, 4]);
end
xlabel('US'); ylabel('VG (volts)')
```

### 16.6

(a) Eq.(16.28) may be viewed as a quadratic equation with  $\sqrt{\phi_S}$  as the variable.

$$(\sqrt{\phi_S})^2 + \frac{K_S}{K_O} x_0 \sqrt{\frac{2qN_A}{K_S \epsilon_0}} \sqrt{\phi_S} - V_G = 0$$

Introducing

$$b \equiv \frac{K_S}{K_O} x_0 \sqrt{\frac{2qN_A}{K_S \epsilon_0}}$$

and choosing the (+) root solution so that  $\sqrt{\phi_S} > 0$ , one obtains,

$$\sqrt{\phi_S} = -\frac{b}{2} + \left[ \left( \frac{b}{2} \right)^2 + V_G \right]^{1/2} = \frac{b}{2} \left\{ \left[ 1 + \frac{V_G}{(b/2)^2} \right]^{1/2} - 1 \right\}$$

or

$$\sqrt{\phi_S} = \left( \frac{K_S}{K_O} x_0 \sqrt{\frac{qN_A}{2K_S \epsilon_0}} \right) \left\{ \left[ 1 + \frac{V_G}{(b/2)^2} \right]^{1/2} - 1 \right\}$$

Substituting the  $\sqrt{\phi_S}$  result into Eq.(16.15) then yields

$$W = \frac{K_S x_0}{K_O} \left[ \sqrt{1 + \frac{V_G}{V_\delta}} - 1 \right]$$

if

$$V_\delta \equiv \left( \frac{b}{2} \right)^2 = \frac{q}{2} \frac{K_S x_0^2}{K_O^2 \epsilon_0} N_A$$

We have indeed obtained the text result.

$$(b) (i) \phi_F = -\frac{kT}{q} \ln(N_D/n_i) = -(0.0259) \ln\left(\frac{10^{15}}{10^{10}}\right) = -0.298V$$

$$W_T = \left[ \frac{2K_S \epsilon_0}{-qN_D} (2\phi_F) \right]^{1/2} = \left[ \frac{(2)(11.8)(8.85 \times 10^{-14})(2)(0.298)}{(1.6 \times 10^{-19})(10^{15})} \right]^{1/2} = 0.882 \mu m$$

(From Fig. 16.9 with  $N_D = 10^{15}/cm^3$  one would estimate  $W_T \approx 0.9 \mu m$ .)

(ii) From Eq.(16.34d),

$$\begin{aligned}\frac{C}{C_0} &= \frac{1}{1 + \frac{K_O W_T}{K_S x_0}} \quad \dots \text{inv}(\omega \rightarrow \infty) \\ &= \frac{1}{1 + \frac{(3.9)(0.882)}{(11.8)(0.1)}} = 0.255\end{aligned}$$

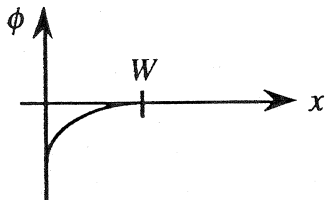
(iii) Some care must be exercised in working this part of the problem. An acceptable approach is to proceed as in Problem 16.4, first calculating  $\mathcal{E}_S$  using Eq.(16.12) and then substituting into Eq.(16.26). In fact, the parameters are the same as in Prob. 16.4 and thus the expected answer is  $V_T = -1.00V$ . Alternatively, one might consider substituting into Eq.(16.28) directly;  $V_G = V_T$  when  $\phi_S = 2\phi_F$ . However, Eq.(16.28) is only valid for *p*-type devices and simply changing  $N_A$  to  $-N_D$  will not yield the correct  $V_T$ . [For an *n*-type device the "+" between the two right-hand terms in Eq.(16.28) is replaced with a "-" sign.] Nevertheless, Eq.(16.28) can be used if we first act as if the doping was *p*-type, and then just change the sign of the result noting the voltage symmetry between ideal *n*- and *p*-type devices.

$$\begin{aligned}V_T &= - \left[ (2\phi_F) + \frac{K_S}{K_O} x_0 \sqrt{\frac{2qN_A}{K_S \epsilon_0} (2\phi_F)} \right] \quad (\phi_F > 0) \\ &= - \left\{ (2)(0.298) + \frac{(11.8)(10^{-5})}{3.9} \left[ \frac{(2)(1.6 \times 10^{-19})(10^{15})(2)(0.298)}{(11.8)(8.85 \times 10^{-14})} \right]^{1/2} \right\} \\ &= -1.00 \text{ V} \leftarrow \text{expected result}\end{aligned}$$

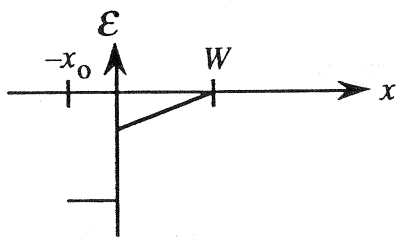
(iv) The parameters used in this problem are identical to those assumed in constructing Fig. 16.13. Thus the part (ii)  $C/C_0$  value should correspond to the high-frequency inversion value on the figure and the  $V_T$  calculated in part (iii) should be the depletion/inversion transition voltage shown in the figure. This is indeed the case.

16.7

(a)  $\phi$  has the same shape as the "upside down" of the bands.



(b)  $\mathcal{E}$  is proportional to the slope of the bands. Also, as emphasized in a footnote on p. 581,  $\mathcal{E}_{ox} \equiv 3\mathcal{E}_S$  in an ideal MOS-C.

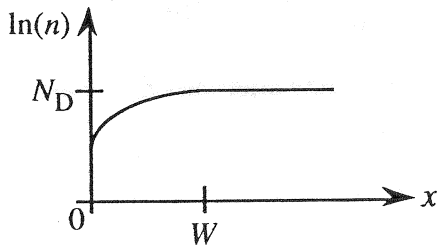


(c) [Yes]. Inside the semiconductor  $E_F$  is position independent.

(d) Noting

$$n = n_i e^{(E_F - E_i)/kT}$$

we conclude



(e) Since  $E_F = E_i$  at the Si-SiO<sub>2</sub> interface,  $n|_{x=0} \equiv n_i = 10^{10}/\text{cm}^3$ .

(f)  $N_D \equiv n_{\text{bulk}} = n_i e^{[E_{FS} - E_i(\text{bulk})]/kT} = (10^{10}) e^{0.29/0.0259} = 7.29 \times 10^{14}/\text{cm}^3$

(g)  $\phi_S = (1/q)[E_i(\text{bulk}) - E_i(\text{surface})] = -0.29 \text{ V}$

(h) Some care must be exercised in completing this part of the problem. Simply employing Eq. (16.28) with  $N_A$  replaced by  $-N_D$  yields an incorrect result because  $\mathcal{E}_S < 0$  when an *n*-bulk MOS-C is depletion biased. Specifically, for an *n*-bulk device

$$\mathcal{E}_S = -\left[\frac{2qN_D}{K_S \epsilon_0}(-\phi_S)\right]^{1/2}$$

and

$$V_G = \phi_S - \frac{K_S x_0}{K_O} \sqrt{\frac{2qN_D}{K_S \epsilon_0} (-\phi_S)}$$

Thus here

$$V_G = -0.29 - \frac{(11.8)(2 \times 10^{-5})}{(3.9)} \left[ \frac{(2)(1.6 \times 10^{-19})(7.29 \times 10^{14})}{(11.8)(8.85 \times 10^{-14})} (0.29) \right]^{1/2}$$

or

$$V_G = -0.78 \text{ V}$$

$$(i) V_G = \Delta\phi_{ox} + \phi_S$$

$$\Delta\phi_{ox} = V_G - \phi_S = -0.78 + 0.29 = -0.49 \text{ V}$$

$$(j) V_\delta = -\frac{q}{2} \frac{K_S x_0^2}{K_O^2 \epsilon_0} N_D = -\frac{(1.6 \times 10^{-19})}{2} \frac{(11.8)(2 \times 10^{-5})^2 (7.29 \times 10^{14})}{(3.9)^2 (8.85 \times 10^{-14})} = 0.2045 \text{ V}$$

$$\frac{C}{C_O} = \frac{1}{\sqrt{1 + V_G/V_\delta}} \approx \frac{1}{\sqrt{1 + 0.78/0.20}} = 0.45$$

(Eqs. 16.15 and 16.34b may alternatively be used to compute  $C/C_O$ .)

## 16.8

Inversion	... e, 4
Depletion	... c, 3
Flat band	... b, 1
$V_G = V_T$	... d, 2
Accumulation	... a, 5

### 16.9

- (a) [Yes]. The Fermi level *inside the semiconductor* is position independent.
- (b)...  $\phi_F = (1/q)[E_i(\text{bulk}) - E_F] = 0.3 \text{ V}$
- (c)...  $\phi_S = (1/q)[E_i(\text{bulk}) - E_i(\text{surface})] = \phi_F = 0.3 \text{ V}$
- (d)...  $E_F(\text{metal}) - E_F(\text{semi}) = -qV_G \quad \dots \text{Eq. (2.1)}$   
 $V_G = (1/q)[E_F(\text{semi}) - E_F(\text{metal})] = 0.6 \text{ V}$

(e) Based on the delta-depletion approximation,

$$V_G = \phi_S + \frac{K_S x_0}{K_O} \sqrt{\frac{2qN_A}{K_S \epsilon_0} \phi_S} \quad \Leftarrow \text{Eq.(16.28)}$$

where from prior parts of the problem  $V_G = 0.6 \text{ V}$  and  $\phi_S = 0.3 \text{ V}$ . Also,

$$\phi_F = (kT/q) \ln(N_A/n_i)$$

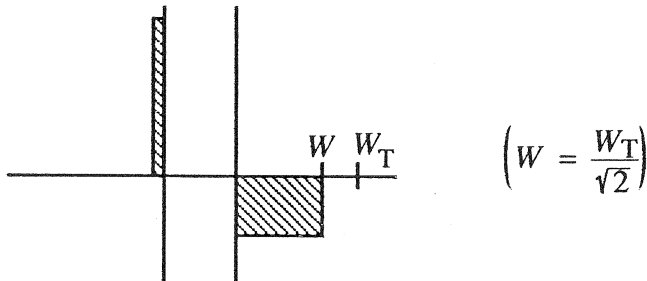
or

$$N_A = n_i e^{\phi_F/(kT/q)} = (10^{10}) e^{0.3/0.0259} = 1.073 \times 10^{15}/\text{cm}^3$$

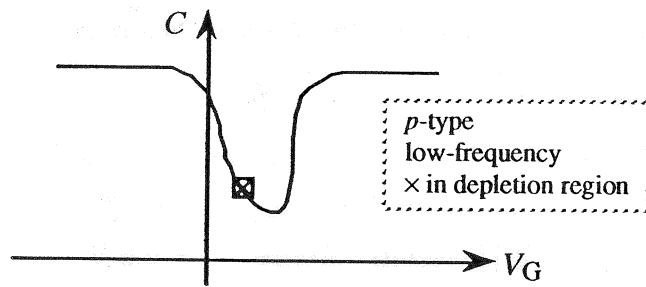
Thus

$$x_0 = \frac{V_G - \phi_S}{\frac{K_S}{K_O} \sqrt{\frac{2qN_A}{K_S \epsilon_0} \phi_S}} = \frac{0.6 - 0.3}{\left(\frac{11.8}{3.9}\right) \left[ \frac{(2)(1.6 \times 10^{-19})(1.073 \times 10^{15})(0.3)}{(11.8)(8.85 \times 10^{-14})} \right]^{1/2}} = 0.10 \mu\text{m}$$

(f)



(g)



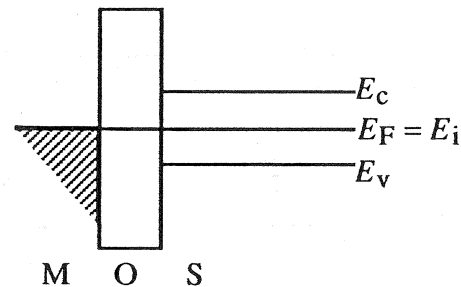
(b) Expressions (i) and (iv) are clearly wrong because they do not apply to depletion. Employing Eq. (16.28), we conclude  $V_T \approx 1V$  and  $V_G \approx 0.6V_T$ . Thus referring to Eq. (16.37), expression (ii) is close but not the correct expression. Finally, noting that at the specified bias point,

$$\phi_S = \phi_F \text{ and } W = \left[ \frac{2K_S \epsilon_0}{qN_A} \phi_F \right]^{1/2} = W_T \sqrt{2}$$

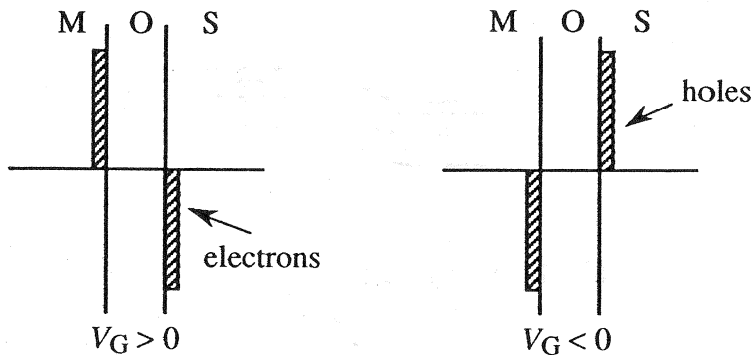
we conclude

$$C = \frac{C_0}{1 + \frac{K_O W}{K_S x_0}} = \frac{C_0}{1 + \frac{K_O W_T}{\sqrt{2} K_S x_0}} \quad \Leftarrow \boxed{\text{Expression (iii)}}$$

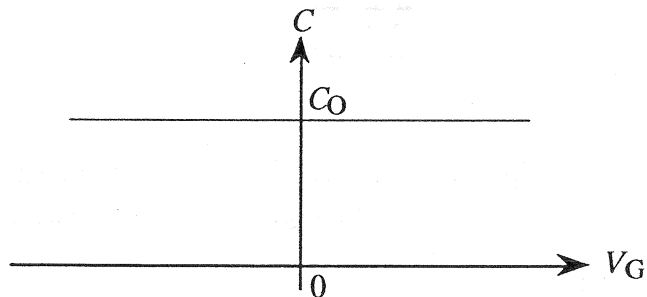
16.10  
(a)



(b)



(c)

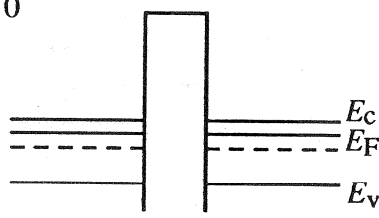


*Justification:* When  $V_G > 0$ , electrons pile-up in the Si immediately adjacent to the oxide giving rise to a low-frequency  $C = C_O$ . Similarly, when  $V_G < 0$ , holes pile-up in the Si immediately adjacent to the oxide giving rise to a low-frequency  $C = C_O$ . (Actually,  $C \equiv C_O$ , but in the delta-depletion formulation the carrier layers are taken to be  $\delta$ -functions at the Si surface.) Note that, within the framework of the delta-depletion formulation, there is no "depletion" or depletion-like region inside the given device.

16.11

Part (a) ↓

(i)  $V_G = 0$

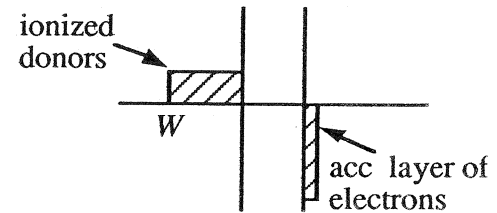
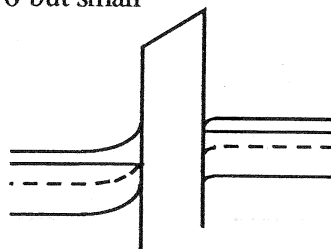


Part (b) ↓

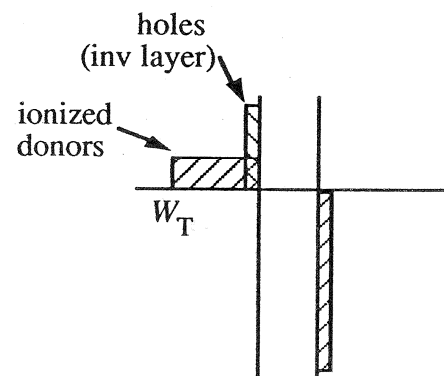
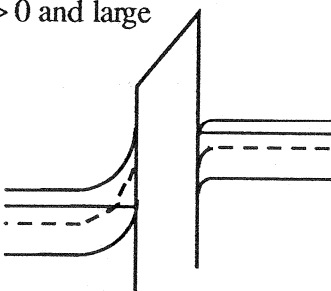
No charge anywhere

S O S

(ii)  $V_G > 0$  but small



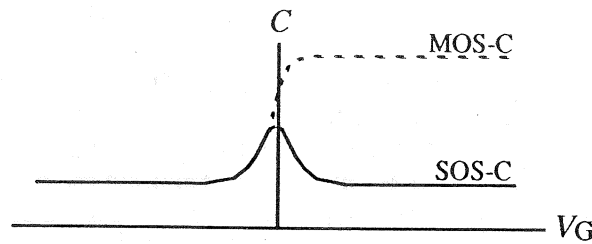
(iii)  $V_G > 0$  and large



(iv)  $V_G < 0$  but small — (ii) answer with semiconductor regions interchanged.

(v)  $V_G < 0$  and large — (iii) answer with semiconductor regions interchanged.

(c)



### 16.12

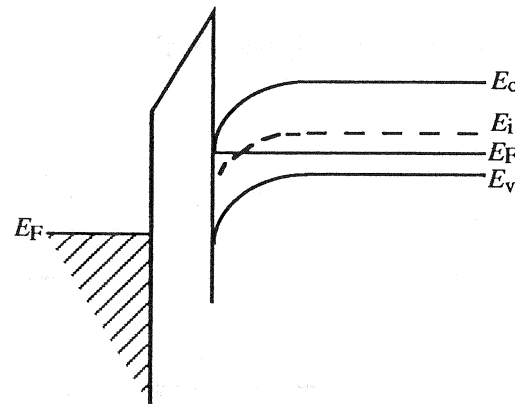
(a) Curves *a* and *b* are standard low- and high-frequency C-V curves that result when the semiconductor component of the MOS-C is in equilibrium under d.c. biasing conditions. Curve *c* is a nonequilibrium deep-depletion characteristic.

(b) In accumulation  $C \rightarrow C_0 = K_O \epsilon_0 A_G / x_0$ . Since both devices exhibit the same capacitance in accumulation, the two devices have the same oxide thickness. With  $x_0$  being the same, the lower capacitance of device *b* in inversion indicates this device has a lower doping. ( $W_T$  increases with decreasing doping, thereby giving rise to a smaller capacitance; also see Fig. 16.14b.)

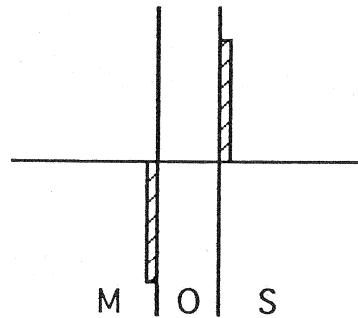
### 16.13

(a) *p-type* ...For *p*-type devices accumulation ( $C_{\max}$ ) occurs for negative  $V_G$  and inversion ( $C_{\min}$ ) occurs at positive  $V_G$ . The exact opposite is true for *n*-type devices.

(b) At point (2) the *p*-type MOS-C is far into inversion. Thus



(c) At point (1) the MOS-C is clearly deep into accumulation.



(d) From Fig. P16.13,  $C_{\max} = 100 \text{ pF}$ . However,

$$C_{\max} = C_0 = \frac{K_O \epsilon_0 A_G}{x_0}$$

$$x_0 = \frac{K_O \epsilon_0 A_G}{C_{\max}} = \frac{(3.9)(8.85 \times 10^{-14})(3 \times 10^{-3})}{(10^{-10})} = 0.104 \mu\text{m}$$

(e) In the delta-depletion formulation

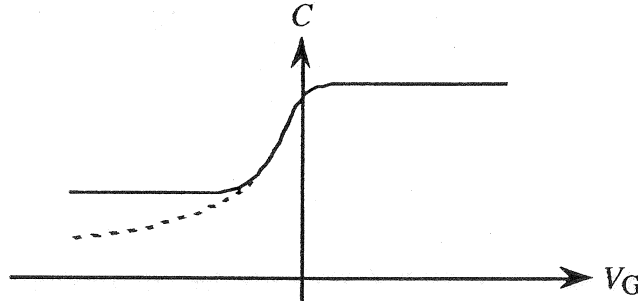
$$C = \frac{C_0}{1 + \frac{K_O W_T}{K_S x_0}} \quad \text{inv } (\omega \rightarrow \infty) \quad (16.34d)$$

Thus

$$W_T = \frac{K_S x_0}{K_O} \left( \frac{C_0}{C} - 1 \right) = \frac{(11.8)(0.104)}{(3.9)} \left( \frac{100}{20} - 1 \right) = 1.26 \mu\text{m}$$

Employing Fig. 16.9, we conclude  $N_A \approx 5 \times 10^{14}/\text{cm}^3$ .

16.14  
(a)



$$(b) C_{\max} = C_0 = \frac{K_O \epsilon_0 A_G}{x_0} = \frac{(3.9)(8.85 \times 10^{-14})(10^{-3})}{10^{-5}} = 34.5 \text{ pF}$$

$$(c) \phi_F = -(kT/q) \ln(N_D/n_i) = -0.0259 \ln(2 \times 10^{15}/10^{10}) = -0.316$$

$$W_T = \left[ \frac{2K_S \epsilon_0}{qN_D} (-2\phi_F) \right]^{1/2} = \left[ \frac{(2)(11.8)(8.85 \times 10^{-14})(2)(0.316)}{(1.6 \times 10^{-19})(2 \times 10^{15})} \right]^{1/2} = 6.42 \times 10^{-5} \text{ cm}$$

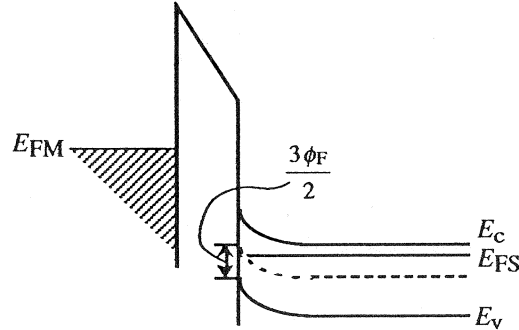
$$C_{\text{MIN}} = \frac{C_0}{1 + \frac{K_O W_T}{K_S x_0}} = \frac{34.5}{1 + \frac{(3.9)(6.42 \times 10^{-5})}{(11.8)(10^{-5})}} = 11.1 \text{ pF}$$

(d) By definition, if  $V_G = V_T \dots \phi_S = 2\phi_F = -0.632 \text{ V}$

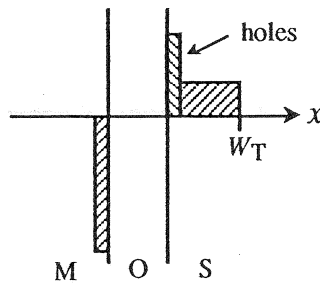
$$(e) V_T = (2\phi_F) - \frac{K_S x_0}{K_O} \sqrt{\frac{2qN_D}{K_S \epsilon_0} (-2\phi_F)} \quad (\text{Also see Prob. 16.7h.})$$

$$= -2(0.316) - \frac{(11.8)(10^{-5})}{(3.9)} \left[ \frac{(2)(1.6 \times 10^{-19})(2 \times 10^{15})(0.632)}{(11.8)(8.85 \times 10^{-14})} \right]^{1/2} = 1.23 \text{ V}$$

(f)



(g)  $|\phi_S| = |5\phi_F/2| > |2\phi_F|$  and the MOS-C is therefore inversion biased with  $W = W_T$ .



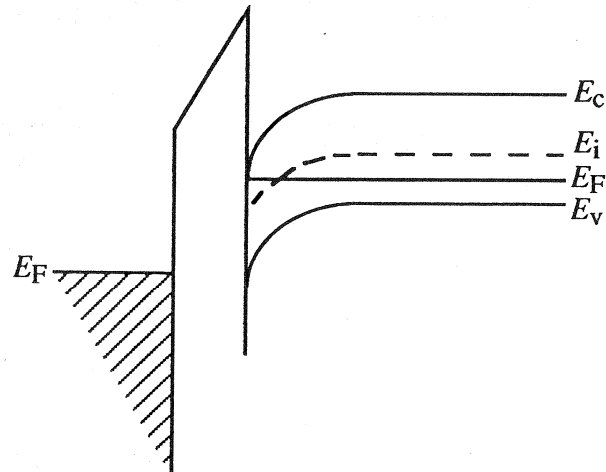
(h) Under the specified operating conditions, the MOS-C is expected to exhibit a total deep-depletion characteristic exemplified by the dashed line in the part (a) answer.

16.15

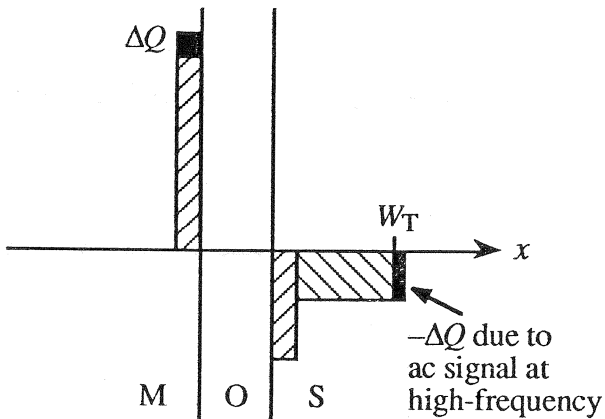
(a) **[p-type]** ...There is an inversion-layer of negative charge — electrons — shown in the block charge diagram. The semiconductor must therefore be *p*-type. (Also, the depletion-region charge is negative or clearly due to acceptor ions.)

(b) **[Inversion biased]** ...As noted in part (a), there is an inversion layer with  $n_s > N_A$  shown on the diagram.

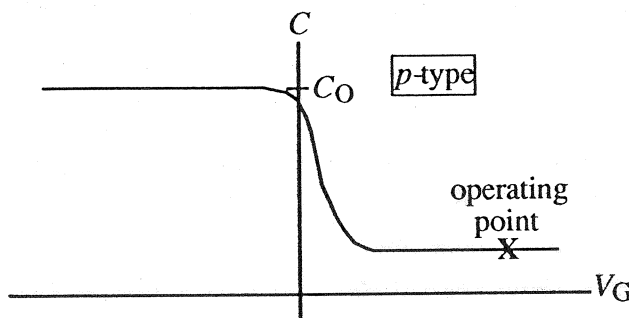
(c)



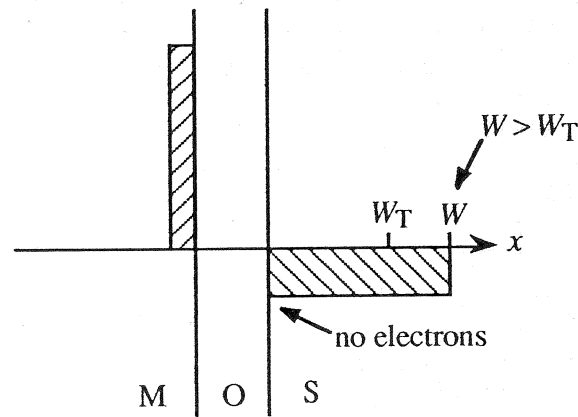
(d)



(e)



(f)



NOTE: Because the added depletion-layer charge is farther from the surface than the inversion layer charge, there is NOT a one-to-one correspondence between the two charges. Also, the charge on the metal will be slightly different than under equilibrium inversion conditions at the same  $V_G$  bias.

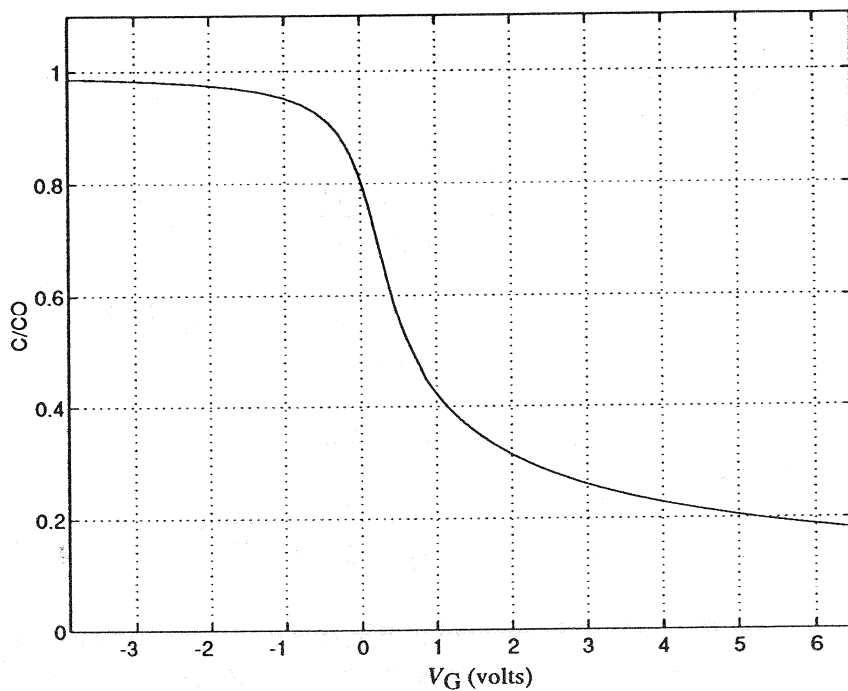
### 16.16

The MATLAB program script yielding deep-depletion *p*-type MOS-C *C*–*V* characteristics and a sample plot ( $x_0 = 0.2\mu\text{m}$ ,  $N_A = 7.8 \times 10^{14}/\text{cm}^3$ ) are reproduced below. Note that the sample plot has been extended to  $V_G = 5V_T$  (as opposed to stopping at  $V_G = 3V_T$  per the directions in the first printing of the book). If the sample *C*–*V* curve is converted to an *n*-type characteristic AND translated approximately 2V along the voltage axis in the negative direction, the sample plot becomes a very good match to the experimental total-deep-depletion data displayed in Fig. 16.17.

MATLAB program script...

```
%p-type Deep Depletion MOS-C C-V Characteristics
%Initialization and Input
clear; close
format compact
NA=input('Please input the bulk doping in /cm3, NA=');
xo=input('Please input the oxide thickness in cm, xo=');
%Constants and Parameters
e0=8.85e-14;
q=1.6e-19;
k=8.617e-5;
KS=11.8;
KO=3.9;
ni=1.0e10;
T=300;
kT=k*T;
%Computed Constants
UF=log(NA/ni);
LD=sqrt((kT*KS*e0)/(2*q*ni));
%C-V Computation for US < UF ( or VG < VI)
US=UF-21:0.5:UF;
F=sqrt(exp(UF).* (exp(-US)+US-1)+exp(-UF).* (exp(US)-US-1));
VG1=kT*(US+ (US./abs(US)).*(KS*xo)/(KO*LD).*F);
DENOM1=exp(UF).* (1-exp(-US))+exp(-UF).* (exp(US)-1);
W1=(US./abs(US)).*LD.* (2*F).*/DENOM1;
c1=1.0./(1+(KO*W1)./(KS*xo));
%C-V Computation for US > UF (or VI < VG < 5VT)
FI=sqrt(exp(UF).* (exp(-UF)+UF-1)+exp(-UF).* (exp(UF)-UF-1));
VI=kT*(UF+ (KS*xo)/(KO*LD).*FI);
oF=kT*UF;
VT=2*oF+(KS*xo/KO)*sqrt((4*q*NA*oF)/(KS*e0));
Vdelta=(q/2)*(KS*xo^2*NA)/(KO^2*e0);
VG2=VI+0.1:0.1:5*VT;
c2=1./sqrt(1+VG2./Vdelta);
```

```
%Combining and Plotting results
c=[c1,c2];
VG=[VG1,VG2];
plot(VG,c); grid
axis([-3*VT,5*VT,0, 1.1])
xlabel('VG (volts)'); ylabel('C/CO')
```



16.17

(a)

$$C_O = \frac{K_O \epsilon_0 A_G}{x_0} \Rightarrow x_0 = \frac{K_O \epsilon_0 A_G}{C_O}$$

$$x_0 = \frac{(3.9)(8.85 \times 10^{-14})(4.75 \times 10^{-3})}{82 \times 10^{-12}} = 0.200 \mu\text{m}$$

(b) From Fig. 16.17,  $C/C_O(\text{inv}) \approx 0.39$ .

$$C(\text{inv}) = \frac{C_O}{1 + \frac{K_O W_{\text{eff}}(\text{inv})}{K_S x_0}}$$

$$W_{\text{eff}}(\text{inv}) = \frac{K_S x_0}{K_O} \left[ \frac{C_O}{C(\text{inv})} - 1 \right] = \frac{(11.8)(0.2)}{(3.9)} \left( \frac{1}{0.39} - 1 \right)$$

$$= 0.946 \mu\text{m}$$

and

$$\frac{W_{\text{eff}}(\text{inv})}{L_D} = \frac{9.46 \times 10^{-5}}{2.91 \times 10^{-3}} = 3.25 \times 10^{-2}$$

(c) If  $W_{\text{eff}}(\text{inv})$  is equated to  $W_T$ , one estimates from Fig. 16.9 that  $N_D \approx 8.5 \times 10^{14}/\text{cm}^3$  or  $U_F = -\ln(N_D/n_i) = -\ln(8.5 \times 10^{14}/1.00 \times 10^{10}) = -11.35$ . Substituting  $U_F = -11.35$  into the expression for  $W_{\text{eff}}/L_D$  one computes  $W_{\text{eff}}/L_D = 3.374 \times 10^{-2}$ .  $W_{\text{eff}}/L_D$  is too large implying  $N_D$  and  $|U_F|$  are somewhat larger. Trying  $U_F = -11.45$  yields  $W_{\text{eff}}/L_D = 3.223 \times 10^{-2}$ ; trying  $U_F = -11.40$  yields  $W_{\text{eff}}/L_D = 3.298 \times 10^{-2}$ . Clearly  $U_F$  is bracketed between  $-11.40$  and  $-11.45$ . Subsequent calculations give  $W_{\text{eff}}/L_D = 3.268 \times 10^{-2}$ ,  $3.253 \times 10^{-2}$ ,  $3.238 \times 10^{-2}$  when  $U_F = -11.42$ ,  $-11.43$ , and  $-11.44$ , respectively. The best value appears to be

$U_F = -11.43$	and	$N_D = n_i e^{-U_F} = (10^{10}) e^{11.43} = 9.20 \times 10^{14}/\text{cm}^3$
----------------	-----	--

NOTE: We actually pushed the calculation here beyond the accuracy of the data to illustrate the procedure.

## CHAPTER 17

### 17.1

- (a) Carriers enter the channel at the source contact and leave the channel (or are "drained") at the drain contact.
- (b) Channel...inversion layer beneath the MOS gate which electrically connects the source and drain.
- (c) The portion of the characteristics where  $V_D > V_{D\text{sat}}$  for a given  $V_G$  (the approximately horizontal portion of the characteristics) is referred to as the saturation region of operation.
- (d) The depletion-inversion transition point voltage and the threshold voltage are one and the same voltage.
- (e) There is an additional carrier scattering mechanism in the surface channel of a MOSFET; namely, surface scattering. With increased scattering the mobility decreases.
- (f) The square-law name arises from the fact that  $I_{D\text{sat}}$  varies as the square of  $V_{D\text{sat}}$  in this first-order formulation (see Eq. 17.22).
- (g) The bulk-charge theory gets its name from the fact that source-to-drain variations in the depletion-layer or "bulk" charge are modeled correctly in the formulation.
- (h)  $I_D$  versus  $V_G$  with  $V_D$  held constant.
- (i) 
$$g_d \equiv \left. \frac{\partial I_D}{\partial V_D} \right|_{V_G=\text{constant}} ; \quad g_m \equiv \left. \frac{\partial I_D}{\partial V_G} \right|_{V_D=\text{constant}}$$
- (j) The source and drain islands in a MOSFET supply the minority carriers required to obtain a low-frequency characteristic. Under inversion conditions minority carriers merely use the surface channel to flow laterally into and out of the MOS gate area in response to the applied ac signal.

17.2  
(a)

$$\phi_F = \frac{kT}{q} \ln(N_A/n_i) = 0.0259 \ln(10^{15}/10^{10}) = 0.298V$$

$$V_T = 2\phi_F + \frac{K_S x_0}{K_O} \sqrt{\frac{4qN_A}{K_S \epsilon_0} \phi_F} \quad \dots(17.1a)$$

$$= (2)(0.298) + \frac{(11.8)(5 \times 10^{-6})}{(3.9)} \left[ \frac{(4)(1.6 \times 10^{-19})(10^{15})(0.298)}{(11.8)(8.85 \times 10^{-14})} \right]^{1/2}$$

$$V_T = 0.800 V$$

(b) In the square-law theory

$$I_{Dsat} = \frac{Z\bar{\mu}_n C_0}{2L} (V_G - V_T)^2 \quad \dots(17.22)$$

$$C_0 = \frac{K_O \epsilon_0}{x_0} = \frac{(3.9)(8.85 \times 10^{-14})}{(5 \times 10^{-6})} = 6.90 \times 10^{-8} F/cm^2$$

$$I_{Dsat} = \frac{(5 \times 10^{-3})(800)(6.9 \times 10^{-8})(2-0.8)^2}{(2)(5 \times 10^{-4})} = 0.397 mA$$

(c) In the bulk-charge theory we must first determine  $V_{Dsat}$  using Eq.(17.29). We know  $\phi_F$  and  $V_T$  from part (a), but must compute  $V_W$  before substituting into the  $V_{Dsat}$  expression.

$$W_T = \left[ \frac{2K_S \epsilon_0}{qN_A} (2\phi_F) \right]^{1/2} = \left[ \frac{(2)(11.8)(8.85 \times 10^{-14})(2)(0.298)}{(1.6 \times 10^{-19})(10^{15})} \right]^{1/2} = 0.882 \mu m$$

$$V_W \equiv \frac{qN_A W_T}{C_0} = \frac{(1.6 \times 10^{-19})(10^{15})(8.82 \times 10^{-5})}{(6.90 \times 10^{-8})} = 0.205V$$

Noting that  $V_G - V_T = 1.20V$ , substituting into Eq.(17.29) then gives

$$V_{Dsat} = 1.20 - 0.205 \left\{ \left[ \frac{(1.20)}{(2)(0.298)} + \left( 1 + \frac{(0.205)}{(4)(0.298)} \right)^2 \right]^{1/2} - \left[ 1 + \frac{(0.205)}{(4)(0.298)} \right] \right\}$$

or

$$V_{D\text{sat}} = 1.06\text{V} \quad \dots \text{smaller than } V_{D\text{sat}} \text{ of square-law theory as expected}$$

Now

$$\frac{Z \bar{\mu}_n C_0}{L} = \frac{(5 \times 10^{-3})(800)(6.90 \times 10^{-8})}{(5 \times 10^{-4})} = 5.52 \times 10^{-4} \text{ amps/V}^2$$

Finally, substituting into Eq.(17.28) gives  $I_{D\text{sat}}$  if  $V_D = V_{D\text{sat}}$ . Thus

$$I_{D\text{sat}} = (5.52 \times 10^{-4}) \left\{ (1.20)(1.06) - \frac{(1.06)^2}{2} - \frac{4}{3} (0.205)(0.298) \left[ \left( 1 + \frac{(1.06)}{(2)(0.298)} \right)^{3/2} - \left( 1 + \frac{(3)(1.06)}{(4)(0.298)} \right) \right] \right\}$$

$$I_{D\text{sat}} = 0.349\text{mA} \quad \Leftarrow \text{bulk charge result (smaller than the square-law result as expected)}$$

(d) Clearly here the device is biased below pinch-off. From Table 17.1 we note that both the square-law and bulk-charge theories reduce to the same result if  $V_D = 0$ .

$$g_d = \frac{Z \bar{\mu}_n C_0}{L} (V_G - V_T) = (5.52 \times 10^{-4})(2 - 0.8) = 0.662\text{mS}$$

(e) In the square-law theory,  $V_{D\text{sat}} = V_G - V_T$ . Thus  $V_{D\text{sat}} = 1.20\text{V}$  and  $V_D = 2\text{V}$ . Since  $V_D > V_{D\text{sat}}$ , the device is saturation (above-pinch-off) biased, and from Table 17.1

$$g_m = \frac{Z \bar{\mu}_n C_0}{L} (V_G - V_T) = 0.662\text{mS} \quad \dots \text{same as } g_d \text{ of part (d)}$$

(f) In part (c) we calculated the bulk-charge  $V_{D\text{sat}} = 1.06\text{V}$ . Since  $V_D > V_{D\text{sat}}$ , the device is above-pinch-off biased, and from Table 17.1

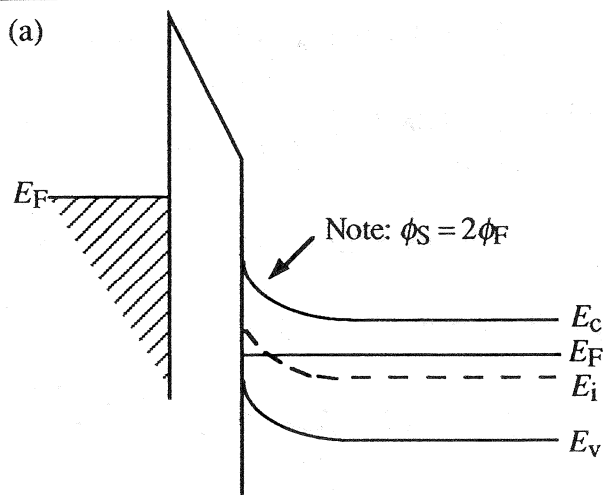
$$g_m = \frac{Z \bar{\mu}_n C_0}{L} V_{D\text{sat}} = (5.52 \times 10^{-4})(1.06) = 0.585\text{mS}$$

(g) For the applied  $V_G = 2\text{V}$ ,  $V_{D\text{sat}} = 1.20\text{V}$  in the square-law theory and  $V_{D\text{sat}} = 1.06\text{V}$  in the bulk-charge theory. Since in either case  $V_D < V_{D\text{sat}}$ , we can utilize the second form of Eq.(17.37).

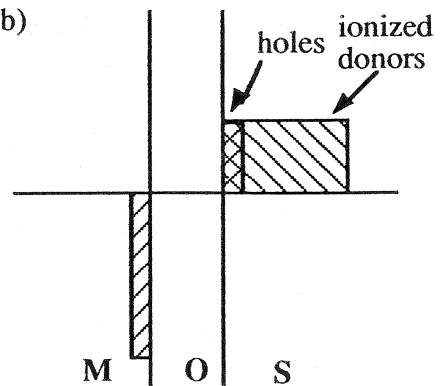
$$f_{\max} = \frac{\bar{\mu}_n V_D}{2\pi L^2} = \frac{(800)(1)}{(2\pi)(5 \times 10^{-4})^2} = 509\text{MHz}$$

17.3

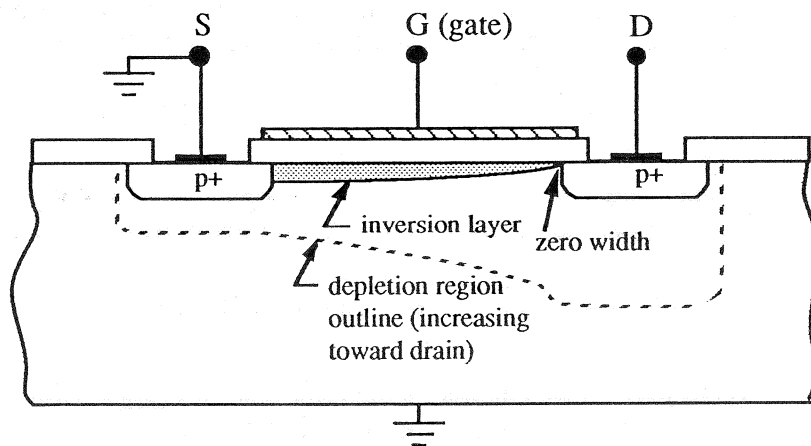
(a)



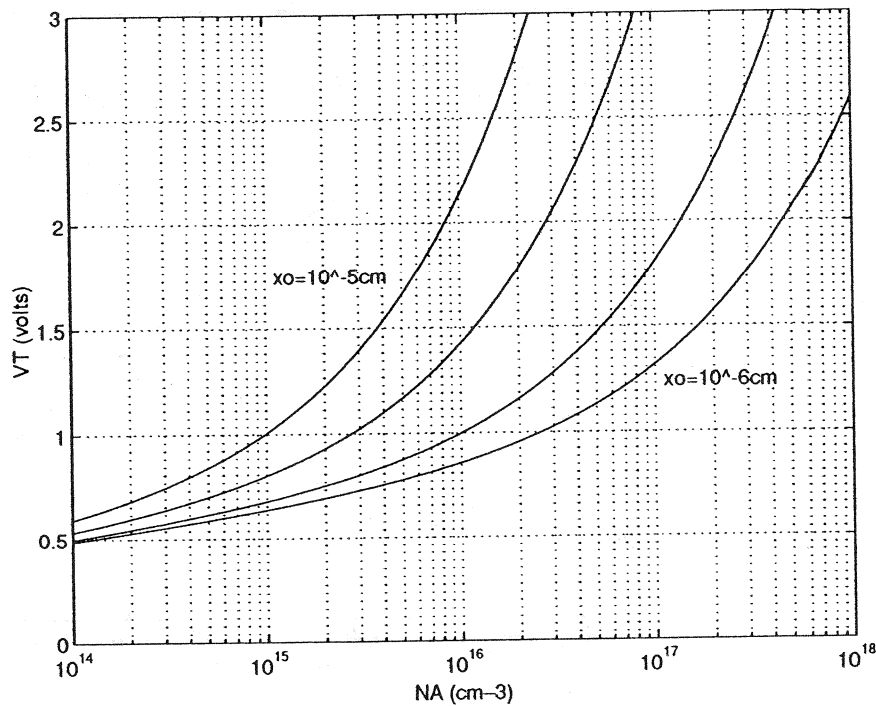
(b)



(c)



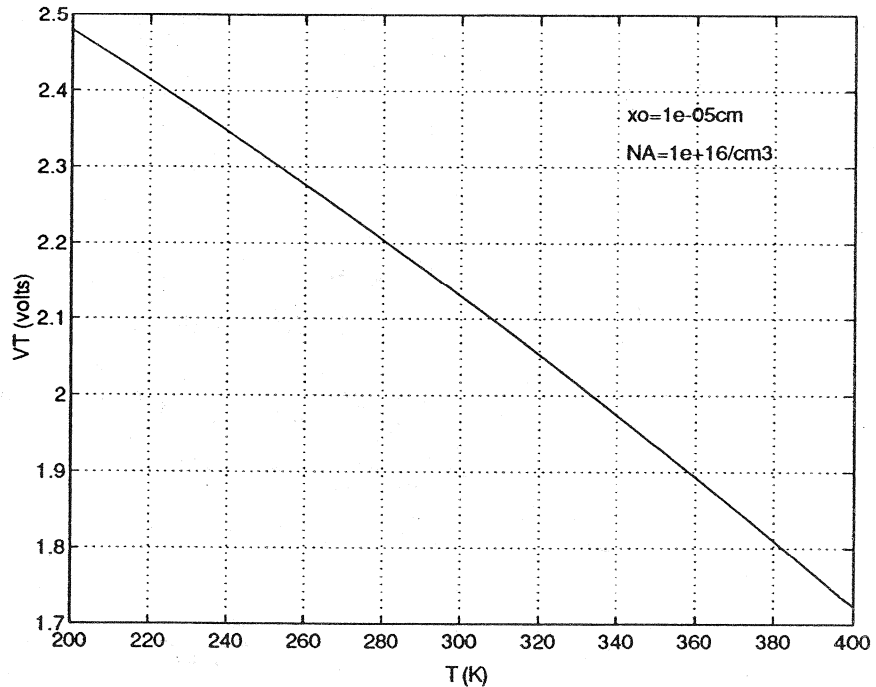
17.4



MATLAB program script...

```
%Problem 17.4...VT vs. NA with xo as a parameter
%Initialization
clear; close
%Constants and Parameters
q=1.6e-19; e0=8.85e-14;
kT=0.0259; ni=1.0e10;
KS=11.8; KO=3.9;
NA=logspace(14,18);
xo=[1.0e-6 2.0e-6 5.0e-6 1.0e-5];
%VT Computation
øF=kT.*log(NA./ni);
for i=1:4,
    xoo=xo(i);
    VT= 2 .*øF+((KS*xoo)/KO).*sqrt((4 .*q.*NA.*øF)./(KS*e0));
    semilogx(NA,VT); axis([1.0e14,1.0e18,0,3])
    hold on
end
grid; xlabel('NA (cm-3)'); ylabel('VT (volts)')
text(1.1e17,1.25,'xo=10-6cm'); text(1.1e15,1.75,'xo=10-5cm');
hold off
```

17.5



The threshold voltage is seen to decrease in an almost linear fashion with increasing  $T$ .

MATLAB program script...

```
%Problem 17.5...VT vs. T
%Initialization
clear; close
%Constants and Parameters
q=1.6e-19; k=8.617e-5;
e0=8.85e-14;
KS=11.8; KO=3.9;
T=linspace(200,400);
kT=k.*T;
xo=input('Input the oxide thickness in cm, xo = ');
NA=input('Input the Si doping in cm^-3, NA = ');
%ni versus T
%Constants
A=2.510e19;
Eex=0.0074;
%Band Gap vs. T
EG0=1.17;
```

```

a=4.730e-4;
b=636;
EG=EG0-a.* (T.^2) ./ (T+b);
%Effective mass ratio (mnr=mn*/m0, mpr=mp*/m0)
mnr=1.028 + (6.11e-4).*T - (3.09e-7).*T.^2;
mpr=0.610 + (7.83e-4).*T - (4.46e-7).*T.^2;
%Computation of ni
ni=A.*((T./300).^1.5).*((mnr.*mpr).^(0.75)).*exp(-(EG-Eex)./(2
.*k.*T));
%VT Computation
øF=kT.*log(NA./ni);
VT= 2 .*øF+((KS*xo)/KO).*sqrt((4 .*q.*NA.*øF)./(KS*e0));
plot(T,VT); grid
xlabel('T (K)');
ylabel('VT (volts)')
text(342,2.37,['xo=',num2str(xo),'cm'])
text(342,2.32,['NA=',num2str(NA),'/cm^3'])

```

### 17.6

Differentiating Eq.(17.17) with respect to  $V_D$  with  $V_G$  held constant yields

$$\frac{\partial I_D}{\partial V_D} \Big|_{V_G=\text{constant}} = \frac{Z \bar{\mu}_n C_0}{L} (V_G - V_T - V_D) \stackrel{\text{set}}{=} 0$$

Solving we obtain

$$V_G - V_T - V_{D\text{sat}} = 0$$

or

$$V_{D\text{sat}} = V_G - V_T$$

### 17.7

$$J_P \equiv J_{Py} \equiv q\mu_p p \mathcal{E}_y \equiv -q\mu_p p \frac{d\phi}{dy} \quad (17.7')$$

$$I_D = \int \int J_{Py} dx dz = Z \int_0^{x_c(y)} J_{Py} dx \quad (17.8a')$$

(Note that  $I_D$  is defined to be positive flowing *out-of* the drain.)

$$I_D = \left( -Z \frac{d\phi}{dy} \right) \left( q \int_0^{x_c(y)} \mu_p(x,y) p(x,y) dx \right) \quad (17.8b')$$

$$Q_P(y) = q \int_0^{x_c(y)} p(x,y) dx \quad (17.3')$$

$$\bar{\mu}_p = \frac{q}{Q_P(y)} \int_0^{x_c(y)} \mu_p(x,y) p(x,y) dx \quad (17.4')$$

$$I_D = -Z \bar{\mu}_p Q_P \frac{d\phi}{dy} \quad (17.9')$$

$$\int_0^L I_D dy = I_D L = -Z \int_0^{V_D} \bar{\mu}_p Q_P d\phi \quad (17.10')$$

$$I_D = -\frac{Z \bar{\mu}_p}{L} \int_0^{V_D} Q_P d\phi \quad (\text{NOTE: } V_D \leq 0, \text{ which gives } I_D \text{ the correct sign.}) \quad (17.11')$$

$$\Delta Q_{\text{gate}} = -\Delta Q_{\text{semi}} \equiv -Q_P \quad (17.12')$$

$$\Delta Q_{\text{gate}} = C_o(V_G - V_T) \quad (17.13')$$

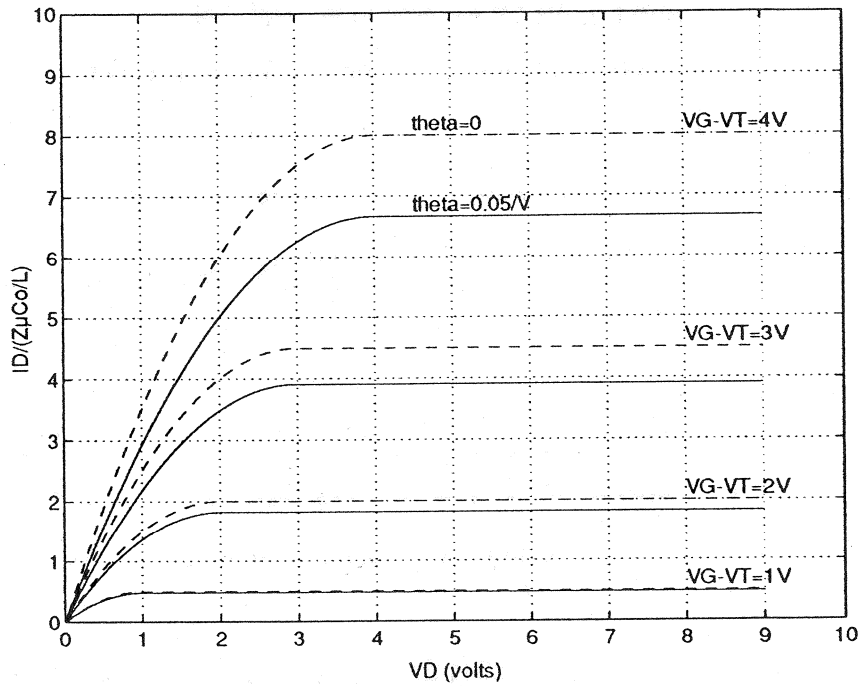
$$Q_P \equiv -C_o(V_G - V_T) \quad (17.14')$$

$$Q_P(y) \equiv -C_o(V_G - V_T - \phi) \quad (17.16')$$

$$I_D = \frac{Z \bar{\mu}_p C_o}{L} [(V_G - V_T)V_D - V_D^2/2] \quad \dots 0 \geq V_D \geq V_{D\text{sat}} \quad \dots V_G \leq V_T \quad (17.17')$$

Note that Eq.(17.17') is the same as the text Eq.(17.17) except  $\bar{\mu}_n \rightarrow \bar{\mu}_p$  and there is a polarity reversal in the inequalities specifying the range of valid  $V_D$  and  $V_G$  values.

17.8



MATLAB program script...

```
%Problem 17.8...effective mobility per Eq. (17.5)
%ID-VD Characteristics /// Square-Law Theory

%Initialization
clear; close

%Let VGT = VG - VT;
for VGT=4:-1:1,
    %Primary Computation
    VD=linspace(0,VGT);
    ID0=VGT.*VD-VD.*VD./2;
    ID0sat=VGT*VGT/2;
    ID0=[ID0, ID0sat];
    ID1=(VGT.*VD-VD.*VD./2)./(1+0.05*VGT);
    ID1sat=(VGT*VGT/2)./(1+0.05*VGT);
    ID1=[ID1, ID1sat];
    VD=[VD, 9];
    %Plotting and Labeling
    if VGT==4,
        plot(VD, ID0, 'g--', VD, ID1, 'r');
        grid
        axis([0 10 0 10])
        xlabel('VD (volts)');
        ylabel('ID/(ZμCo/L)');
    else,
        plot(VD, ID0, 'g--', VD, ID1, 'r');
        %Labeling of VG-VT curves < 4
        if VGT==3,
            text(8, ID0sat+0.2, 'VG-VT=4V');
            text(4.5, ID0sat+0.2, 'theta=0');
            text(4.5, ID1sat+0.2, 'theta=0.05/V');
            hold on
        elseif VGT==2,
            text(8, ID0sat+0.2, 'VG-VT=3V');
        elseif VGT==1,
            text(8, ID0sat+0.2, 'VG-VT=2V');
        end
    end
end
```

### 17.9

(a) From Fig. P17.9 we note in general that

$$V_G = V_D + V_B \quad \text{or} \quad V_D = V_G - V_B$$

In the square-law formulation  $V_{Dsat} = V_G - V_T$ . If  $V_B = V_T/2$ , then  $V_D = V_G - V_T/2 > V_{Dsat}$  and the MOSFET is *always biased into saturation*. Noting  $I_D = 0$  if  $V_G < V_T$  or  $V_D < V_T/2$ , and using Eq.(17.22), we conclude

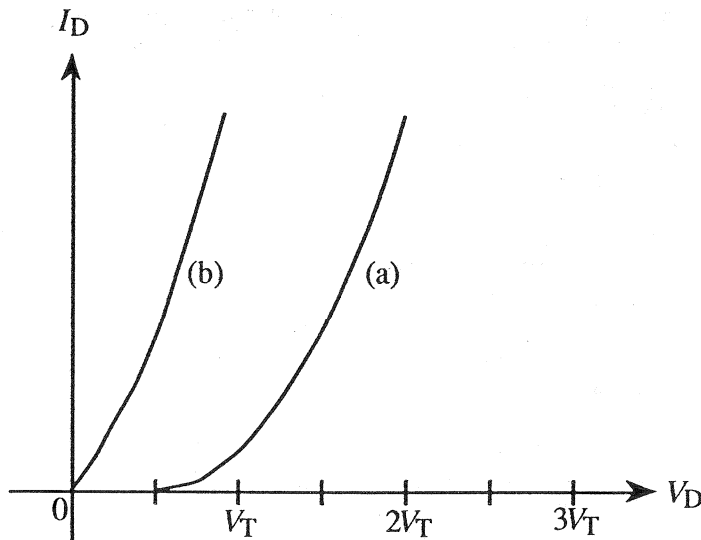
$$I_D = \frac{Z\bar{\mu}_n C_o}{2L} (V_G - V_T)^2 = \frac{Z\bar{\mu}_n C_o}{2L} (V_D - V_T/2)^2 \quad \dots V_D > V_T/2$$

and

$$I_D = 0 \quad \dots V_D < V_T/2$$

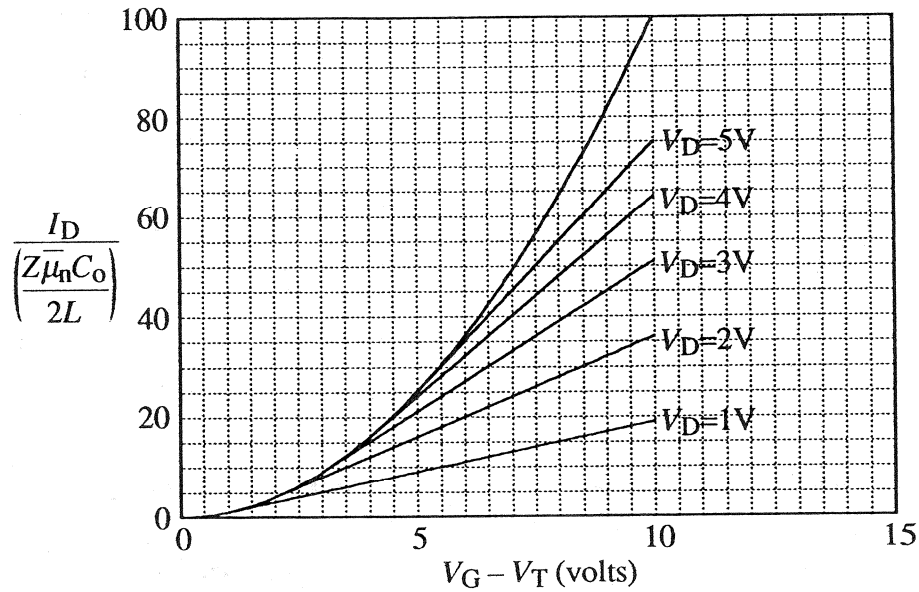
(b) If  $V_B = 2V_T$ , then  $V_D = V_G - 2V_T < V_G - V_T = V_{Dsat}$  and the MOSFET is always biased in the linear region of operation. The device turns on for  $V_G > V_T$  or  $V_D > -V_T$  and is therefore on for all  $V_D \geq 0$ . Using Eq.(17.17) we obtain

$$\begin{aligned} I_D &= \frac{Z\bar{\mu}_n C_o}{L} [(V_G - V_T)V_D - V_D^2/2] = \frac{Z\bar{\mu}_n C_o}{L} [(V_D + V_T)V_D - V_D^2/2] \\ &= \frac{Z\bar{\mu}_n C_o}{L} (V_D^2/2 + V_T V_D) = \frac{Z\bar{\mu}_n C_o}{2L} [(V_D + V_T)^2 - V_T^2] \quad \dots V_D \geq 0 \end{aligned}$$



Note that both curves have the same general shape; the part (b) curve is simply shifted to the left and displaced downward.

17.10



The above  $I_D$  versus  $V_g - V_T$  characteristics were arrived at as follows:

- (i) Suppose we systematically increase  $V_g - V_T$  from zero with  $V_D$  held constant. Initially  $V_D$  is greater than  $V_g - V_T$  and the device is in saturation. (Use is being made of the square-law theory.) Thus initially

$$I_D = I_{D\text{sat}} = \frac{Z\bar{\mu}_n C_0}{2L} (V_g - V_T)^2$$

and we conclude  $I_D$  varies as the square of  $V_g - V_T$  if  $V_g - V_T < V_D$ .

- (ii) When  $V_g - V_T$  becomes equal to  $V_D$ , the device moves into the linear region of operation. In the linear region

$$I_D = \frac{Z\bar{\mu}_n C_0}{L} [(V_g - V_T)V_D - V_D^2/2]$$

and  $I_D$  varies linearly with  $V_g - V_T$ .

- (iii) With increased  $V_D$ , one stays on the voltage-squared part of the curve for a longer and longer range of voltages. Once  $V_g - V_T > V_D$ , a linear region whose slope increases with increasing  $V_D$  is observed.

17.11

(a)

$$J_N = J_{Nr} = q\mu_n n \mathcal{E}_r = -q\mu_n n \frac{d\phi}{dr} \quad (17.7')$$

If the z-direction points from the surface into the bulk,

$$\begin{aligned} I_D &= - \int \int J_{Nr} dz d\theta = - \int_0^{z_c} 2\pi r J_{Nr} dz \quad \dots z_c \text{ is the channel depth} \\ &= \left( -2\pi r \frac{d\phi}{dr} \right) \left( -q \int_0^{z_c} \mu_n n dz \right) \end{aligned} \quad (17.8')$$

Since the second quantity enclosed in parentheses above is just  $\bar{\mu}_n Q_N$ , we can write

$$I_D = -2\pi r \bar{\mu}_n Q_N \frac{d\phi}{dr} \quad (17.9')$$

Integrating over the  $r$ -width of the channel,

$$\int_{r_1}^{r_2} \frac{I_D}{2\pi r} dr = \frac{I_D}{2\pi} \int_{r_1}^{r_2} \frac{dr}{r} = \frac{I_D}{2\pi} \ln(r_2/r_1) = -\bar{\mu}_n \int_0^{V_D} Q_N d\phi \quad (17.10')$$

and

$$I_D = -\frac{2\pi}{\ln(r_2/r_1)} \bar{\mu}_n \int_0^{V_D} Q_N d\phi \quad (17.11')$$

The change in geometry does not modify Eqs.(17.12) through (17.16). Thus

$$Q_N = -C_0(V_G - V_T - \phi)$$

and

$I_D = \frac{2\pi}{\ln(r_2/r_1)} \bar{\mu}_n C_0 [(V_G - V_T)V_D - V_D^2/2]$

(b) Setting  $r_2 = r_1 + L$ , we can write

$$\ln(r_2/r_1) = \ln\left(\frac{r_1+L}{r_1}\right) = \ln(1 + L/r_1)$$

If  $L/r_1 \ll 1$

$$\ln(1 + L/r_1) = (L/r_1) - \frac{1}{2}(L/r_1)^2 + \dots \approx L/r_1$$

Thus

$$\frac{2\pi}{\ln(r_2/r_1)} \rightarrow \frac{2\pi r_1}{L} = \frac{Z}{L}$$

and one obtains the usual  $I_D - V_D$  result.

### 17.12

(a) Utilizing the Eq. (17.22) square-law result,

$$I_{D\text{sat}} = \frac{Z \bar{\mu}_n C_0}{2L} (V_G - V_T)^2$$

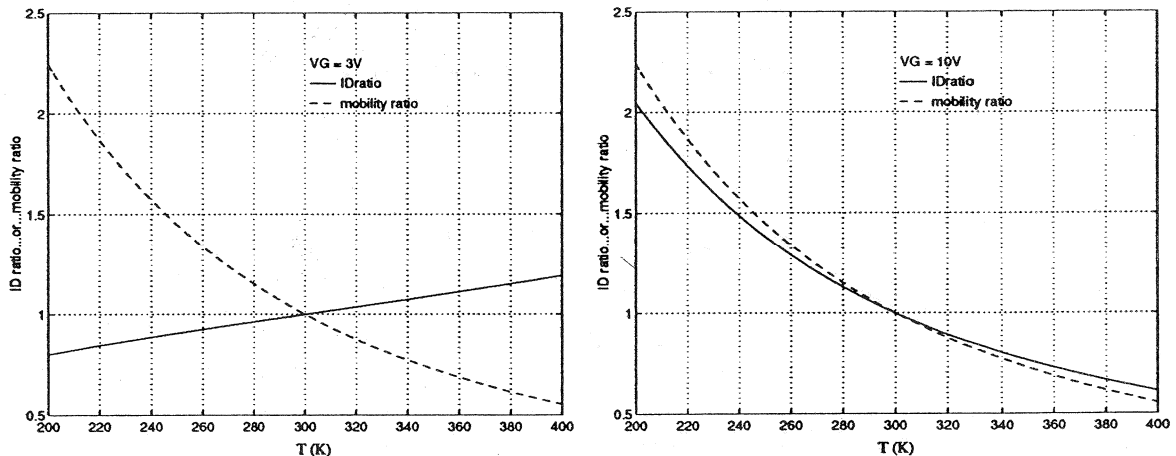
and

$$\frac{I_{D\text{sat}}(T)}{I_{D\text{sat}}(300\text{K})} = \frac{\bar{\mu}_n(T)}{\bar{\mu}_n(300\text{K})} \left[ \frac{V_G - V_T(T)}{V_G - V_T(300\text{K})} \right]^2$$

Assuming  $\bar{\mu}_n$  has the same temperature dependence as  $\mu_n$  (and neglecting any differences in the effective mobility as a function of temperature that may result from operating at slightly different  $V_G - V_T$  points), we obtain the computational expression

$$\frac{I_{D\text{sat}}(T)}{I_{D\text{sat}}(300\text{K})} = \frac{\mu_n(T)}{\mu_n(300\text{K})} \left[ \frac{V_G - V_T(T)}{V_G - V_T(300\text{K})} \right]^2$$

(b)



The results here are rather interesting. If the device is  $V_G$  biased far above turn-on, then the  $V_G - V_T$  term in the part (a) expression becomes approximately unity and the characteristics exhibit essentially the same temperature dependence as the mobility — generally decreasing with temperature. However, the threshold voltage change with temperature is sufficiently large that a totally different  $I_{Dsat}$  temperature-dependence is observed if the chosen  $V_G$  is only slightly greater than  $V_T$ . — The change in the degree of surface inversion becomes more important than the change in mobility.

It should be noted that in performing the computations the  $\mu_n$  value in  $N_A$ -doped Si was assumed to be the same as that in equivalently  $N_D$ -doped Si.

MATLAB program script...

```
%Problem 17.12... IDsat(T)/IDsat(300K) vs. T
%Initialization
clear; close
%Constants and Parameters
q=1.6e-19;
k=8.617e-5;
KS=11.8;
KO=3.9;
e0=8.85e-14;
T=linspace(200,400,101); %Note: T(51)=300K;
kT=k.*T;
xo=1.0e-5;
NA=1.0e16;
VG=input('Input gate voltage in volts, VG = ');
```

```

%ni versus T
%Constants
A=2.510e19;
Eex=0.0074;
%Band Gap vs. T
EG0=1.17;
a=4.730e-4;
b=636;
EG=EG0-a.* (T.^2) ./ (T+b);
%Effective mass ratio (mnr=mn*/m0, mp*/m0)
mnr=1.028 + (6.11e-4).*T - (3.09e-7).*T.^2;
mpr=0.610 + (7.83e-4).*T - (4.46e-7).*T.^2;
%Computation of ni
ni=A.*((T./300).^1.5).*((mnr.*mpr).^(0.75)).*exp(-(EG-Eex)./(2.*k.*T));
%VT Computation
øF=kT.*log(NA./ni);
VT= 2 .*øF+((KS*xo)/KO).*sqrt((4 .*q.*NA.*øF)./(KS*e0));
%Mobility Computation
%Fit Parameters
NDref=1.3e17; TNref=2.4;
µnmin=92; Tµmin=-0.57;
µn0=1268; Tµn0=-2.33;
an=0.91; Ta=-0.146;
%Mobility Calculation
NDrefT=NDref*(T./300).^TNref;
µnmint=µnmin.* (T./300).^Tµmin;
µn0T=µn0.* (T./300).^Tµn0;
anT=an.* (T./300).^Ta;
µn=µnmint+µn0T./(1+(NA./NDrefT).^anT);
%IDsat Computation and Plot
%IDratio=IDsat(T)/IDsat(300K) and µnratio=µn(T)/µn(300K);
µnratio=µn/µn(51);
IDratio=µnratio.*((VG-VT)/(VG-VT(51))).^2;
%Plotting result
plot(T, IDratio, T, µnratio, 'g--'); grid
xlabel('T (K)'); ylabel('ID ratio...or...mobility ratio')
%Key
text(302, 2.25, ['VG = ', num2str(VG), 'V'])
x=[302, 312]; y1=[2.15, 2.15]; y2=[2.05, 2.05]
hold on; plot(x, y1, x, y2, 'g--')
text(314, 2.15, 'IDratio')
text(314, 2.05, 'mobility ratio')
hold off

```

### 17.13

With  $R_S$  and  $R_D$  taken into account, the channel voltages at  $y=0$  and  $y=L$  become  $V(0) = I_D R_S$  and  $V(L) = V_D - I_D R_D$ . Inserting the revised voltage limits into Eq. (17.10), and likewise modifying Eq. (17.11), we obtain

$$I_D = -\frac{Z\bar{\mu}_n}{L} \int_{I_D R_S}^{V_D - I_D R_D} Q_N d\phi \quad (17.11')$$

where in the square-law theory

$$Q_N = -C_0(V_G - V_T - \phi) \quad (17.16)$$

Substituting the Eq. (17.16) expression for  $Q_N$  into Eq. (17.11') and integrating yields

$$I_D = \frac{Z\bar{\mu}_n C_0}{L} \left\{ (V_G - V_T)[V_D - I_D(R_S + R_D)] - \frac{(V_D - I_D R_D)^2}{2} + \frac{(I_D R_S)^2}{2} \right\}$$

or

$$I_D = \frac{Z\bar{\mu}_n C_0}{L} \left\{ (V_G - I_D R_S - V_T)[V_D - I_D(R_S + R_D)] - \frac{[V_D - I_D(R_S + R_D)]^2}{2} \right\} \quad (17.17')$$

Turning next to the modification of Eq. (17.21), we note that when  $V_D = V_{Dsat}$ ,  $Q_N(L) = 0$ ,  $\phi(L) = V_{Dsat} - I_{Dsat} R_D$ , and from Eq. (17.16),

$$0 = -C_0[V_G - V_T - (V_{Dsat} - I_{Dsat} R_D)]$$

or

$$V_{Dsat} - I_{Dsat} R_D = V_G - V_T \quad (17.21')$$

Finally, setting  $V_D = V_{Dsat}$  and  $I_D = I_{Dsat}$  in Eq. (17.17'), and simplifying the result using Eq. (17.21'), one obtains

$$I_{Dsat} = \frac{Z\bar{\mu}_n C_0}{2L} (V_G - I_{Dsat} R_S - V_T)^2 \quad (17.22')$$

Note that replacing  $V_D$  by  $V_D - I_D(R_S + R_D)$  and  $V_G$  by  $V_G - I_D R_S$  in Eqs. (17.17), (17.21), and (17.22) does indeed yield Eqs. (17.17'), (17.21'), and (17.22').

**17.14**

Following the text suggestion, we set  $Q_N(L) = 0$  in Eq.(17.27) when  $V(L) = V_D \rightarrow V_{Dsat}$ .

$$Q_N(L) = -C_0 [V_G - V_T - V_{Dsat} - V_W (\sqrt{1 + V_{Dsat}/2\phi_F} - 1)] \leq 0$$

or

$$V_G - V_T - V_{Dsat} - V_W (\sqrt{1 + V_{Dsat}/2\phi_F} - 1) = 0$$

Manipulating the preceding into a form which can be solved for  $V_{Dsat}$  we note

$$V_G - V_T + V_W - V_{Dsat} = V_W \sqrt{1 + V_{Dsat}/2\phi_F}$$

Squaring

$$V_{Dsat}^2 - 2(V_G - V_T + V_W)V_{Dsat} + (V_G - V_T + V_W)^2 = V_W^2 + V_W^2 V_{Dsat}/2\phi_F$$

or

$$V_{Dsat}^2 - \left[ \frac{V_W^2}{2\phi_F} + 2(V_G - V_T + V_W) \right] V_{Dsat} + (V_G - V_T + V_W)^2 - V_W^2 = 0$$

Solving the quadratic equation gives

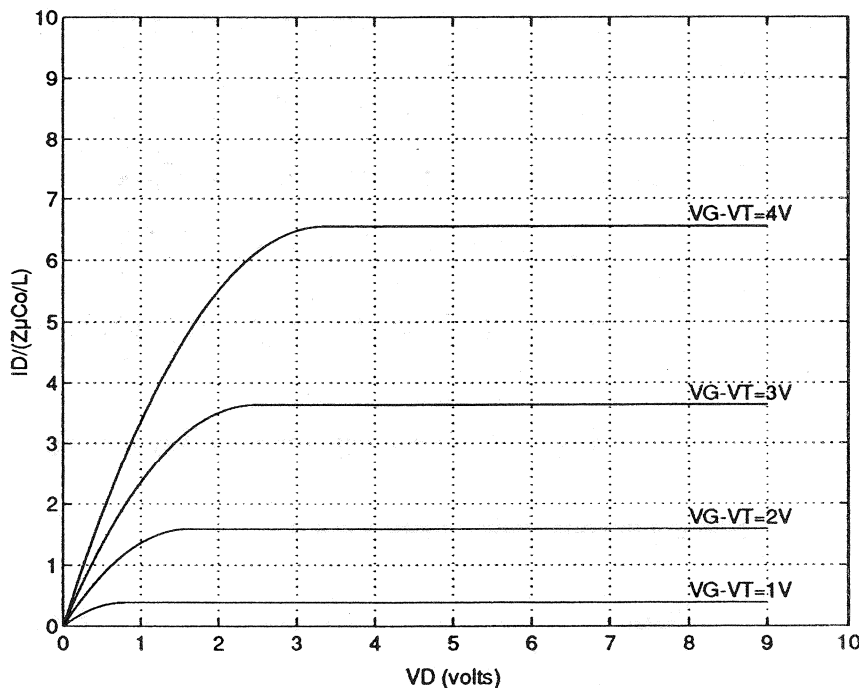
$$\begin{aligned} V_{Dsat} &= \frac{V_W^2}{4\phi_F} + (V_G - V_T + V_W) \pm \left\{ \left[ \frac{V_W^2}{4\phi_F} + (V_G - V_T + V_W) \right]^2 - (V_G - V_T + V_W)^2 + V_W^2 \right\}^{1/2} \\ &= V_G - V_T + V_W \left( 1 + \frac{V_W}{4\phi_F} \right) \pm \left[ \left( \frac{V_W^2}{4\phi_F} \right)^2 + 2 \frac{V_W^2}{4\phi_F} (V_G - V_T + V_W) + V_W^2 \right]^{1/2} \\ &= V_G - V_T + V_W \left( 1 + \frac{V_W}{4\phi_F} \right) \pm V_W \left[ \left( \frac{V_W}{4\phi_F} \right)^2 + 2 \frac{V_W}{4\phi_F} + \frac{V_G - V_T}{2\phi_F} \right]^{1/2} \\ &= V_G - V_T + V_W \left( 1 + \frac{V_W}{4\phi_F} \right) \pm V_W \left[ \frac{V_G - V_T}{2\phi_F} + \left( 1 + \frac{V_W}{4\phi_F} \right)^2 \right]^{1/2} \end{aligned}$$

Note that if the (+) root is chosen  $V_{Dsat}(+root) > V_G - V_T$ . Choosing the (-) root on the other hand yields  $V_{Dsat} < (V_G - V_T)$ . As discussed in the text, in the bulk-charge formulation, part of the change in the gate charge goes into balancing changes in the depletion-layer charge. Thus, there is less inversion-layer charge at a given  $V_G$  relative to the square-law formulation. Consequently  $V_{Dsat}$  occurs at a lower voltage than  $V_G - V_T$ . We choose the (-) root and slightly rearrange our result to finally obtain Eq.(17.29).

$$V_{Dsat} = V_G - V_T - V_W \left\{ \left[ \frac{V_G - V_T}{2\phi_F} + \left( 1 + \frac{V_W}{4\phi_F} \right)^2 \right]^{1/2} - \left( 1 + \frac{V_W}{4\phi_F} \right) \right\}$$

### 17.15

The required computer program and a sample output is reproduced below.



**MATLAB program script...**

```
%ID-VD Characteristics /// Bulk-Charge Theory
%Initialization
clear; close
%Constants and Parameters
q=1.60e-19;
e0=8.85e-14;
kT=0.0259;
ni=1.0e10;
KS=11.8;
KO=3.9;
NA=input('input the doping in cm-3, NA = ');
xo=input('input the oxide thickness in cm, xo = ');
%Computed Parameters
øF=kT*log(NA/ni);
WT=sqrt((4*KS*e0*øF)/(q*NA));
Co=KO*e0/xo;
VW=q*NA*WT/Co;
```

```

%ID-VD Computation and Plot
for VGT=4:-1:1,    %VGT = VG - VT;
%Computation
A=VGT/(2*øF);   B=1+VW/(4*øF);
VDSat=VGT-VW*(sqrt(A+B^2)-B);
VD=linspace(0,VDSat);
ID1=VGT.*VD-VD.*VD/2;
VDF=VD./(2*øF);
ID2=(4/3)*VW*øF.*((1+VDF).^1.5-(1+1.5*VDF));
ID=ID1-ID2;
IDSat1=VGT.*VDSat-VDSat.*VDSat/2;
VDFsat=VDSat./(2*øF);
IDSat2=(4/3)*VW*øF.*((1+VDFsat).^1.5-(1+1.5.*VDFsat));
IDSat=IDSat1-IDSat2;
VD=[VD,9];
ID=[ID,IDSat];
%Plotting and Primary Labeling
if VGT==4,
plot(VD,ID); grid;
axis([0 10 0 10]);
xlabel('VD (volts)'); ylabel('ID/(ZµCo/L)');
text(8,IDSat+0.2,'VG-VT=4V');
hold on
else,
plot(VD,ID);
%The following 'if' labels VG-VT curves < 4
if VGT==3,
text(8,IDSat+0.2,'VG-VT=3V');
elseif VGT==2,
text(8,IDSat+0.2,'VG-VT=2V');
else,
text(8,IDSat+0.2,'VG-VT=1V');
end
end
end
hold off

```

17.16 (Solution not supplied.)

17.17 (Solution merely involves straightforward mathematical manipulations.)

17.18

(a) Given  $V_D = 0$ , then  $\phi(y) = 0$  and

$$Q_N(\text{all } y) = -C_0(V_G - V_T) = \frac{K_O \epsilon_0}{x_0} (V_G - V_T) = \frac{(3.9)(8.85 \times 10^{-14})(2)}{5 \times 10^{-6}}$$
$$= -1.38 \times 10^{-7} \text{ coul/cm}^2$$

(b)  $g_d|_{V_D=0} = \frac{Z\bar{\mu}_n C_0}{L} (V_G - V_T)$  ...making use of Table 17.1

$$= -\frac{Z\bar{\mu}_n Q_N}{L} = \frac{(70 \times 10^{-4})(550)(1.38 \times 10^{-7})}{7 \times 10^{-4}}$$
$$= 7.59 \times 10^{-4} \text{ S}$$

17.19

$|V_T|$  is the same in ideal *p*-channel and *n*-channel MOSFETs with the same  $x_0$  and bulk doping concentration. Thus, with the devices also equivalently biased, one concludes from Table 17.1 that the same  $g_m$ 's will result if

$$\frac{Z_p}{L_p} \bar{\mu}_p = \frac{Z_n}{L_n} \bar{\mu}_n$$

where the subscripts indicate the channel type. This same conclusion is reached whether one uses the square-law theory or bulk-charge theory and whether the devices are biased below or above pinch-off.

Next, examining the first form of Eq.(17.37), we again quite generally conclude that  $C_O(p\text{-channel})$  must equal  $C_O(n\text{-channel})$  for the  $f_{\max}$  values to be the same. Since  $C_O = K_O \epsilon_0 Z L / x_0$ , we therefore require

$$Z_p L_p = Z_n L_n$$

Substituting  $Z_p$  from the first relationship into the second relationship and simplifying, one obtains

$$L_p = \sqrt{\frac{\mu_p}{\mu_n}} L_n$$

and

$$Z_p = \frac{Z_n L_n}{L_p} = \sqrt{\frac{\mu_n}{\mu_p}} Z_n$$

The mobilities deduced from Fig. 3.5a yield  $\bar{\mu}_n = \mu_n/2 = 673 \text{ cm}^2/\text{V-sec}$  and  $\bar{\mu}_p = \mu_p/2 = 229 \text{ cm}^2/\text{V-sec}$ . Thus the required *p*-channel device dimensions are

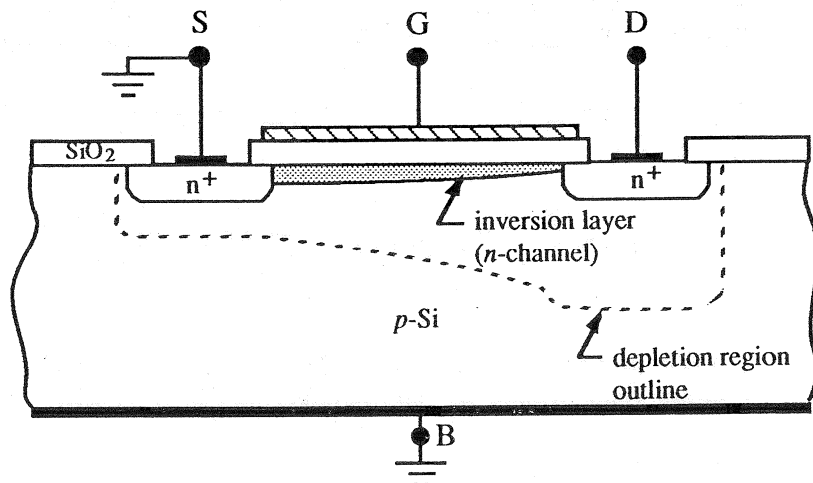
$$Z = \sqrt{673/229} \times 50 = 85.7 \mu\text{m}$$

and

$$L = \sqrt{229/673} \times 5 = 2.92 \mu\text{m}$$

### 17.20

- (a) Since the applied  $V_D$  is greater than zero, we infer the given MOSFET is an *n*-channel device. Also, at point (1) the MOSFET is biased below saturation. Thus the channel narrows near the drain but is not pinched-off.



(b) In the square-law theory  $V_{Dsat} = V_G - V_T$ . Thus

$$V_G = V_{Dsat} + V_T = 6V$$

(c) The point (2) bias corresponds to the pinch-off point. At the pinch-off point, and based on the square-law theory, the charge in the MOSFET channel goes to zero at the drain.

$$Q_N(L) = 0$$

(d) With  $V_D = 4V$  and  $V_G - V_T = 3V$ ,  $V_D > V_{Dsat} = V_G - V_T$ . Consequently, for the readjusted gate voltage, the MOSFET is being operated in the saturation region. Since  $I_{Dsat} \propto (V_G - V_T)^2$ , it follows that

$$\frac{I_{Dsat1}}{I_{Dsat2}} = \left( \frac{V_{G1} - V_T}{V_{G2} - V_T} \right)^2$$

Here identifying the desired  $I_D = I_{Dsat1}$  ( $V_{G1} - V_T = 3V$ ) and  $I_{Dsat2} = 10^{-3}A$  ( $V_{G2} - V_T = 5V$ ) from the given characteristics, we conclude

$$I_D = (10^{-3}) \left( \frac{3}{5} \right)^2 = 3.6 \times 10^{-4} A$$

(e) By definition  $g_d = \partial I_D / \partial V_D$  with  $V_G$  held constant. Inspecting the given characteristic, we conclude  $\partial I_D / \partial V_D = 0$  at bias point (3) and  $g_d = 0$ . Alternatively, in the saturation region of operation,  $I_{Dsat}$  is not a function of  $V_D$ . Consequently  $\partial I_{Dsat} / \partial V_D = 0$  and  $g_d = 0$ .

(f) At bias point (3) the MOSFET is in the above pinch-off region of operation and from Table 17.1

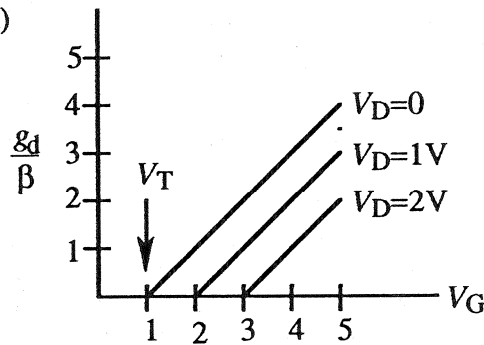
$$g_m = \frac{Z\bar{\mu}_n C_0}{L} (V_G - V_T) = \frac{2I_{Dsat}}{V_G - V_T} = \frac{(2)(10^{-3})}{5} = 4 \times 10^{-4} S$$

(g) For an  $n$ -channel ( $p$ -bulk) MOSFET, one expects a low-frequency MOS-C type characteristic similar to that displayed in Fig. 17.13(b).

17.21

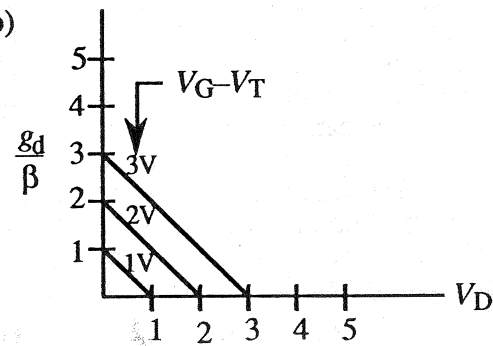
Making use of Table 17.1 and defining  $\beta = Z \bar{\mu}_n C_0 / L$ , we conclude:

(a)



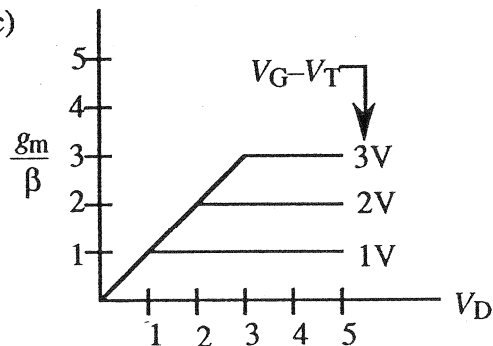
$$\frac{g_d}{\beta} = \begin{cases} 0 & \dots V_G - V_T \leq V_D \\ V_G - V_T - V_D & \dots V_G - V_T \geq V_D \end{cases}$$

(b)



$$\frac{g_d}{\beta} = \begin{cases} V_G - V_T - V_D & \dots V_D \leq V_G - V_T \\ 0 & \dots V_D \geq V_G - V_T \end{cases}$$

(c)



$$\frac{g_m}{\beta} = \begin{cases} V_D & \dots V_D \leq V_G - V_T \\ V_G - V_T & \dots V_D \geq V_G - V_T \end{cases}$$

## 17.22

There is of course no set answer to this question. The answer, however, should include some of the following points:

Externally the J-FET and MOSFET yield similar electrical characteristics and even appear similar physically, with the terminal leads being designated the source, drain, and gate.

The gate voltage in both devices determines the maximum conductance of the internal channel. However, there are major differences in the nature of the conducting channel and the substructure used to modulate the channel conductance. The J-FET channel is a narrow piece of bulk material; in the basic transistor configuration the MOSFET channel is an inversion layer which is created by the applied gate voltage. Manipulation of the channel conductance is accomplished by reverse biasing a *pn* junction in the J-FET; the MOSFET channel conductance is modulated by the bias applied to the MOS structure.

The first and even second-order quantitative analyses leading to the dc characteristics are quite similar for the two devices. Nonetheless, there are two complicating factors which enter the MOSFET analysis, factors which are not present in the J-FET analysis. First of all, carriers in a surface channel experience motion-impeding collisions with the Si surface which lower the mobility of the carriers and necessitate the introduction of an effective carrier mobility. Secondly, the carrier concentration and current density in the surface channel are strong functions of position, dropping off rapidly as one proceeds into the semiconductor bulk. For the device structure analyzed in the text, the carrier concentration and current density are of course constant across the J-FET channel.

Both first order theories give rise to an  $I_{D\text{sat}}$  which varies (or varies approximately) as the square of the gate voltage. The general ac response and first order equivalent circuits for the two devices are identical.

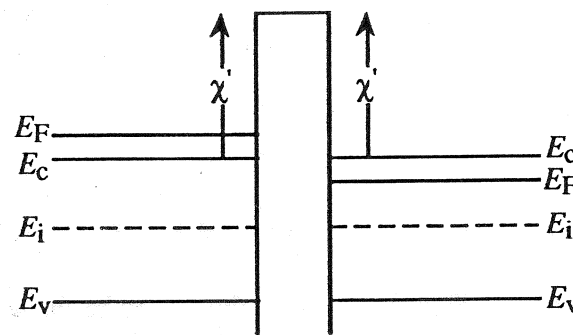
## **CHAPTER 18**

### 18.1

- (a) In theory the two quantities are numerically identical.
- (b) The MOS-C or MOSFET under test is heated to an elevated temperature and a bias is applied to the gate of the device. Typical conditions for a bias-temperature stress to detect sodium ion contamination would be  $T = 150^\circ\text{C}$ ,  $V_G$  such that  $\mathcal{E}_{\text{ox}} < 10^6 \text{ V/cm}$ , and  $t = 5$  minutes.
- (c) The fixed oxide charge is thought to be due to excess ionic silicon that has broken away from the silicon proper and is waiting to react in the vicinity of the Si-SiO<sub>2</sub> interface when the oxidation process is abruptly terminated.
- (d)  $D_{IT}$  is greatest on {111} Si surfaces, smallest on {100} Si surfaces, and the ratio of midgap states on the two surfaces is approximately 3:1.
- (e) MOS device structures exhibit both an increase in the apparent fixed charge within the oxide and an increase in the interfacial trap concentration.
- (f) In response to -BT stressing, the negative-bias instability causes a shifting of the C-V curve toward negative biases. Alkali ion contamination leads to a C-V curve voltage translation in the direction *opposite* to the applied bias.
- (g) The  $V_T = V_T' + V_{FB}$  relationship was derived assuming  $Q_{IT}$  changes little over the range of surface potentials between  $\phi_S = 0$  and  $\phi_S = 2\phi_F$ . This becomes a poor assumption if the device contains a large density of interfacial traps — if the device is unannealed, for example.
- (h) A depletion-mode transistor is a MOSFET that is "on" or conducting when  $V_G = 0$ .
- (i) The field-oxide lies outside the active region in MOS devices and integrated circuits; the gate-oxide lies directly beneath the MOS gates. The field-oxide is typically much thicker than the gate-oxide.
- (j) Simply stated, the "body effect" refers to the deep depletion condition that is created beneath the gate when the back or body of a MOSFET is reverse biased relative to the source. The body effect is utilized to adjust the threshold voltage.

18.2

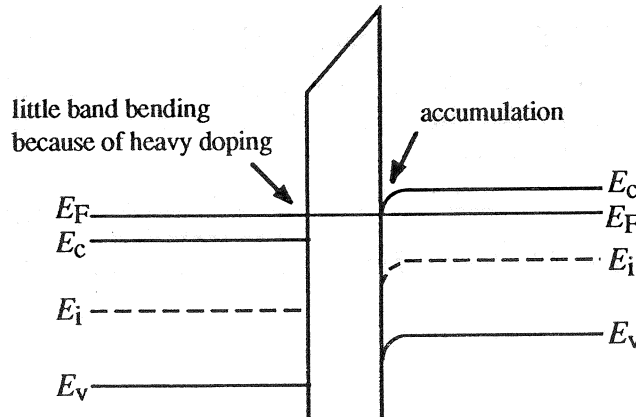
(a)



$$\begin{aligned}
 \text{(b)} \quad \phi_{MS} &= \frac{1}{q}(\Phi_M - \Phi_S) = [\chi' - (E_F - E_c)_{\text{poly-Si}}] - [\chi' + (E_c - E_F)_{\text{FB, crystalline-Si}}] \\
 &= \frac{1}{q}[(E_c - E_F)_{\text{poly-Si}} - (E_c - E_F)_{\text{FB, crystalline-Si}}] \\
 &= \mathbf{-0.4 \text{ V}}
 \end{aligned}$$

(Note that the computational equation developed here is the same as Eq. 18.24.)

(c) [Accumulation] biased. When  $V_G = 0$  the polysilicon side of the part (a) diagram is lowered, yielding



### 18.3

In general

$$\phi_{MS} = \frac{1}{q} [\Phi_M' - \chi' - (E_c - E_F)_{FB}]$$

where

$$\Phi_M' - \chi' = \begin{cases} -0.03\text{eV} & \dots \text{Al} \\ -0.18\text{eV} & \dots n^+ \text{ poly} \\ (E_0 - E_F)_{p^+ \text{ poly}} - \chi' = (\chi' + E_G) - \chi' = E_G = 1.12\text{eV} & \dots p^+ \text{ poly} \end{cases}$$

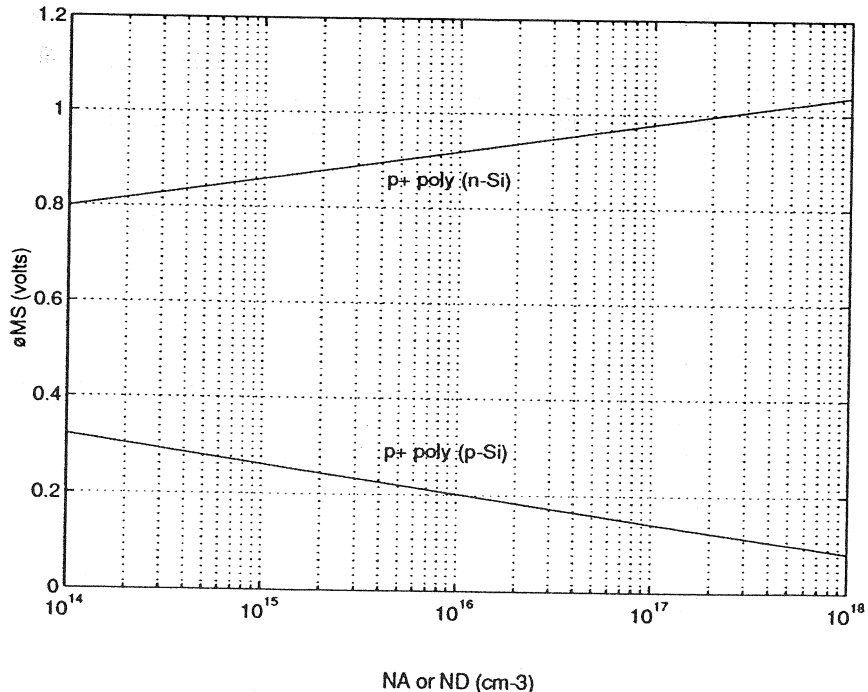
Also

$$(E_c - E_F)_{FB} = (E_c - E_i) + (E_i - E_F)_{FB} \approx E_G/2 + (E_i - E_F)_{FB}$$

or

$$(E_c - E_F)_{FB} = \begin{cases} E_G/2 - (kT/q)\ln(N_D/n_i) & \dots n\text{-type crystalline Si} \\ E_G/2 + (kT/q)\ln(N_A/n_i) & \dots p\text{-type crystalline Si} \end{cases}$$

The results of the  $p^+$  polycrystalline-gate computation based on the above relationships are presented in the following plot. The MATLAB program script used to generate the plot is also listed on the next page. Although it leads to only a minor difference, it should be mentioned that, instead of employing  $E_c - E_i \approx E_G/2$ , the more accurate value of  $E_c - E_i = 0.57\text{eV}$  was used in constructing Fig. 18.3.



### MATLAB program script...

```
%Metal-Semiconductor Workfunction Difference
%Initialization
clear; close
%Constants and Parameters
ni=1.0e10;
EG=1.12;
kT=0.0259;
s=menu('Specify the gate material','Al','n+ poly','p+ poly');
if s==1,
    A=-0.03;
elseif s==2,
    A=-0.18;
else
    A=EG;
end
%Calculate M-S Workfunction Difference
%EcEF=(Ec-EF)FB
NB=logspace(14,18);
EcEFn=EG/2-kT.*log(NB./ni);
EcEFp=EG/2+kT.*log(NB./ni);
oMSn=A-EcEFn;
oMSp=A-EcEFp;
%Plotting result
semilogx(NB,oMSn,NB,oMSp); grid
xlabel('NA or ND (cm-3)'); ylabel('oMS (volts)')
```

### 18.4

(a) Given  $\rho_{\text{ion}} = \rho_0 = \text{constant}$ ,

$$\begin{aligned}\Delta V_G^{\text{(mobile)}} &= -\frac{1}{K_O \epsilon_0} \int_0^{x_0} x \rho_0 dx = -\frac{\rho_0 x_0^2}{2 K_O \epsilon_0} \\ &= -\frac{(1.6 \times 10^{-19})(10^{18})(10^{-5})^2}{(2)(3.9)(8.85 \times 10^{-14})} \\ &= -23.2 \text{V}\end{aligned}$$

(b) Here

$$\rho_{\text{ion}} = Q_M \delta(x_0)$$

where

$$Q_M = \int_0^{x_0} \rho_{\text{ion}}(x) dx = \rho_0 x_0$$

Substituting  $\rho_{\text{ion}} = Q_M \delta(x_0)$  into Eq.(18.13) gives

$$\Delta V_G^{\text{(mobile)}} = -\frac{Q_M}{C_0} = -\frac{x_0}{K_O \epsilon_0} \rho_0 x_0 = -\frac{\rho_0 x_0^2}{K_O \epsilon_0}$$

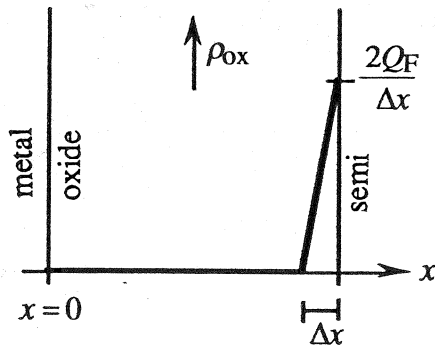
Clearly the  $\Delta V_G$  here is twice that in part (a).

$$\Delta V_G = -46.4 \text{V}$$

### 18.5

(a)  $\Delta V_G(\text{fixed charge}) = -Q_F/C_0$  ...Eq. (18.15)

(b) We are given



or mathematically

$$\rho_{\text{ox}} = \begin{cases} 0 & \dots 0 \leq x \leq x_0 - \Delta x \\ \frac{2Q_F}{\Delta x^2} x' & \dots 0 \leq x' \leq \Delta x, \text{ where } x' = x - x_0 + \Delta x \end{cases}$$

Substituting  $\rho_{\text{ox}}$  into Eq.(18.11) gives

$$\Delta V_G = -\frac{1}{K_0 \epsilon_0} \int_0^{x_0} x \rho_{\text{ox}} dx = -\frac{1}{K_0 \epsilon_0} \left( \frac{2Q_F}{\Delta x^2} \right) \int_0^{\Delta x} x'(x'+x_0-\Delta x) dx'$$

and

$$\boxed{\Delta V_G = -\frac{Q_F}{C_0} \left( 1 - \frac{\Delta x}{3x_0} \right)}$$

(c)  $\frac{\Delta V_G(\text{part b})}{\Delta V_G(\text{part a})} = 1 - \frac{\Delta x}{3x_0}$

If  $\Delta x = 10^{-7}\text{cm}$  and  $x_0 = 10^{-5}\text{cm}$   $\rightarrow \Delta V_G(\text{b})/\Delta V_G(\text{a}) = 0.997$

If  $\Delta x = 10^{-7}\text{cm}$  and  $x_0 = 10^{-6}\text{cm}$   $\rightarrow \Delta V_G(\text{b})/\Delta V_G(\text{a}) = 0.967$

Provided  $x_0 \gg \Delta x$ , it is essentially impossible to distinguish between charge distributed a short distance into the oxide and charge right at the interface. For very thin oxides the difference becomes detectable, but not all that significant, even when  $x_0$  is only  $10\Delta x$ .

### 18.6

(a) If the MOS-C is ideal except for  $\phi_{MS} \neq 0$  and  $Q_F \neq 0$ , then

$$V_{FB} = \phi_{MS} - \frac{Q_F}{C_0} = \phi_{MS} - \frac{x_0}{K_O \epsilon_0} Q_F$$

A plot of  $V_{FB}$  versus  $x_0$  data should be a straight line with an extrapolated  $V_{FB}$ -axis intercept equal to  $\phi_{MS}$  and a slope of  $-Q_F/K_O \epsilon_0$ .

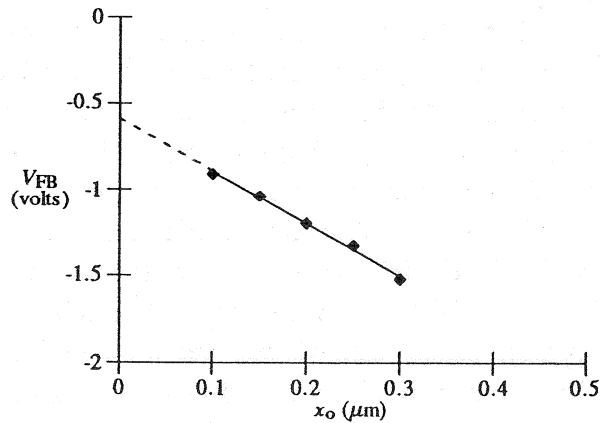
(b) The given  $V_{FB}$  versus  $x_0$  data is plotted below. A least squares fit through the data yields

$$V_{FB} = -0.596 - (3.02 \times 10^4)x_0 \quad \dots x_0 \text{ in cm}$$

Thus

$$\phi_{MS} = -0.596 \text{ V}$$

$$Q_F/q = -K_O \epsilon_0 (\text{slope})/q = \frac{(3.9)(8.85 \times 10^{-14})(3.02 \times 10^4)}{1.6 \times 10^{-19}} = 6.52 \times 10^{10}/\text{cm}^2$$



## 18.7

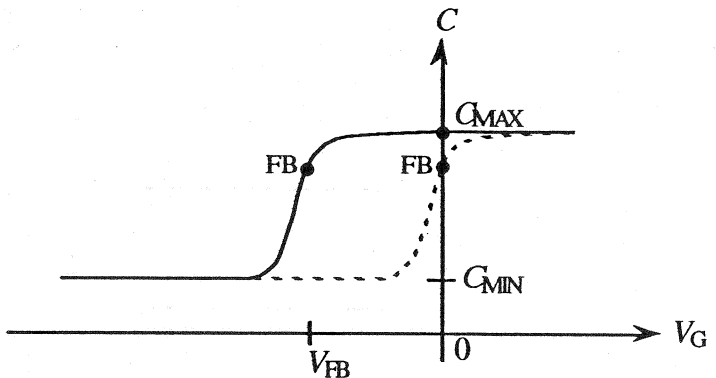
(a)  $Q_M \neq 0$ . If there is no charge in the oxide, if  $\rho_{ox} = 0$ , then  $\mathcal{E}_{ox} = \text{constant}$  and the oxide energy bands are a linear function of position. However, if  $\rho_{ox} \neq 0$ ,  $\mathcal{E}_{ox}$  becomes a function of position and the oxide energy bands in turn exhibit curvature. A concave curvature as pictured in Fig. P18.7 is indicative of a significant positive charge, alkali ions, in the oxide.

(b)  $Q_F \neq 0$ . The normal component of the  $D$ -field, where  $D = \epsilon \mathcal{E}$ , must be continuous if there is no plane of charge at an interface between two dissimilar materials (see Sub-section 16.3.2). When a plane of charge does exist, there is a discontinuity in the  $D$ -field equal to the charge/cm<sup>2</sup> along the interface. Note from Fig. P18.7 that the slope of the bands is zero and therefore  $\mathcal{E} = (1/q)(dE_c/dx) = 0$  on the oxide side of the interface. On the semiconductor side of the interface  $\mathcal{E}$  is decidedly nonzero and positive. Thus, there must be a plane of charge at or near the interface. For the pictured situation we in fact require  $Q_{\text{interface}} = K_S \epsilon_0 \mathcal{E}_S$  and the interface charge must be positive. The interfacial charge could arise from alkali ions, interfacial traps, or the fixed charge. In real devices, alkali ions typically give rise to a spread-out volume charge, making alkali ions an unlikely source of  $Q_{\text{interface}}$ . Moreover, the interfacial trap charge is assumed to be negligible in the statement of the problem. That leaves the fixed charge which closely approximates a plane of positive charge at the Si-SiO<sub>2</sub> interface. We conclude  $Q_F \neq 0$ .

Although a conclusion has been reached, we need to address an apparent inconsistency. In this problem and in Exercise 18.3, we have indicated that the fixed charge will cause a discontinuity in the interfacial  $D$ -field at the Si-SiO<sub>2</sub> interface. However, in deriving Eq.(18.11), the  $D$ -field was *explicitly* assumed to be continuous across the Si-SiO<sub>2</sub> interface. Eq. (18.11) in turn was used to establish the  $\Delta V_G$ (fixed charge) expression. This apparent inconsistency is resolved if the mathematical development is examined carefully. To be precise, by including  $Q_F$  in  $\rho_{ox}$  in the Eq. (18.11) derivation, we actually took the fixed charge to be slightly inside the oxide. The  $D$ -field discontinuity then occurs at  $x = x_0^-$  instead of exactly at  $x = x_0$ . Whether the discontinuity occurs exactly at the interface or an imperceptible distance into the oxide cannot be detected physically, and clearly does not affect the mathematical results.

### 18.8

(a) In an ideal version of an MOS-C, flat band always occurs at  $V_G = 0$ , with the ideal device exhibiting the same value of  $C$  at flat band as the non-ideal device. Because  $Q_{IT} = 0$ , the ideal  $C-V$  curve is obtained by simply translating the given  $C-V$  curve along the voltage axis until the flat band point is at  $V_G = 0$ .



(b) Given  $C_{MAX} = C_0 = \frac{K_0 \epsilon_0 A_G}{x_0}$

we conclude

$$x_0 = \frac{K_0 \epsilon_0 A_G}{C_0} = \frac{(3.9)(8.85 \times 10^{-14})(2.9 \times 10^{-3})}{200 \times 10^{-12}} = 5.00 \times 10^{-6} \text{ cm}$$

Also

$$C_{MIN} = \frac{C_0}{1 + \frac{K_0 W_T}{K_S x_0}}$$

making  $W_T = \frac{K_S x_0}{K_0} \left( \frac{C_0}{C_{MIN}} - 1 \right) = \frac{(11.8)(5 \times 10^{-6})}{(3.9)} \left( \frac{200}{67} - 1 \right) = 3.00 \times 10^{-5} \text{ cm} = 0.3 \mu\text{m}$

Referring to Fig. 16.9, the plot of  $W_T$  versus  $N_A$  or  $N_D$ , we conclude a  $W_T = 0.3 \mu\text{m}$  results when

$$N_D \approx 10^{16}/\text{cm}^3$$

(c) Since  $Q_M = 0$  and  $Q_{IT} = 0$ ,

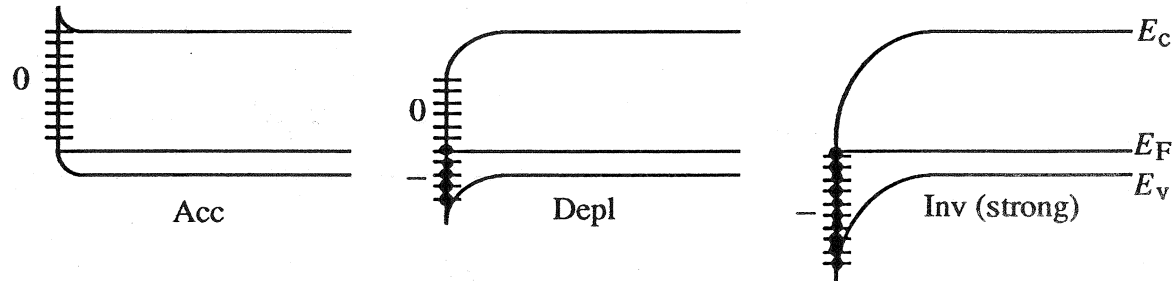
$$\Delta V_G|_{\text{flat band}} = V_{FB} = \phi_{MS} - \frac{Q_F}{C_0}$$

$V_{FB} = -0.71$  in the statement of the problem. Also, for an  $N_D = 10^{16}/\text{cm}^3$  Al(*n*-Si) device, we conclude from Fig. 18.3 that  $\phi_{MS} = -0.24\text{V}$ . Thus

$$\begin{aligned} Q_F &= C_0(\phi_{MS} - V_{FB}) = \frac{C_0}{A_G} (\phi_{MS} - V_{FB}) = \frac{200 \times 10^{-12}}{2.9 \times 10^{-3}} (-0.24 + 0.71) \\ &= 3.24 \times 10^{-8} \text{ coul/cm}^2 \end{aligned}$$

### 18.9

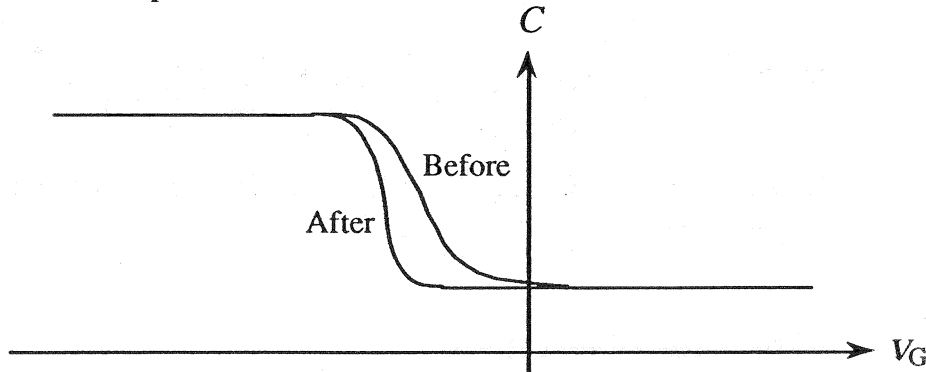
We infer from the  $C-V$  characteristics that the MOS-C is a p-bulk device. Also, we know that acceptor-like traps are negatively charged when filled with an electron and neutral when empty. For a p-bulk MOS-C the effect of biasing on the occupation and charge state of the acceptor-like traps is summarized in the following figure.



We also note

$$\Delta V_G = -\frac{Q_{IT}}{C_0}$$

Thus, relative to the "after" or negligible  $Q_{IT}$  situation, the "before" characteristics will be shifted positively ( $Q_{IT}$  is negative) and the displacement will systematically increase as one progresses from accumulation, through depletion, to inversion. The deduced "before" characteristics are pictured below.

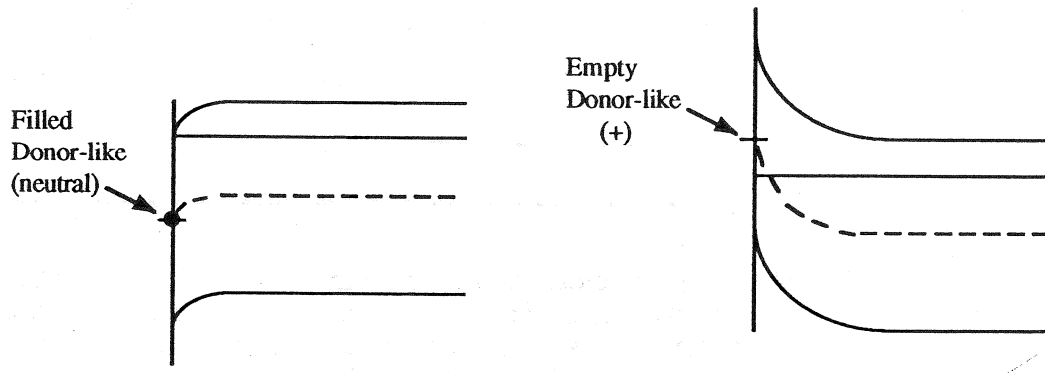


### 18.10

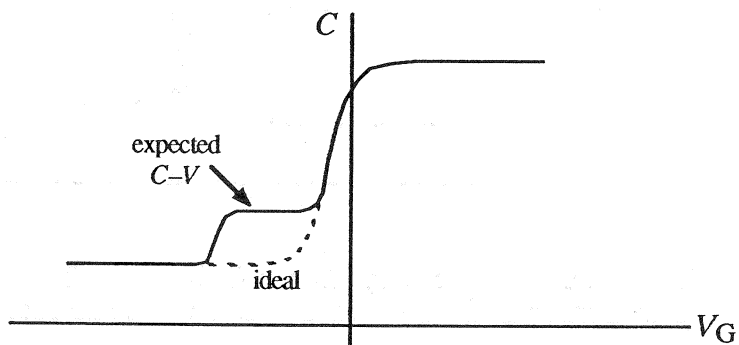
From the answer to Problem 1.5 (see Solutions Manual pages 1-2 and 1-3), we know that there are  $6.78 \times 10^{14}$  atoms/cm<sup>2</sup> and  $9.59 \times 10^{14}$  atoms/cm<sup>2</sup> on the (100) and (110) surface planes, respectively. If one assumes the number of residual "dangling bonds" is proportional to the number of Si surface atoms, then the (110) surface should exhibit the higher density of residual "dangling bonds" or interfacial traps. (Experiments confirm the above conclusion.)

### 18.11

(a) We note that the interfacial traps will be neutral when the MOS-C is accumulation or lightly depletion biased, but become positively charged when the device is  $|\phi_S| > |\phi_F|$  depletion biased or inversion biased.



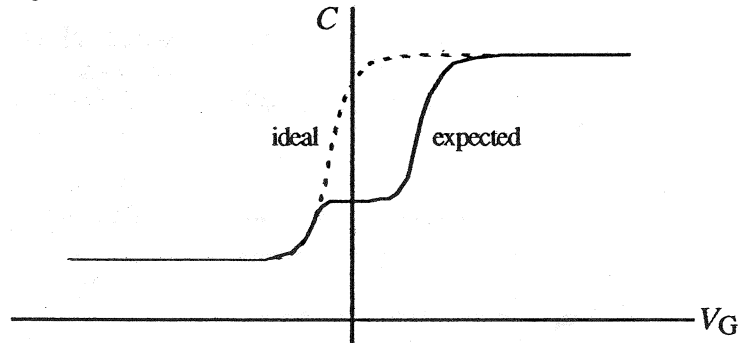
Clearly, there is no shift in the  $C-V$  curve when the device is accumulation and  $|\phi_S| < |\phi_F|$  depletion biased. However, when  $|\phi_S| > |\phi_F|$  depletion biased or inversion biased, the characteristics are translated  $\Delta V_G = -Q_{IT}/C_0 = \text{constant negative value along the voltage axis}$ .



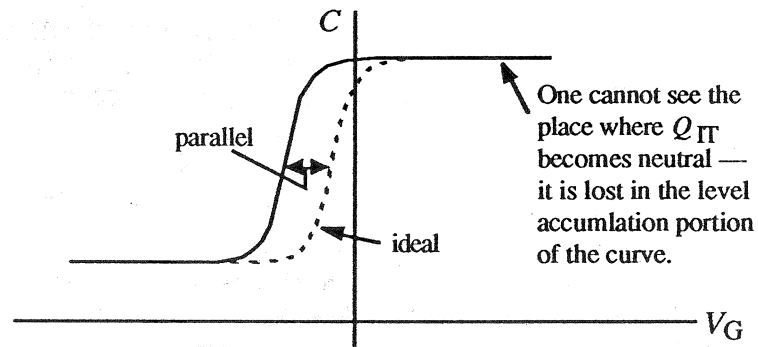
(b) For acceptor-like interfacial traps

Bias	Position of $E_F$	Trap Occupation	Charge State	$\Delta V_G$ shift
acc, $ \phi_S  <  \phi_F $ depl	above $E_{IT}$	filled	negative	toward $+V_G$
$ \phi_S  >  \phi_F $ depl, inv	below $E_{IT}$	empty	neutral	none

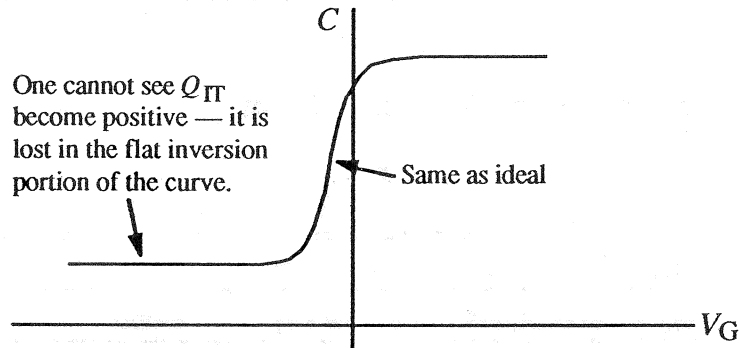
From the preceding one concludes,



- (c) If the states are very close to  $E_C$  they retain the same charge over the non-constant capacitance portion of the  $C$ - $V$  characteristic. Since the states are donor-like and always empty for all depletion biasing, one expects a positive  $Q_{IT}$  and a negative shifting for the entire depletion part of the  $C$ - $V$  characteristic.



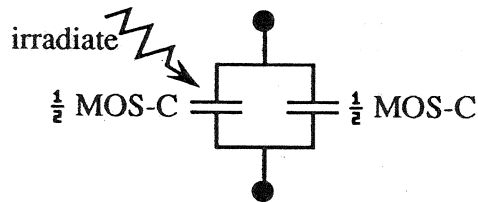
- (d) A donor-like level very close to  $E_V$  is always filled and neutral for the non-constant capacitance portion of the  $C$ - $V$  curve. There will be no observable  $C$ - $V$  shift due to such states.



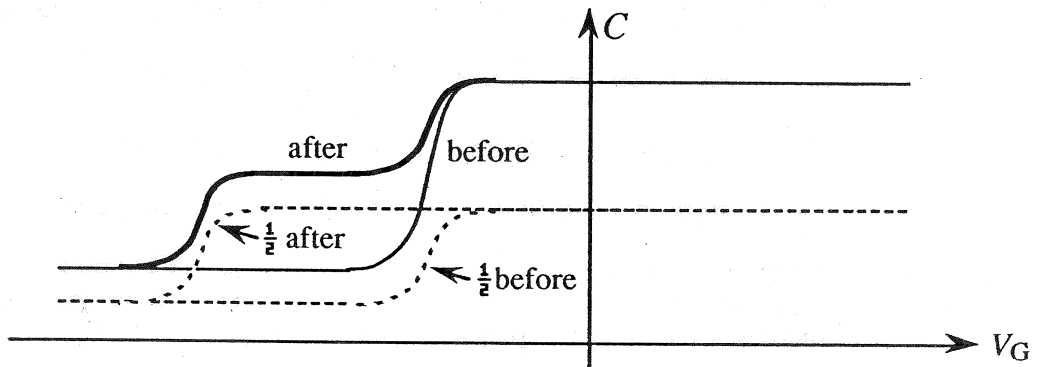
*Note:* This problem points out the difficulty of detecting  $E_{IT}$  states that are very close to the band edges.

### 18.12

The two halves of the MOS-C may be viewed as separate capacitors.



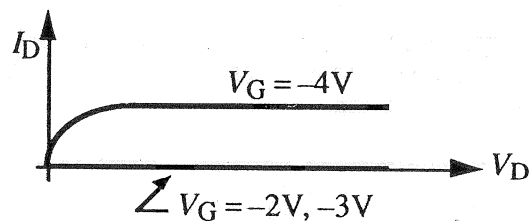
Before irradiation, each half will contribute precisely one-half of the observed capacitance, each yielding a C-V characteristic like that labeled " $\frac{1}{2}$  before" in the figure below. After irradiation, the C-V characteristic of the affected half (labeled " $\frac{1}{2}$  after" in the figure below) will be shifted toward negative voltages due to the apparent  $Q_F$ . Graphically combining the " $\frac{1}{2}$  before" and " $\frac{1}{2}$  after" curves yields the total expected "after" curve.



### 18.13

(a) The shift in the  $g_d - V_G$  characteristic after +BT stressing is symptomatic of *mobile ions* in the oxide.

(b) Conceptually extrapolating the  $g_d - V_G$  curves into the  $V_G$  axis, we conclude that the turn-on voltage has shifted negatively  $\sim 2V$  after +BT stressing. The device is now obviously "off" when  $V_G = -2V$  and  $V_G = -3V$ . Moreover, the  $V_G = -4V$  state after stressing is equivalent to the  $V_G = -2V$  state before stressing. Thus,

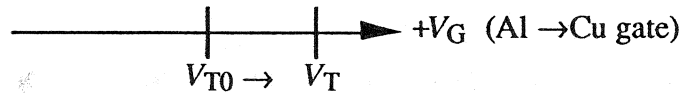


18.14

(a)  $V_T$  will shift in the  $-V_G$  direction. Since  $Q_F$  is positive, an apparent  $Q_F \neq 0$  causes a negative shift in the threshold voltage.



(b) The gate material affects  $\phi_{MS}$ . With  $\Phi_M' - \chi' = -0.03$  eV for Al (see the Fig. 18.3 caption) and  $\Phi_M' - \chi' = 0.63$  eV for Cu (from Table 18.1),  $\phi_{MS}$  and hence  $V_T$  will increase by 0.66V in going from an Al to a Cu gate.



(c) The substrate doping affects both  $\phi_{MS}$  and  $V_T'$ . As given by Eq.(18.22),

$$V'_T = 2\phi_F + \frac{K_S}{K_O} x_0 \sqrt{\frac{4qN_A}{K_S \epsilon_0}} \phi_F \quad \text{where} \quad \phi_F = \frac{kT}{q} \ln \left( \frac{N_A}{n_i} \right)$$

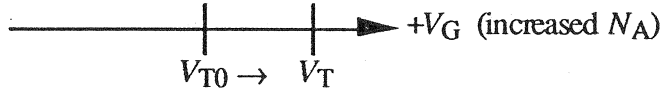
Also

$$(E_c - E_F)_{FB} \cong E_G/2 - (E_i - E_F)_{FB} = E_G/2 + q\phi_F$$

and

$$\phi_{MS} = (1/q)[\Phi_M' - \chi' - (E_c - E_F)_{FB}] = (1/q)[\Phi_M' - \chi' - E_G/2] - \phi_F$$

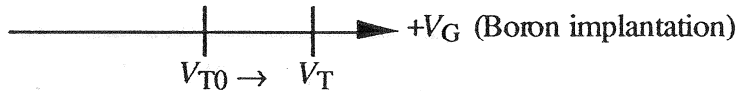
Since  $\phi_F$  increases with doping,  $\phi_{MS}$  decreases and  $V_T'$  increases with increasing  $N_A$ . However, the increase in  $V_T'$  is greater than the decrease in  $\phi_{MS}$ , and  $V_T = V_T' + \phi_{MS}$  increases with an increase in substrate doping.



(d) In general,  $x_0$  enters into the determination of both  $V_T'$  and  $V_{FB}$ . However, because the MOSFET is specified to be ideal except for  $\phi_{MS} \neq 0$ ,  $x_0$  in this problem affects only  $V_T'$ . Inspecting the  $V_T'$  expression quoted in part (b), one rapidly concludes  $V_T'$ , and therefore  $V_T$ , decrease with decreasing  $x_0$ .



(e) To first order, the implantation of Boron into the near surface region of the Si is equivalent to adding a negative fixed charge to the system. — The threshold voltage shifts in the  $+V_G$  direction.



18.15

(a) Adding the voltage shift due to the ion implanted charge (Eq. 18.25) to the regular flat band expression (Eq. 18.20), one obtains

$$V_{FB} = \phi_{MS} - \frac{Q_F}{C_0} - \frac{Q_M \gamma_M}{C_0} - \frac{Q_{IT}(0)}{C_0} - \frac{Q_I}{C_0}$$

$$= \phi_{MS} - q \frac{x_0}{K_O \epsilon_0} \left[ \frac{Q_F}{q} + \frac{Q_M \gamma_M}{q} + \frac{Q_{IT}(0)}{q} + \frac{Q_I}{q} \right]$$

For the given device

$$V_{FB} = -0.46 - \frac{(1.6 \times 10^{-19})(5 \times 10^{-6})}{(3.9)(8.85 \times 10^{-14})} (2 \times 10^{11} + 0 + 0 - 4 \times 10^{11}) \equiv 0$$

(b)

$$V_T = 2\phi_F - \frac{K_S}{K_O} x_0 \sqrt{\frac{4qN_D}{K_S \epsilon_0} (-\phi_F)}$$

$$\phi_F = -\frac{kT}{q} \ln(N_D/n_i) = -0.0259 \ln(10^{15}/10^{10}) = -0.298V$$

$$V_T = -(2)(0.298) - \frac{(11.8)}{(3.9)} (5 \times 10^{-6}) \left[ \frac{(4)(1.6 \times 10^{-19})(10^{15})(0.298)}{(11.8)(8.85 \times 10^{-14})} \right]^{1/2}$$

$$= -0.80V$$

and

$$V_T = V_T + V_{FB} = V_T = -0.80V$$

(c) [Enhancement mode] device. For the given *p*-channel device there is no inversion-layer at zero bias and therefore no drain current when  $V_G = 0$ . A MOSFET which is "off" at zero bias is referred to as an enhancement mode device.

### 18.16

Combining Eqs.(18.21), (18.20), and (18.25), one can write

$$V_T = V_T' + \phi_{MS} - \frac{Q_F}{C_0} - \frac{Q_M Y_M}{C_0} - \frac{Q_{IT}(0)}{C_0} - \frac{Q_I}{C_0}$$

Since there are no interfacial traps and no mobile ions in the oxide,  $Q_M = 0$  and  $Q_{IT} = 0$ . Also  $C_0 = K_O \epsilon_0 / x_0$  and  $Q_I = -qN_I$ . Thus the  $V_T$  expression simplifies to

$$V_T = V_T' + \phi_{MS} - q \frac{x_0}{K_O \epsilon_0} (Q_F/q - N_I)$$

Solving the preceding equation for  $N_I$  then gives

$$\left[ N_I = \frac{Q_F}{q} + \frac{1}{q} \frac{K_O \epsilon_0}{x_0} (V_T - V_T' - \phi_{MS}) \right]$$

$Q_F/q$  and  $V_T$  are specified in the statement of the problem. However, we need to determine  $\phi_{MS}$  and  $V_T'$ . Because the MOSFET is an Al-SiO<sub>2</sub>-Si device, we can read  $\phi_{MS}$  directly from Fig. 18.3. For  $N_A = 10^{17}/\text{cm}^3$ , one finds  $\phi_{MS} = -1.02\text{V}$ . The ideal-device threshold voltage can be computed using Eq.(18.22).

$$V_T' = 2\phi_F + \frac{K_S}{K_O} x_0 \sqrt{\frac{4qN_A}{K_S \epsilon_0} \phi_F}$$

$$\phi_F = \frac{kT}{q} \ln(N_A/n_i) = 0.0259 \ln(10^{17}/10^{10}) = 0.417\text{V}$$

$$V_T' = (2)(0.417) + \frac{(11.8)}{(3.9)} (10^{-6}) \left[ \frac{(4)(1.6 \times 10^{-19})(10^{17})(0.417)}{(11.8)(8.85 \times 10^{-14})} \right]^{1/2}$$

$$= 1.32\text{V}$$

Finally, substituting into the  $N_I$  expression, we obtain

$$N_I = 10^{11} + \frac{(3.9)(8.85 \times 10^{-14})}{(1.6 \times 10^{-19})(10^{-6})} (0.5 - 1.32 + 1.02)$$

or

$$N_I = 5.31 \times 10^{11} \text{ boron ions/cm}^2$$

## CHAPTER 19

### 19.1

(a) True

(b) (i) Severely distorted  $I_D$ - $V_D$  characteristics. (Curves fail to saturate and  $I_D \propto V_D^2$  curves observed for gate voltages below threshold.)

(ii) Subthreshold transfer characteristics which vary with  $V_D$ .

(iii) A threshold voltage which is a function of the gate dimensions and the applied biases.

(c) differ ...  $|V_T|$  decreases with  $L$  but increases with  $Z$ .

alike ... Both effects have a similar cause; the gate charge required to achieve the threshold point changes because of the increasing importance of channel-edge charges.

(d) As noted in Subsection 19.1.1,  $L_{min}$  can be made smaller, and hence small-dimension effects minimized, by reducing the depth of the source/drain islands and by increasing the substrate doping.

(e) (i) punch-through

(ii) carrier multiplication and regenerative feedback

(f) In the vicinity of the drain under operational conditions, channel carriers, and carriers entering the drain depletion region from the substrate, periodically gain a sufficient amount of energy to surmount the Si-SiO<sub>2</sub> surface barrier and enter the oxide. Neutral centers in the oxide trap a portion of the injected charge and thereby cause a charge build-up within the oxide.

(g) Primarily because a larger percentage of the gated region is affected in the smaller devices. (However, the oxide charging is made worse by the common practice of using bias voltages that have not been scaled down in proportion to the device dimensions.)

(h) First,  $I_{Dsat}$  for a given  $V_G$  is significantly reduced. Second, the saturation current exhibits an almost linear dependence on  $V_G - V_T$  as opposed to the conventional square-law dependence.

(i) *ballistic transport* — the projectile-like motion of carriers through a semiconductor region where there is very little or no scattering.

(j) *velocity overshoot* — an average carrier velocity greater than  $v_{sat}$ .

(k) A lightly doped drain (LDD) region is introduced between the end of the channel and the drain proper.

- (l) With a material lattice constant different than that of the underlying substrate, a pseudomorphic film is a thin layer of the material (typically  $\lesssim 1000\text{\AA}$ ) that conforms to the lattice pattern of the substrate.
- (m) (i) The SiGe enhanced-mobility MOSFET picture in Fig. 19.12 contains a strained pseudomorphic Si film that conforms to the larger lattice constant of the underlying  $\text{Si}_{0.7}\text{Ge}_{0.3}$  layer.  
(ii) The pseudomorphic MODFET or PHEMT pictured in Fig. 19.15 contains a pseudomorphic  $\text{In}_x\text{Ga}_{1-x}\text{As}$  layer positioned between the  $\text{AlGaAs}$  and  $\text{GaAs}$ .
- (n) A high dose of oxygen is implanted into a silicon wafer and the wafer subsequently annealed to produce an oxide layer beneath the top surface of the wafer. An SOI layer is thereby created. (See Fig. 19.13.)
- (o) There is no difference. MODFET and HEMT are just two different names for the same device.

## 19.2

LD...lightly doped drain

DMOS...double-diffused metal oxide semiconductor

SOI...silicon on insulator

SOS...silicon on sapphire

ELO...epitaxial layer overgrowth

SIMOX...separation by implantation of oxygen

BESOI...bonded silicon on insulator

BOX...buried oxide layer

MODFET...modulation doped field effect transistor

PHEMT...pseudomorphic high electron mobility transistor

### 19.3

(a) Given...  $x_0 = 0.028\mu\text{m} = 280\text{\AA}$ ,  $r_j = 1\mu\text{m}$ , and

$$W = \left[ \frac{2K_S \epsilon_0}{qN_A} (V_{bi} - V_A) \right]^{1/2} \quad \begin{aligned} \text{with } V_{bi} &= 0.915\text{V} \text{ (read from Fig. E5.1)} \\ V_A &\Rightarrow 0 \quad \text{source junction} \\ V_A &\Rightarrow -V_D = 0.125\text{V} \quad \text{drain junction} \end{aligned}$$

$$W_S = \left[ \frac{(2)(11.8)(8.85 \times 10^{-14})}{(1.6 \times 10^{-19})(8 \times 10^{15})} (0.915) \right]^{1/2} = 0.386\mu\text{m}$$

$$W_D = \left[ \frac{(2)(11.8)(8.85 \times 10^{-14})}{(1.6 \times 10^{-19})(8 \times 10^{15})} (0.915 + 0.125) \right]^{1/2} = 0.412\mu\text{m}$$

$$L_{min} = 0.4 [r_j x_0 (W_S + W_D)]^{1/3} = 0.4 [(1)(280)(0.386 + 0.412)]^{1/3} = 2.25\mu\text{m}$$

The calculated  $L_{min}$  is right on target. The  $V_D = 0.125\text{V}$  data in Fig. 19.3 show a significant change in the threshold voltage for  $L \leq 2\mu\text{m}$ . [It should be noted that  $W_D = 0.896\mu\text{m}$  and  $L_{min} = 3.09\mu\text{m}$  if one employs  $V_D = 4\text{V}$ . This  $L_{min}$  for  $V_D = 4\text{V}$  appears to be decidedly too low. The  $V_D$  dependence noted in Fig. 19.3 is much stronger than that expected from the  $L_{min}$  dependence.]

$$(b) \phi_F = (kT/q) \ln(N_A/n_i) = 0.0259 \ln(8 \times 10^{15}/10^{10}) = 0.352\text{V}$$

$$W_T = \left[ \frac{2K_S \epsilon_0}{qN_A} (2\phi_F) \right]^{1/2} = \left[ \frac{(2)(11.8)(8.85 \times 10^{-14})}{(1.6 \times 10^{-19})(8 \times 10^{15})} (2)(0.352) \right]^{1/2} = 0.339\mu\text{m}$$

$$\Delta V_T = - \frac{qN_A W_T}{K_O \epsilon_0} x_0 \frac{r_j}{L} \left( \sqrt{1 + \frac{2W_T}{r_j}} - 1 \right)$$

$$= - \frac{(1.6 \times 10^{-19})(8 \times 10^{15})(3.39 \times 10^{-5})(2.8 \times 10^{-6})(10^{-4})}{(3.9)(8.85 \times 10^{-14})(10^{-4})} \left\{ \left[ 1 + \frac{(2)(0.339)}{1} \right]^{1/2} - 1 \right\}$$

$$= -0.104\text{V}$$

The computed result here is very close to the observed  $\Delta V_T \approx -0.13\text{V}$ .

(c) No...The Eq.(19.13) result is derived assuming  $V_D \approx 0$ .

#### 19.4

- (a) A lightly doped drain region ( $n^-$  versus  $n^+$  of the drain proper) which lies between the end of the channel and the drain proper.
- (b) A short channel length ( $\sim 1\mu\text{m}$ ) formed by the difference in the lateral distances diffused by two impurities. The short channel length can be achieved without using small-dimension lithographic masks.
- (c) A surface layer beneath the gate with the same doping as the drain and source islands.
- (d) The channel region of the MOSFET is a strained pseudomorphic Si layer with a higher carrier mobility than equivalently-doped bulk Si.
- (e) Si device layers formed *over* an insulating film or substrate.